NUMERICAL MODELLING OF SMALL GROUPS OF STONE COLUMNS

by

Micheál Killeen B.E.

A thesis submitted to the College of Engineering and Informatics, National University of Ireland, Galway, in partial fulfilment of the requirements for the Degree of Doctorate in Philosophy

June 2012

Academic Supervisor: Dr. Bryan McCabe

Professor of Civil Engineering: Prof. Padraic O'Donoghue

Declaration

I hereby declare that this thesis has not been submitted in whole or in part to any other University as an exercise for a degree. I further declare that, except where reference is given in the text, it is entirely my own work.

This thesis may be lent or copied by the library.

Signed: _____ Date: _____

Micheál Killeen

To my parents Michael and Kitty,
and sisters Maria and Áine

Acknowledgements

I would like to express my sincere appreciation and deep gratitude to my supervisor, Dr. Bryan McCabe, who devoted so much time and effort to this research project. I am extremely grateful for all his support, encouragement and advice throughout my studies. Most of all, I appreciate his friendship.

I would also like to extend a special thanks to my academic mentors, Dr. Annette Harte and Prof. Padraic O' Donoghue, for their contributions throughout the duration of this research.

I would like to acknowledge Keller Foundations (UK) for their generous financial support provided to this research project. I am especially grateful to Dr. Alan Bell and Dr. Derek Egan for their highly practical advice and valuable contributions to many technical problems.

This thesis on the behaviour of small groups of stone columns was conducted in collaboration with research partners. I would like to thank Dr. V. Sivakumar (Queen's University, Belfast), Dr. Jonathan Black (University of Sheffield, UK) and also Dr. Minna Karstunen and Dr. Daniela Kamrat-Pietraszewska (Strathclyde University, Glasgow) for their assistance to this research project. I would also like to thank Dr. Jorge Castro and Dr. Bostjan Pulko for their help in patiently answering my many questions. I would also like to acknowledge the advice from the PLAXIS support team.

I greatly appreciate the financial scholarship provided by the Irish Research Council for Science, Engineering and Technology (IRCSET) to support this research project. I would also like to express my sincere gratitude to the Geotechnical Society of Ireland for funding my trip to Egypt to participate in the International Young Geotechnical Engineers conference in 2009. I thoroughly enjoyed this experience and it has encouraged me to pursue future studies in geotechnical research.

I am indebted to the staff in the Department of Civil Engineering at NUI Galway who through their dedication and enthusiasm helped to instil a passion for engineering in me during my undergraduate studies.

I am extremely grateful to my fellow postgraduate students, all my friends and my relatives (including those who have passed away) for their support, advice and warm friendship they have provided to me.

Finally, my last and most important acknowledgement goes to my parents and sisters. I am forever indebted to you for the never-ending support provided to me and all the sacrifices made.

Míle buíochas

Abstract

Vibro stone columns, installed using the vibro replacement technique, are a cost-effective form of ground improvement for enhancing the bearing capacity and settlement characteristics of various soil types. Large groups of stone columns (such as used to support embankments) are conventionally modelled using the unit cell concept, which is based on an infinite grid of columns supporting an infinitely wide load area. Therefore all columns are equally confined on all sides and are subject to a constant increment of vertical stress with depth. The behaviour of small groups of stone columns supporting small area footings is quite complex as peripheral columns are subject to a loss of lateral confinement and the increment of vertical stress decays sharply with depth. This research is the first comprehensive three-dimensional numerical study of the factors affecting both the mechanisms of load transfer from columns to soil and the settlement performance of small column groups at working loads.

PLAXIS 3D Foundation is used for this research in conjunction with the advanced elasto-plastic Hardening Soil model, which is adopted for the parent soil and stone backfill. The soft soil modelled is that at Bothkennar, Scotland, the former UK geotechnical test bed. The influence of key design parameters such as area ratio, column length, stiffness, strength and installation effects upon the settlement performance and deformational behaviour of small groups of stone columns was investigated through a total of 45 numerical analyses.

The modelling has shown that the area ratio and column length have a significant influence on the settlement performance of stone columns. Moreover, they appear to be inter-dependent as the effect of column length becomes more pronounced at low area ratios. The influence of column confinement (i.e. increasing number of columns) was also found to have a positive influence on the settlement performance of small groups of stone columns. It was also shown that the influence of key design parameters upon the settlement performance of stone columns is dependent upon the mode of deformation.

New parameters called compression and punching ratios were defined to help identify three distinct mechanisms referred to as "punching", "block failure" and "bulging". The

occurrence of these mechanisms was verified by analysing the distribution of total shear strain within columns and the surrounding soil and also examining the variation of stress and strain along the length of columns. It was found that area ratio and column length, rather than the number of columns, dictates the load transfer mechanism for small groups of stone columns.

A more in-depth analysis of the deformational behaviour reveals that some combination of punching and bulging occurs simultaneously, with one particular mode of deformation more influential for a given area ratio and column length. This is consistent with the finding that settlement improvement factors increase with column length for all configurations of columns and suggests that a unique critical length, as proposed by previous laboratory studies, does not exist for small groups of stone columns. The presence of a stiff crust, an important feature of soft soil stratigraphy not captured in the laboratory tests, was shown to have a significant influence upon the deformational behaviour of columns. The observation of a critical length from laboratory studies is shown in part to be due to the absence of a stiff crust (i.e. homogeneous soil samples) as columns are more susceptible to bulging in the upper layers and thus cannot transfer the applied load to their base.

The stress concentration ratios at the ground surface were also examined and it was found that they are related to the mode of deformation. Moreover, it was shown that stress concentration ratios vary considerably with column position and as such, do not uniquely reflect the settlement performance of stone columns. Instead, the stress concentration ratios with depth were noted and it was observed that they are constant with depth in the yielded sections of the column and decrease towards unity at the base of floating columns thereafter.

The numerical output in this thesis has been developed into a simplified design method which allows the settlement of a column group to be related to that of a unit cell with knowledge of the footing to column length ratio and the column length to layer thickness ratio (and thereby caters for floating column groups).

Table of Contents

8 Conclusions

List of Figures

2 Literature review

3 Background and preliminary checks for Finite Element Analysis

4 Development and validation of soft soil profile

5 Results of FEA: Settlement performance, deformational behaviour and stress concentration ratios

6 Results of FEA: Distribution of total shear strains and characteristic column behaviour

7 Development of simplified design method and comparison of findings with previous research

List of Tables

2 Literature review

3 Background and preliminary checks for Finite Element Analysis

4 Development and validation of soft soil profile

5 Results of FEA: Settlement performance, deformational behaviour and stress concentration ratios

Nomenclature

Unless otherwise stated, the following abbreviations and symbols are used in this thesis. However, when referring to specific publications, the original notation has been used.

Abbreviation:

CCET	Cylindrical Cavity Expansion Theory
FEA	Finite Element Analysis
FEM	Finite Element Method

Symbols:

A	Tributary area of soil per column in a large grid
A_C	Area of the stone column
A/A_C	Area ratio
B	Width of square footing
C_C, C_S	Compression and swelling indices, respectively
C_k	Hydraulic change index (= $\Delta e/\Delta \log(k)$)
D	Diameter of circular footing
E	Young's modulus
E_{50}	Secant Young's modulus at 50% deviatoric stress
E_{ur}	Young's modulus for unload-reload
E_{col}/E_{soil}	Modular ratio
G	Shear modulus
H	Thickness of soil deposit
I_L	Liquidity index
I_P	Plasticity index
K_0	Coefficient of lateral earth pressure at rest
K_A, K_P	Coefficient of active and passive earth pressure, respectively
L	Column length
N	Diameter ratio (= d_e/d_c)
R_f	Failure ratio (Hardening Soil model)
R_{inter}	Strength reduction factor (Hardening Soil model)
a	Column radius
b	Unit cell radius
c	Cohesion
c_u	Undrained shear strength

c_r, c_v	Coefficients of consolidation in radial and vertical direction, respectively
d	Column diameter (= 2a)
d_e	Unit cell diameter (= 2b)
e_0	Initial voids ratio
f_d	Depth factor (cf. Priebe, 1995)
k_{vert}, k_{horz}	Coefficients of vertical and horizontal permeability, respectively
m_v	Modulus of volume compressibility
m	Power for stress dependency (Hardening Soil model)
n	Settlement improvement factor (= $s_{untreated}/s_{treated}$)
p, p'	Mean principal total and effective stress, respectively
p_A	Applied pressure
p^{ref}	Reference pressure (Hardening Soil model)
p_{lim}	'Limit pressure' at which indefinite expansion of a cavity occurs (cf. CCET)
q	Deviatoric stress
s	Column spacing
s	Settlement of a finite group of stone columns
s_{uc}	Settlement of an infinite grid of stone columns
s/s_{uc}	Settlement ratio
u	Vertical displacement
z	Depth
w	Water content

α	Slope of s/s_{uc} versus B/L line
β	Settlement reduction factor (= $s_{treated}/s_{untreated}$)
γ	Bulk unit weight
	Shear strain
ε_y, ε_h	Vertical and horizontal strain, respectively
κ	Slope of unload/reload line on plot of υ versus ln(p')
λ	Slope of isotropic normal compression line on plot of υ versus ln(p')
μ, υ	Poisson's ratio
σ, σ'	Total and effective normal stress, respectively
σ_1, σ_2, σ_3	Major, intermediate and minor principal stress, respectively
$\sigma'_{col}/\sigma'_{soil}$	Stress concentration ratio
$\sigma'_{y,\,0}$, $\sigma'_{y,\,max}$	*In situ* and maximum vertical effective stress, respectively
τ (= τ')	Shear stress
φ	Angle of internal friction
ψ	Angle of dilatancy

Chapter 1
Introduction

1.1 Background

Vibro replacement is a popular form of ground improvement which is used to enhance the settlement and bearing capacity characteristics of soft soils. Vertical columns of compact stone are formed in the ground using either the top or bottom feed systems. The vibro replacement process typically involves replacing 10–35% of the *in situ* soil with crushed gravel. The high stiffness properties of the crushed gravel reduce the overall and differential settlements of treated soil. The consolidation time is also reduced due to the high permeability of the crushed gravel. Stone columns can be used to provide support for a variety of loading scenarios ranging from small footings (i.e. pad/strip footings) to wide area loadings (i.e. embankments and large floor slabs).

The design of foundations on soft soils is usually governed by settlement criteria rather than bearing capacity due to their high compressibility. The majority of analytical design methods developed to date contain many simplifying assumptions, such as the unit cell concept, which assumes an infinite grid of columns supporting an infinitely wide load area. Therefore, they do not account for the loss of lateral confinement associated with groups of columns supporting small footings. In addition, the reduction in vertical stress with depth beneath small footings is much sharper than that beneath wide area loadings and, therefore, offers the possibility of partial depth treatment. While some correction factors exist to account for the loss of lateral confinement, current design methods do not consider the loss of lateral confinement for small groups of floating stone columns.

While the bearing capacity of small groups of stone columns has been well researched, a dearth of information exists regarding the settlement performance of small groups of columns. This is highlighted by McCabe *et al.* (2009) whose settlement database of over 20 case studies comprised only three case studies related to small groups of columns. Similarly, the majority of numerical studies conducted are axisymmetric analyses on

large groups of columns. The lack of information regarding the settlement performance of small groups of stone columns was identified by Black (2006) who conducted some high quality laboratory research; however, it is difficult to extrapolate the findings due to scale effects associated with laboratory tests and also as some of the area ratios considered are at the high end of typical values used in practice.

1.2 Aims and objectives

This research aims to investigate the loss of lateral confinement and reduction of vertical stress with depth for small groups of floating stone columns. The following milestones are outlined below to achieve this objective:

(a) Determine the influence of area ratio, column length and the number of columns (i.e. column confinement) upon the settlement performance and deformational behaviour of small groups of stone columns.

(b) For a select number of column configurations, examine the influence of column arrangement, the position of columns relative to the footing edge, column compressibility, column strength, column installation effects and the presence of a stiff crust upon the settlement performance and deformational behaviour of stone columns.

(c) Develop a simplified design method which accounts for the loss of lateral confinement and reduction of vertical stress with depth associated with small groups of floating stone columns.

1.3 Methodology

A series of three-dimensional finite element analyses are proposed to investigate the settlement performance and deformational behaviour of small groups of stone columns in soft soil. PLAXIS 3D Foundation is a FE program which is specially developed for geotechnical engineering and is adopted for this thesis. The stress-strain behaviour of the soil and stone columns is simulated using advanced constitutive models. The soil profile adopted is that of the well characterised Bothkennar test site, which consists of soft uniform clay overlain by a stiff crust. The adopted soil profile and material parameters are validated and the analysis is extended to study the influence of key design parameters such as area ratio, column length, stiffness, strength, installation effects and the presence of a stiff crust.

Two parameters are introduced to study the deformational behaviour of stone columns, column compression and column punching ratios. These ratios are determined from the displacement at the top and bottom of columns and are a simple method to investigate the influence of various design parameters upon the mode of deformation of columns.

A more detailed analysis of load-transfer mechanisms for small groups of stone columns is conducted by examining the distribution of total shear strains within stone columns and the surrounding soil. This analysis is conducted for a select number of column lengths, which are specifically chosen to display each mode of deformation. The effect of column spacing and confinement upon column-column interaction and column-soil interaction for each mode of deformation is identified.

The distribution of stress and strain along the column is also examined. These parameters play a key role in the settlement performance of stone columns and allow a link between the settlement performance and the deformational behaviour of columns to be established.

1.4 Outline of thesis

Chapter 2 provides a detailed description of the vibro replacement technique. A comprehensive review into the deformational behaviour, settlement performance and installation effects of vibro stone columns is presented. The main analytical design methods used in practice to calculate the settlement of stone columns are also reviewed.

A background to the finite element analysis is presented in Chapter 3. The material models used in PLAXIS 3D Foundation are described and the results of preliminary studies on mesh sensitivity and boundary effects are presented. Other issues such as simulating the long term behaviour of soft soil, modelling the column-soil interface and incorporating column installation effects into the finite element model are discussed.

The accuracy of PLAXIS 3D Foundation to capture the load-deformational behaviour of stone columns is assessed in Chapter 4. A series of load tests on stone columns in a layered estuarine deposit are simulated and the predicted load-settlement curves are compared with field measurements and two axisymmetric FEA. A soil profile and set of material parameters are developed for the Bothkennar test site. The adopted soil profile and set of material

parameters are validated by simulating a load test reported by Jardine *et al.* (1995) at the test site. The settlement performance of an infinite grid of columns at the Bothkennar test site is also simulated with PLAXIS 3D Foundation and compared with one-dimensional compression theory, a settlement improvement database and analytical design methods.

The results from the primary analysis of this thesis regarding the settlement performance, deformational behaviour and stress concentration ratios for small groups of columns are presented and interpreted in Chapter 5. The interaction between column confinement, length and area ratio and their influence upon the settlement performance of columns is examined. Three modes of modes deformation are identified, which are referred to as "punching", "block failure" and "bulging", at typical working loads levels. Finally, the relationship between the stress concentration ratio at the surface and the mode of deformation is examined.

The modes of deformation identified in Chapter 5 are verified by examining the distribution of total shear strain, normal strain and stress concentration ratios within columns for specific column lengths in Chapter 6. The distribution of shear strains within columns and the surrounding soil allows the column-column and column-soil interactions to be investigated. The characteristic behaviour of individual columns (i.e. corner, edge and centre columns) is examined though the distribution of vertical and horizontal strains along the length of columns. The variation of stress concentration ratio with depth is also examined and its relationship with the mode of deformation is highlighted.

A simplified design method which accounts for the loss of lateral confinement and reduction of vertical stress with depth for groups of columns supporting small loaded areas is developed in Chapter 7. The findings from PLAXIS 3D Foundation are discussed in relation to previous research and the existence of a critical length and the effect of the stiff crust are highlighted. The influence of the mode of deformation upon the settlement performance of stone columns is also discussed. Finally, the stress concentration ratios at the surface and at depth are compared with a field and laboratory measurements and also analytical design methods.

Finally, the conclusions of the research are presented in Chapter 8. A better understanding of small groups of stone columns is gained and the findings can be used by practitioners to relate the settlement of small groups and infinite grids of columns.

Chapter 2
Literature review

2.1 Background

2.1.1 Introduction

Deep vibratory techniques such as vibro compaction and vibro replacement are forms of ground improvement which are used to enhance the bearing capacity and settlement characteristics of weak soils. The vibro compaction technique was developed in 1936 by the Keller group and one of its first applications was to densify non-cohesive river-borne granular soils (McCabe *et al.*, 2007). The technique consists of lowering a vibrating poker into the ground, which imparts horizontal forces to the surrounding soil and causes the soil particles to re-arrange into a denser state. However, it was found that vibro compaction reaches its technical and economic limits in saturated sands with high silt contents, as fine particles attenuate the horizontal forces imparted by the vibrating poker (Sondermann & Wehr, 2004).

The limitation of vibro compaction in cohesive soils (i.e. soils composed of a high proportion of fine particles) was overcome in 1956 by the development of the vibro replacement technique. As with the vibro compaction technique, a vibrating poker penetrates the soil to form a borehole. The resulting borehole is then backfilled in stages with coarse aggregate, which is compacted by re-lowering the poker. This process results in stone columns which are tightly inter-locked with the surrounding soil. Stone columns can readily be formed up to 15 m and typically replace 10–35% of the *in situ* soil (McKelvey *et al.*, 2004). Figure 2.1 illustrates how the vibro replacement technique extends the range of soils types treatable by deep vibratory techniques. Vibro stone columns offer a cost-effective alternative to traditional piled solutions when supporting moderately loaded residential, commercial and industrial structures.

Other variations of vibro stone columns include geotextile-encased columns and vibro concrete columns. Geotextile-encased stone columns are used in very weak soils where

insufficient lateral support is provided by the surrounding soil and excessive bulging of stone columns occurs. The geotextile material develops tensile forces which constrain the column and reduce bulging.

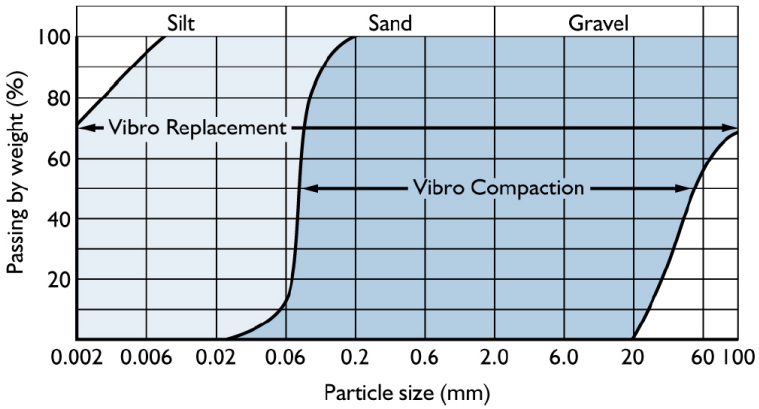

Figure 2.1 - Range of soil types treatable by vibro compaction and vibro replacement techniques (courtesy of Keller Ground Engineering)

2.1.2 Construction processes

Poker

The vibrating pokers used for the dry and wet top feed systems are depth vibrators suspended from a crane. The vibrating pokers are 300–500 mm in diameter and range in length from 2–5 m. This length can be increased with extension tubes to reach depths of up to 26 m (Sondermann & Wehr, 2004). The poker consists of a cylindrical steel shell and the horizontal vibratory forces are generated from an eccentric weight located in the lower section. An elastic coupling is used at the top of the vibrator to prevent any vibratory forces being transferred to the extension tubes. Supply tubes for compressed air and water, which are used to aid the poker penetration, are also incorporated into the vibrator shell (Figure 2.2).

Dry top feed system

The poker is inserted into the ground which displaces the soil laterally. Compressed air is delivered to the cavity as the poker is withdrawn from the ground in order to prevent the cavity collapsing. A controlled volume of crushed stone is then tipped into the cavity from the ground surface and subsequently compacted by re-lowering the poker. This process is repeated until a stone column, which is tightly interlocked with the surrounding soil, is formed up to the ground surface. This construction method is limited to competent soils that can sustain an open borehole.

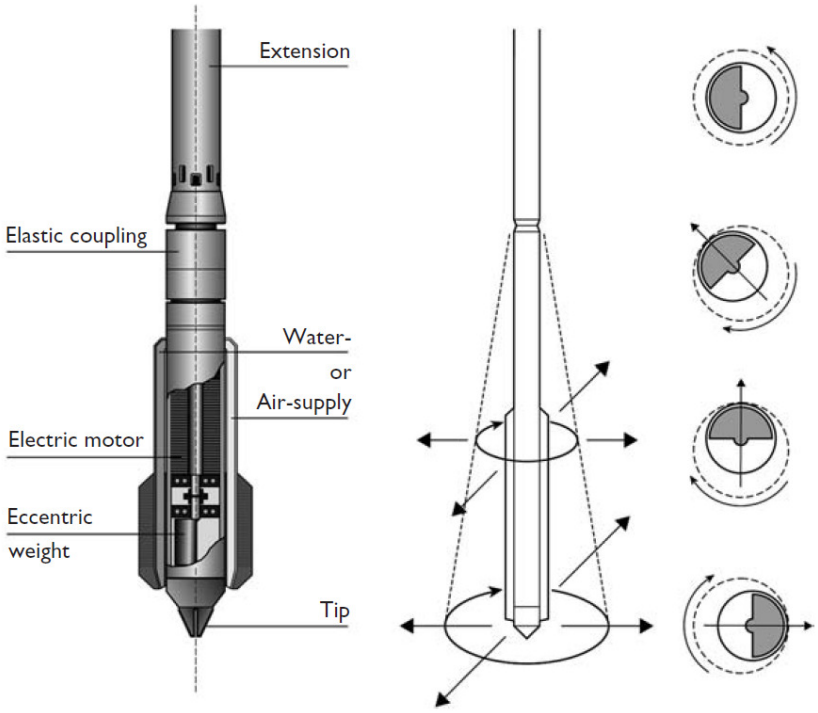

Figure 2.2 - Depth vibrator and principle of vibro compaction (Sondermann & Wehr, 2004)

Wet top feed system

The poker penetration for the wet top feed system is aided by water jets at the poker tip. The jets support the cavity wall and dislodge any loose material during penetration. The flushed out material is carried upwards through the annulus surrounding the poker and treated in settlement lagoons. Field experience indicates that penetration is more effective when a larger volume of water is used, rather than a higher pressure (Sondermann & Wehr, 2004). Once the design depth is reached, the poker is raised slightly and crushed stone is added to the cavity through the annulus surrounding the poker. The poker is then re-lowered to compact the stone and this process is repeated until a stone column is formed up to the ground surface. This system is not commonly used due to the onerous task of treating the flushed out material and also as the water jets create a smear zone surrounding the cavity which reduces the drainage capacity of stone columns.

Dry bottom feed system

A specially developed machine called a 'vibrocat' is used for the dry bottom feed system (Figure 2.3). The vibrocat is different from traditional crane suspended vibrators as the vibrator is mounted on leaders, thus ensuring vertical columns. The vibrator can also generate pull down forces using a hydraulic winch to aid poker penetration. The supply tube for the

crushed stone is attached to the vibrator and bends inwards at the tip. Therefore columns are formed without removing the poker, which allows the poker to case the borehole thereby preventing collapse. Once at the design depth the poker is raised by 100–500 mm, depending on soil conditions, and crushed stone flows into the cavity through the supply tube. The poker is then raised and lowered a number of times until satisfactory compaction of the stone backfill is achieved. This cycle is repeated until a column of compact stone is formed up to the ground surface.

Figure 2.3 - Dry bottom feed system using 'vibrocat'

2.1.3 Applications of vibro replacement

Settlement Control

Vibro replacement can be used to support a variety of structures in soft cohesive soils. Columns can be spaced on large grids to support wide area loadings or in small groups beneath pad/strip footings. The area ratio (A/A_C) is a measure of the proportion of soil replaced by stone, where A is the tributary area of soil per column in a large grid and A_C is the area of the stone column (Figure 2.4). The area ratio for footings is determined as the total area of the footing divided by the total area of the columns.

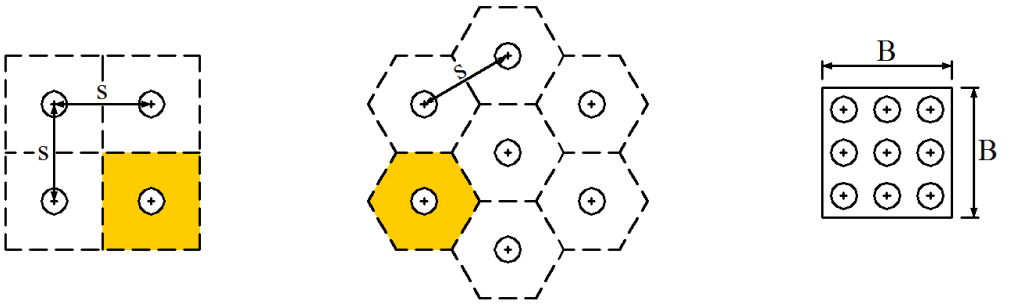

$$\frac{A}{A_C} = \frac{s^2}{\pi r^2} \quad \text{(i)}$$

$$\frac{A}{A_C} = \frac{1.5s^2}{\pi r^2} \quad \text{(ii)}$$

$$\frac{A}{A_C} = \frac{B^2}{(\#\ of\ cols) \times \pi r^2} \quad \text{(iii)}$$

Figure 2.4 - Area ratios for (i) square grids, (ii) triangular girds and (iii) pad footings

Vibro replacement primarily enhances the settlement performance of treated soils due to the high stiffness of granular columns. If equal strain (i.e. uniform deformation) is assumed beneath the base of footings, it can be shown from equilibrium that a larger proportion of the applied load is taken by the stiffer stone columns (Figure 2.5). Therefore, stress concentration ratios develop in stone columns. Field experience indicates that stress concentration ratios typically range from 2.5–5.0 (Barksdale & Bachus, 1983). The stress concentrations which occur in columns reduce the vertical stress on the surrounding soil which, consequently, reduces the settlement.

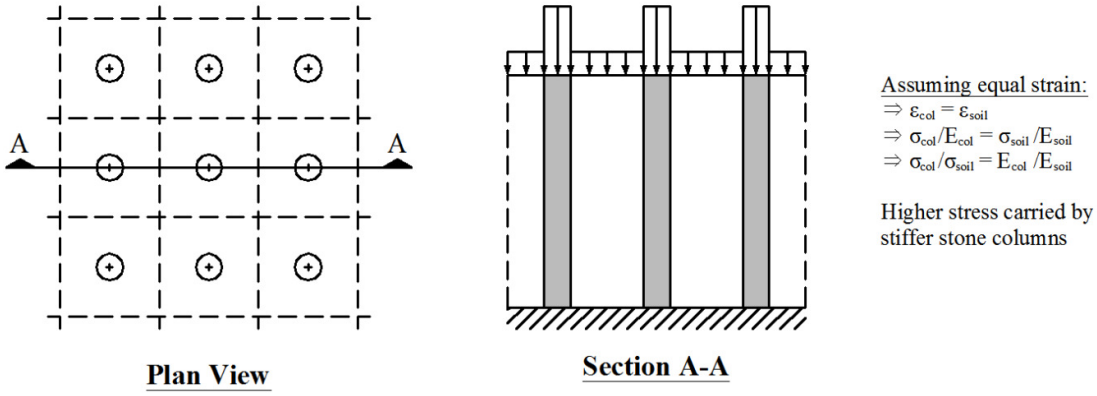

Figure 2.5 - Development of stress concentration ratios in stiffer stone columns

A comprehensive review of over twenty case studies by McCabe *et al.* (2009) highlights the effectiveness of vibro stone columns in enhancing the settlement performance of soft soils. In addition to reducing the magnitude of settlement, vibro stone columns also homogenise treated soil deposits and thus reduce differential settlement. Therefore, it is not necessary to span ground beams between compaction points, as is required with piled solutions, and shallow footings can be used to support the foundations.

Vibro stone columns also act as vertical drains due to the high permeability of the stone backfill. This allows excess pore pressure to dissipate rapidly which decreases consolidation time. However, the drainage capacity of stone columns may be reduced slightly by the creation of a smear zone around the vibrating poker upon penetration.

Slope stability

The vibro replacement technique can be used to increase the stability of embankment side slopes if stone columns are installed deeper than the rotational failure surface. Stone columns have a higher shear strength than the surrounding soil and therefore increase the shearing resistance along the failure surface. Moreover, stress concentrations ensure that a larger proportion of the applied load is carried by the stronger column material. The effectiveness of stone columns at increasing the stability of two full scale test embankments, founded in deep deposits of very soft cohesive soil, was investigated by Munfakh *et al.* (1984). The authors report that in addition to reducing the settlement and consolidation time, stone columns increased the load-carrying capacity of *in situ* soil by approximately 50%.

Mitigation of liquefaction

Liquefaction is initiated when excess pore pressures generated from seismic motions increase to equal the inter-granular stresses. As a result, soil loses all its shear strength and large deformations follow. The vibro replacement technique mitigates against liquefaction by densifying *in situ* soils and acting as vertical drains. The initial poker penetration densifies granular soils which increases inter-granular forces between soil particles. Stone columns also act as vertical drains which allows for a rapid dissipation of excess pore pressure. Vibro stone columns were employed to support a wastewater treatment plant in Santa Barbara, USA, which was located in a seismically active zone affected by liquefaction (Mitchell & Huber, 1985).

2.1.4 Limitations of vibro replacement

Barksdale & Bachus (1983) state that the vibro replacement technique is most effective in very soft to soft compressible clays/silts and in loose silty sands. However, vibro stone columns are highly dependent on the lateral support provided by the surrounding soil and consequently are not suitable for use in very weak soils. If the strength of the surrounding soil is insufficient, excessive column deformation will occur. Experience indicates that stone

columns should not be installed in soils which contain layers of peat or decomposable organics greater than 1d–2d (d = column diameter) in thickness (Barksdale & Bachus, 1983). McCabe *et al.* (2009) state that considerable evidence exists to suggest that stone columns can be formed successfully in soils with undrained shear strengths (c_u) well below 15–20 kPa, which is often quoted as the lower practical limit of the system. A small scale laboratory study conducted by Wehr (2006a) indicates that columns can be installed in soil with $c_u \geq 4$ kPa.

The vibro replacement technique is also not appropriate in high sensitivity soils. The shear strength of high sensitivity soils dramatically reduces once the grain structure is disturbed. Therefore, the vibratory forces imparted from the poker during column installation may remould the soil and, thus, significantly reduce the soil strength.

2.2 General deformational behaviour of stone columns

2.2.1 Behaviour of single columns

Hughes & Withers (1974)

The behaviour of single stone columns was analysed by Hughes & Withers (1974) in small scale laboratory tests. The deformation of columns was observed by taking radiographs of lead shot markers which were located in the clay. The behaviour of various column lengths was investigated, with length to diameter ratios (L/d) ranging from 4 to 12. Columns were loaded to failure in a stress-controlled manner which ensured drained conditions in the clay. While significant column bulging was observed in upper sections, negligible strain occurred beyond a depth of 4d (Figure 2.6). Therefore the ultimate strength of single columns is dependent upon the lateral resistance provided by the surrounding soil in the bulging zone and installing stone columns beyond 4d will not enhance the ultimate strength. The authors postulate that uniform bulging occurs in the upper section of the column and use cylindrical cavity expansion theory to determine the ultimate column capacity. It is also suggested that columns shorter than 4d would fail by punching, as the shear stress and end-bearing pressure are lower than the bulging capacity for columns shorter than $L < 4d$. Another interesting finding from the laboratory study is that only the clay within a cylinder of diameter of 2.5d is significantly strained, which suggests that 2.5d may be the upper limit for the spacing of stone columns.

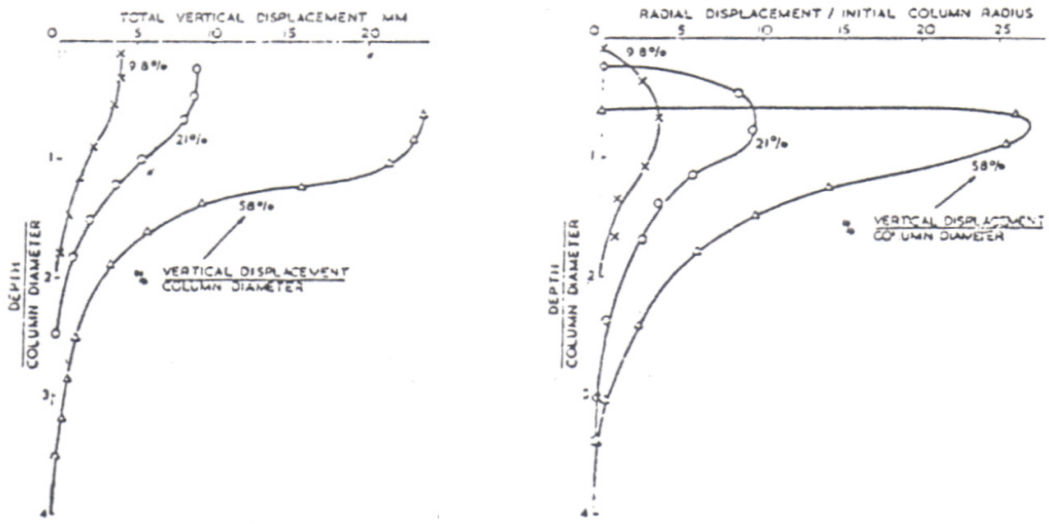

(a) (b)

Figure 2.6 - (a) Vertical displacement within the column against depth and (b) Radial displacement at the edge of the column / initial column radius against depth (Hughes & Withers, 1974)

Narasimha Rao et al. (1992)

Small scale laboratory tests were conducted by Narasimha Rao *et al.* (1992) to examine the ultimate bearing capacity of single stone columns. The influence of the column diameter, length and footing diameter was investigated by varying the L/d ratio from 3 to 9 and examining a range of footing diameters, D = 1d–2d (Figure 2.7). The tests indicate that the ultimate capacity of stone columns increases with the L/d ratio, which the authors suggest is the governing factor of column capacity. A critical L/d ratio appears to exist between 5 and 7, beyond which no further increase in ultimate capacity is gained. The ultimate capacity of stone columns was also observed to increase with footing size; however, this increase was only noticeable for columns shorter than 7d.

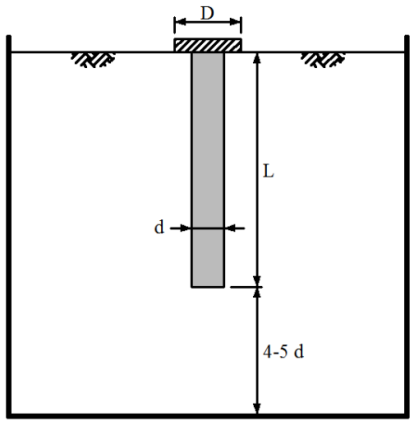

Figure 2.7 - Typical test setup examined by Narasimha Rao *et al.* (1992)

2.2.2 Behaviour of column groups

Muir Wood et al. (2000)

Muir Wood *et al.* (2000) conducted a series of laboratory tests in reconstituted kaolin clay to examine the deformational behaviour of a group of floating stone columns. The spacing, length and diameter of columns were all varied, with L/d ranging from 6 to 15. The loading was applied through a rigid circular footing at a constant rate of displacement, which was slow enough (0.061 mm/min) to ensure drained conditions in the clay.

The findings from the laboratory tests were verified by a plane strain Finite Element Analysis (FEA). Four modes of deformation were observed; bulging, shearing, punching and bending. The occurrence of column bulging was found to be dependent on the lateral restraint provided by neighbouring columns (A in Figure 2.8); the magnitude of bulging increases and the depth of bulging becomes shallower with increasing area ratio (A/A_C). Shearing of columns occurred when low lateral restraint is provided to columns and is most noticeable beneath the edge of footings near the ground surface (B in Figure 2.8). The zone of influence for the footing may be defined by a cone of undeforming soil, located directly beneath the footing and bound by the shear planes occurring in the soil. The depth of the zone of influence is dependent on the mobilised angle of friction of the composite soil mass, which increases at low A/A_C. Punching of columns is evident in Figure 2.8(a) and occurs when columns are not long enough to transfer the load to depth; this mode of deformation becomes more pronounced for closely-spaced columns, i.e. low A/A_C. Bending of stone columns occurs when columns are subject to lateral loads and can be seen in Figure 2.8(c).

The findings from the laboratory tests also indicate that columns located at mid-radius (i.e. between central and edge columns) are the most heavily loaded, followed by central columns and then edge columns. The authors attribute the reduced load carrying ability of edge columns to their decreased lateral restraint. However, the reason for the reduced performance of central columns is less clear, as the stiffness of the soil increases towards the footing centre. The authors also suggest that a critical length may exist; however, the dominant strain in the column is dependent on the footing diameter (D) and not the column diameter. Wehr (2004) simulated the laboratory tests with a plane strain FEA and suggests that a critical column length exists at 1.5D, where a marked change in column behaviour occurs. Central and edge columns shorter than this length exhibit punching and buckling failure, respectively.

(a) (b) (c)

Figure 2.8 - Photographs of deformed sand columns exhumed at the end of footing penetration (Muir Wood *et al.*, 2000)

The findings from the laboratory tests also indicate that columns located at mid-radius (i.e. between central and edge columns) are the most heavily loaded, followed by central columns and then edge columns. The authors attribute the reduced load carrying ability of edge columns to their decreased lateral restraint. However, the reason for the reduced performance of central columns is less clear, as the stiffness of the soil increases towards the footing centre. The authors also suggest that a critical length may exist; however, the dominant strain in the column is dependent on the footing diameter (D) and not the column diameter. Wehr (2004) simulated the laboratory tests with a plane strain FEA and suggests that a critical column length exists at 1.5D, where a marked change in column behaviour occurs. Central and edge columns shorter than this length exhibit punching and buckling failure, respectively.

Woo-Seok Bae et al. (2002)

Woo-Seok Bae *et al.* (2002) examine the horizontal resistance at the stone-soil interface for various configurations of stone columns by conducting small scale laboratory tests, the findings of which were verified by FEA. It was observed that failure of single end-bearing stone columns occurs by bulging between depths 1.6d–2.8d, and also that failure is dependent on the column diameter as opposed to the length. The failure zone for a group of stone columns is a conical zone of undeforming soil, which corresponds to Muir Wood *et al.* (2000). The depth of the conical zone of undeforming soil was found to increase for longer columns and at lower area ratios (A/A_C). It was also observed that column bulging occurred deeper at lower A/A_C, which is attributed to the increased lateral confinement. The influence of a granular mat, which acts as a stress distribution layer, also tends to push column bulging

deeper. The authors conclude that the ultimate capacity of stone columns is influenced by column spacing and diameter rather than column length and the granular mat.

McKelvey et al. (2004)

McKelvey *et al.* (2004) investigated the deformed shape, bearing capacity and stress concentration of small groups of stone columns beneath circular, strip and pad footings. The tests were conducted on floating stone columns, with lengths L = 6d and 10d, in both a transparent material and kaolin clay. The transparent material, with clay-like properties, allows for the deformed shape of the columns to be observed throughout loading. Columns tended to deform away from neighbouring columns and bulging in central columns beneath strip footings was significantly reduced, possibly due to the restraining effect of the two adjacent columns (Figure 2.9). It was also observed that short columns bulged over their entire length and tended to punch into the underlying soil. This is in contrast to long columns which exhibit no punching and only bulged in their upper regions. The authors report that a negligible increase in the bearing capacity of stone columns is gained by increasing column length beyond 6d. However, the undrained stiffness of footings is observed to increase for columns longer than 6d, which suggests that there is some merit in installing columns longer than this critical length for settlement control. For the initial stages of loading, it was observed that long stone columns carried a significant portion of the load ($\sigma_{col}/\sigma_{soil} > 4$) in comparison to short stone columns ($\sigma_{col}/\sigma_{soil} < 2$). The stress concentration ratio for both long and short stone columns tends to a constant value ($\sigma_{col}/\sigma_{soil} = 3$) at higher loads.

Ambily & Gandhi (2007)

Ambily & Gandhi (2007) investigated the behaviour of stone columns using small scale laboratory experiments and an axisymmetric FEA. The tests are performed on kaolin clay in a cylindrical tank and examine the influence of various design parameters. The findings indicate that the ultimate capacity of stone columns reduces as column spacing increases and that the loss of ultimate capacity is negligible for columns spaced further than 3d apart. It was also observed that the ultimate column capacity increases with undrained shear strength, surcharge load and the angle of internal friction of the stone backfill. Bulging was observed at a depth of 0.5d when the column area alone was loaded, whereas no bulging was observed when the entire area was loaded.

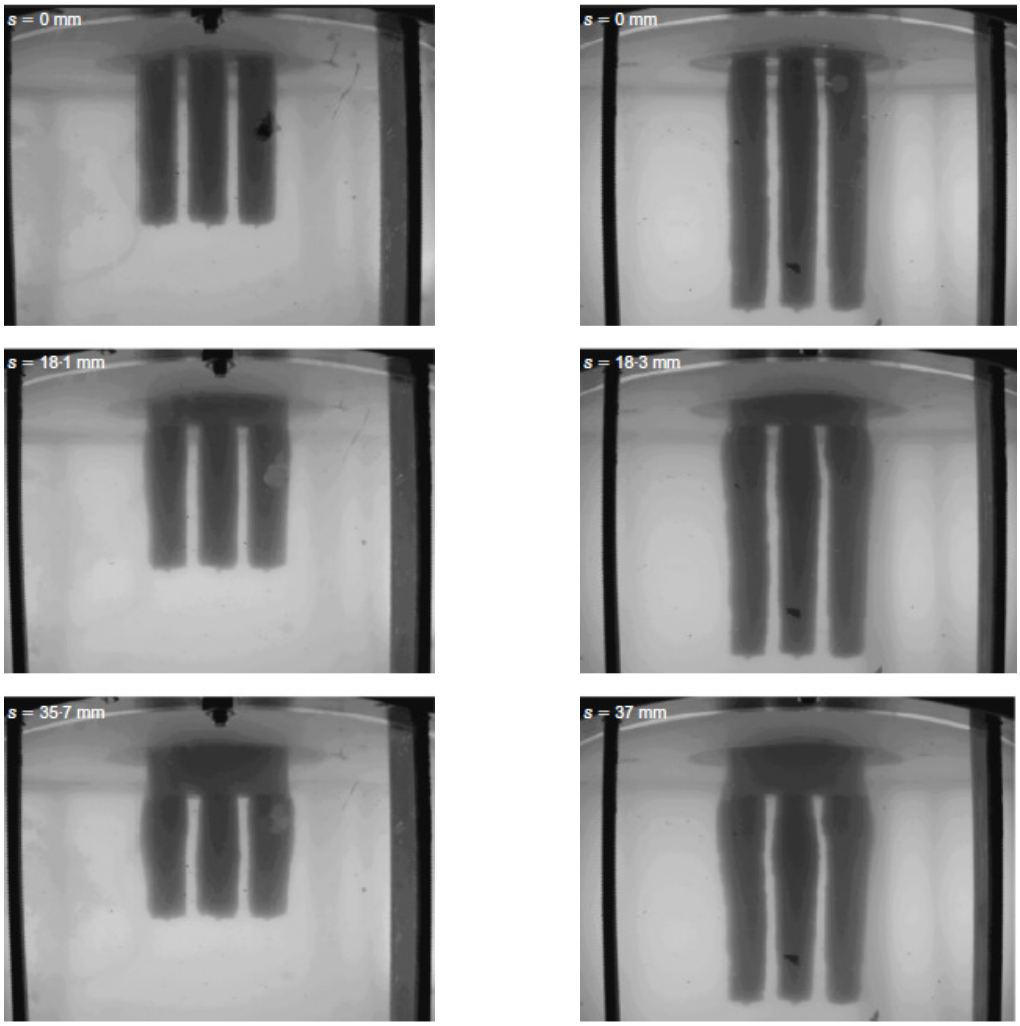

Figure 2.9 - Photographs of sand columns beneath strip footings at beginning, middle and end of foundation loading process: (a) L/d = 6; (b) L/d = 10 (McKelvey *et al.*, 2004)

Wehr (2004)

Wehr (2004) examined the behaviour of a single stone column and a group of stone columns using a plane strain FEA, which employed an elasto-plastic constitutive law in a Cosserat continuum. The results from the FEA for the single column and the group of columns are compared with experimental studies by Brauns/Witt (1978) and Hu (1995), respectively. A wedge of undeforming stone, which induces radial and vertical displacement, is observed from the experimental tests on a single stone column. This failure mechanism, along with a secondary failure mechanism in the form of a shear plane along the column-soil interface, is identified from the FEA. A wedge shaped zone of undeforming soil, which is bounded by shear planes, is also observed from the laboratory tests on a group of stone columns (Figure 2.10). The shear zones intersect beneath the centre of the footing and cause excessive bulging

to occur in central columns. In addition to inclined shear planes, the FEA identifies extra shear zones along the interface of internal and external stone columns. The author suggests that the shear zones between the internal columns may unite if the spacing of the stone columns is reduced and the lateral deformation is limited. The unification of shear zones is also dependent upon the relative movement of the column and soil. Another interesting observation from the FEA is that the thickness of the inclined shear planes increases with column length and that the 'bulging' observed by Hu (1995) in outer columns, is actually a large shear zone. The influence of an edge row of columns, as investigated by Hu (1995), is quantified using the FEM and its influence on bearing capacity was found to be negligible (peak force increased by 7%).

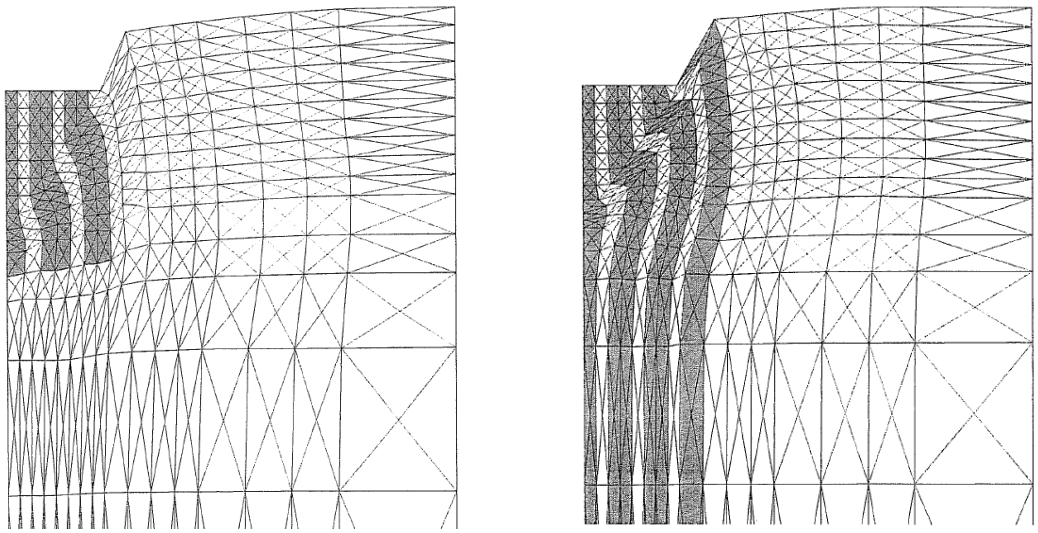

(a) (b)

Figure 2.10 - Deformed group of (a) short columns and (b) long slender columns with additional column outside the footing, upper part, u = 10 mm, clay (white) and column (grey) (Wehr, 2004)

Wehr (2006b)

Wehr (2006b) extended the previous analysis (Wehr, 2004) to study the effects of footing flexibility. A wedge shaped zone of undeforming soil was not observed for a flexible footing and columns tended to bulge rather than buckle. However failure mechanisms in the form of a broad vertical shear zone at the edge of the footing and several approximately wedge shaped and parallel shear zones were observed. The number of shear zones increased with the flexibility of the footing. The shear zones also extend to a limited depth and are dependent on the movement of the columns relative to the soil. Wehr (2006b) concluded that a flexible footing has a better load-carrying capacity than a rigid footing due to the formation of wider shear zones near the footing edge and the additional shear zones between columns.

2.2.3 Summary of general deformational behaviour of stone columns

The behaviour of single columns and groups of columns was reviewed in the previous sections. Single columns tended to bulge or punch, depending on column length. A critical length, beyond which no increase in column capacity is gained was observed for single stone columns within a range L = 4d–7d.

It appears that column interaction influences the deformational behaviour of stone columns as groups of stone columns exhibit bulging, punching, shearing and bending. The occurrence of each mode of deformation was found to be dependent upon the geometrical properties of columns and the footing, i.e. column spacing, length, position beneath footing and footing diameter. The critical length for groups of columns was found to be dependent on the column diameter and the footing diameter, with L = 1.5D and L = 6d suggested by Muir Wood *et al.* (2000) and McKelvey *et al.* (2004), respectively.

The stress concentration ratio which develops in stone columns appears to be related to the mode of deformation (McKelvey *et al.* 2004). Stress concentration ratios are low for columns which are punching into the underlying soil and increase with column length to a maximum when column bulging is occurring. It was also observed that the position of columns beneath footings influences the magnitude of stress concentration ratio as edge columns carry a lower proportion of the applied load at failure due to the loss of lateral confinement.

2.3 Settlement performance of stone columns

Vibro stone columns can be used to treat soft clayey soils, which are typically characterised by poor strength, stiffness and drainage properties. Consequently foundations on these soils undergo large displacements at relatively low loads and settlement is usually the governing criterion in foundation design. The rate of settlement is also another important feature of stone column design. Consolidation time can significantly affect the progress of construction projects, such as embankments, and therefore increase the cost of projects. By adopting vibro stone columns, consolidation time is reduced and the indigenous soil consolidates more quickly. As a result, the shear strength of the soil develops at a faster rate which allows embankments to be built in a shorter space of time.

2.3.1 Case studies

McCabe *et al.* (2009) conducted a comprehensive review of case studies involving the treatment of soft soils by vibro stone columns. The authors collated a series of data points from over twenty case studies in order to develop a 'settlement improvement database'. While the majority of the data points are specific to wide area loadings, three case studies relate to pad and strip footings. Figure 2.11 compares the measured data points (for wide area loadings) with the basic improvement curve, as derived by Priebe (1995), and assuming 40° for the angle of internal friction of the stone backfill. It was necessary to assume this value as insufficient data was provided in many of the case studies examined; the value is typical of what would be used in design. While some scatter exists, it is clear that the measured data follows a similar trend to that predicted by Priebe (1995).

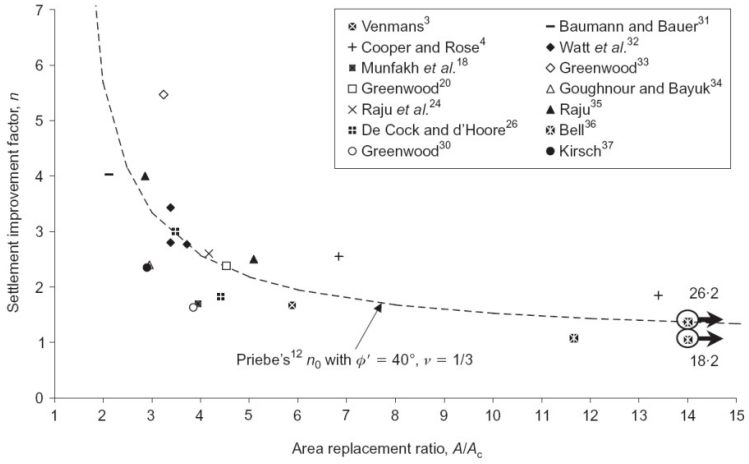

Figure 2.11 - Settlement improvement factor against area replacement ratio for sites with widespread loading (McCabe *et al.*, 2009)

The authors also examine the effectiveness of different construction techniques by comparing measured and predicted settlement improvement factors in Figure 2.12. It appears that the construction technique has a significant influence on settlement performance of stone columns and also that the bottom feed system is the preferred choice for installing vibro stone columns in soft soils. Some of the data points in Figure 2.12 suggest that vibro stone columns are behaving worst than predicted, which may be due to a number of factors such as workmanship and uncertainties in the measured data. The authors stress the importance of workmanship in installing stone columns and state that the disturbance caused by imparting excessive energy in the installation sequence may offset the benefit of a stone column. Uncertainties also exist with the measured data, such as the methods used to predict settlement and the 'as-built' dimensions of columns. On consideration of these facts and the

excellent performance of the bottom feed system, Figure 2.12 indicates that the assumed angle of internal friction of 40° for the stone backfill is somewhat conservative.

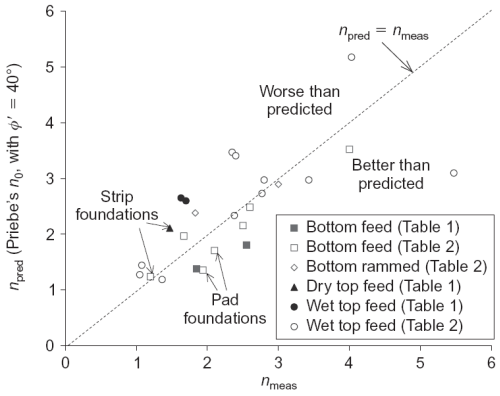

Figure 2.12 - Predicted versus measured settlement improvement factors for all widespread loadings and footings (McCabe *et al.*, 2009)

2.3.2 Laboratory studies

Black (2006) examined the behaviour of large diameter single stone columns and small groups of columns beneath a circular footing (diameter = 60 mm), using small scale laboratory tests. Three area ratios (A/A_C = 2.5, 3.6 and 5.8) were adopted for the analysis and the effect of column length was also investigated by varying the length L = 125–400 mm.

Based on the initial slope of the 'load versus settlement' curve for both area ratios, it appears that the group of stone columns are under-performing as the stiffness for groups is half of that for single columns (Figure 2.13). This is attributed to a ‘block failure’ that manifests itself in column groups, where all the columns act together and punch into the underlying soil, and also to the reduced shoulder length between the edge of columns and the edge of the footing (Figure 2.14).

The deformation patterns of columns were found to be dependent on both the column length and arrangement. It was observed that both single columns and column groups that were 125 mm long, with a length to diameter ratio (L/d) ranging from 3 to 5, all punched into the underlying soil. As the length was increased to 250 mm, it was observed that the single column (L/d = 7–10) bulged whereas the group of columns (L/d = 11–14) continued to punch into the underlying soil. However, column groups act as a 'block' and re-defining the L/d ratios on the basis that the diameter for the group is more appropriate (i.e. d = 60 mm) leads to revised L/d ratios of 4 and 6. Punching is precluded for end-bearing columns and it was

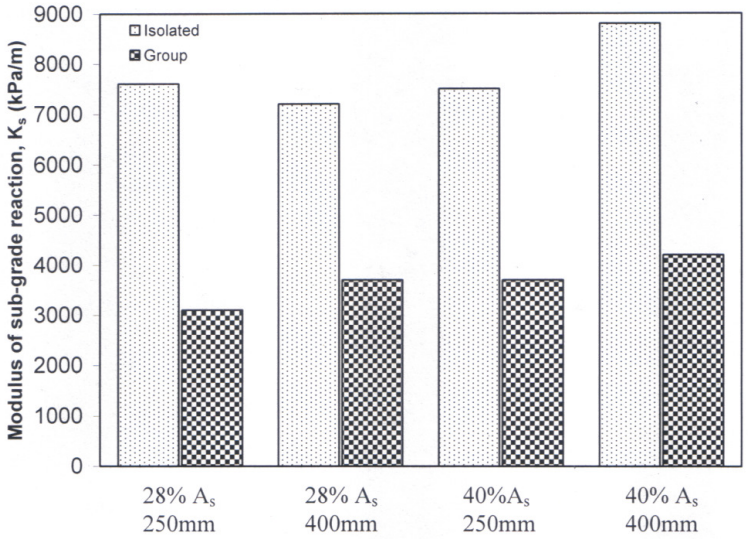

Figure 2.13 - Comparison of Ks for isolated and group formation (Black, 2006)

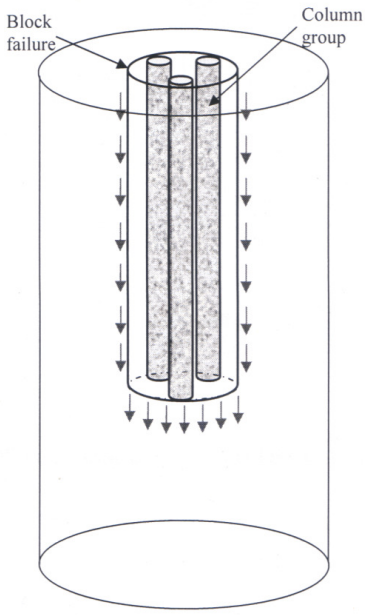

Figure 2.14 - Illustration of block failure in group columns (Black, 2006)

observed that all 400 mm long columns bulged. Black (2006) suggests that the critical L/d ratio which defines the cross-over from punching to bulging failure is approximately 8 for these drained analyses.

Another interesting finding from the tests is the relationship between the stress concentration ratio ($\sigma_{col}/\sigma_{soil}$) and column length. No increase of vertical stress was observed in short columns, as columns failing by end-bearing cannot sustain any extra vertical stress. However, stress concentration ratios are observed to increase with column length, which reflects the

higher ultimate capacity of columns which are bulging. It was also observed for column groups that the pressure recorded beneath the centre of the footings was higher than in the columns. The increased pressure in the centre of the footing imparts a lateral force on the surrounding columns, forcing them to bulge outwards and away from neighbouring columns. This may explain the reduced settlement performance of groups of columns compared to single columns, which are positioned beneath the centre of the footing.

2.3.3 Numerical studies

Balaam et al. (1977)

Balaam *et al.* (1977) conducted a numerical analysis to investigate the influence of column length, spacing and stiffness upon the settlement performance of stone columns. An infinite array of stone columns supporting an infinite load area is modelled using the unit cell concept (see Section 2.5.1) to simplify the analysis. A uniform pressure is applied to the column-soil unit which simulates a flexible loading (i.e. large raft, embankment).

The long term settlement performance of stone columns is estimated using the FEM and accordingly both the column and soil are modelled as drained materials. The authors examined the settlement performance of stone columns using an elastic and elasto-plastic analysis. While the elastic analysis was found to slightly under-predict the settlement of the column-soil unit at working loads (maximum discrepancy = 6%), it was deemed sufficiently accurate and was adopted for the subsequent analyses. It is shown in Figure 2.15(a) that the ratio of the column and soil moduli has a minor influence on the settlement performance of stone columns. It is also noted by the authors that columns shorter than L/h = ¼ (h = thickness of soil deposit) or columns spaced wider than $d_e/d = 5$ ($A/A_C = 25$) yield negligible settlement improvement factors (n). It can be seen in Figure 2.15(b) that the influence of column length is more pronounced for closely-spaced columns. It is also interesting to note the identical settlement performance of floating columns spaced at $d_e/d = 2$ and end-bearing columns spaced at $d_e/d = 5$, which occupy 12.5 % and 4 % of the soil volume, respectively. This emphasises the importance of column length upon the settlement performance of large arrays of columns.

The rate of settlement is determined from a finite difference solution, which uses diffusion theory to approximate consolidation theory developed by Biot (1941). The diffusion theory is

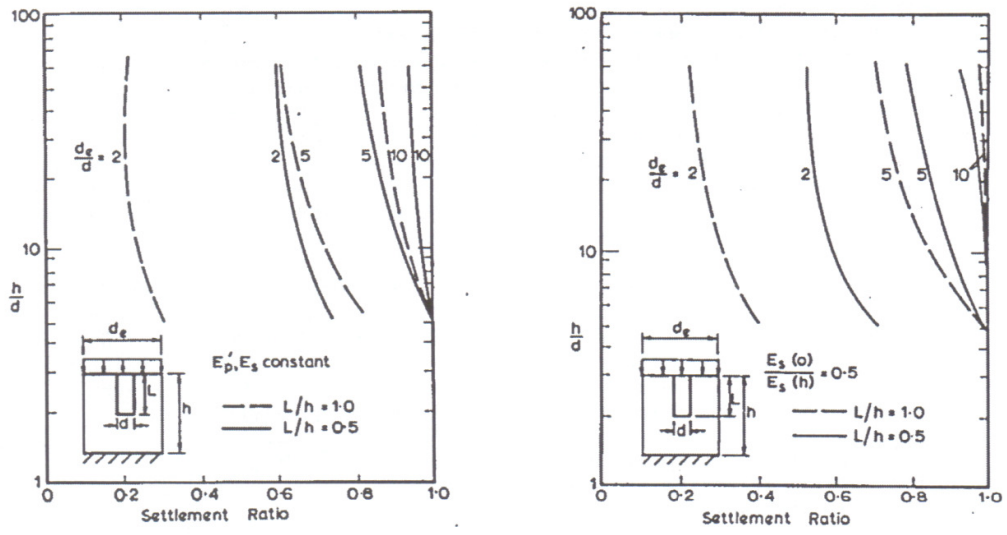

(a) (b)

Figure 2.15 - Settlement variation with (a) E_P/E_S ratio and (b) degree of penetration of piles (Balaam *et al.*, 1977)

an extension of the Terzaghi theory of one-dimensional consolidation (Terzaghi, 1925). The influence of increasing L/h significantly increases the rate of consolidation and this effect becomes more pronounced at close column spacings.

Domingues et al. (2007)

Domingues *et al.* (2007a) and Domingues *et al.* (2007b) conducted axisymmetric FEA to examine the influence of column spacing and compressibility upon an infinite grid of columns supporting a 2 m high embankment. As the embankment is a wide area loading, it is possible to model the behaviour of the column using the unit cell concept and a flexible loading. The p-q-θ critical state model, which is an extension of the Modified Cam Clay model into a three dimensional stress space using the Mohr-Coulomb failure criteria, is adopted to simulate the behaviour of both the stone and the soft soil. The end-bearing columns are 1.0 m in diameter and formed in 5.5 m deep normally consolidated clay. The coefficient of lateral earth pressure of the clay is increased (K_0 = 0.7) to account for the effects of column installation; this was chosen as an intermediate value between K_0 = 1 – sin(φ') (Jaky, 1944) and K_0 = 1.0 (Priebe, 1995).

The influence of the column spacing was examined by conducting analyses over a range of area ratios A/A_C = 3–10. As expected, settlement improvement factors increase (n = 1.2→2.0) at lower A/A_C. However, no change in differential settlement was observed. Stone

columns act as vertical drains due to their high permeability and it was found that the rate of consolidation increased at lower A/A_C. The horizontal displacement at the column-soil interface was also found to decrease with lower A/A_C, which may be attributed to the confining effects of neighbouring columns.

The influence of column compressibility was also investigated by varying the modular ratio ($\lambda_{col}/\lambda_{soil}$) from 10 to 100, for columns spaced at A/A_C = 5.3. It was observed that both settlement improvement factors (n = 1.3→3.8) and differential settlement increase with increasing column stiffness. The rate of consolidation is also influenced by the column stiffness as the time taken to reach consolidation reduces for higher column stiffness, i.e. time taken to reach $\delta = 0.9\delta_{max}$ (δ and δ_{max} = average settlement and final settlement on the ground surface, respectively) was 16 weeks and 10 weeks for $\lambda_{col}/\lambda_{soil}$ = 20 and 100, respectively. The stress concentration ratio was observed by Domingues *et al.* (2007b) to increase linearly from 3.9 to 14.0 with increasing modular ratio.

Andreou & Papadopoulos (2006)

Andreou & Papadopoulos (2006) investigated the influence of the applied load, area ratio, angle of internal friction and undrained shear strength upon the horizontal displacement of a stone column. The column is subject to a wide area loading via a rigid footing and is modelled using the unit cell concept. The horizontal displacement is estimated using an axisymmetric FEA, where the stone and the soil are modelled using the simple Mohr-Coulomb model. The 20 m long end-bearing stone columns are 0.8 m in diameter. The depth of plasticity increases in the column with increasing load (10–120 kPa) and settlement improvement factors decrease (n = 3.1→1.9). It also appears that decreasing the area ratio (A/A_C = 14.2→5.1) and increasing the angle of internal friction (φ = 38→44°) reduces the extent of the plastic zone in the column, which improves the settlement performance. Finally, the authors observed that increasing the undrained shear strength of the surrounding soil (c_u = 10→60 kPa) did not influence the horizontal displacements of the column.

Kirsch & Sondermann (2003)

The stress concentration occurring in stone columns is a critical parameter in numerous settlement and slope stability design methods. Kirsch & Sondermann (2003) investigated this parameter and compared the estimates from a FEA with two analytical solutions and a case

study. The authors present the results of the development of stress concentration as a function of applied loading for an embankment site in Kuala Lumpur. The curve presented in Figure 2.16 indicates that the stress concentration increases with applied load; this curve is specific to columns installed on a square grid ($A/A_C = 4$) to 14 m, in a 16 m deposit.

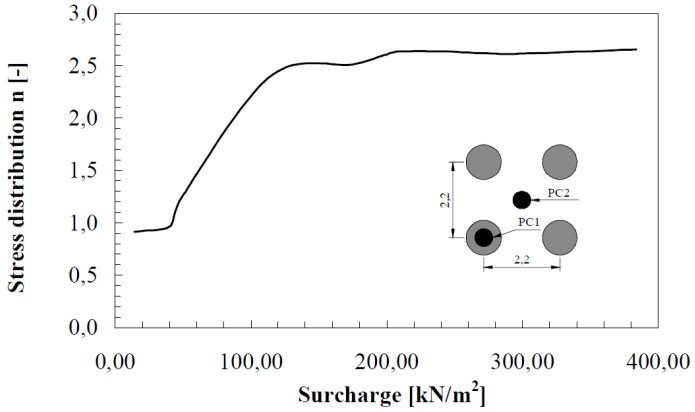

Figure 2.16 - Measurement of stress concentration below an embankment (Kirsch & Sondermann, 2003)

Wehr & Herle (2006)

Wehr & Herle (2006) determined the magnitude and rate of settlement for an embankment supported by vibro stone columns using a FEA and analytical design methods. The 9 m high embankment was supported by 6 m long floating stone columns, which were 0.9 m in diameter and spaced on a triangular grid at $A/A_C = 6.3$. The embankment was constructed in three distinct phases: (i) the initial 6 m was constructed in 40 days; (ii) rest period for consolidation of 120 days; (iii) the final 3 m was constructed in 40 days. The magnitude of the settlement was estimated using an analytical software program which is based upon Priebe (1995). The rate of settlement was determined using Balaam & Booker (1981), which is based upon Biot's consolidation theory. A two-dimensional plane strain FEA was undertaken where the stone and the soil are both modelled using the Mohr Coulomb model. The stone columns were converted to two-dimensional stone walls for the FEA, by keeping the volume of the improved soil constant. The results indicate that the stone columns significantly reduce the settlement of the embankment (up to 40%) and also that consolidation occurs very quickly (within 16 days). The predictions from both the FEA and the analytical design method agree very well. The authors attribute this to the fact that the same material model is used for both the analytical design methods and the FEA. Consolidation also occurs very quickly which allows for compatibility between the analytical method and the FEA.

Elshazly et al. (2008a)

Elshazly *et al.* (2008a) conducted an axisymmetric FEA to investigate the applicability of settlement design methods based upon the unit cell concept (see Section 2.5.1) to groups of stone columns. The majority of design methods are based on the unit cell concept which assumes an infinite grid of columns supporting an infinitely wide load. However, this concept is clearly not applicable to groups of columns as exterior columns along the edge of the footing experience a loss of lateral confinement and also the distribution of vertical stress decays with depth beneath small footings.

Elshazly *et al.* (2008a) develop modification factors to relate the settlement of finite groups of columns (s) with the settlement of an infinite grid of columns (s_{uc}). The column length (L) and area ratio (A/A_C = 3.4) were both constant, while the number of columns beneath footings was varied to yield normalised footing widths (B/L) from 0.5 to 4.7. Two soil profiles were adopted for the investigation; the first soil profile is a layered estuarine deposit, which is described in detail by Mitchell & Huber (1985), and the second soil profile is developed from typical parameters for soft soil. The ratio of the Young's modulus of the stone column to the soil ranges from 1.3 to 2.6 for the first soil profile and is 8.5 for the second soil profile. The installation effects associated with stone column installation are incorporated by increasing the coefficient of lateral earth pressure (K_0) of the soil immediately surrounding the stone columns to 1.5 and 1.2 for the first and second soil profiles, respectively. The loads are applied through a stone distribution blanket and the long term settlements are determined using an axisymmetric FEA.

The authors identify two counteracting effects which are associated with the unit cell model. The first effect concerns the distribution of vertical stress beneath pad footings and wide area loadings. Vertical stress reduces sharply with depth beneath small footings and is negligible beyond a depth of z = 2B. This is in contrast to the unit cell which stresses the soil profile to the full depth and therefore increases settlement. The second effect is related to the loss of lateral confinement that is experienced by exterior columns beneath small footings, which increases the settlement. However, full lateral confinement is provided on all sides of columns within an infinite grid, which results in enhanced lateral support and less settlement.

It can be seen in Figure 2.17(a) for a layered deposit that the settlement of small footings (B/L < 2) is less than the settlement of a unit cell. Therefore it appears that the beneficial

effect of stress reduction with depth overrides the loss of lateral confinement for small footings. However, as footing width increases (B/L > 2) it can be seen that the settlement of small footings exceeds the settlement of a unit cell. This may be attributed to an increase in the vertical stress in the soil with increasing footing width.

It can be seen in Figures 2.17(b) and 2.17(c) for the soft soil deposit that the settlement of finite groups is always less than that of a unit cell. The increased footing settlement may be attributed to the low lateral support provided by the soft soil deposit.

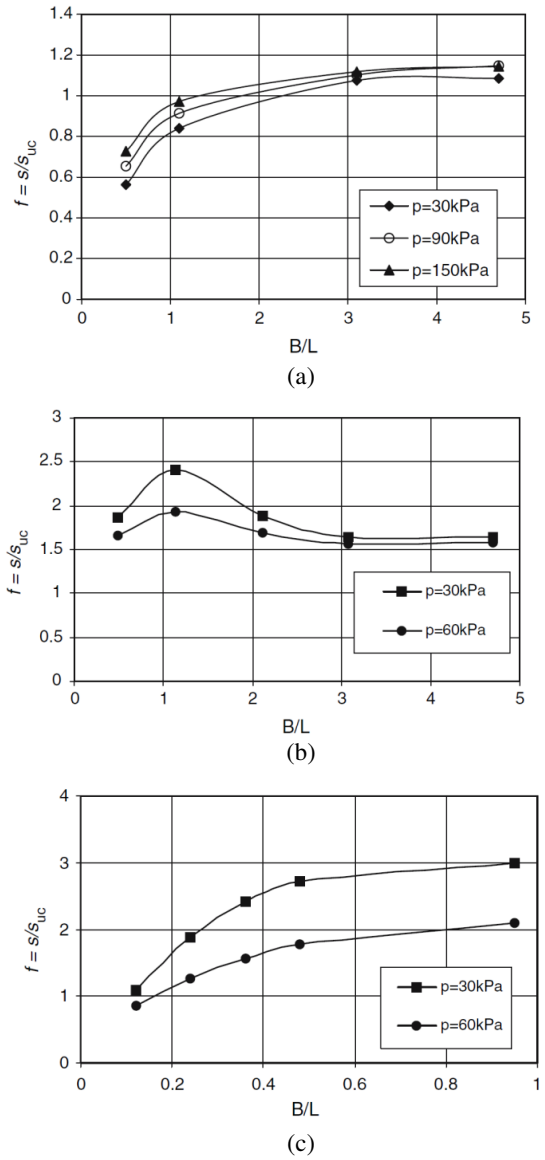

Figure 2.17 - Settlement correction factor versus size ratio (a) case of layered soil, (b) case of 10.8 m thick soft clay layer and (c) case of 30 m thick soft clay layer (Elshazly *et al.*, 2008a)

Kirsch (2008)

Kirsch (2008) conducted a FEA on two footings, which are supported by 25 columns. Installation effects, which are based on a previous study by Kirsch (2006), are incorporated into the FE model. The stress concentration ratio ($\sigma_{col}/\sigma_{soil}$) was measured in a sand layer above the stone columns and was found to increase with load from 1.4 to 1.6 for central columns and from 1.4 to 2.8 for corner columns. The measured stress-concentration ratios increased upon reloading. The FEA is compared with field data and despite over-predicting the ultimate capacity of columns it predicts the settlement behaviour quite well at working loads. The influence of increasing the column length and the angle of internal friction is found to be more pronounced at low A/A_C. Another interesting finding from the study is that column stiffness has a negligible influence on the settlement behaviour of the footing. Kirsch (2008) suggests that columns undergo plastic deformations at relatively low loads due to stress concentrations and are therefore insensitive to elastic stiffness parameters.

2.3.4 Summary of settlement performance of stone columns

A review of the settlement performance of stone columns from field, laboratory and numerical studies was presented in the previous sections. The settlement performance of large groups of columns is well understood. Field experience indicates that Priebe (1995) predicts the settlement performance quite well and also that an angle of internal friction for the stone column $\varphi' = 40°$ is somewhat conservative for the bottom feed system. The influence of column length and area ratio upon the settlement performance of stone columns is very important and the arrangement of columns can be tailored to achieve a specific settlement performance. It was found that the influence of column length becomes more pronounced for large groups of closely-spaced columns and that long, widely-spaced columns require less stone than short, closely-spaced columns to achieve the same settlement performance. It was also found that columns shorter than $L/h \leq ¼$ (h = thickness of soil deposit) and wider than $A/A_C > 25$ yield negligible settlement improvement factors.

The settlement performance of small groups of stone columns was also reviewed. It appears that the mode of deformation changes with the number of columns, as closely-spaced columns act together and punch as a 'block' into the underlying soil. A comparison of small groups of columns and infinite grids of columns highlights the importance of the lateral support to columns and the distribution of vertical stress beneath pad footings in determining

the settlement of small groups of columns. The influence of column length and the angle of internal friction for the stone columns were found to be more pronounced at low A/A_C.

Stress concentration ratios were found to vary with applied load and also with position beneath pad footings, as corner columns carry a higher proportion of the vertical load than centre columns.

2.4 Column installation effects

As the vibrating poker penetrates the ground, it displaces the soil and imparts horizontal vibratory forces to the surrounding soil. However, horizontal forces are attenuated by fine particles (Sondermann & Wehr, 2004) and any alteration to the *in situ* stress state of fine grained soils may, therefore, be attributed to the displacing effects of the poker. Yu (2000) states that soil displacement due to the installation of a driven pile can be predicted using cylindrical and spherical cavity expansion theories along the shaft and at the tip of the pile respectively, and that the soil near the ground surface is locally affected by surface heave (Figure 2.18).

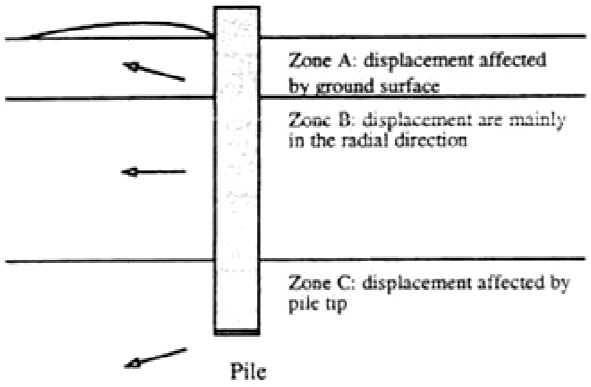

Figure 2.18 - Soil displacement due to pile installation (Yu, 2000)

2.4.1 Laboratory investigations

Randolph *et al.* (1979a) conducted small scale laboratory tests to investigate soil displacement patterns associated with the installation of a closed ended pile. As the pile tip advances, the soil particles are displaced downwards and outwards, similar to that predicted by spherical cavity expansion theory. However, once the pile tip passes the soil particles, significant radial displacement occurs. The displacement of the soil reaches a steady state relative to the advancing pile tip once the pile tip is more than 4d–5d (d = pile diameter)

beyond the soil particles. The ultimate displacement pattern of the soil is similar to that of cylindrical cavity expansion.

The use of a video camera to observe soil displacement surrounding the installation of a flat bottomed penetrometer was adopted by Gill & Lehane (2001). This non-intrusive method determines the soil displacement by tracking the movement of dark beads against a light background, which consisted of a transparent artificial material. This artificial material has properties similar to that of a lightly over-consolidated natural clay and consists of silica particles and paraffin. The findings show that the soil is displaced both outwards and downwards as the penetrometer tip advances towards the beads. Once the tip passes the beads, the soil displacement becomes radial and upwards. It was also observed that negligible displacement occurred once the penetrometer tip was more than five penetrometer diameters deeper than the level of the beads. The results compare well with experimental data from other authors, which reinforces the assumption by Baligh (1985) that the kinematics of deep penetration are such that the displacement paths are relatively insensitive to the properties of the soil.

2.4.2 Observed field measurements

Kirsch (2006) analysed the changes to the *in situ* stress regime in sandy silt due to the installation of two groups of twenty five stone columns. The variation of pore water pressure, effective horizontal stress and soil stiffness was analysed in order to determine the post-installation stress state of the soil. A rise in pore water pressure was recorded at various locations immediately after installation. The data was compared with theoretical values, predicted using an analytical formula developed by Cunze (1985) based upon cylindrical cavity expansion theory. A good relationship was found to exist between the field and theoretical data, although there was considerable scatter in the results. The horizontal stress and soil stiffness, shown in Figures 2.19 and 2.20, respectively, both appear to be increased within a zone which ranges from 4d to 8d from the centreline of columns. The horizontal stress and soil stiffness increased as the vibrating poker advanced towards the measuring locations. However, increases in horizontal stress and soil stiffness were offset by the effects of remoulding and dynamic excitation within a distance 4d.

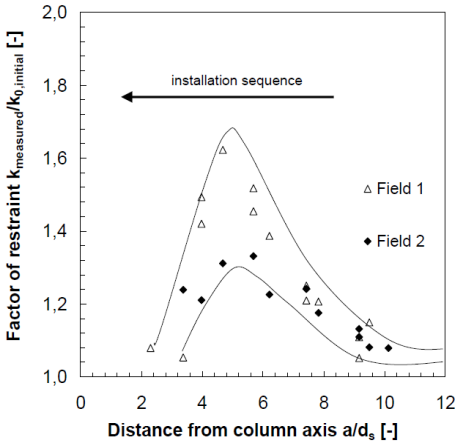

Figure 2.19 - Factor of restraint measured during the installation of stone columns (Kirsch, 2006)

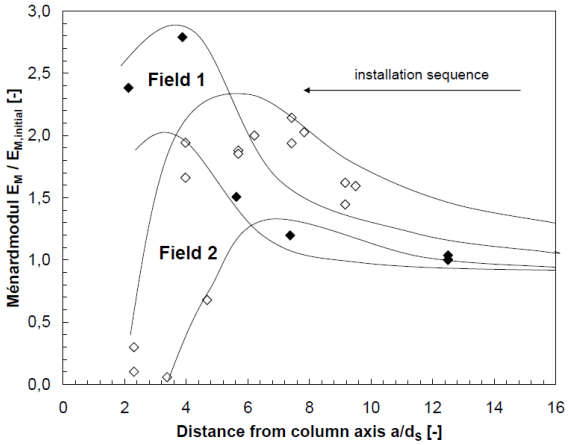

Figure 2.20 - Development of ground stiffness during column installation (Kirsch, 2006)

Castro (2007) recorded the development and dissipation of excess pore water pressure which resulted from the installation of seven stone columns in a normally consolidated clay. The pore water pressure rose upon poker penetration and peaked as the poker tip passes the level of the piezometers. Despite significant heave occurring at the ground surface, it was deemed reasonable to assume that plane strain conditions exist and cylindrical cavity expansion theory may be used to simulate the poker installation. The increase in excess pore water pressure recorded during the initial poker penetration agreed favourably with theoretical values, which were predicted using an analytical formula derived by Randolph *et al.* (1979b). An additional assumption was required that the undrained shear strength of the surrounding soil iss reduced, due to the increase in excess pore water pressure, which is a common phenomenon associated with driven pile installation. However, the agreement between field and theoretical values breaks down with the installation of subsequent columns, as the assumed boundary conditions of plane strain are violated. The dissipation of excess pore water pressure occurred very quickly (within 15 minutes), which is 100 times less than the

theoretical dissipation time, predicted using a finite difference technique based upon theory developed by Soderburg (1962). This is attributed to fractures in the clays, which result from the high pressures due to column installation and act as drainage channels.

Gäb *et al.* (2007) measured the pore water pressure and settlement due to the construction of a large embankment. The embankment was founded on 11 m of loose-medium dense lacustrine sand which was underlain by 50 m of clayey silt. The stone columns were installed to 14.5 m and on a triangular grid at $A/A_C = 7.7$. In total 37 columns were installed in 4 rings, with construction starting at the outer ring and progressively moving towards the centre. The excess pore water pressure increased as the construction sequence moved closer to the piezometers. This increase in excess pore water pressure was a maximum at 12 m, near the column base and was even noticeable at 20 m depth. The excess pore water pressure dissipated very quickly in the sand (< 1 day) and very slowly in the clay. Slight heave was also measured at the site.

Egan *et al.* (2008) collate data relating to the installation of stone columns from various sites including that of Castro (2007). The authors observe that heave may occur during the installation of stone columns and tentatively suggest a relationship between column density and the amount of heave. The authors suggest that heave is also a function of column size, spacing and construction method. The footing arrangement also influences the amount of heave as small groups and strips of stone columns do not generate as much heave as large grids.

2.4.3 Simulation of installation effects in numerical models

Increased coefficient of lateral earth pressure

The installation effects associated with stone columns may be accounted for by increasing the coefficient of lateral earth pressure (K_0) in the surrounding soil. This relatively simple technique has been adopted by many authors, as shown in Table 2.1. Elshazly *et al.* (2006) conduct an axisymmetric FEA to determine the increase in K_0 by back-calculating field load tests on stone columns, which are described by Mitchell & Huber (1985). A central column located within a large array of columns is loaded by a circular footing. The stone columns were installed using the *'wet technique'* to a depth of 10.8 m, in a layered estuarine deposit. The soil properties adopted are determined from post-installation soil samples and therefore

incorporate any change to soil properties due to column installation. The authors then attribute any discrepancy in the load-settlement curve to a change in the stress state of the surrounding soil and adjust K_0 until the load-settlement curves match. Assuming full confidence in the adopted soil parameters, an axisymmetric FEA indicates that K_0 = 1.5 yields the best match between the actual and predicted load-settlement curves.

Elshazly *et al.* (2008b) extended to the previous analysis to investigate the effect of column spacing upon the post-installation stress state of the soil. A range of column spacings were analysed, which corresponded to A/A_C ranging from 2.5 to 4.8. The back-calculated values for the K_0 ranged from 0.7 to 2.0, depending on the level of confidence in the soil parameters. The best conservative estimates of K_0 are 1.7, 1.2 and 0.85 for A/A_C = 2.5, 3.7 and 4.8, respectively. This indicates that installation stresses reduce at high A/A_C (i.e. widely-spaced columns).

Table 2.1 - Increase in K_0 to account for stone column installation effects by various authors

Reference	A/A_C	Coefficient of lateral earth pressure, K
Balaam & Booker (1977)	4 – 100	1.00
Barksdale & Bachus (1983)	4 – 10	0.75
Mitchell & Huber (1985)	2.0 – 4.9	1.00
Elshazly *et al.* (2006)	3.4	1.50
Domingues *et al.* (2007a)	3.3 – 10.0	0.70
Elshazly *et al.* (2008b)	2.0 – 4.9	0.85-1.70

Cylindrical cavity expansion

Debats *et al.* (2003) and Guetif *et al.* (2007) both simulate the installation effects associated with stone columns using an axisymmetric FEA. The authors apply an undrained cylindrical expansion to a 'dummy material' and then convert this material into a stone column. In order to replicate the actual installation process, it would be necessary to expand the cavity from a zero initial diameter to the final column diameter. However, this is theoretically impossible to implement in a numerical model as infinite strain would be generated. A numerical analysis by Randolph *et al.* (1979a) in the context of pile installation reveals that expanding a cavity by doubling the radius is sufficient to simulate expanding a cavity from a zero initial diameter. The 'dummy material' is expanded from an initial diameter of 500 mm, which is close to a typical poker diameter, to a final column diameter of 1100 mm. A 'dummy material', which is assigned a nominal stiffness, is adopted for this procedure in order to reduce high stresses that would occur in the column during the expansion.

Both authors conducted numerical investigations into the influence of this technique upon the stiffness development of the surrounding soil and zone of influence of the expanding column. The increase in soil modulus is estimated from the change in mean effective stress, using an experimental relationship developed by Biarez *et al.* (1998). It is postulated by Brinkgreve & Broere (2006) that soil stiffness is directly proportional to the mean effective stress for soft soils. The undrained cavity expansion induces large excess pore water pressures in the surrounding soil, which are magnified at low A/A_C. Following consolidation of the soil, the mean effective stress and hence the soil stiffness are increased. Debats *et al.* (2003) report a 30% and 40% increase in soil stiffness within a cylindrical zone of radius 2d in the surrounding soil for column spacings of 6 m and 10 m, respectively. However, these findings are specific to the Mohr-Coulomb model and even higher increases in soil stiffness in a greater zone of influence are observed when the Hardening Soil model is adopted. Guetif *et al.* (2007) also observe that a stress concentration occurs in the stone column and that the lateral coefficient of earth pressure is increased above unity in the surrounding soil.

Cylindrical cavity expansion & increased soil stiffness

Based on measurements from field tests on two groups of twenty five columns, Kirsch (2006) simulates the installation effects of stone columns by applying both an individual cylindrical expansion to each column and also by increasing the stiffness in an enhancement zone surrounding the footing. Kirsch (2006) found that the best match between the predicted and actual 'load-settlement' curves was achieved by applying a moderate cylindrical expansion to the stone column (lateral strain, $\varepsilon_r = 4\%$) and doubling the stiffness in the enhancement zone, which exists between 2d and 5d from the centre-line of outer row columns. The load-settlement performance of both footings was back-calculated using the FEM (incorporating the installation effects), which was found to agree favourably with field data and analytical design methods (Priebe, 1995 and Goughnour & Bayuk, 1979).

Kirsch (2006) investigated the influence of both the individual and the global column installation effects upon the settlement improvement factor for a 7.2 m square footing, supported by 25 columns. The results indicate that increasing the radial expansion of the individual column to 8% results in a 45% increase in the settlement improvement factor. An examination of the global installation effects suggests that increasing the stiffness of this zone (2d–5d from the centre-line of the outer row columns) by three times its initial value yields a 25% increase in the settlement improvement factor. However, it is observed that the

additional improvement is highly dependent upon the loading stage, and that at high loads the additional improvement gained drops once stone columns yield and plastic deformation becomes dominant. Therefore, the installation effects do not influence the ultimate behaviour of stone columns but they do play a positive role in enhancing the settlement behaviour.

2.4.4 Summary of column installation effects

Stone columns are formed with the aid of a vibrating poker which displaces the soil and imparts horizontal vibrations. The forces imparted from the horizontal vibrations are attenuated in fine grained soils and any change to *in situ* stress state may be attributed to the displacing effects of the poker. It was shown in a series of small scale laboratory experiments that the soil displacement due to the installation of a driven pile can be predicted using cylindrical cavity expansion theory and authors have used this approach in two-dimensional axisymmetric FEA to model stone column installation.

Field experience indicates that horizontal stress and soil stiffness increase within a zone which ranges from 4d–8d from the centre-line of columns. However, increases in horizontal stress and soil stiffness are offset by the effects of remoulding and dynamic excitation within 4d. It was also found that an increase in excess pore water pressure due to initial poker penetration agrees favourably with the analytical formula developed by Randolph *et al.* (1979b). Column installation effects tend to improve settlement behaviour of stone columns. However, the additional improvement drops once stone columns yield and plastic deformation becomes dominant. Therefore, the installation effects do not influence the ultimate behaviour of stone columns.

A number of methods to simulate column installation effects are summarised below:

1. Increase the coefficient of lateral earth pressure (K_0) in soil
   - Increases in K_0 ranges from 0.75 to 1.50 ($K_{0,\,average} = 1.0$)
2. Apply cylindrical cavity expansion to stone column
   - Expand a dummy material (with a nominal stiffness)
   - Convert properties to stone backfill after expansion
3. Apply cylindrical cavity expansion to stone column and increase in soil stiffness
   - Apply cavity expansion to stone columns
   - Increase the stiffness in an enhancement zone (2d–5d from centreline of outer columns)

2.5 Design methods

2.5.1 Unit cell concept

Large arrays of columns are typically spaced on square or triangular grids to support wide loaded areas. Figure 2.21 illustrates that the shape of the zone of influence depends upon the column arrangement adopted. It follows from symmetry that the behaviour of each stone column and its surrounding zone of influence within a large array will be identical. It also follows from symmetry that the sides of the zones of influence are free of radial displacements and shear stresses. Therefore the analysis may be simplified to one column and its surrounding zone of influence. The unit cell concept approximates the zone of influence by a circle of equivalent area. This concept applies to interior columns beneath wide loaded areas, the proportion of which increases with group size (e.g. embankments, large floor slabs). The unit cell concept is not valid for edge columns beneath wide loaded areas or small groups of columns beneath pad/strip footings due to a loss of lateral confinement.

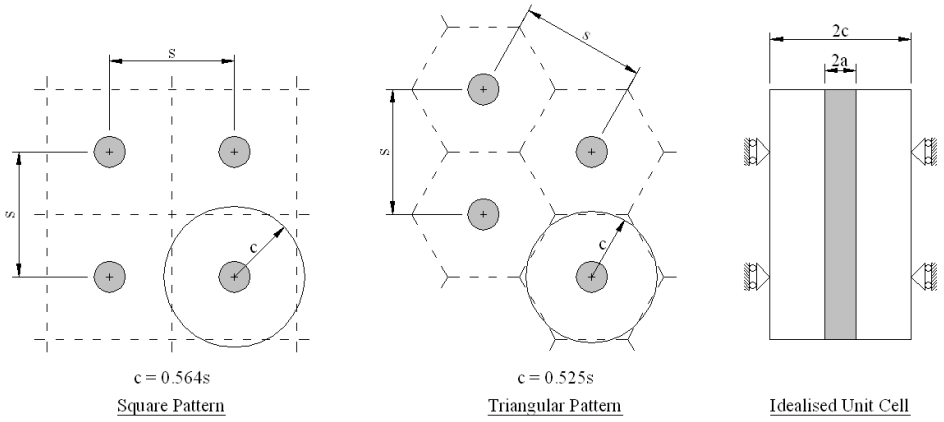

Figure 2.21 - Zones of influence for square and triangular arrangements of stone columns

2.5.2 Cylindrical Cavity Expansion Theory (CCET)

If an internal pressure is applied to a cavity wall, the wall will expand as shown in Figure 2.22. Suppose a general cylindrical shell at radial distance r expands by an amount y and also that another cylindrical shell, at a radial distance r + dr expands by an amount y + dy.

The radial ($\Delta\varepsilon_r$) and tangential ($\Delta\varepsilon_\theta$) strain are defined as:

$$\Delta\varepsilon_r = -\frac{(dr+dy)-dy}{(r+dr)-r} = -\frac{dy}{dr} \quad \textbf{(2.1)}$$

$$\Delta\varepsilon_\theta = -\frac{2\pi(r+y)-2\pi r}{2\pi r} = -\frac{y}{r} \quad \textbf{(2.2)}$$

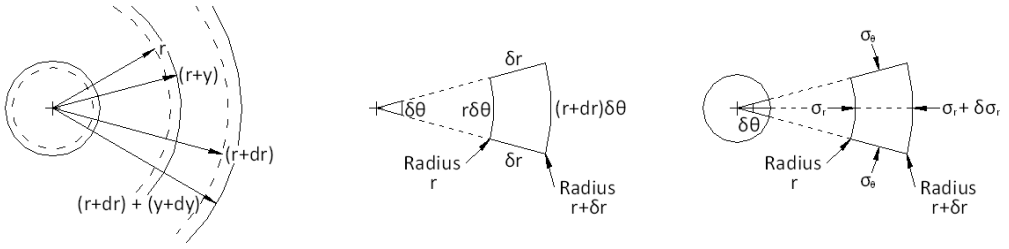

(a) (b) (c)

Figure 2.22 - Equilibrium of soil element (Powrie, 2004)

Assuming the soil can be idealised as a uniform, isotropic and linear elastic material which obeys Hooke's laws, then the principal total stress and strain increments in the radial (r), tangential (θ) and vertical (z) directions are related as follows:

$$\Delta\sigma_r = \lambda(\Delta\varepsilon_r + \Delta\varepsilon_\theta + \Delta\varepsilon_z) + 2G\Delta\varepsilon_r \quad \textbf{(2.3)}$$

$$\Delta\sigma_\theta = \lambda(\Delta\varepsilon_r + \Delta\varepsilon_\theta + \Delta\varepsilon_z) + 2G\Delta\varepsilon_\theta \quad \textbf{(2.4)}$$

$$\Delta\sigma_z = \lambda(\Delta\varepsilon_r + \Delta\varepsilon_\theta + \Delta\varepsilon_z) + 2G\Delta\varepsilon_z \quad \textbf{(2.5)}$$

where $\lambda = \frac{\nu E}{(1-2\nu)(1+\nu)}; G = \frac{E}{2(1+\nu)}$

Considering equilibrium of the element in Figure 2.20(b) and 2.20(c), the equation for radial equilibrium is as follows:

$$[(\sigma_r + \delta\sigma_r)(r + \delta r)\delta\theta] = [\sigma_r r\delta\theta] + [(2\sigma_\theta \delta r)sin(\delta\theta/2)] \quad \textbf{(2.6)}$$

$\delta\theta \; is \; small \implies sin(\delta\theta/2) \approx \delta\theta/2$

$$[(\sigma_r + \delta\sigma_r)(r + \delta r)\delta\theta] = [\sigma_r r\delta\theta] + [(2\sigma_\theta \delta r)(\delta\theta/2)] \quad \textbf{(2.7)}$$

$Ignoring \; small \; quantities \; (e.g. \delta\sigma_r \times \delta r)$

$$\sigma_r\delta r + r\delta\sigma_r = \sigma_\theta\delta r \quad \textbf{(2.8)}$$

$$\frac{\sigma_r}{r} + \frac{\delta\sigma_r}{\delta r} = \frac{\sigma_\theta}{r} \quad \textbf{(2.9)}$$

$Limit \; as \; \delta r \; and \; \delta\sigma_r \to 0$:

$$\frac{d\sigma_r}{dr} = \frac{\sigma_\theta - \sigma_r}{r} \quad \textbf{(2.10)}$$

Assuming plane strain conditions (i.e. $\Delta\varepsilon_z = 0$) and combining the stress-strain equations (2.3, 2.4 and 2.5) and equation of equilibrium (2.10):

$$\frac{d\Delta\sigma_r}{dr} = \frac{\Delta\sigma_\theta - \Delta\sigma_r}{r} = \frac{d}{dr}[\lambda(\Delta\varepsilon_r + \Delta\varepsilon_\theta + \Delta\varepsilon_z) + 2G\Delta\varepsilon_r] = \frac{1}{r}[2G\Delta\varepsilon_\theta - 2G\Delta\varepsilon_r] \quad \textbf{(2.11)}$$

$$\frac{d}{dr}[\lambda(\Delta\varepsilon_r + \Delta\varepsilon_\theta) + 2G\Delta\varepsilon_r] = \frac{1}{r}[2G\Delta\varepsilon_\theta - 2G\Delta\varepsilon_r] \quad \textbf{(2.12)}$$

$$\frac{d}{dr}[(\lambda + 2G)\Delta\varepsilon_r + \lambda\Delta\varepsilon_\theta] = \frac{1}{r}[2G\Delta\varepsilon_\theta - 2G\Delta\varepsilon_r] \quad \textbf{(2.13)}$$

$$\frac{d}{dr}\left[(\lambda + 2G)\left(-\frac{dy}{dr}\right) + \lambda\Delta\varepsilon_\theta\left(-\frac{y}{r}\right)\right] = \frac{1}{r}\left[2G\left(-\frac{y}{r}\right) - 2G\left(-\frac{dy}{dr}\right)\right] \quad \textbf{(2.14)}$$

$$-(\lambda + 2G)\frac{d^2y}{dr^2} - \lambda\frac{1}{r}\frac{dy}{dr} + \lambda\frac{y}{r^2} = -2G\frac{y}{r^2} + 2G\frac{1}{r}\frac{dy}{dr} \quad \textbf{(2.15)}$$

$$-(\lambda + 2G)\frac{d^2y}{dr^2} - (\lambda + 2G)\frac{1}{r}\frac{dy}{dr} + (\lambda + 2G)\frac{y}{r^2} = 0 \quad \textbf{(2.16)}$$

$$\frac{d^2y}{dr^2} + \frac{1}{r}\frac{dy}{dr} - \frac{y}{r^2} = 0 \quad \textbf{(2.17)}$$

Powrie (2004) states that equation 2.17 is a differential equation in terms of a single variable y (y = radial movement). Its general solution, which may be verified by substitution, is:

$$y = \frac{A}{r} + Br \quad \textbf{(2.18)}$$

2.5.3 Ultimate bearing capacity

Thorburn & MacVicar (1968)

Thorburn & MacVicar (1968) present empirical and semi-empirical design curves to calculate allowable working loads on stone columns formed in granular and cohesive soils, respectively. The design curves were developed as the authors sought an alternative design solution to piled foundations for low-rise developments in Glasgow, where soil types range from fresh water alluvium to beach deposits and glacial till. A load test on a strip of three stone columns indicated that this technique was a preferred design alternative to piles as it reduced overall and differential settlements. The authors developed the design chart for cohesive soils from load tests carried out at various sites and undrained axial compression tests (Figure 2.23). The authors state that stone columns cannot be satisfactorily installed in soils with a $c_u < 400$ lb/ft^2 (19.2 kPa), as these soils have very low passive resistances and present difficulties in forming the stone columns.

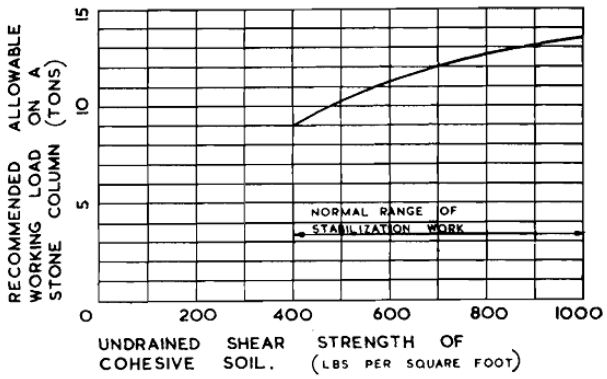

Figure 2.23 - Relationship between allowable vertical stress on stone column and undrained shear strength (Thorburn & MacVicar, 1968)

Hughes & Withers (1974)

As outlined in Section 2.2.1, Hughes & Withers (1974) conducted a series of laboratory tests on single stone columns. Significant column deformation occurred in the upper sections of columns, while negligible strain was observed below 4d (Figure 2.6). Column deformation is idealised as uniform bulging and CCET developed by Gibson & Anderson (1961) can be used to predict the limiting radial stress. However, on the basis of field records of quick expansion tests the authors approximate the limiting radial stress (σ_{rL}) by:

$$\sigma_{rL} = \sigma_{r0} + 4c + u \quad \textbf{(2.19)}$$

where σ_{r0} = total in situ lateral stress

c = undrained cohesion

u = pore water pressure

Assuming columns are in a critical state, the ultimate vertical stress (σ_v') is related to the limiting radial stress by:

$$\sigma_v' = \left(\frac{1+sin\varphi'}{1-sin\varphi'}\right)\sigma_r' \quad \textbf{(2.20)}$$

where σ_r' = lateral effective stress

φ' = angle of internal friction of column material

Therefore, the ultimate vertical stress for column bulging is:

$$\sigma_v' = \left(\frac{1+sin\varphi'}{1-sin\varphi'}\right)(\sigma_{r0} + 4c + u) \quad \textbf{(2.21)}$$

If the vertical forces exceed the shear resistance along the sides of the column and the ultimate bearing capacity at the base, then column punching will occur.

2.5.4 Magnitude of settlement

Greenwood (1970)

Greenwood (1970) presents design curves for estimating consolidation settlement of soft clay strengthened by stone columns under wide spread loadings (Figure 2.24). The curves are developed empirically for the wet and dry methods of construction. It appears that columns installed using the wet method provide a better settlement performance. However, this may be attributed to the larger column diameters which result from this construction technique. The curves neglect immediate settlement and shear displacements. In addition, columns are assumed to be resting on firm clay, sand or harder ground.

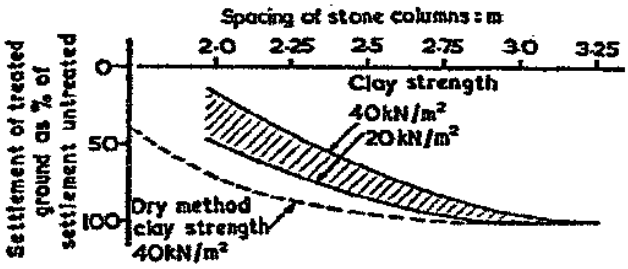

Figure 2.24 - Settlement diagram for stone columns in uniform soft clay (Greenwood, 1970)

Aboshi et al. (1979)

Aboshi *et al.* (1979) propose a simple design method to determine the settlement of large diameter sand columns. The distribution of vertical stress within sand columns (σ_S) and the surrounding clay (σ_C) is determined by the stress concentration ratio (n) and the area ratio (a_S), which are defined as σ_S/σ_C and $A_C/(A_S+A_C)$, respectively. The following expressions are obtained from the equilibrium of stresses:

$$\sigma = \sigma_S a_S + \sigma_C(1 - a_S) \quad \textbf{(2.22)}$$

$$\sigma_C = \sigma/[1 + (n-1)a_S] = \mu_C \sigma \quad \textbf{(2.23)}$$

$$\sigma_S = n\sigma/[1 + (n-1)a_S] = \mu_S \sigma \quad \textbf{(2.24)}$$

The stress concentration ratio is estimated based on field experience. Aboshi *et al.* (1979) present stress concentration ratios measured at several construction sites which range from

1.6–11.5. However, Barksdale & Bachus (1983) suggest that stress concentration ratios typically range from 2.5–5.0. The proposed design method is based on an infinite grid of columns and the settlement of an untreated S and treated S' soil deposit is:

$$S = m_V PH \quad \textbf{(2.25)}$$

$$S' = m_V(\mu_C P)H \quad \textbf{(2.26)}$$

where m_v = modulus of volume compressibility

P = applied pressure

H = thickness of soil deposit

Therefore the settlement reduction factor is:

$$\beta = \mu_C = 1/[1 + (n-1)a_S] \quad \textbf{(2.27)}$$

Priebe (1995)

Priebe (1995) developed a semi-empirical design method to estimate the settlement of an infinite grid of end-bearing stone columns. The columns are assumed to be in an active state and bulge uniformly along their length. The surrounding soil is idealised as an isotropic elastic material, with an increased coefficient of lateral earth pressure ($K_0 = 1$) to account for the effects of column installation. The relationship between the applied vertical stress and the expansion of the column is determined using CCET, the fundamental equations of which are outlined in 2.5.2. The columns are assumed to be incompressible and a basic settlement improvement factor (n_0), which is defined as the ratio of settlements for an untreated footing to a treated footing, is developed:

$$n_0 = 1 + \frac{A_C}{A}\left[\frac{1/2 + f(\mu_c, A_C/A)}{K_{A,C} f(\mu_c, A_C/A)} - 1\right] \quad \textbf{(2.28)}$$

where $f(\mu_c, A_C/A) = \frac{1-\mu^2}{1-\mu-2\mu^2}\frac{(1-2\mu)(1-A_C/A)}{1-2\mu+A_C/A}$

$K_{A,c}$ = coefficient of active earth pressure of column = $\tan^2(45 - \varphi_c/2)$

φ_c = angle of internal friction of column

μ = Poisson's ratio of soil

It is clear from Figure 2.25 that the settlement improvement factors are significantly influenced by both column spacing (A/A_C) and the strength of the stone backfill (φ_c).

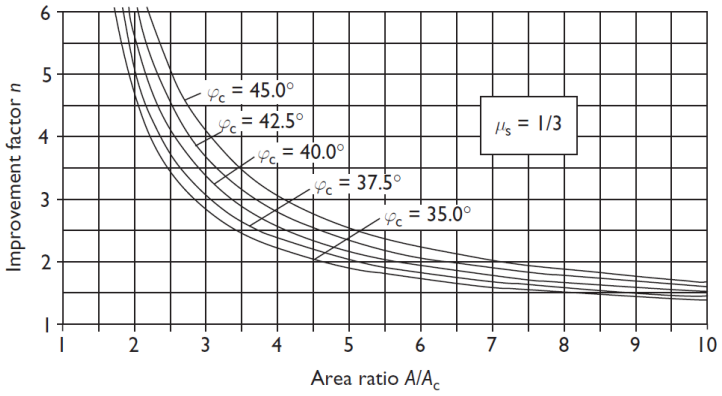

Figure 2.25 - Design curves for basic settlement improvement factor n_0 with Poisson's ratio υ = ⅓ (Priebe, 1995)

Priebe (1995) modifies the basic settlement improvement factor (n_0) to account for column compressibility and the effect of overburden stress. The assumption of column incompressibility yields infinite settlement improvement factors for an area ratio $A/A_C = 1$. This is clearly unrealistic as settlement improvement factors should at best be equal to the ratio of the compression moduli of the column and soil. The effect of column compressibility is accounted for by increasing the area ratio A/A_C by an amount $\Delta A/A_C$, which is dependent on the ratio of the compression moduli of the column and soil. The modification for column compressibility results in lower settlement improvement factors (n_1).

The basic settlement improvement factor also neglects the effect of overburden stress. The pressure difference at the column-soil interface is assumed to be constant with depth and does not account for the unit weight of the column and the surrounding soil. Overburden stress increases with depth and reduces the pressure difference at the column-soil interface. Therefore, consideration of the overburden stress reduces column bulging and yields higher settlement improvement factors. A depth factor (f_d) is introduced to account for the effect of overburden stress. The depth factor is defined as the ratio of the original pressure difference to the 'new' pressure difference (which incorporates overburden stress). The settlement of stone columns is directly related to the depth factor and modified settlement improvement factors are calculated as $n_2 = f_d \times n_1$.

Priebe (1995) develops design charts relating the settlement of a group of columns beneath pad footings (s) to the settlement of an infinite grid of columns (s_∞). The design curves account for the stress distribution beneath pad footings and assume a reduced bearing capacity for the outer columns. It appears from Figure 2.26 that the settlement ratio (s/s_∞) is

independent of footing area (A). However Priebe states that the footing area must be calculated from the area ratio A/A_C, which compensates for footing size as larger footing areas have higher A/A_C ratios and hence yield lower settlement improvement factors. Priebe also states that this compensation provides acceptable results for area ratios A/A_C up to 10.

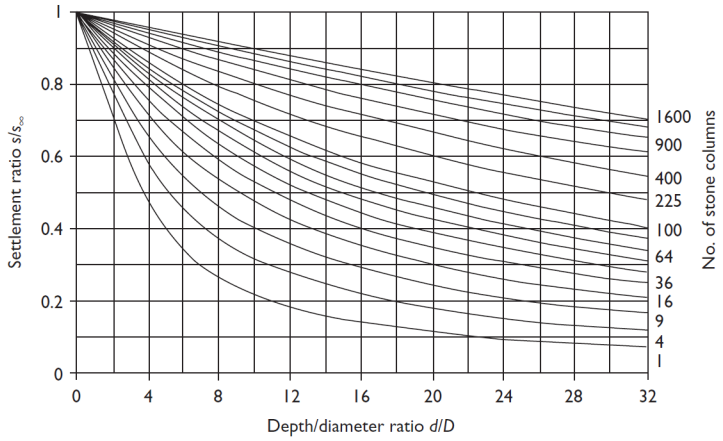

Figure 2.26 - Settlement of single footings on groups of columns (Priebe, 1995)

The curves in Figure 2.26 indicate that the settlement ratio (s/s_∞) reduces rapidly with depth, especially for smaller groups of columns. This results from a decay of vertical stress with depth beneath pad footings and hence the influence of the depth factor (f_d) is reduced for pad footings. Therefore, Priebe suggests dividing the subsoil into layers and calculating the settlement of each layer individually to avoid over-estimating settlements of pad footings. The settlement is calculated using the following formula:

$$\Delta s = \frac{p}{D_S\, n_2}[(s/s_\infty)_L d_L - (s/s_\infty)_U d_U] \qquad \textbf{(2.29)}$$

where d_L and d_U are the lower and upper bound depths of the layer considered.

Balaam & Booker (1981)

Balaam & Booker (1981) propose an analytical solution to determine the settlement of an infinite array of end-bearing stone columns. The stone backfill and the surrounding soil are both idealised as linear elastic materials, which are defined by Young's modulus (E) and Poisson's ratio (ν); the selection of appropriate values must take into consideration the stress level encountered beneath the foundation. The analysis is essentially the compression of a cylindrical body between smooth (raft) and rough (substratum) plates, with a laterally restrained smooth wall. An axisymmetric FEA undertaken by the authors indicates that a triaxial state of stress exists in the column and also that field quantities remote from the

substratum are insensitive to a smooth or rough boundary condition being assumed at the substratum. Therefore, it is possible to assume a smooth substratum and hence to find an exact analytical solution. This solution is based on CCET, the fundamental equations of which are outlined in 2.5.2.

As a first approximation (solution A), the column is assumed to be laterally restrained. The authors report that this assumption yields reasonable results, however a stress discontinuity ($\Delta\sigma_r$) occurs at the column-soil interface. As the column is much stiffer than the surrounding soil, it will attract more load and hence will develop a higher radial stress than the surrounding soil. This stress discontinuity displays itself as column bulging in reality and it is necessary to account for this. Therefore a second solution (B) is developed for zero vertical movement of the raft and a laterally expanding column, which imparts a radial stress equal and opposite to $\Delta\sigma_r$ at the column-soil interface (Figure 2.27).

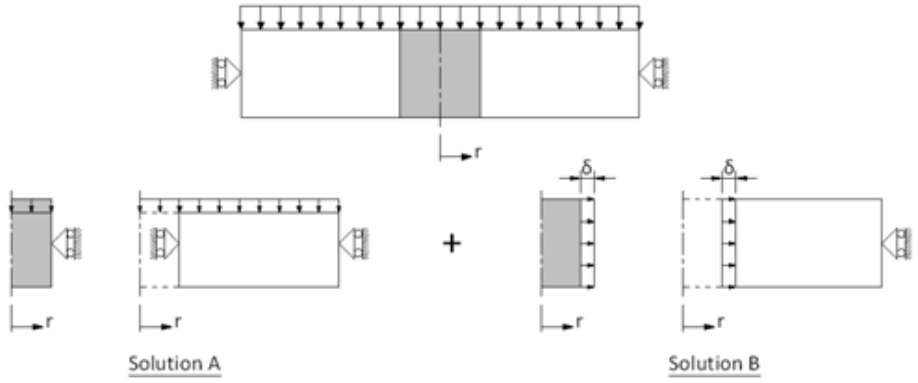

Figure 2.27 - Boundary conditions for solutions A & B proposed by Balaam & Booker (1981)

The final solution is found by super-imposing solutions A & B (Table 2.2). The relationship between strain and the average applied stress q_A is determined by integrating the vertical stresses across the soil surface.

Table 2.2 - Final solution for stresses and strains in column and soil (Balaam & Booker, 1981)

	Region 1 Stone column	Region 2 Clay
ε_z	ε	ε
y	$Fr\varepsilon$	$\left[F\frac{a^2}{r}\frac{(b^2-r^2)}{b^2-a^2}\right]\varepsilon$
σ_r	$[\lambda_1 - 2(\lambda_1+G_1)F]\varepsilon$	$\left[\lambda_2 + \frac{2a^2F}{b^2-a^2}\left(\lambda_2+G_2+G_2\frac{b^2}{r^2}\right)\right]\varepsilon$
σ_θ	$[\lambda_1 - 2(\lambda_1+G_1)F]\varepsilon$	$\left[\lambda_2 + \frac{2a^2F}{b^2-a^2}\left(\lambda_2+G_2-G_2\frac{b^2}{r^2}\right)\right]\varepsilon$
σ_z	$[\lambda_1 + 2G_1 - 2\lambda_1F]\varepsilon$	$\left[\lambda_2 + 2G_2 + 2\lambda_2\frac{Fa^2}{b^2-a^2}\right]\varepsilon$

Lame's parameters: $\lambda = \frac{\upsilon E}{(1-2\nu)(1+\nu)}$; $G = \frac{E}{2(1+\nu)}$

and where $F = \frac{(\lambda_1-\lambda_2)(b^2-a^2)}{2[a^2(\lambda_2+G_2-\lambda_1-G_1)+b^2(\lambda_1+G_1+G_2)]}$

a = radius of stone column

b = radius of unit cell

Relationship between strain and average applied stress, q_A:

$$q_A b^2 = [(\lambda_1 + 2G_1)a^2 + (\lambda_2 + 2G_2)(b^2 - a^2) - 2a^2(\lambda_1 - \lambda_2)F]\varepsilon \quad \textbf{(2.30)}$$

$$q_A = [(\lambda_1 + 2G_1)(A_C/A) + (\lambda_2 + 2G_2)(1 - A_C/A) - 2(A_C/A)(\lambda_1 - \lambda_2)F]\varepsilon \quad \textbf{(2.31)}$$

$$\varepsilon = q_A/[(\lambda_1 + 2G_1)(A_C/A) + (\lambda_2 + 2G_2)(1 - A_C/A) - 2(A_C/A)(\lambda_1 - \lambda_2)F] \quad \textbf{(2.32)}$$

The settlement reduction factor (β) is defined as:

$$\beta = \varepsilon/q_A m_{V2} \quad \textbf{(2.33)}$$

$$\beta = E_{oed}/[(\lambda_1 + 2G_1)(A_C/A) + (\lambda_2 + 2G_2)(1 - A_C/A) - 2(A_C/A)(\lambda_1 - \lambda_2)F] \quad \textbf{(2.34)}$$

Balaam & Booker (1985)

Several authors have found that under certain circumstances an elastic analysis can grossly overestimate the effectiveness of stone columns in reducing the settlement of a foundation. Balaam & Booker (1985) propose an interaction analysis which contains some simplifying assumptions to account for column yielding. The analytical solution for the elastic response developed by Balaam & Booker (1981) indicates that the major principal stresses will be close to vertical. Furthermore, there may also be significant yielding of the column, but little yield in the surrounding clay. As a result, Balaam & Booker (1985) make the following assumptions:

(i) stone columns are in a triaxial stress state

(ii) yielding may occur in columns and no yielding occurs in the surrounding soil

(iii) no shear stress develops along the stone-soil interface

(iv) the behaviour of stone columns is idealised as an elasto-plastic material satisfying the Mohr-Coulomb yield criterion

The proposed solution which incorporates these assumptions was validated by a comparison with a FEA. The clay and the column material were both treated as dilatant materials, which

satisfy the Mohr-Coulomb yield criterion and have a non-associated flow rule. Appropriate material parameters and geometrical dimensions were selected to comprehensively test the validity of the assumptions. A good agreement exists between both methods and, therefore, the solution proposed by Balaam & Booker (1985) is an efficient and accurate way to calculate the reduction in settlement due to stone columns.

Pulko & Majes (2005)

Pulko & Majes (2005) extend the elastic analysis proposed by Balaam & Booker (1981) to account for confined column yielding. Therefore the soil is assumed to remain in an elastic state and the column material is assumed to behave as a perfectly elastic-plastic material satisfying the Mohr-Coulomb yield criterion. The design method accounts for both applied stress levels and the *in situ* overburden stress. Column yielding, which is accounted for by dilatancy theory developed by Rowe (1962), occurs once active conditions are reached in the column. The elastic strains, and if applicable plastic strains, are integrated along the length of the column to determine settlement improvement factors. The settlement results of the design method are in excellent agreement with a FEA for non-dilatant soil and stone materials.

2.5.5 Rate of settlement

Han & Ye (2001)

It is well established from field studies that stone columns increase the rate of consolidation. The high permeability of stone backfill ensures that columns act as vertical drains. The low compressibility of stone columns further increases the rate of consolidation as stress concentrations develop in columns which reduces the vertical stress on the soil. Han & Ye (2001) develop a simplified method to compute the rate of consolidation of stone column reinforced foundations. The formats of vertical and radial flows are similar to those of the Terzaghi 1D solution and the Barron solution for drain wells in fine grained soils, respectively. Modified coefficients of consolidation in the radial (c_r') and vertical (c_v') directions are introduced to account the stone column-soil modular ratio:

$$c_r' = c_r\left(1 + n_s \frac{1}{N^2-1}\right) \qquad c_v' = c_v\left(1 + n_s \frac{1}{N^2-1}\right)$$

where c_r, c_v = coefficient of consolidation in radial and vertical direction, respectively

n_s = steady state stress concentration ratio

N = diameter ratio (= d_e/d_c)

The effectiveness of stone columns in increasing the rate of consolidation is shown Figure 2.28, where the proportion of excess pore pressure dissipation due to the stiffness of the stone column is shown. It can also be seen that vertical stress transfers from the soil to the stone columns as consolidation proceeds. The proposed solution was compared with a numerical study by Balaam & Booker (1981) and a reasonable agreement was observed. However, the proposed solution tends to under-estimate the rate of consolidation initially, while a reverse in this trend is observed for rates of consolidation greater than 40 %. The may be explained as the proposed solution does not account for lateral expansion of columns. Initially, the pore water pressure in the soil takes the entire load which forces the column to compress. This mechanism acts as a relief for the soil which increases the rate of consolidation. However, as consolidation occurs, stress concentration increases in columns which cause columns to expand into surrounding soil. This increases the excess pore water pressure in the soil and reduces the rate of consolidation.

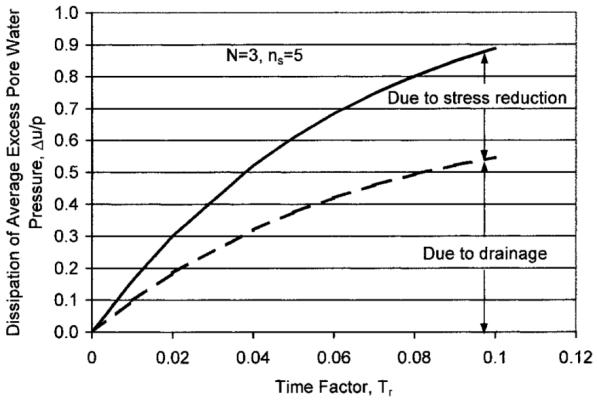

Figure 2.28 - Dissipation of excess pore water pressure (Han & Ye, 2001)

Castro & Sagaseta (2009)

Castro & Sagaseta (2009) develop equivalent coefficients of consolidation which account for the lateral movement of the stone column during the consolidation process. The behaviour of the column is modelled as an elastic material or as an elasto-plastic dilatant material with a Mohr-Coulomb failure criterion. Vertical stress increases in columns with consolidation and column yielding may occur. The stiffness of columns reduces once yielding occurs, which results in increased radial deformability of the column. Therefore columns in a plastic state expand and increase the excess pore water pressure in the soil. The solution developed by Castro & Sagaseta (2009) allows the depth and time of column yielding to be determined. Therefore it is possible to accurately determine the stresses and strains occurring in columns

at any stage in the loading history. A comparison with Han & Ye (2001) of the development of stress concentration ratio with time is shown in Figure 2.29.

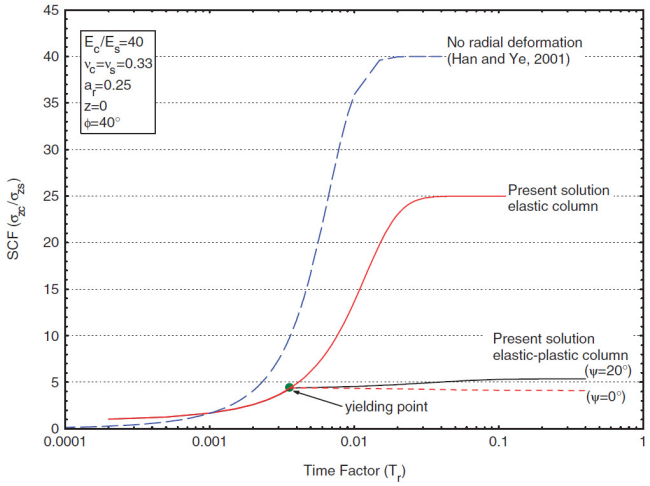

Figure 2.29 - Stress concentration factor. Influence of radial deformation and plastic strains (Castro & Sagaseta, 2009)

2.5.6 Summary of design methods

The majority of design methods for the ultimate bearing capacity and settlement performance of stone columns are based on the unit cell concept and Cylindrical Cavity Expansion Theory (CCET). The unit cell concept assumes that an infinite grid of columns support an infinitely wide load area. It follows from symmetry that the behaviour of each column within an infinite grid is identical and the analysis may be simplified to one column and its surrounding zone of influence. Consequently, the unit cell concept is only applicable to interior columns within large groups. The stresses and strains which develop in the soil surrounding an expanding cylindrical shell may be determined using CCET.

Empirical and analytical design methods to determine the ultimate bearing capacity of columns were presented in the previous section. These design methods indicate that the ultimate bearing capacity of stone columns is highly dependent upon the passive resistance of the surrounding soil, especially in the upper sections of columns (i.e. near the ground surface).

A series of design methods, ranging from empirical to analytical, are presented in the previous section to determine the magnitude of settlement for stone columns. Priebe (1995) develops a semi-empirical design method which contains some simplifying assumptions.

Columns are assumed to be in an active state and uniform bulging occurs along the length of columns. Modification factors are introduced to account for column compressibility and overburden stresses. Balaam & Booker (1981) propose a more rigorous theoretical solution than Priebe (1995), but model the stone columns and surrounding soil as linear elastic materials and, therefore, fail to account for column yielding. This can significantly over-estimate the effectiveness of stone columns at reducing the settlement of foundation. Balaam & Booker (1985) and Pulko & Majes (2005) extend this solution to account for column yielding through an interaction analysis and analytical design method, respectively. The behaviour of stone columns is idealised as elastic-rigid plastic and column yielding is captured using dilation theory developed by Rowe (1962).

Stone columns are an effective method to increase the rate of consolidation as their high permeability allows them to act as vertical drains and also as stress concentrations, which develop in stone columns, reduce the vertical stress on the surrounding soil. Han & Ye (2001) develop a simplified solution to compute the rate of consolidation for stone column reinforced foundations. This solution is extended by Castro & Sagaseta (2009) who model the stone column as an elasto-plastic dilatant material and account for lateral expansion. This design method can be used to determine the depth and time of yielding, which allows for an accurate determination of stresses and strains occurring in columns at any stage in the loading history.

2.6 Summary of literature review

Vibro stone columns are a popular form of ground improvement, which enhance the settlement performance and bearing capacity of treated soils. Vertical columns of compact stone are formed in the ground using the top or bottom feed systems. Stone columns can be used to support a wide variety of loading scenarios ranging from small footings to wide area loadings.

The deformational behaviour of stone columns is well understood and it is established that single columns or large groups of columns exhibit either a punching or bulging mode of deformation. However, the behaviour of small groups of stone columns is more complex and Muir Wood *et al.* (2000) demonstrate that small groups of columns can fail by punching, bulging, bending and shearing. This may be attributed to the loss of lateral confinement for

peripheral columns and also the reduction in vertical stress with depth beneath small loaded areas.

Stone columns can be adopted to treat soft clayey soils, which are typically characterised by poor strength, stiffness and drainage properties. Consequently, foundations on these soils undergo large displacements at relatively low loads, and settlement is usually the governing criterion in foundation design. While the deformational behaviour of small groups of columns is well understood, there exists a dearth of information regarding the settlement performance of small groups of columns. This is highlighted by McCabe *et al.* (2009), who collated a settlement database from field records, and observed that only three out of 20 case studies relate to small groups of stone columns. Analytical design methods contain many simplifying assumptions, such as the unit cell concept which is only applicable to large groups of stone columns. Elshazly *et al.* (2008) conduct an axisymmetric FEA to examine the settlement performance of finite groups of columns; however, the majority of numerical studies are based on large groups of columns supporting wide area loadings. The lack of information regarding the settlement performance of small groups of stone columns was identified by Black (2006), who conducted a series of high quality laboratory tests. However, it is difficult to extrapolate the findings due to scale effects and also as some of the area ratios considered are at the high end of typical values used in practice.

It was shown in the laboratory tests that column interaction plays an important role in the deformational behaviour of small groups of stone columns. Therefore, it is necessary to model columns at discrete locations, rather than approximating their presence by cylindrical rings, as is the case with axisymmetric analyses. Furthermore, the decay of vertical stress with depth will have an important role on the settlement performance of stone columns, and must be captured when analysing the settlement performance of small groups of stone columns. It is proposed in this thesis to conduct a three-dimensional FEA using PLAXIS 3D Foundation to examine the influence of various design parameters, such as area ratio, column length and the number of columns, upon the settlement performance and deformational behaviour of small groups of stone columns.

Chapter 3
Background and preliminary checks for Finite Element Analysis

3.1 Introduction

The Finite Element Method (FEM) is a powerful tool used for analysing complex engineering problems. The FEM is an approximate technique which uses the principle of virtual work to estimate the distribution of stresses and strains throughout a continuum. PLAXIS 3D Foundation is a three-dimensional FE program which is specifically tailored for geotechnical applications. This program is ideal for capturing the complex behaviour of small groups of stone columns and was adopted for the subsequent FEA. The behaviour of the soil and stone is simulated with advanced constitutive models, which are described in the following chapter. In addition, as the FEM is an approximate technique it is necessary to carry out a number of preliminary checks, such as mesh sensitivity and distance to the boundary, to ensure accurate numerical analyses.

3.2 Description of material models

The behaviour of real soil is highly non-linear, with both strength and stiffness depending on the stress and strain level (Potts & Zdravkovic, 1999). Furthermore, real soil often exhibits time-dependent behaviour and anisotropic tendencies. The behaviour of soil may be approximated to varying degrees of accuracy using material models. An overview of the material models used in the subsequent FEA is given below:

Linear Elastic model

This is based on Hooke's law of elasticity and idealises soil as a linear elastic material, thus precluding the development of irreversible strains. The material behaviour is defined by two parameters, Young's modulus (E) and Poisson's ratio (ν). This model is too crude to accurately capture the complicated stress-strain behaviour of soil and is only adopted to represent structural elements e.g. concrete, steel.

Mohr-Coulomb model

This is a first order model which idealises soil as an elastic-perfectly plastic material. The behaviour of soil before failure is approximated by Hooke's law of elasticity. The failure of soil is based upon the Mohr-Coulomb failure criterion which is defined by two parameters, angle of internal friction (φ) and cohesion (c). This failure criterion is an extension of Coulomb's friction theory and its yield surfaces in principal stress space are shown in Figure 3.1. The model does not generate irreversible strains below the yield surfaces (Mar, 2002). However, irreversible plastic strains resulting from shearing are captured using a non-associated flow rule, which is defined by an angle of dilation (ψ).

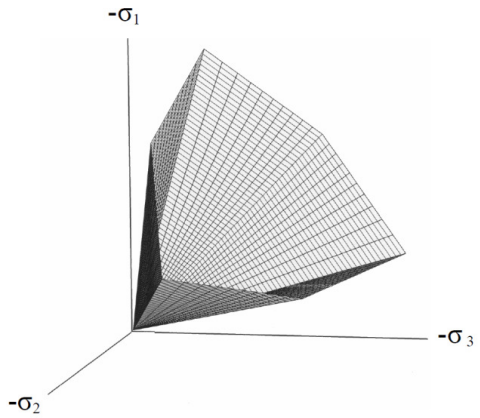

Figure 3.1 - Mohr-Coulomb yield surface in principal stress space (c = 0 kPa) (Brinkgreve & Broere, 2006)

A constant Young's modulus defines the behaviour of soil before failure and it is important to choose an appropriate value which reflects the stress path and stress level experienced by the soil. A drawback to the Mohr-Coulomb model is that it fails to accurately capture the stiffness response of soils due to the simplistic assumption of linear elasticity before failure and is only used as a first approximation of soil behaviour (Brinkgreve & Broere, 2006).

While the Mohr-Coulomb model captures the failure behaviour of soil quite well in drained conditions, it over-estimates the undrained shear strength, as continuous dilation is assumed once yielding occurs (Potts & Zdravkovic, 2001).

Hardening Soil model

The Hardening Soil model is an advanced elasto-plastic constitutive model which can be used to simulate the behaviour of both soft and stiff soils (Schanz, 1998). The model is an extension of the hyperbolic model developed by Duncan & Chang (1970). It supersedes the hyperbolic model as it is based on the theory of plasticity rather than elasticity, includes soil

dilatancy and introduces a yield cap (Schanz *et al.*, 1999). It accounts for both shear and volumetric hardening, thus capturing irreversible strains caused by deviatoric and compression loadings, respectively.

The basis for the Hardening Soil model is that the relationship between the deviatoric stress (q) and the vertical strain (ε_1) for a primary triaxial loading may be approximated by a hyperbola. Therefore, the yield curve for a standard drained triaxial test, which is shown in Figure 3.2, can be defined by:

$$\varepsilon_1 = \frac{q_a}{2E_{50}} \frac{q}{q_a - q} \qquad for\ q < q_f \tag{3.1}$$

where q_a = asymptotic value of shear strength

q_f = ultimate deviatoric stress

E_{50} = secant Young's modulus at 50% deviatoric stress

The secant Young's modulus is used instead of the initial modulus (E_i) as this is easier to define from triaxial tests. The Hardening Soil model also captures the stress path dependency of soil stiffness using an unload-reload modulus (E_{ur}). The ultimate deviatoric stress (q_f) is derived from the Mohr-Coulomb failure criterion and related to the asymptotic value of shear strength (q_a) by a failure ratio (R_f):

$$q_f = \frac{6sin\varphi}{3 - sin\varphi}(p + c.cot\varphi) \qquad R_f = \frac{q_a}{q_f} \tag{3.2}$$

where φ = angle of internal friction

c = cohesion

p = mean total stress

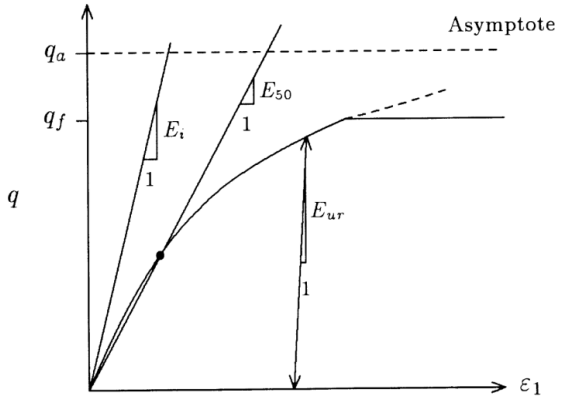

Figure 3.2 - Hyperbolic stress-strain relation in primary loading for a standard drained triaxial test (Schanz *et al.*, 1999)

Soils tend to exhibit a stress level dependency which results in an increasing stiffness with increasing confining pressure. The stress dependency of soil stiffness is captured by the Hardening Soil model using a power law:

$$\frac{E}{E_{ref}} = \left(\frac{\sigma}{\sigma_{ref}}\right)^{m} \quad \textbf{(3.3)}$$

where E_{ref} is the reference stiffness corresponding to the reference confining pressure (σ_{ref}). The confining pressure is taken as the minor or major principal stress for triaxial or oedometer tests, respectively. The stress dependency is determined by the parameter, m, which ranges from 0.5 for Norwegian sands and silts (Janbu, 1963) to 1.0 for soft clays (Brinkgreve & Broere, 2006).

Once the ultimate deviatoric stress is reached, the Mohr-Coulomb failure criterion is satisfied and perfectly plastic yielding occurs. In addition to capturing plastic shear strains, which result from decreasing stiffness, the Hardening Soil model also accounts for the volumetric strains due to dilatancy. Plastic volumetric strains are determined from the stress-dilatancy theory developed by Rowe (1962). A cap yield surface is introduced to account for volumetric strains resulting from isotropic loadings. The yield surfaces for the Hardening Soil model in principal stress space are shown in Figure 3.3.

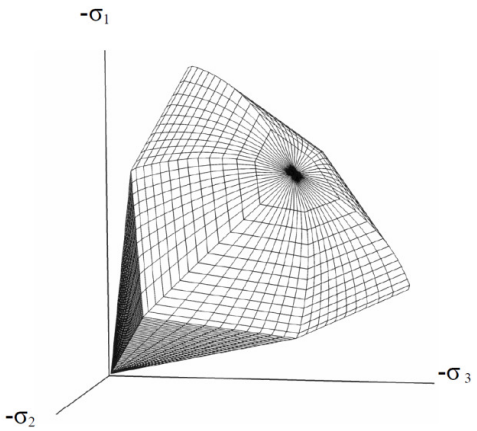

Figure 3.3 - Hardening Soil yield surface in principal stress space (c = 0 kPa) (Brinkgreve & Broere, 2006)

The Hardening Soil model does not include anisotropic strength and stiffness or time dependent behaviour of soil. Also, it does not account for the strain dependent nature of soil stiffness and therefore its application to dynamic loadings is limited.

3.3 Preliminary checks to ensure accurate numerical analyses

3.3.1 Mesh sensitivity analyses

The accuracy of the FEM depends not only on the level of sophistication of the material model, but also on the number and type of the elements into which the domain is discretised. PLAXIS 3D Foundation uses 15 node wedge elements which are composed of 6 node triangles in the horizontal direction and 8 node quadrilaterals in the vertical direction (Figure 3.4).

(i) (ii)

Figure 3.4 - Distribution of (i) nodes and (ii) stress points within 15 node wedge elements

The influence of the number of elements upon the accuracy of the FEM was investigated by conducting a mesh sensitivity analysis. In the subsequent parametric studies, both the number of columns and column spacing are varied beneath pad footings which results in various footing sizes. Mesh sensitivity analyses are conducted for six different footing sizes where the accuracy of medium and fine meshes are compared against very fine (vf) meshes.

The vertical displacement (u_y) and mean effective stress (p') were measured at three points A, B and C which are 0, 1 and 2 m below the centre of footings, respectively (Figure 3.5). When conducting mesh sensitivity analyses it is prudent to examine stresses in the zone of interest, as the distribution of stress within elements is derived from lower order equations than the displacement. Therefore, stress converges slower than displacement with increasing mesh density and, consequently, the distribution of stress within an element will not be as accurate as the displacement. Vertical displacements were also examined for the mesh sensitivity analysis as the settlement performance of stone columns is the primary focus of this thesis. The soil profile adopted for the subsequent FEA and the mesh sensitivity analysis is that of the well characterised Bothkennar test site, which is described in detail in Section 4.4.

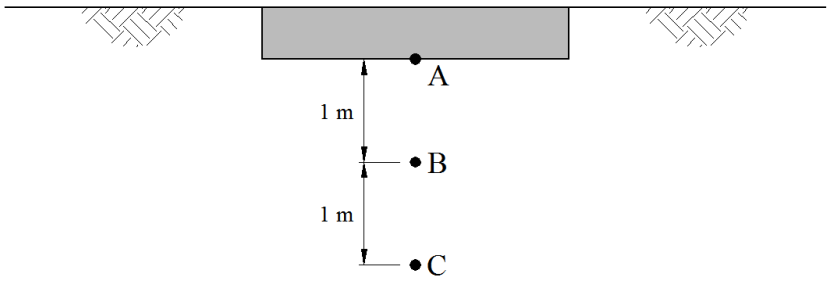

Figure 3.5 - Points A, B and C beneath pad footing

The accuracy of medium and fine meshes is determined by comparing the normalised error for vertical displacement (u_y) and mean effective stress (p') against very fine meshes:

Normalised error for vertical displacement, $u_y = \left(\frac{u_{y,vf} - u_y}{u_{y,vf}}\right) \times 100$

Normalised error for mean effective stress, $p' = \left(\frac{p'_{vf} - p'}{p'_{vf}}\right) \times 100$

In addition to checking convergence of stress and strain with an increasing number of elements, the mesh is also checked for discontinuities at inter-element boundaries. Discontinuities typically occur in regions of rapid changes of stress and strain, i.e. beneath the edge of footings, and can be overcome by refining the mesh in these regions. An example of continuous displacement contours at inter-element boundaries is shown in Figure 3.6.

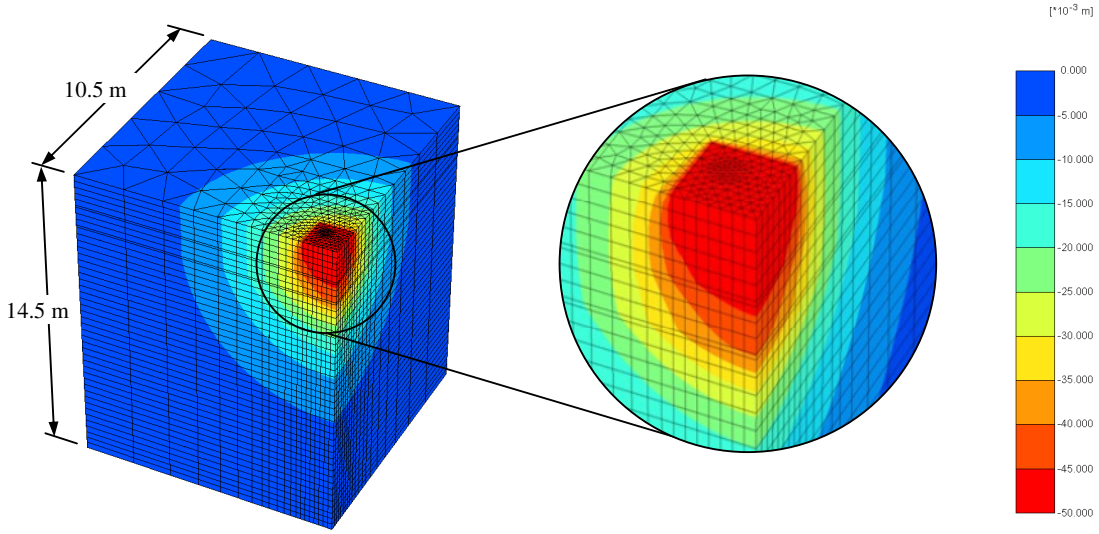

Figure 3.6 - Continuous displacement contours along inter-element boundaries beneath a 3 m square footing

In the subsequent FEA, the settlement performance and deformational behaviour of various configurations of columns is examined at 50 kPa, which is a typical working load for the

Bothkennar test site. However, most of the mesh sensitivity analyses were conducted at 25 kPa in order to save computational time.

A flowchart outlining the steps taken to ensure accurate numerical analyses is shown in Figure 3.7.

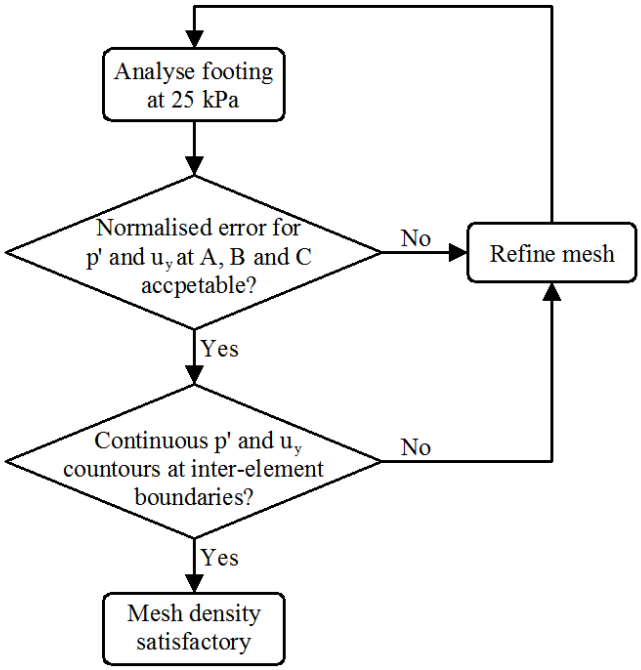

Figure 3.7 - Flowchart outlining preliminary analysis checks

The number of elements used for each mesh and the normalised error for the vertical displacement and mean effective stress is shown in Table 3.1. It is clear that the values for medium and fine meshes are converging towards the very fine mesh and also that the normalised error between the fine and very fine meshes for the vertical displacement and mean effective stress is quite low (maximum error is no greater than 2%).

3.3.2 Influence of distance to boundary

The pad footings modelled in the subsequent parametric studies are surrounded by a zone of soil, which undergoes no lateral displacement along its outer boundary. Therefore, it is necessary to position the boundary at a sufficient distance from the footing so that boundary conditions do not influence the results. A sensitivity analysis was conducted on a 3 m square footing, where the distance to the boundary from the footing centre ranged from 2B–12B. The footings were loaded to 25 kPa and the vertical displacement and mean effective stress at points A, B and C for the different boundary distances are listed in Table 3.2. It appears that

Table 3.1 - Vertical displacement and mean effective stress at points A, B and C

Ftg width, B (m)	Mesh	No. of elements in top work plane	No. of elements in 3D mesh	Vert displ, u_y (mm)			Normalised Error (%)			Mean eff stress, p' (kPa)			Normalised Error (%)		
				A	B	C	A	B	C	A	B	C	A	B	C
2	Medium	302	7852	11.6	10.8	9.2	0.9	2.4	8.1	21.5	24.6	25.5	3.1	0.3	0.9
	Fine	**302**	**12684**	**11.7**	**10.5**	**8.5**	**0.5**	**0.4**	**0.3**	**20.8**	**24.5**	**25.3**	**0.4**	**0.1**	**0.0**
	Very fine	700	29400	11.7	10.6	8.5				20.9	24.5	25.3			
3	Medium	356	11036	48.3	45.4	38.4	1.5	1.5	0.9	26.5	29.7	29.2	2.2	0.5	0.1
	Fine	**356**	**16376**	**48.7**	**45.7**	**38.6**	**0.8**	**0.8**	**0.5**	**25.8**	**29.7**	**29.2**	**0.5**	**0.3**	**0.1**
	Very fine	678	31188	49.1	46.1	38.7				25.9	29.8	29.3			
4	Medium	536	16616	59.4	55.7	43.5	1.1	1.1	0.9	25.7	30.4	24.4	0.4	0.4	0.0
	Fine	**536**	**23048**	**59.9**	**56.2**	**43.8**	**0.3**	**0.3**	**0.3**	**25.8**	**30.5**	**24.4**	**0.1**	**0.1**	**0.0**
	Very fine	822	35346	60.1	56.3	43.9				25.9	30.5	24.4			
4.5	Medium	480	20640	85.4	82.1	71.3	1.8	1.8	1.6	25.9	30.7	32.6	0.8	0.6	0.5
	Fine	**1124**	**48332**	**86.8**	**83.5**	**72.4**	**0.2**	**0.2**	**0.2**	**26.1**	**30.9**	**32.8**	**0.1**	**0.1**	**0.1**
	Very fine	1370	58910	87.0	83.6	72.5				26.1	30.9	32.8			
6	Medium	392	10976	122.8	118.8	105.6	2.7	2.6	2.5	273.2	32.3	36.2	25.0	1.0	2.0
	Fine	**738**	**31734**	**125.5**	**121.3**	**107.8**	**0.6**	**0.6**	**0.5**	**370.9**	**32.6**	**35.4**	**1.7**	**0.2**	**0.2**
	Very fine	1476	63468	126.2	122.0	108.4				364.5	32.6	35.5			
8	Medium	738	20664	170.2	165.1	149.2	1.3	1.2	1.2	30.7	34.5	37.6	6.0	0.4	0.4
	Fine	**738**	**31734**	**171.5**	**166.2**	**150.2**	**0.5**	**0.5**	**0.5**	**28.8**	**34.6**	**37.7**	**0.2**	**0.2**	**0.2**
	Very fine	1532	58216	172.4	167.1	151.0				28.9	34.6	37.8			

Table 3.2 - Influence of the distance to boundary upon the settlement of a 3 m square footing

Distance to boundary (B = footing width)	Vertical displacement, u_y (mm)			Normalised Error (%)			Mean effective stress, p' (kPa)			Normalised Error (%)		
	Point A	Point B	Point C	Point A	Point B	Point C	Point A	Point B	Point C	Point A	Point B	Point C
2B	61.9	58.4	50.2	26.2	26.8	29.3	26.8	30.6	29.9	0.5	2.8	2.0
4B	53.2	50.0	42.1	8.4	8.5	8.5	26.2	30.1	29.5	1.7	1.0	0.6
6B	49.4	46.3	38.9	0.6	0.6	0.3	25.9	29.8	29.3	2.9	0.1	0.1
8B	49.1	46.1	38.7	0.0	0.0	0.2	25.9	29.8	29.3	2.9	0.1	0.2
10B	48.9	45.9	38.7	0.3	0.3	0.2	26.6	29.8	29.3	0.1	0.1	0.1
12B	49.1	46.1	38.8	0.0	0.0	0.0	26.7	29.8	29.3	0.0	0.0	0.0

positioning the boundary closer than 6B to the centre of the footing induces more settlement in the pad footing. The distance to the boundary from the centre of the footing is conservatively chosen at 8B for all the subsequent FEA.

3.4 Other modelling issues

3.4.1 Modelling of soft soil behaviour

The long term behaviour of cohesive soils, which develop excess pore pressure during loading, can be modelled by two methods with PLAXIS 3D Foundation:

(i) Undrained loading followed by consolidation analysis

(ii) Drained analysis

Method (i) is a closer simulation of reality than method (ii), however it is far more time consuming. In method (i), the soil is specified to behave in an undrained manner during the application of footing loads. Initial undrained settlements are computed and long term settlements are then determined by conducting a consolidation analysis. The soil can be defined using either total or effective strength parameters for this method. However, it is not possible to capture the increase in soil shear strength with consolidation or the stress dependency of soil stiffness when using total strength parameters and, consequently, effective strength parameters are used in all the subsequent FEA. The initial undrained response of the soil is simulated by adding a very large bulk modulus to the pore water stiffness matrix, which ensures that all of the stresses generated from the footing loading will be taken by the pore water. The consolidation analysis is then conducted by removing the extra bulk modulus. The stresses in the pore water pressure are then transferred to the soil matrix and the resulting settlements for primary consolidation are computed. The behaviour of the soil for method (ii) is again defined using effective strength and stiffness parameters. However, it is not possible to separate the settlements from the initial undrained response and primary consolidation for the second method.

The consistency of methods (i) and (ii) is compared in Figure 3.8, which shows the variation of settlement improvement factors with column length for three arrangements of stone columns beneath a 3 m square footing. For the purposes of comparing the consistency of both methods it suffices to examine their relative performance; a detailed analysis of the results is provided in chapter 5. It appears that method (ii) predicts slightly higher settlement

improvement factors than method (i) for footings supported by 9 columns, while the opposite is observed for the footing supported by 5 columns. However, both methods predict a similar variation of settlement improvement factor with column length for all configurations of columns (maximum normalised error is no greater than 7%). To save computational time, method (ii) is therefore adopted for all the subsequent FEA, unless otherwise stated.

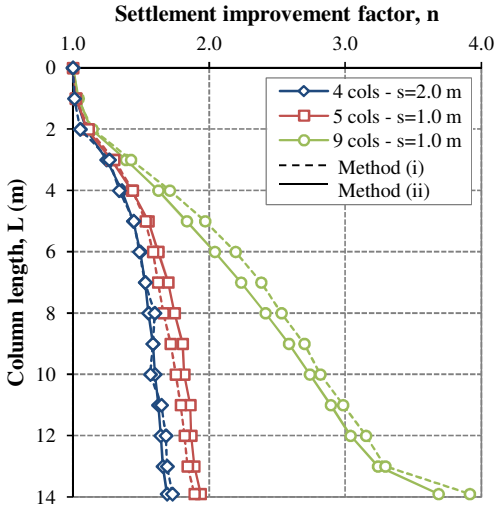

Figure 3.8 - Influence of analysis type upon the settlement improvement factors for various groups of columns

3.4.2 Modelling of column-soil interface

Interface elements are available in PLAXIS 3D Foundation to model the interaction between smooth and rough surfaces i.e. between piles/basement walls and soil. Interface elements can simulate gap and slip displacements which are normal and parallel to the interface, respectively. The 16 node elements consist of 8 pairs of nodes (2 nodes at the same point; 1 for the soil and 1 for the wall) and are shown in Figure 3.9.

The element behaviour is modelled as elastic-plastic, with the Coulomb criterion adopted to distinguish between elastic and plastic behaviour. The loss of strength at the interface is modelled with a strength reduction factor (R_{inter}), which relates the interface strength to the soil strength through friction angle (φ) and cohesion (c):

$$c_i = R_{inter} c_{soil} \quad \textbf{(3.4)}$$

$$tan\varphi_i = R_{inter} tan\varphi_{soil} \leq tan\varphi_{soil} \quad \textbf{(3.5)}$$

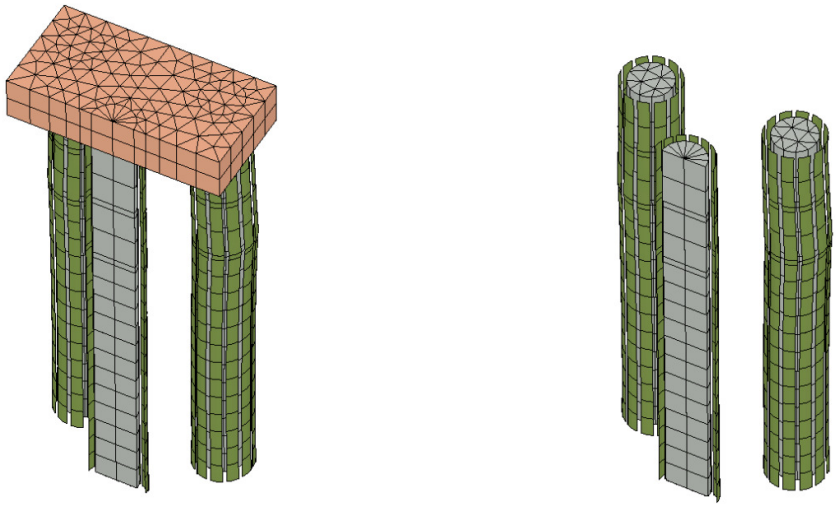

Figure 3.9 - Interface elements for a group of 5 columns beneath a 3 m square pad footing

In reality elements have zero thickness, but are assigned a virtual thickness in order to determine element stiffness. Gap and slip displacements are calculated from the oedometric ($E_{oed,i}$) and shear (G_i) moduli, respectively. The moduli are related by the expression:

$$E_{oed,i} = 2G_i \frac{1-\nu_i}{1-2\nu_i} \quad \textbf{(3.6)}$$

where $\upsilon_i = 0.45$

Guetif *et al.* (2007) adopt rigid interface elements (i.e. $R_{inter} = 1$) on the basis that stone columns are tightly interlocked with the surrounding soil and a perfect bond exists along the column-soil interface. However Gäb *et al.* (2008), Elshazly *et al.* (2008a), Domingues *et al.* (2007a) and many other authors model a perfect bond along the column-soil interface by omitting interface elements.

The influence of interface elements upon the settlement performance of various configurations of columns beneath a 3 m square footing is presented in Figure 3.10. It can be seen that column arrangements with interface elements yield lower settlement improvement factors i.e. they over-predict the settlement of stone columns. This may be attributed to the elastic-plastic material model and the increased Poisson's ratio ($\upsilon_i = 0.2 \rightarrow 0.45$) assigned to interface elements in PLAXIS 3D Foundation. It can be shown in equation 3.6 that an increased Poisson's ratio yields lower shear moduli, which increases slip displacement.

The influence of interface elements also appears to become more pronounced with an increasing number of columns. It will be shown in chapter 5 that closely-spaced columns punch into the underlying soil, whereas columns at higher A/A_C tend to bend and bulge. Therefore, as A/A_C decreases, a larger proportion of the applied load is transferred along the side of columns and along the interface elements, which induces more displacement.

It is clear from Figure 3.10 that a similar variation of settlement improvement factors with column length was observed for columns modelled with and without interface elements. As columns are tightly interlocked with the surrounding soil it was deemed appropriate to model the column-soil interface in the subsequent FEA by omitting interface elements, in keeping with the prior work of several other authors.

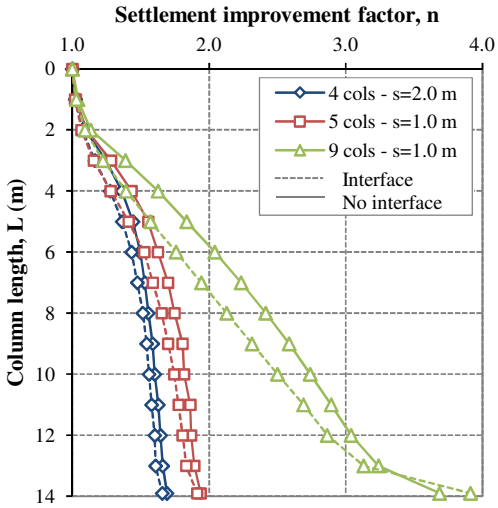

Figure 3.10 - Influence of interface elements upon settlement improvement factors for various groups of columns

3.4.3 Modelling of column installation effects

It was shown in the literature review (see Section 2.4) that column installation effects increase the horizontal stress and stiffness in the surrounding soil. It was also postulated that any changes to the *in situ* stress levels in fine grained soils are solely due to the displacing effects of the poker, as the forces generated from horizontal vibrations are attenuated. Measurements from field and laboratory studies suggest that the effects of column installation can be accurately predicted by Cylindrical Cavity Expansion Theory (CCET). McCabe *et al.* (2008) conducted a three-dimensional FEA to assess the ability of PLAXIS 3D Foundation to simulate the column installation process using cavity expansion.

The change in the stress state of the soil due to column installation may be predicted by an undrained CCE formulation developed by Gibson & Anderson (1961). As the poker expands a hole from an initial diameter of zero to the final diameter of a constructed stone column, the lateral strain is effectively infinite. Consequently, Egan *et al.* (2008) state that it is necessary to assume cavity expansion pressure reaches its limit value (p_{lim}) in order to accurately simulate column installation effects.

The relationship between cavity pressure and lateral expansion is derived from CCET and is shown in Figure 3.11, where the cavity pressure (p) is normalised by the limit pressure and the current borehole radius (a) is normalised by the initial radius (a_0). It can be seen that considerable lateral expansion is required to reach the limit pressure.

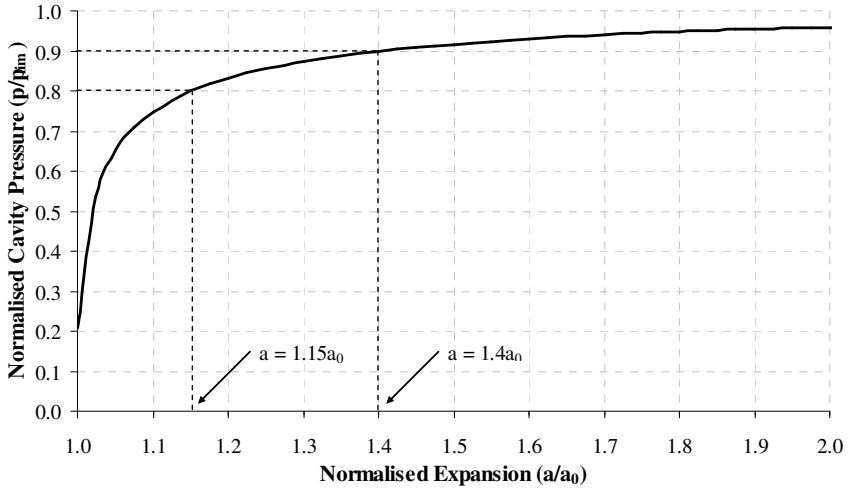

Figure 3.11 - Variation of cavity pressure with radius (undrained CCE) (McCabe *et al.*, 2008)

McCabe *et al.* (2008) simulated the lateral expansion of a 600 mm diameter column in the Bothkennar soil profile using PLAXIS 3D Foundation. The Mohr Coulomb and Hardening Soil models were adopted to simulate the behaviour of the stone column and soil, respectively. Various degrees of lateral expansion were applied (a/a_0 = 1.03, 1.06, 1.1, 1.33, 1.67) and the excess pore pressure and radial stress in the soil were measured at mid-depth along a 5 m long column.

The variation of excess pore pressure and radial stress with normalised radial distance from the centre of the stone column is shown in Figures 3.12(a) and 3.12(b), respectively. The excess pore pressure and radial stress is also compared with theoretical curves, developed by Randolph *et al.* (1979b) and Gibson & Anderson (1961), respectively. Two curves are

presented for radial stress in Figure 3.12(b); the first curve corresponds to limit pressure in the expanding cavity (i.e. field conditions) and the second curve corresponds to the actual lateral expansion applied in the numerical analysis.

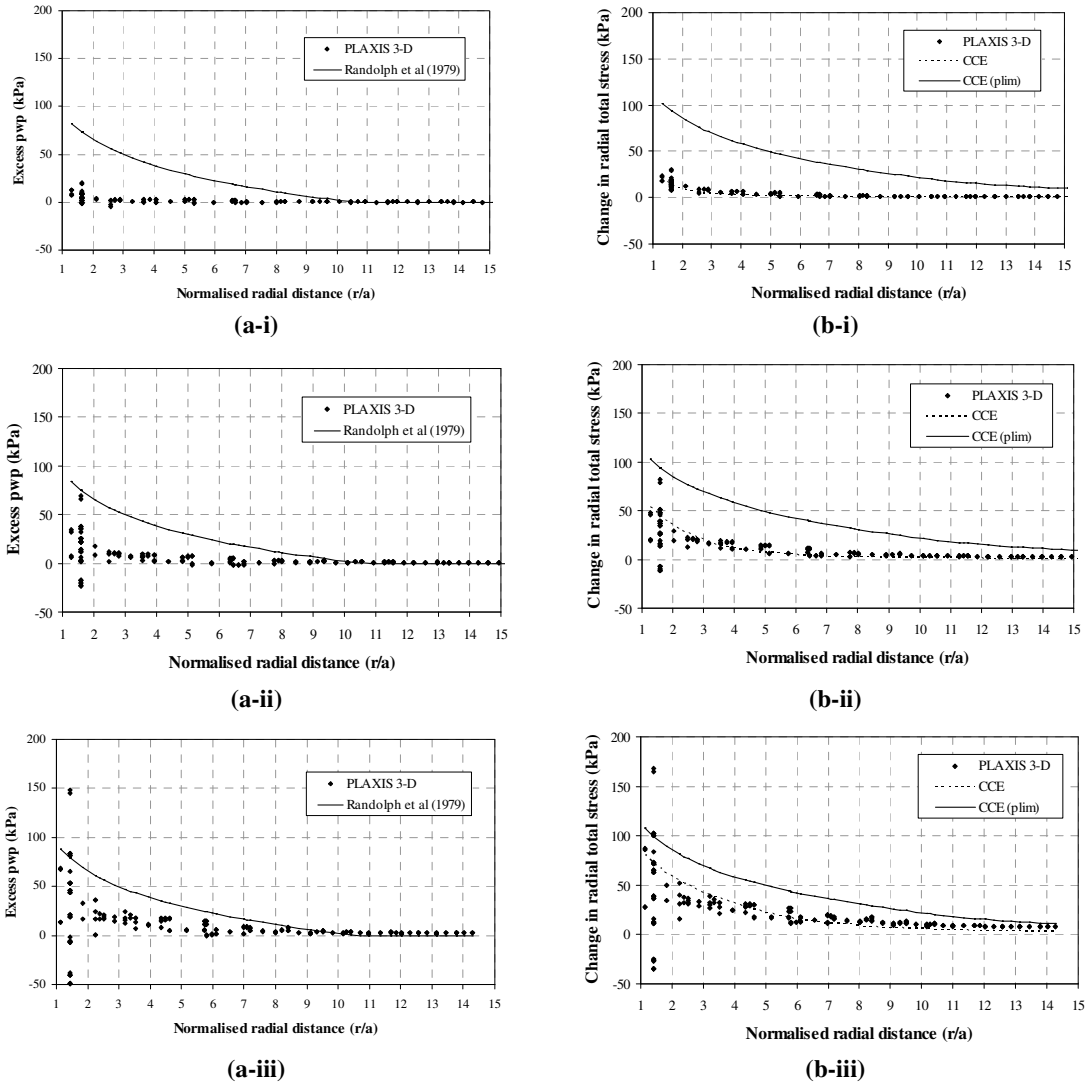

Figure 3.12 - Variation of (a) Excess pore pressure (pwp) and (b) total radial stress with normalised radial distance for lateral expansions (a/a_0) of (i) 1.03, (ii) 1.1 and (iii) 1.33 (McCabe *et al.*, 2008)

It can be seen in Figure 3.12 that PLAXIS 3D Foundation data tends towards the p_{lim} curve as lateral expansion increases. It can also be seen that PLAXIS 3D Foundation captures the variation of radial stress with radial distance from the stone column quite well. However, a large scatter for excess pore pressure and radial stress is evident, especially for $a < r < 2a$. The level of scatter increases with lateral expansion and would not be acceptable at the level required to reach p_{lim}. Furthermore, the lateral extent of the scatter precludes this technique

for simulating the installation effects of groups of stone columns. The results suggest that PLAXIS 3D Foundation is currently incapable of simulating the column installation process by applying large strain cavity expansions. An approximate technique to increase the stress state of the soil by increasing the coefficient of horizontal stress (K_0) is recommended by the authors and this is investigated in chapter 5.

Chapter 4
Development and validation of soft soil profile

4.1 Introduction

The FEM is a powerful investigative tool which has many advantages over laboratory experiments and large scale field tests. However, the FEM is still an approximate technique which idealises real-life situations into a set of continuum components and adopts constitutive models to simulate soil behaviour. As a result, it is necessary to validate the output of the FEM to ensure that the real-life situation is accurately modelled.

The ability of PLAXIS 3D Foundation to accurately capture the settlement performance of stone columns is validated by simulating three field load tests, described by Mitchell & Huber (1985). The load tests were conducted on single columns within a large group, which are founded in a layered estuarine deposit. The predicted load-settlement curves are compared with observed field data and also with two independent axisymmetric FE simulations of the field tests, which also allows the merits of a three-dimensional FEA to be evaluated.

The main aim of this thesis is to examine the behaviour of small groups of stone columns in soft clay. A model of the soft soil profile at the well-characterised Bothkennar test site is developed (using the Hardening Soil model in PLAXIS) in this chapter. The Bothkennar test site consists of a soft uniform clay, which is overlain by a stiff crust and is representative of many sites where the applicability of stone columns is of growing interest. The adopted soil profile and material parameters are validated by back-analysing a load test on an unreinforced rigid pad footing at the Bothkennar test site, described by Jardine *et al.* (1995).

Finally, the accuracy of PLAXIS 3D Foundation to predict the settlement performance of stone columns in the Bothkennar soil profile is examined. The settlement performance of an infinite grid of columns is simulated and compared against one-dimensional compression

theory, a settlement improvement database (collated by McCabe *et al.*, 2009) and a selection of analytical design methods.

4.2 Description of load tests in a layered estuarine deposit

4.2.1 Background

In 1976 the vibro replacement technique was used to support a waste water treatment plant located in Santa Barbara, California. Over 6500 stone columns were installed at the site in what was the first major application of the vibro replacement technique along the west coast of America (Mitchell & Huber, 1985). The vibro replacement technique was preferred to traditional foundation solutions such as piling and 'remove and replace' as it generated less noise and required less construction time. The technique also offered the extra benefit of reducing the liquefaction potential of the site, which is located in a seismically active area. The settlement performance of the stone column foundations was assessed by conducting 28 load tests on individual columns within large groups of columns as construction proceeded. The field tests are described in detail by Mitchell & Huber (1985) who also conduct an axisymmetric FEA to simulate the field load tests and to predict the long term settlements of the wastewater treatment plant.

4.2.2 Description of site conditions

The site is adjacent to the Pacific Ocean and is located in a historic tidal estuary. The upper 1–3 m is a recent fill of clayey sand containing wood, masonry, rubble, asphalt, glass and metal in variable concentrations. The recent fill is underlain by soft estuarine deposits which increase in thickness from 5–16 m across the site. The estuarine deposits consist of inter-layered silty and sandy clay to clayey and silty sand, with occasional layers of sandy silt. Some layers and lenses of sand, with minor amounts of gravel are locally present, usually in the lower portions of the deposits. The estuarine deposits are underlain by older marine deposits, which are thought to extend to 600 m. These deposits consist of clayey sand and silty sand, with lesser amounts of sandy clay and sandy silt. The ground water level is located at 1.5 m below the ground surface.

4.2.3 Stone column design & construction

The stone columns were formed using the 'wet' system, whereby a poker penetrated the soil with the aid of water jets. A controlled quantity of stone was tipped into the resulting borehole and the poker was re-lowered to compact the stone and force it laterally into the surrounding soil. This process of adding and compacting stone was repeated until a stone column, which was tightly inter-locked with the surrounding soil, was formed up to the ground surface. The final diameter of stone columns ranged from 0.81–1.22 m, with an average of 1.07 m. The stone columns were installed on square or rectangular patterns and spacing ranged from 1.2 m × 1.5 m in the most heavily loaded areas to 2.1 m × 2.1 m in areas between buildings. The length of columns varied from 9–15 m across the site and all columns penetrated 0.3 m into the underlying older marine deposits.

4.2.4 Material parameters

Undisturbed soil samples were obtained from various depths using thin walled Shelby tubes after column installation. Despite a large degree of variation within estuarine and marine deposits, Mitchell & Huber (1985) classify the samples as either cohesive or cohesionless, depending on whether the predominant soil type was clay or sand, respectively. The cohesionless soils were assumed to be free draining in the vicinity of the stone columns and were only subject to drained triaxial compression tests. The cohesive soils were not considered to be completely free draining and were subject to both consolidated undrained and drained triaxial tests; these tests were used to establish the short and long term behaviour of the cohesive soils, respectively. The gravel used for the stone columns was reconstituted into specimens and subjected to consolidated drained triaxial tests. Mitchell & Huber (1985) average the results of several triaxial tests and convert the results into parameters for the Duncan & Chang (1970) material model.

While the majority of the parameters for the Hardening Soil model can be readily converted from the Duncan & Chang (1970) material model, the latter model does not account for stress path dependency or formulate a cap yield surface. Therefore, it is necessary to define unload-reload (E_{ur}) and oedometric (E_{oed}) moduli for the soil layers. However, the settlement of the field load tests are insensitive to E_{ur} and E_{oed}, as the field load tests are monotonically loaded and do not develop large isotropic stresses (Elshazly *et al.*, 2008a). Therefore, practicable values of $E_{ur} = 5E_{50}$ and $E_{oed} = E_{50}$ are selected for the Hardening Soil model. A Poisson's

ratio $\upsilon = 0.2$ is adopted for both the estuarine and marine deposits, which yields reasonable lateral deformations and does not under-estimate final settlements.

Elshazly *et al.* (2008b) state that it is not appropriate to use high permeability values for the stone column and cohesionless layers as the column is infiltrated with silt and clay particles resulting from column installation and also as a large proportion of fine particles exist in the cohesionless layers. Accordingly, a vertical permeability $k_z = 10^{-5}$ m/s and 10^{-6} m/s is adopted for the stone columns and cohesionless soil layers, respectively. The vertical permeability for cohesive layers is within the range $10^{-8} < k_z < 10^{-7}$ m/s, as suggested by Lambe & Whitman (1979) for low liquid limit silts and clays. Elshazly *et al.* (2008b) adopt a ratio of horizontal to vertical permeability $k_x/k_z = 2$ and state that this ratio does not affect the settlement of the field load tests, as stone columns act as vertical drains and therefore reduce the influence of horizontal permeability.

A summary of the material parameters for the Santa Barbara wastewater treatment plant quoted by Elshazly *et al.* (2008b) are shown in Table 4.1. It should be noted that the failure ratio (R_f) for the cohesive marine deposit is different to the original value of $R_f = 0.84$ quoted by Mitchell & Huber (1985) and is possibly an error.

Table 4.1 - Material parameters for Santa Barbara wastewater treatment plant (Elshazly *et al.*, 2008b)

Parameter	Estuarine cohesive	Estuarine cohesionless	Marine cohesive	Marine cohesionless	Gravel
Dry unit weight, γ_d (kN/m^3)	15	15	17	17	18.6
Saturated unit weight, γ_{sat} (kN/m^3)	19	19	20	20	21.6
Cohesion, c' (kPa)	0	0	0	0	0
Angle of internal friction, φ' (°)	34	38	34	37	41
Poisson's ratio, υ	0.2	0.2	0.2	0.2	0.2
Secant Young's modulus, E_{50}^{ref} (kPa)	8500	17000	8700	12600	29200
Power for stress dependency, m	0.65	0.69	0.65	0.90	0.59
Reference pressure, p^{ref} (kPa)	100	100	100	100	100
Failure ratio, R_f	0.87	0.69	0.67*	0.67	0.86
Coefficient of vert. permeability, k_z (m/s)	1×10^{-8}	1×10^{-6}	1×10^{-8}	1×10^{-6}	1×10^{-5}
Coefficient of horiz. permeability, k_x (m/s)	2×10^{-8}	2×10^{-6}	2×10^{-8}	2×10^{-6}	2×10^{-5}

* Mitchell & Huber (1985) adopt $R_f = 0.84$

4.2.5 Field load tests

The settlement performance of single columns within large groups was assessed for various column spacings. The tests were conducted in accordance with ASTM D1194-72, with a 1.2 m deep circular concrete slab used as a loading plate. The area of the concrete slab was equal to the tested area for each column and, therefore, increased with column spacing. The load

was applied in 45 kN increments once the settlement rate dropped to 0.25 mm/hr and was increased to a maximum of 350–400 kN, with the final load maintained for 6 hrs after the settlement rate slowed to 0.25 mm/hr. The criterion for increasing the vertical load at 0.25 mm/hr was arbitrarily chosen to reduce the length of the load tests and additional settlement would have occurred if a longer time increment was adopted (Mitchell & Huber, 1985). Therefore, the recorded load-settlement curves are not specific to fully drained conditions.

4.2.6 Axisymmetric FEA

Mitchell & Huber (1985)

Mitchell & Huber (1985) conduct an axisymmetric FEA to simulate field load tests for three configurations of stone columns: (i) 1.2 m × 1.5 m; (ii) 1.75 m × 1.75 m and (iii) 2.1 m × 2.1 m. The behaviour of the soil layers is captured using the hyperbolic model developed by Duncan & Chang (1970). While the thickness of the cohesive and cohesionless layers varied across the site, Mitchell & Huber (1985) assume a thickness of 1–2 m for the estuarine deposits and 1–2.4 m for the marine deposits, with approximately 60% more cohesionless soil in the older marine deposits (Figure 4.1). To account for the vibro-compaction effect due to column installation, K_0 was chosen as 1.0 and 0.5 for the estuarine deposits and older marine deposits, respectively. The presence of the large group of columns surrounding the centrally loaded column is accounted for by modelling cylindrical rings of stone columns in the FEA. The thickness of the rings is chosen to maintain a constant area replacement ratio. The rings of stone columns are concentrically spaced at column spacings for each arrangement.

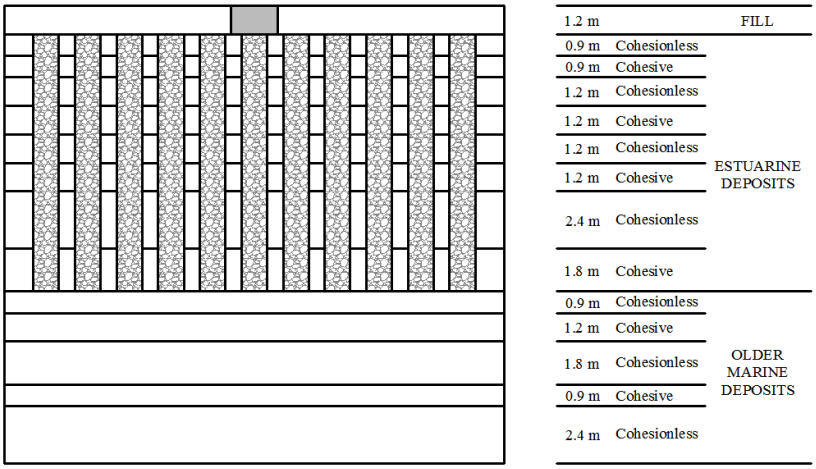

Figure 4.1 - Soil profile for Santa Barbara waste water treatment plant (columns spaced at 1.75 m x 1.75 m)

Elshazly et al. (2008b)

Elshazly *et al.* (2008b) also conduct an axisymmetric FEA similar to Mitchell & Huber (1985), but adopt the more advanced Hardening Soil model and account for the presence of the surrounding group of columns differently. The presence of the columns is again accounted for by modelling cylindrical rings and varying the thickness of the rings to maintain a constant area replacement ratio. However, the spacing between the concentric rings is an average of the distance to the orthogonal and diagonal columns (Figure 4.2).

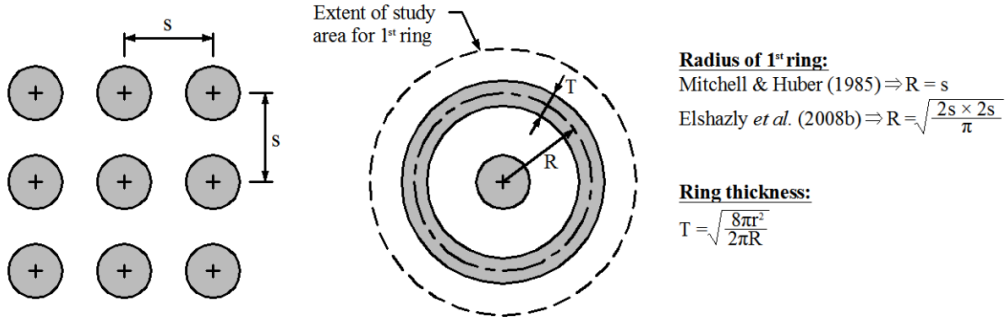

Figure 4.2 - Conversion of surrounding stone columns into a cylindrical ring for axisymmetric FEA

4.3 Simulation of load tests in a layered estuarine deposit

As part of this thesis, the field load tests described by Mitchell & Huber (1985) were simulated for the first time using a three-dimensional FEA in PLAXIS 3D Foundation. Similar to Elshazly *et al.* (2008b), the Hardening Soil model is adopted in conjunction with the material parameters outlined in Table 4.1 - with the exception of the failure ratio (R_f) for the cohesive marine deposit, which was selected as $R_f = 0.84$, in keeping with the original reference Mitchell & Huber (1985). The three-dimensional analysis accurately captures the confinement effect of the surrounding columns, rather than approximating their presence by cylindrical rings. A constant length L = 11.1 m and diameter d = 1.07 m was adopted for the field load tests. The FE mesh for columns spaced on a 1.75 m × 1.75 m grid is shown in Figure 4.3.

The behaviour of the soft clay is modelled using methods (i) and (ii), as outlined in Section 3.4.1. The loading process is accounted for in method (i) by applying the load in 45 kN increments and allowing the soil to consolidate until the settlement rate dropped below 0.25 mm/hr. The extra settlement due to the pause periods can be seen as vertical drops in the load-settlement curves shown in Figure 4.4. In contrast all the layers are assumed to behave in a drained manner for method (ii) and do not develop excess pore pressures.

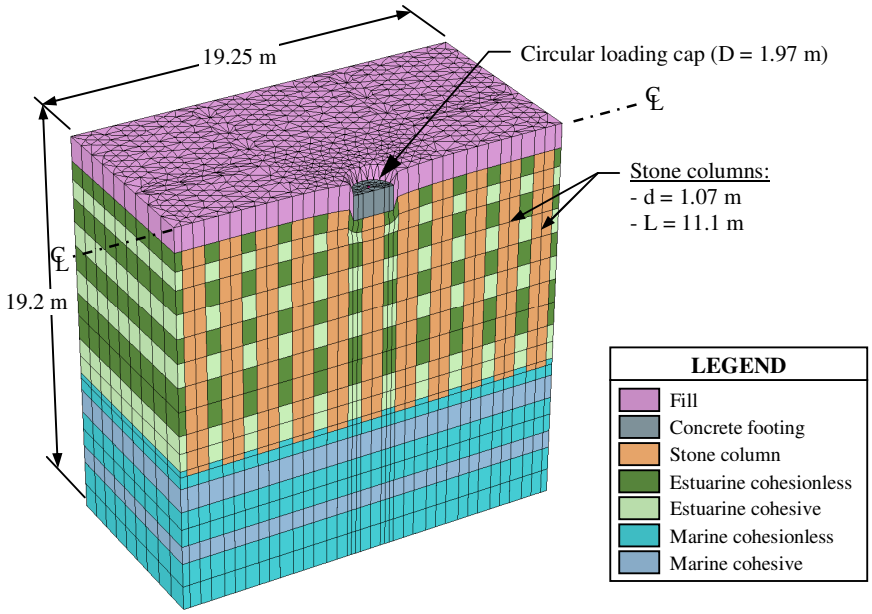

Figure 4.3 - FE mesh for 1.75 m × 1.75 m grid of columns

4.3.1 Comparison of PLAXIS 3D Foundation with field records and axisymmetric FEA

The observed load-settlement curves from the 28 field load tests and numerical simulations are shown in Figure 4.4. A large degree of variation is observed in the field load tests, which Mitchell & Huber (1985) attribute to the non-uniformity of soil properties in the estuarine deposits and the variable depth to older marine deposits.

It can be seen in Figure 4.4 that all the numerical analyses over-predict the load-settlement response from the field tests and this becomes more pronounced as column spacing decreases. The distribution of fine particles throughout the soil profile is quite varied and Mitchell & Huber (1985) state that soil layers defined as cohesionless may have contained enough fine particles to prevent free drainage during the short duration of the load tests. This would explain the stiffer response of the observed field measurements.

A comparison of the two axisymmetric analyses reveals that Mitchell & Huber (1985) tend to predict less settlement than Elshazly *et al.* (2008b), especially for closely spaced columns. This may be explained as Mitchell & Huber (1985) position the cylindrical rings of stone columns at radii equal to the orthogonal distance between columns, while Elshazly *et al.* (2008b) position the cylindrical rings of stone columns at radii equal to average distance between orthogonal and diagonal columns (Figure 4.2). In addition, both analyses are based on different material models, as Mitchell & Huber (1985) adopt the Duncan & Chang (1970)

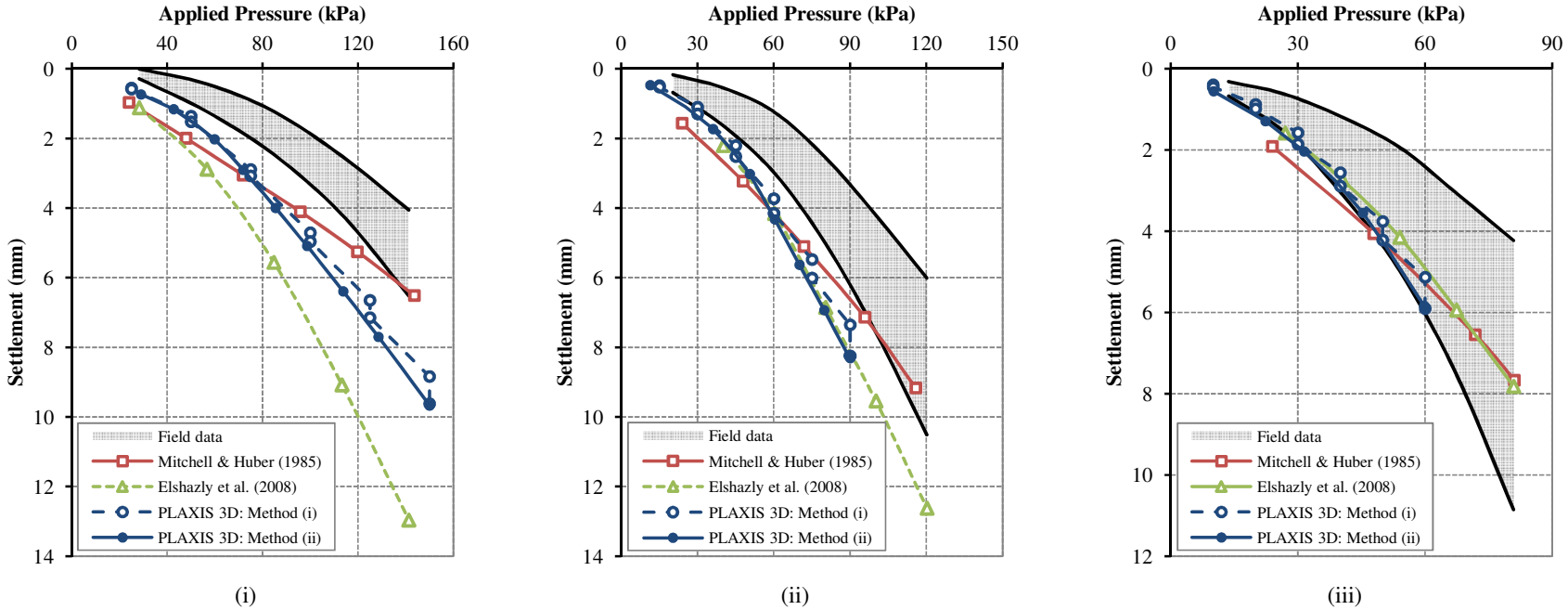

Figure 4.4 - Comparison of field load test data with numerical simulations for columns spaced on (i) 1.2 m × 1.5 m, (ii) 1.75 m × 1.75 m and (iii) 2.1 m × 2.1 m

hyperbolic model and Elshazly *et al.* (2008b) adopt the more advanced Hardening-Soil model. It can be seen that Mitchell & Huber (1985) tend to predict less settlement as the applied load increases. This may be attributed to the limitations of the hyperbolic model, which is based on the theory of elasticity.

The presence of the surrounding columns and the material model are two important factors to consider when modelling the load-deformation behaviour of stone columns. PLAXIS 3D Foundation appears to capture the load-settlement response of the columns closet to the field data (Figure 4.4). This is most noticeable for closely spaced columns and reflects the accurate modelling of the surrounding columns at discrete locations, rather than approximating their presence by cylindrical rings. This highlights the advantage of PLAXIS 3D Foundation over the axisymmetric analyses.

It can also be seen in Figure 4.4 that methods (i) and (ii) predict very similar load-displacement curves. This indicates that the excess pore pressures generated in the cohesive layers from the undrained loading in method (i) are almost fully dissipated by the time the next load increment is applied. This may be due to the short drainage length to the cohesionless layers and to the presence of the stone columns which reduce the radial drainage length. The close agreement between both methods gives confidence to the use of method (ii) for the subsequent FEA.

4.4 Development of Bothkennar soil profile

4.4.1 Description of Bothkennar test site

The Bothkennar test site is located on the south side of the Firth of Forth, near Grangemouth in Scotland (Figure 4.5). The site was purchased in 1987 by the Science, Engineering and Research Council as the national test site for soft soil engineering in the UK. The site primarily consists of soft uniform clay, commonly referred to as Carse clay, which is extensively characterised in Geotechnique (1992). The Carse clay was deposited in a stable marine environment and its thickness ranges from 13–19 m across the site. The Carse clay rests upon Bothkennar gravel and is overlain by a 1.5 m stiff crust. Piezometers indicate that the ground water level is hydrostatic and varies from 0.5–1.0 m below ground level (Hight *et al.*, 1992).

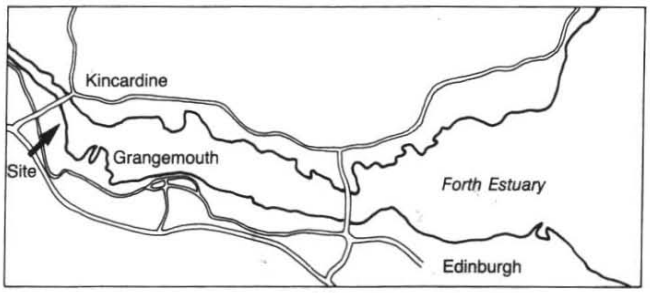

Figure 4.5 - Bothkennar test site location (Nash *et al.*, 1992a)

4.4.2 Soil classification and initial stress state

The soil at the Bothkennar test site was classified by Nash *et al.* (1992a) following a range of index tests, which are presented in Figure 4.6. The moisture content increases from 30% in the crust to 80% at 8 m and then decreases to 40% above the gravel layer. The Atterberg limits are also shown in Figure 4.5 and when plotted on the plasticity chart indicate that the soil is an inorganic clay of high plasticity. However, in accordance with BS 5930, and following findings by Paul *et al.* (1992) that the clay fraction of the soil varies from 35–50%, the soil is classified as a silty clay. The organic content was found by loss on ignition at 425°C and ranges from 3–8%. The bulk density varies from 1600–1800 kg/m^3 and the adopted profile for all subsequent FEA is shown in Figure 4.6.

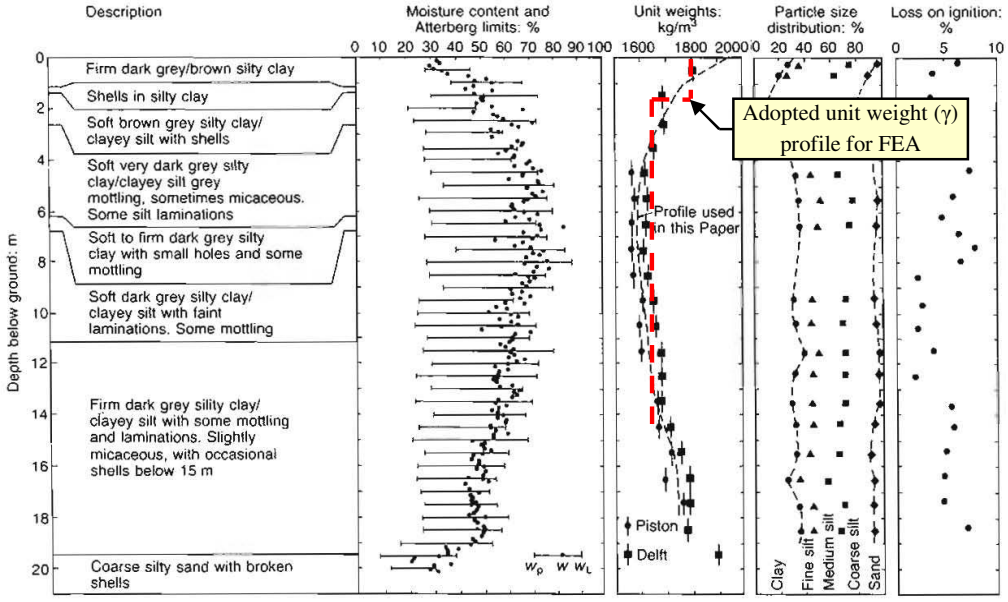

Figure 4.6 - Geotechnical profile at Bothkennar test site (Nash *et al.*, 1992a)

Hight *et al.* (1992) suggest that post depositional processes such as erosion, changes in groundwater levels and bonding occurred at the Bothkennar test site. According to the

geological history a maximum drop of 15 kPa in effective overburden pressure could have occurred at the Bothkennar test site. This implies that over-consolidation ratios should be high in the upper layers of the Carse clay and reduce with depth. The over-consolidation ratio determined on the basis of this stress history is compared with data from incremental load tests by Nash *et al.* (1992a) in Figure 4.7, where yield stress ratio is equivalent to over-consolidation ratio. While the profile agrees favourably in the upper layers, it under predicts the over-consolidation ratio below 4 m where a constant value of 1.55 better represents the actual stress state. It is suggested that the soil below 4 m may be influenced by ageing, which accounts for the observed over-consolidation ratio being larger than that due to the stress history. The profile adopted for all subsequent FEA is shown in Figure 4.7 where the over-consolidation ratio based on a 15 kPa drop in effective overburden pressure defines the upper 2.5 m of the soil profile and a constant over-consolidation ratio of 1.5 defines the soil below this level.

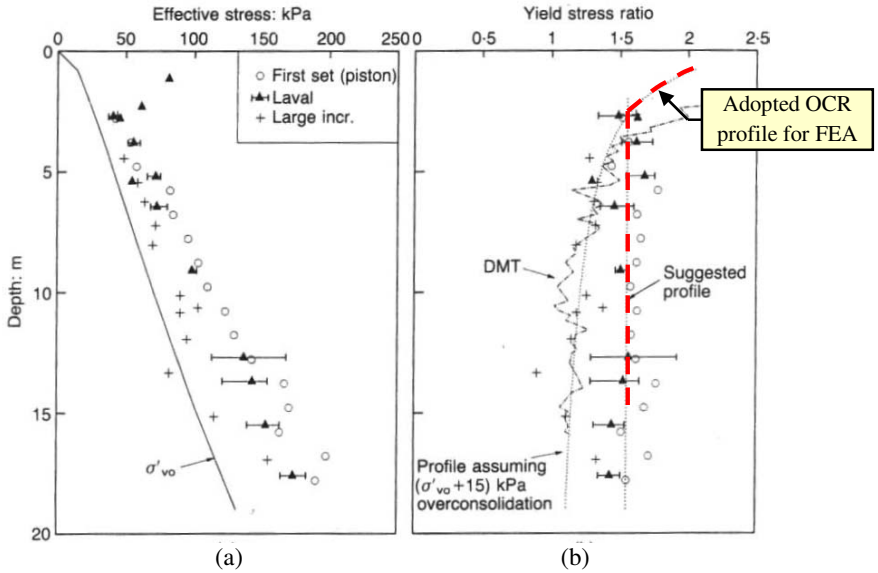

Figure 4.7 - (a) Yield stress and (b) yield stress ratio from incremental load consolidation tests (Nash *et al.*, 1992a)

The profiles of the lateral total stress measured *in situ* and the coefficient of lateral earth pressure (K_0) with depth are presented by Nash *et al.* (1992a) in Figures 4.8(a) and 4.8(b), respectively. The coefficient of lateral earth pressure was determined from a self-boring pressuremeter, spade cells and dilatometer tests. The coefficient of lateral earth pressure is high in the upper layers, which Hight *et al.* (1992) state is consistent with recent groundwater fluctuations, and decreases to 0.6–0.9 in the lower Carse layers. The distribution of horizontal stress with depth adopted for the FEA is shown in Figure 4.8.

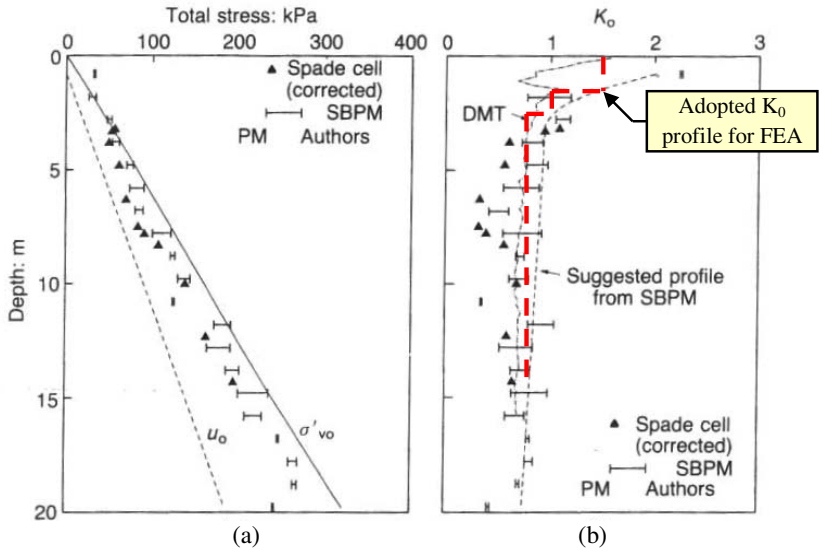

Figure 4.8 - Variation of (a) lateral total stress (b) K_0 with depth (Nash *et al.*, 1992a)

4.4.3 Strength characteristics

The strength characteristics of reconstituted Carse clay were investigated by Allman & Atkinson (1992). Samples were removed from depths between 3.5–6.5 m, reconstituted and formed into a slurry 1.25 times the liquid limit. The slurry was then one-dimensionally consolidated and transferred to the triaxial cell for testing, where the samples were one-dimensionally compressed or swelled to normally-consolidated or slightly over-consolidated states before shearing. Most samples reached well defined constant stress ratios ($M = q/p'$) at shear strains above 15%. The critical stress ratios, which correspond to zero rate of dilation, are $M_c = 1.38$ and $M_e = 1.00$ for compression and extension, respectively. These critical stress ratios are equivalent to critical state friction angles of $\varphi_c = 34°$ and $\varphi_e = 37°$ for compression and extension, respectively. These friction angles are larger than would be expected for a high plasticity clay but this is attributed to the large proportion of angular silt particles present in the Carse clay. While no effective cohesion was observed in the tests, a nominal value of 1 kPa and 3 kPa was adopted for the Carse clay and crust, respectively, to ensure numerical stability in all the subsequent FEA. A higher value of cohesion is adopted for the crust as overburden stresses are lowest in this layer and the stress state is therefore closer to the Mohr Coulomb yield surface.

4.4.4 One-dimensional stiffness properties

Nash *et al.* (1992b) undertook a comprehensive study to examine the one-dimensional stiffness behaviour of Carse clay. Samples were recovered from the ground at various depths and were subject to a series of incremental load, constant rate of strain and restricted flow tests. The majority of the tests were incremental load tests, conducted in a fixed ring oedometer cell, which were used to establish the voids ratio (e) and coefficient of compressibility (C_C) with depth. On the basis of the oedometer results from standard incremental load tests, the soil profile at the Bothkennar test site is divided into a crust, upper and lower Carse clay layers, as shown in Figure 4.9.

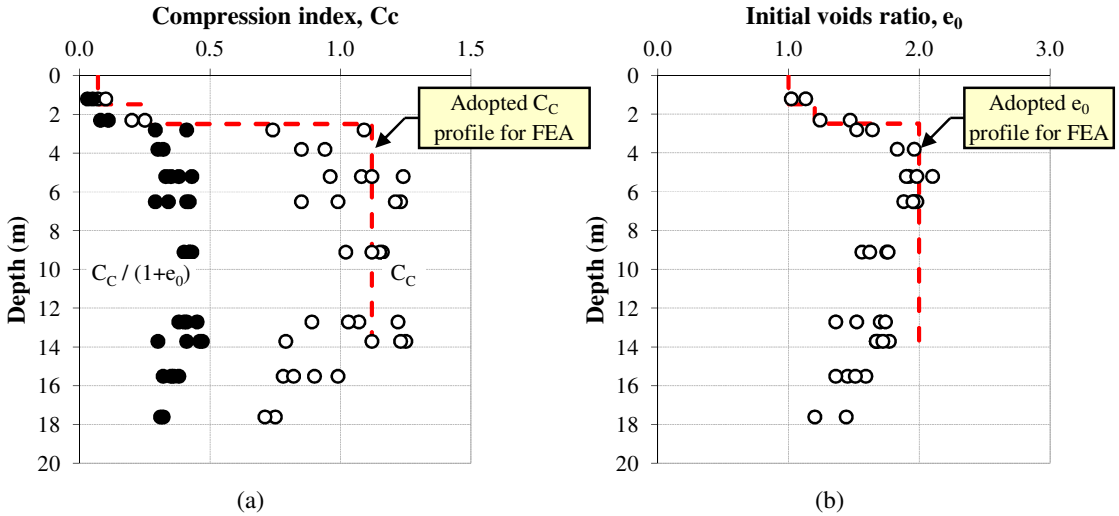

Figure 4.9 - Variation of (a) compression index C_c and (b) initial voids ratio e_0 with depth (Nash *et al.*, 1992b)

The behaviour of the samples prior to yielding was not routinely measured by Nash *et al.* (1992b). However, Allman & Atkinson (1992) also investigated the stiffness behaviour of reconstituted Carse clay and found the slopes of the normal compression (λ) and swelling (κ) lines to be 0.181 and 0.025, respectively. The ratio between these indices (λ/κ = 7.2) was used to determine the coefficients of swelling (C_S) from the one-dimensional data presented by Nash *et al.* (1992b), i.e. $\lambda/\kappa = C_S/C_C = 7.2$. The one-dimensional stiffness parameters are converted into three-dimensional parameters for the Hardening Soil model using the following expressions (Brinkgreve & Broere, 2006):

$$E_{oed}^{ref} = \frac{2.3(1+e_0)p^{ref}}{C_C} \quad \textbf{(4.1)}$$

$$E_{ur}^{ref} = \frac{2.3(1+e_0)(1+\nu)(1-2\nu)p^{ref}}{C_S(1-\nu)} \quad \textbf{(4.2)}$$

It is expected that the influence of the stiff crust will, to a certain extent, mask the behaviour of stone columns in the upper sections, i.e. prevent bulging. In addition, the stiff crust will absorb a higher proportion of the applied load and thus minimise the influence of elevated stress levels beneath the edge of rigid footings. However, the stiff crust is an important feature of soft soil stratigraphy; for example, the soil profile at Kinnegar, Belfast consists of soft Belfast *'sleech'* overlain by relatively stiff layers of fill and silty sand (McCabe, 2002). Therefore, the presence of the stiff crust will yield a more realistic analysis of the settlement performance and deformational behaviour of small groups of stone columns.

4.4.5 Permeability and consolidation coefficients

The hydraulic conductivity characteristics were examined by Leroueil *et al.* (1992) using various laboratory and *in situ* tests. The self boring permeameter gives the most realistic profiles and indicates that the horizontal hydraulic conductivity (k_{h0}) increases from 1.2×10^{-9} m/s at 3 m to 2.1×10^{-9} m/s at 6 m and then decreases to 7.5×10^{-10} m/s at 15 m. The vertical hydraulic conductivities (k_{v0}) observed from laboratory tests are lower than the equivalent horizontal values and an anisotropy ratio (k_{h0}/k_{v0}) of 1.5–2.0 was found. The variation of hydraulic conductivity (k) with voids ratio (e) was examined in order to define a hydraulic change index ($C_k = \Delta e/\Delta \log k$). This was found to be adequately defined by $C_k = 0.5e_0$.

A summary of the parameters developed for the Bothkennar test site is outlined in Table 4.2.

Table 4.2 - Summary of adopted material parameters for the Bothkennar test site

Soil Parameter	Crust	Upper Carse clay	Lower Carse clay
Depth (m)	0.0 – 1.5	1.5 – 2.5	2.5 – 14.5
Bulk unit weight, γ (kN/m^3)	18.0	16.5	16.5
Over-consolidation ratio	-	-	1.5
Pre-overburden stress (kPa)	15	15	-
Coefficient of lateral earth pressure, K_0	1.5	1.0	0.75
Effective cohesion, c' (kPa)	3	1	1
Angle of internal friction, φ (°)	34	34	34
Initial voids ratio, e_0	1.0	1.2	2.0
Compression index, C_C	0.07	0.25	1.12
Swelling index, C_S	0.01	0.03	0.16
Reference pressure, p^{ref} (kPa)	13	20	30
Vert. coefficient of permeability, k_{vert} (m/day)	6.9×10^{-5}	6.9×10^{-5}	6.9×10^{-5}
Horz. coefficient of permeability, k_{horz} (m/day)	1.0×10^{-4}	1.0×10^{-4}	1.0×10^{-4}

4.5 Validation of Bothkennar soil profile

4.5.1 Description of field load test

The bearing capacity and load-displacement behaviour of two rigid pad footings was investigated at the Bothkennar test site by Jardine *et al.* (1995). The short and long term behaviour of the footings was examined as the first footing (Pad A) was loaded to failure and the second footing (Pad B) was loaded to 67% of the ultimate bearing capacity of Pad A. The loading rate is shown in Figure 4.10 and it can be seen that Pad A was loaded to failure in a short space of time while Pad B continued as a maintained load test for more than 2 years. The loading was applied using kentledge blocks; pauses in the loading rate occurred overnight and whenever the settlement rate exceeded 8 mm/hr. The footings were founded at 0.8 m below ground level and Pads A and B were 2.2 m and 2.4 m in width, respectively.

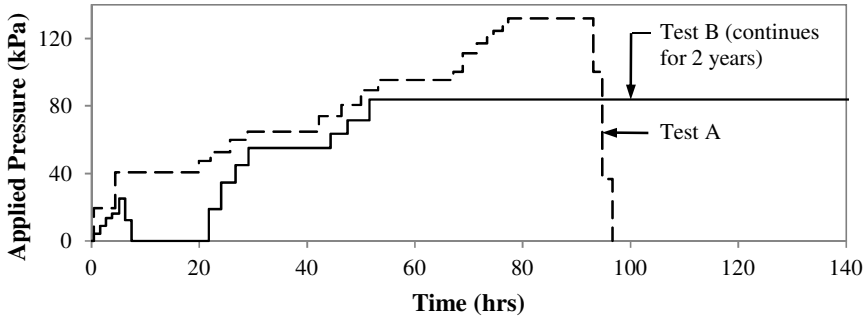

Figure 4.10 - Variation of load with time (Jardine *et al.*, 1995)

The footings were instrumented with pneumatic piezometers, spade cells, inclinometers and magnetic extensometers. The surface settlement was measured with a precise level, giving a nominal resolution of 0.1 mm. In total ten targets were set into the concrete pads and 16 targets were augured into the surrounding soil.

4.5.2 Simulation of field load test with PLAXIS 3D Foundation

The load test on Pad A was simulated with PLAXIS 3D Foundation as an undrained loading due to the short duration of the load test. Consequently, the Carse clay layers were specified to behave in an undrained manner. However, the upper layers of the Bothkennar test site consist of a weathered crust underlain by a shelly layer (Nash *et al.*, 1992a). These layers are combined together to form the *crust* in the adopted soil profile. As the ground water level varies from 0.5–1.0 m below ground level and the lower portion of the crust consists of a shelly layer, it was deemed appropriate to model the *crust* as a drained material.

The load test on Pad B was not simulated with PLAXIS 3D Foundation as this load test contained an unload-reload loop and the recorded footing displacement includes both primary and secondary settlement (Jardine *et al.*, 1995). The aim of this thesis is to examine the long term primary settlement response of small groups of stone columns supporting pad footings. In addition, the Hardening Soil model does not account for secondary settlement and is therefore unable to accurately simulate the load test on Pad B.

4.5.3 Comparison of PLAXIS 3D Foundation with field measurements

The load-displacement behaviour of Pad A recorded by Jardine *et al.* (1995) is shown in Figure 4.11. Pad A reaches an ultimate bearing capacity of 138 kPa and the settlement at the end of the loading was approximately 190 mm. The simulated load-displacement curve from PLAXIS 3D Foundation is also shown in Figure 4.11. It can be seen that PLAXIS 3D Foundation predicts the settlement behaviour of Pad A quite well.

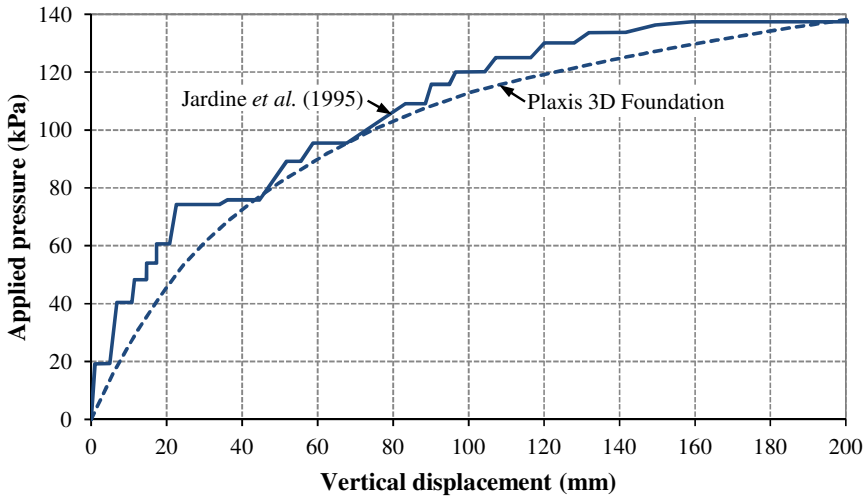

Figure 4.11 - Load-displacement behaviour for pad footings (Jardine *et al.*, 1995)

However, it appears that PLAXIS 3D Foundation slightly under-estimates the stiffness response of the field load test, especially at low applied pressures, which are of interest in this thesis. This may be attributed to increased soil stiffness at low strain levels, which is not accounted for in the Hardening Soil model. The stiffness parameters for the Hardening Soil model are determined from laboratory tests, where the specimens are subject to relatively large strain (Figure 4.12). PLAXIS 3D Foundation under-estimates the stiffness response of Pad A at low applied pressure, as shear strain is lowest at this load level.

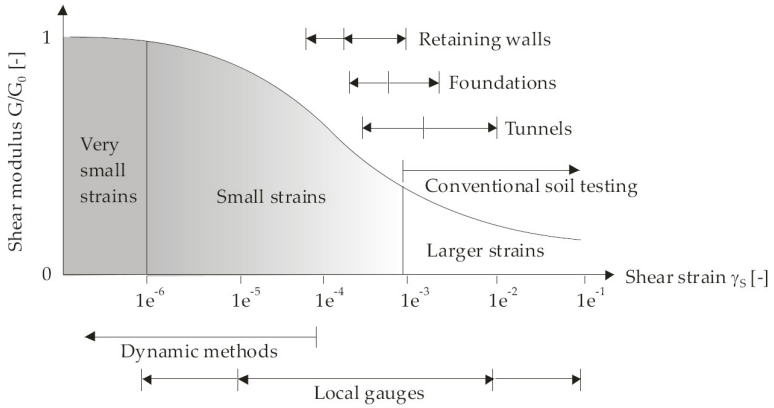

Figure 4.12 - Characteristic stiffness-strain behaviour of soil with typical strain ranges for laboratory tests and structures (after Atkinson & Sallfors, 1991)

Another contributing to the under-estimation of the stiffness response by PLAXIS 3D Foundation may be that the soil profile encountered by Jardine *et al.* (1995) at the test location is slightly different to the soil profile adopted for the FEA. It can be seen in Table 4.3 that Jardine *et al.* (1995) encountered a 0.3 m shelly layer and also that the Carse clay occurs at a shallower depth. The Carse clay would yield a relatively stiff response under undrained loading, which would result in a stiffer footing response.

Table 4.3 - Summary of soil profile to 7 m depth (Jardine *et al.*, 1995)

Stratum	Depth (m)	Soil type	Typical index parameters				
			< 2 μm (%)	w (%)	I_P (%)	I_L	γ (kN/m^3)
I	0.0 – 1.0	Weathered clayey silt crust	15	40	20	0.4	18.0
II	1.0 – 1.3	Shelly layer	Not applicable				
III	1.3 – 2.2	Soft clayey silt with some shell fragments	15	50	30	0.6	17.0
IV	2.2 – 7.0	Soft black silty clay with fine mottling and occasional silt laminae	20 – 40	60 – 75	30 – 50	0.6 – 1.0	15.5 – 16.5

In conclusion, it can be seen that PLAXIS 3D Foundation captures the settlement performance of the field load test in soft clay quite well. This is encouraging and validates the adopted soil profile and the choice of material parameters.

4.6 Simulation of an infinite grid of stone columns in Bothkennar

The settlement performance of an infinite grid of stone columns in the Bothkennar soil profile is simulated using PLAXIS 3D Foundation. A set of material parameters is developed for the stone backfill from previous numerical studies and field records. However, before these material parameters are validated, the settlement performance of an untreated widespread loading is compared with one-dimensional compression theory. This ensures that the

settlements, and not just the settlement improvement factors, are in the correct order of magnitude.

The settlement performance of an infinite grid of stone columns is then analysed over a typical range of A/A_C values presented in the settlement database by McCabe *et al.* (2009). The unit cell concept was adopted to simplify the analysis of an infinite grid of columns to one column and its surrounding zone of influence (see Section 2.5.1). Settlement improvement factors determined from PLAXIS 3D Foundation are compared with a settlement database of field tests (collated by McCabe *et al.*, 2009) and a selection of current analytical design methods.

The settlement performance of stone columns at the Bothkennar test site was determined at 50 kPa. The ultimate bearing capacity recorded by Jardine *et al.* (1995) for an unreinforced footing at the Bothkennar test site was 138 kPa (Figure 4.11). Applying typical factors of safety (2.5–3.0) yields allowable bearing pressures in the range of 46–55 kPa. Therefore, 50 kPa is deemed a typical working load for the Bothkennar test site.

4.6.1 Development of material parameters for stone backfill

The bulk unit weight for the stone backfill $\gamma = 1900$ kg/m^3 is representative of stone columns in soft soils and is similar to values adopted by Mitchell & Huber (1985), Domingues *et al.* (2007a) and Gäb *et al.* (2008). Coefficients of permeability in the vertical and horizontal direction of $k_y = k_h = 1.7$ m/day are adopted for the stone backfill, which are similar to the values adopted by Elshazly *et al.* (2008b).

The angle of internal friction adopted for stone columns $\varphi = 45°$ is chosen on the basis of findings by McCabe *et al.* (2009), who conducted a review of field tests on stone columns and found that $\varphi = 40°$ is conservative for columns formed using the bottom feed system. A nominal value for cohesion $c = 1$ kPa is adopted to ensure numerical stability. The angle of dilatancy is determined from the empirical relationship $\psi = \varphi - 30°$, developed by Bolton (1986). A positive angle of dilatancy ensures that columns dilate when subject to high stress ratios.

Barksdale & Bachus (1983) report that Young's moduli (E) for stone columns, which are back-calculated from measured settlements and recommended by other authors, typically range from 30–58 MPa. However, these values are specific to columns formed using the top feed system and may under-estimate Young's moduli for stone columns following the assertion by McCabe *et al.* (2009) that columns formed using the dry bottom feed system yield a better settlement performance. Consequently, a higher Young's modulus E_{50} = 70 MPa is adopted for the stone columns. A similar value was also adopted by Gäb *et al.* (2008), who conducted a numerical investigation of stone columns supporting an embankment in loose-medium compacted sand and weak clayey silt. The unload-reload Young's modulus E_{ur} = 210 MPa is also similar to Gäb *et al.* (2008) and its selection is based on the relationship ($E_{ur} = 3E_{50}$) proposed by Brinkgreve & Broere (2006).

4.6.2 Comparison of PLAXIS 3D Foundation with one-dimensional compression theory

The accuracy of PLAXIS 3D Foundation to predict the settlement of an untreated infinitely wide footing at the Bothkennar test site is compared with one-dimensional compression theory. The concrete footing is 0.6 m in thickness and is located 0.6 m below ground level. The initial stress state and one-dimensional stiffness parameters, as outlined in Sections 4.3.2 and 4.3.4, respectively, are used in conjunction with equations 4.3 and 4.4 to estimate the settlement of an infinitely wide footing (s_{uc}) at the Bothkennar test site.

If $\sigma'_{y,0} + \Delta\sigma'_y < \sigma'_{y,\,max}$:

$$s_{uc} = H\left[\frac{C_S}{1+e_0} log\left(\frac{\sigma'_{y,0} + \Delta\sigma'_y}{\sigma'_{y,0}}\right)\right] \quad \textbf{(4.3)}$$

If $\sigma'_{y,0} + \Delta\sigma'_y > \sigma'_{y,\,max}$:

$$s_{uc} = H\left[\frac{C_C}{1+e_0} log\left(\frac{\Delta\sigma'_{y,max}}{\sigma'_{y,0}}\right) + \frac{C_S}{1+e_0} log\left(\frac{\sigma'_{y,0} + \Delta\sigma'_y}{\sigma'_{y,max}}\right)\right] \quad \textbf{(4.4)}$$

where $\sigma'_{y,\,0}$ and $\sigma'_{y,\,max}$ = *in situ* and maximum vertical effective stress, respectively

The Bothkennar soil profile is divided into seven layers and the settlement is calculated on the basis of the vertical effective stress at the centre of each layer (Table 4.4). The settlement for each layer and the variation of settlement with depth is shown in Figures 4.13(i) and 4.13(ii), respectively. It can be seen in Figure 4.13(i) that a slight variation exists between PLAXIS 3D Foundation and one-dimensional compression theory for the settlement of each

layer with depth, which may be attributed to a difference in the definition of the cap yield surface. However, it is clear from Figure 4.13(ii) that PLAXIS 3D Foundation predicts the settlement response of an untreated infinitely wide footing at the Bothkennar test site quite well (normalised error for the total settlement is less than 3%).

Table 4.4 - Comparison of one-dimensional compression theory with PLAXIS 3D Foundation

		One-dimensional compression theory				PLAXIS 3D Foundation	
Layer	Thickness (mm)	$\sigma'_{v,0}$ (kPa)	$\sigma'_{v,max}$ (kPa)	$\sigma'_{v,0} + \Delta\sigma'_v$ * (kPa)	s_{uc} (mm)	$\sigma'_{v,0}$ (kPa)	s_{uc} (mm)
1	0.0 - 0.9	18	33	72	12	18	9
2	0.9 - 1.9	25	40	79	36	25	29
3	1.9 - 3.9	35	53	89	185	35	169
4	3.9 - 5.9	49	72	102	127	47	120
5	5.9 - 7.9	62	92	116	88	60	86
6	7.9 - 9.9	76	111	129	61	73	63
7	9.9 - 11.9	89	131	143	40	86	46
8	11.9 - 13.9	102	150	156	23	100	36
				Total settlement	572	*Total settlement*	558

* $\Delta\sigma'_y$ includes additional pressure due to weight of concrete, i.e. $\Delta\sigma'_y = 50 + 0.6\times(24-18) \approx 54$ kPa

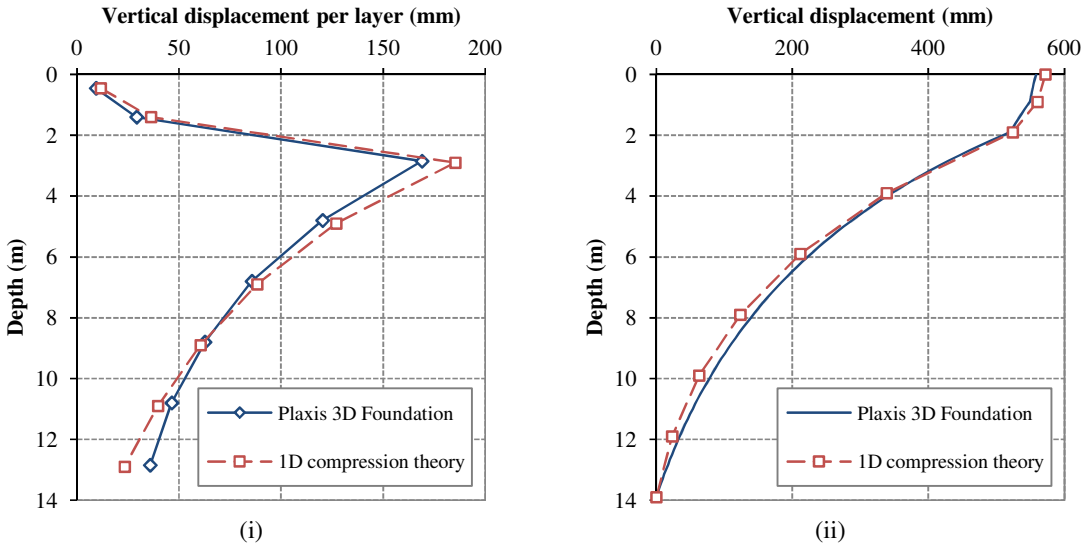

Figure 4.13 - Settlement profile of Bothkennar test site for wide area loading, calculated using one-dimensional compression theory and PLAXIS 3D Foundation

4.6.3 Comparison of PLAXIS 3D Foundation with settlement database

The results from the numerical analysis of an infinite grid of end-bearing columns are compared with a settlement database of field data collated by McCabe *et al.* (2009) in Figure 4.14. The field data agrees quite well with Priebe's (1995) basic design curve (n_0), assuming an angle of friction $\varphi = 40°$. It can also be seen in Figure 4.14 that while PLAXIS 3D Foundation captures the variation of settlement improvement factors (n) with area ratio (A/A_C) quite well, it tends to over-estimate the field data.

However, McCabe *et al.* (2009) suggest that settlement improvement factors for some of the case studies may have been under-estimated due to the following reasons:

(i) The time at which settlement was measured may not be consistent for all tests and untreated settlement may be under-estimated, as primary consolidation was not complete when the measurements were taken.

(ii) Not all of the field data are specific to end-bearing columns and, therefore, the measured settlement includes the settlement of the soil deposit underneath the base of columns.

The high n values predicted by PLAXIS 3D Foundation may also be related to the high compressibility of the lower Carse clay layer relative to the stone columns, i.e. high modular ratio (E_{col}/E_{soil}). Field experience suggests that E_{col}/E_{soil} typically ranges from 10–50 (Castro & Sagaseta, 2009). However, columns at the Bothkennar test site are formed in a soft clay with an average E_{col}/E_{soil} = 100 (see Figure 6.7) for the lower Carse clay layer. This is significantly higher than the upper limit suggested by Castro & Sagaseta (2009), but is not unrealistic as a finite element study by Barksdale & Bachus (1983) indicates E_{col}/E_{soil} up to 100 for columns formed in soft cohesive soil.

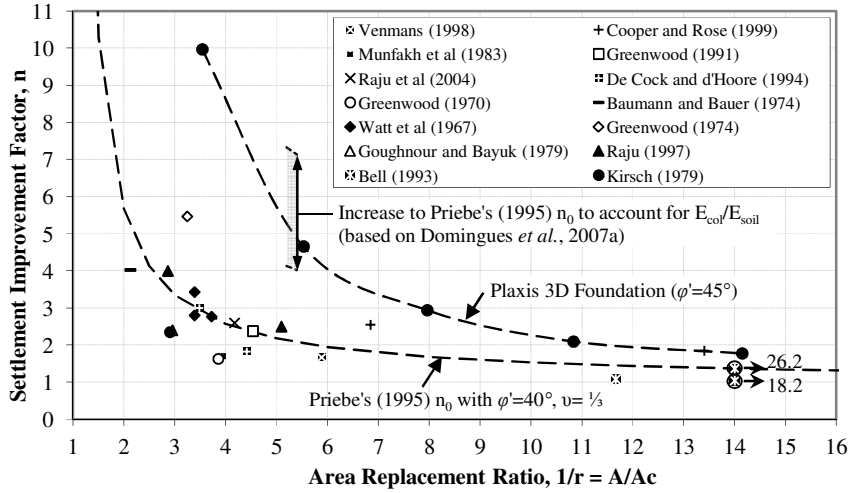

Figure 4.14 - Comparison of settlement improvement factors for an infinite grid of end-bearing columns with field data collated by McCabe *et al.* (2009)

A finite element study by Domingues *et al.* (2007a) shows that high E_{col}/E_{soil} leads to an increase in n values. The authors observed that increasing E_{col}/E_{soil} from 10 to 100 and from 40 to 100 yielded an increase of n values in the range 80–200%. These increases are applied to Priebe's (1995) basic design (n_0) and are shown in Figure 4.14. It can be seen that PLAXIS 3D Foundation agrees quite well with field data when adjusted for a high E_{col}/E_{soil}. This gives

confidence to the selection of the material parameters adopted for the stone backfill (see Section 4.6.1) and also the ability of PLAXIS 3D Foundation to predict the settlement performance of large groups of stone columns in soft clay.

4.6.4 Comparison of PLAXIS 3D Foundation with analytical design methods

The settlement performance of an infinite grid of stone columns from PLAXIS 3D Foundation is compared with various analytical design methods in this section. The analytical design methods chosen for comparison are Balaam & Booker (1981), Pulko & Majes (2005) and Priebe (1995). All of these design methods are based on the unit cell concept, which is consistent with the boundary conditions adopted for the numerical analysis. Analytical design methods are based on more simplified material models than those adopted by PLAXIS 3D Foundation and, consequently, it is necessary to adopt an initial stress state and a set of material parameters which are consistent with the numerical analysis.

Determination of initial stress state

The influence of the initial stress state upon the settlement performance of stone columns is taken into account by both Priebe (1995) and Pulko & Majes (2005):

- Priebe (1995) sets a minimum coefficient of lateral earth pressure $K_{0,soil} = 1.0$ to account for the effects of column installation. However, $K_0 > 1.0$ for the crust and upper Carse clay at the Bothkennar test site (see Section 4.3.2). Priebe (1995) is modified to account for higher K_0 values in the upper layers by changing the pressure difference causing bulging ($= K_{A,col}.\sigma_{col} - K_{0,soil}.\sigma_{soil}$) at the column-soil interface.
- Pulko & Majes (2005) do not specify a minimum K_0 and the K_0 profile developed in Section 4.3.2 for the numerical analysis is adopted for this design method.

The coefficients of lateral earth pressure and material parameters adopted for the stone backfill in the analytical design methods are outlined in Table 4.5.

Table 4.5 - Summary of material parameters for Bothkennar soil profile

	Soil		Stone backfill		
Depth (m)	Unit weight, γ (kN/m^3)	K_0	Unit weight, γ (kN/m^3)	φ (°)	ψ (°)
0.6 – 1.5	18	1.50	19	45	15
1.5 – 2.5	16	1.00	19	45	15
2.5 – 14.5	15	0.75*	19	45	15

*$K_0 = 1.0$ for Priebe (1995)

Determination of Young's moduli

The Hardening Soil model is adopted by PLAXIS 3D Foundation to simulate the behaviour of stone columns and the surrounding soil. This is an advanced constitutive model that accounts for the stress path and stress level dependency of soil stiffness. In contrast the more simplistic models adopted for the analytical design methods (i.e. Mohr-Coulomb) define the stiffness response of each soil layer with a constant Young's modulus. Therefore, the selection of appropriate stiffness parameters must take into consideration the stress path and stress level experienced by the stone column and the surrounding soil. These factors are discussed below:

(i) Consideration of the stress path

The Hardening Soil model accounts for the stress path dependency of soil by defining two stiffness moduli: (i) E_{50}, a secant modulus at 50% strength and (ii) E_{ur}, an unload-reload modulus. E_{50} is appropriate for primary loading of soils, while E_{ur} is used for excavation or tunnelling problems. The loading of an infinite grid of stone columns at the Bothkennar test site is considered as a primary loading and E_{50} is chosen to represent the stiffness response of the stone and surrounding soil in the analytical design methods.

(ii) Consideration of the stress level

Soils exhibit stress level dependency which results in an increasing stiffness with confining pressure. The relationship between soil stiffness and confining pressure is defined in equation 3.3 using a power law. The confining pressure is taken as the minor or major principal stress for triaxial or oedometer tests, respectively.

The parameter 'm' for the Bothkennar soil profile can be determined from one-dimensional stiffness data presented by Nash *et al.* (1992b). The values presented by Nash *et al.* (1992b) are converted into oedometric moduli (E_{oed}) using equation 4.1. The oedometric moduli are then normalised by the effective overburden stress ($\sigma'_{y,0}$), at the level which the samples were taken from the soil, and plotted against $\sigma'_{y,0}$ in Figure 4.15. In this case the major principal stress is adopted for the confining pressure as the samples are subject to oedometric tests. It can be seen for the lower Carse clay that $E_{oed}/\sigma'_{y,0}$ is constant with an increasing $\sigma'_{y,0}$, which suggests that E_{oed} is directly proportional to $\sigma'_{y,0}$. This indicates that m = 1 is appropriate for the lower Carse clay layer, which is consistent with Brinkgreve & Broere (2006) for soft soils. Insufficient data is available to determine the parameter 'm' for the crust and the upper

Carse clay and similar values to the lower Carse clay were adopted. A lower value of 'm' is more appropriate for the granular material and m = 0.3 is used for stone columns, which is similar to Gäb *et al.* (2008).

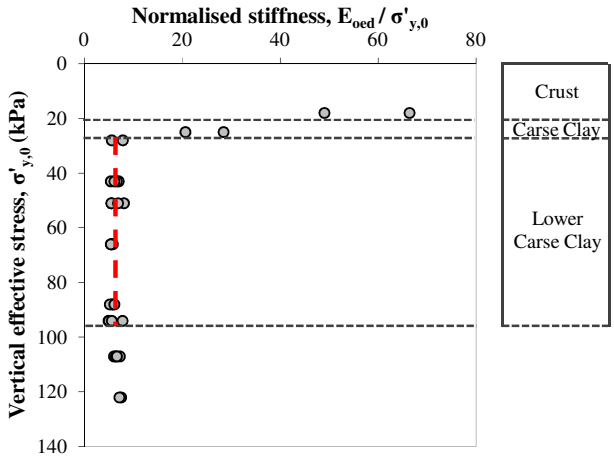

Figure 4.15 - Variation of normalised oedometric moduli with vertical effective stress for Bothkennar test site

While the parameter 'm' is now determined for the Bothkennar soil profile and stone columns, it is still necessary to define the confining pressure for stone columns in the field condition. A FEA conducted by Balaam & Booker (1985) indicates that columns are in a triaxial state of stress during loading. Therefore, the minor principal stress (σ_3) defines the confining pressure for the stone column. The surrounding soil also carries a proportion of the applied vertical load and, consequently, is compressed in vertical direction. As with stone columns, the minor principal stress is used to define the confining pressure for the surrounding soil.

The variation of minor principal stress with depth for stone columns and the surrounding soil is presented in Figure 4.16 for an infinite grid of end-bearing columns ($A/A_C = 3.5$). It can be seen that the average minor stress is slightly higher in the stone column, which may be explained as this material is stiffer than the surrounding soil and therefore takes more load. The average minor stress for each layer is tabulated in Table 4.6 and the resulting Young's moduli are determined from equation 3.3.

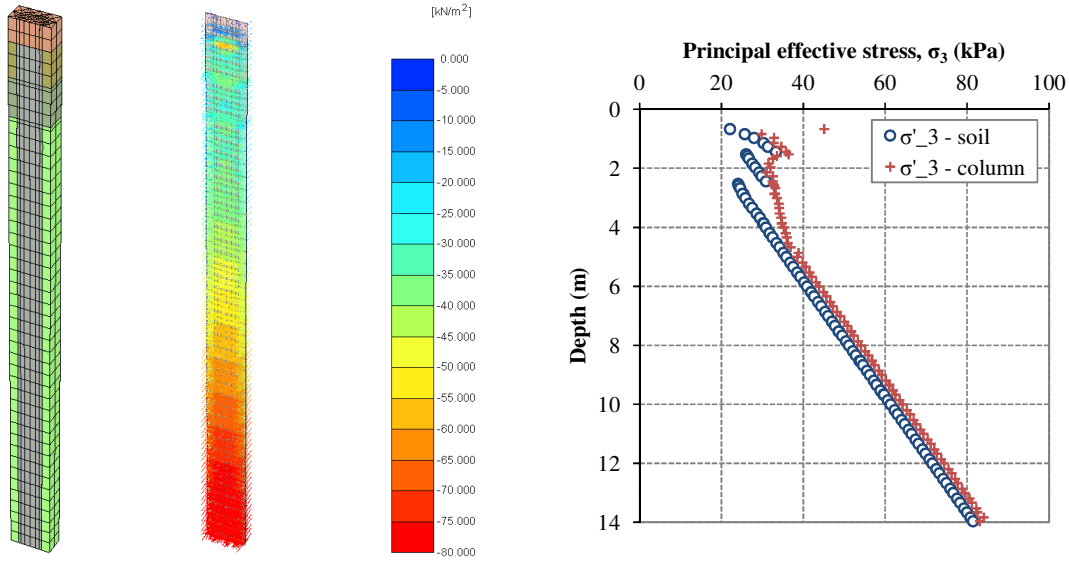

Figure 4.16 - Distribution of minor principal stress σ_3 in end-bearing stone column and surrounding soil (A/Ac = 3.5; L = 13.9 m; Infinite grid of columns)

Table 4.6 - Average minor principal stresses (σ'_3) and Young's moduli (E) for Bothkennar soil profile

	Soil				Stone backfill			
Depth (m)	σ'_{ref} (kPa)	E_{ref} (= E_{50}) (kPa)	σ'_3 (kPa)	E (kPa)	σ'_{ref} (kPa)	E_{ref} (= E_{50}) (kPa)	σ'_3 (kPa)	E (kPa)
0.6 – 1.5	13	1068	28	2304	100	70000	35	51215
1.5 – 2.5	20	506	28	703	100	70000	32	49848
2.5 – 14.5	30	231	53	410	100	70000	57	59120

Comparison of n values from PLAXIS 3D Foundation with analytical design methods

The settlement performance of an infinite grid of columns predicted by PLAXIS 3D Foundation is compared with the analytical design methods in Figure 4.17. It appears that PLAXIS 3D Foundation captures the variation of settlement improvement factors with area ratio quite well.

The design method proposed by Balaam & Booker (1981) significantly over-estimates the settlement performance of stone columns, which is due to the simplified assumption of linear elasticity for the stone backfill (Castro & Sagaseta, 2009). This design method is shown as it forms the basis of Pulko & Majes (2005) and, also, as it demonstrates that linear elasticity is not a valid assumption for stone columns.

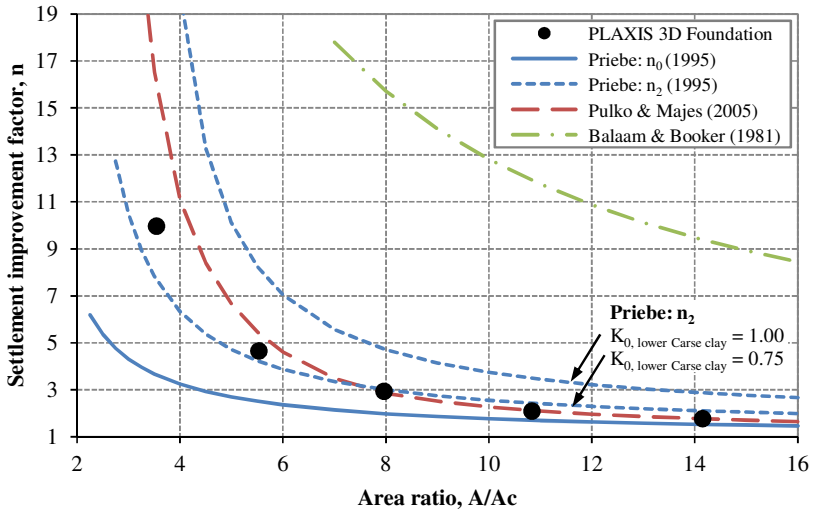

Figure 4.17 - Comparison of settlement improvement factors for an infinite grid of end-bearing columns with analytical design methods

The design method proposed by Pulko & Majes (2005) is an extension of Balaam & Booker (1981) which accounts for column yielding and, hence, predicts more realistic n values. While Pulko & Majes (2005) predicts a similar settlement performance to PLAXIS 3D Foundation for $A/A_C > 8.0$, it tends to over-predict n values at low A/A_C. This may be attributed to the assumption of rigid-plastic behaviour for stone columns by Pulko & Majes (2005), in contrast to elasto-plastic behaviour (i.e. Hardening Soil model) adopted in PLAXIS 3D Foundation. The main difference between these models is that the rigid-plastic model does not account for elastic strains developed when columns are in a plastic state. Therefore, the rigid-plastic model predicts less settlement, and thus higher n values, than the elasto-plastic model. The extent of plasticity becomes more pronounced for an infinite grid of columns at low A/A_C, as columns are better confined and can carry a larger proportion of the applied load. Consequently, the discrepancy between the rigid-plastic model and the elasto-plastic model is most pronounced at low A/A_C.

The basic (n_0) and modified (n_2) settlement improvement factors determined from Priebe (1995) are also shown in Figure 4.17. It appears that the basic design curve (n_0) under-estimates the settlement performance of stone columns. Priebe (1995) modifies the basic design curve to account for column compressibility and the effect of overburden stress, which leads to a significant increase in n values. The modified n_2 values agree favourably with the numerical analysis, although the settlement performance is slightly over-estimated. This over-estimation may be attributed to the assumption of $K_0 = 1$ for the lower Carse clay layer,

which is higher than that adopted in Pulko & Majes (2005) and PLAXIS 3D Foundation. Settlement improvement factors were re-calculated for Priebe (1995) n_2 with $K_0 = 0.75$ for the lower Carse clay layer. It can be seen that the re-calculated n values are very close to Pulko & Majes (2005) and PLAXIS 3D Foundation.

4.7 Summary of development and validation of soft soil profile

Field load tests on single columns, located within large groups and founded in a layered estuarine deposit were simulated using PLAXIS 3D Foundation. The predicted load-settlement curves were compared against field measurements and two independent axisymmetric FEA. It was found that PLAXIS 3D Foundation predicts the load-settlement curves closest to the field measurements, which reflects the ability of a three-dimensional analysis to model the surrounding columns at discrete locations, rather than approximating their presence by a cylindrical ring, as is the case with axisymmetric analyses. This highlights the importance of accurately capturing the presence of surrounding columns and gives confidence to the use of PLAXIS 3D Foundation for the subsequent FEA.

A soil profile and set of material parameters were developed for the well characterised Bothkennar test site, which consists of a soft uniform clay overlain by a stuff crust. This soil profile is representative of many sites where the applicability of stone columns is of growing interest and, therefore, forms the basis for the subsequent FEA. The adopted soil profile and choice of material parameters were validated by simulating a field load test, which was conducted on an unreinforced (i.e. no stone columns) rigid pad footing at the Bothkennar test site.

The ability of PLAXIS 3D Foundation to capture the load deformation behaviour of stone columns in the Bothkennar soil profile was also assessed. The settlement performance of an infinite grid of columns was simulated and the settlement performance was compared with a settlement database of field measurements and various analytical design methods. The importance of modular ratio upon the settlement performance of stone columns was highlighted and it was also shown that linear elasticity is not valid assumption for the behaviour of stone columns.

Chapter 5
Results of FEA: Settlement performance, deformational behaviour and stress concentration ratios

5.1 Background

The main focus of this research is to develop a better understanding of the behaviour of small groups of stone columns in soft soils. A series of FEA were conducted using PLAXIS 3D Foundation to examine the influence of key design parameters upon the settlement performance and deformational behaviour of small groups of stone columns. The key design parameters and considerations investigated are as follows:

- Column length (L)
- Area ratio (A/A_C)
- Column confinement
- Column arrangement
- Column position relative to footing edge
- Column compressibility
- Column strength
- Column installation effects
- The presence of a stiff crust

The design of foundations on soft soils is usually governed by settlement rather than bearing capacity criteria, due to their high compressibility (Priebe, 1976). Therefore, the settlement performance of stone columns at working load levels is of the upmost importance. The degree of confinement provided to columns is dependent upon the number of columns and the area ratio. The influence of column confinement is investigated by analysing the settlement performance of different configurations of columns (i.e. different group sizes) over a range of area ratios. The settlement performance of each configuration of columns is examined for various column lengths, which allows the relationship between column

length, area ratio and column confinement to be determined. Finally, the influence of the key design parameters and practical considerations outlined above is investigated for a select number of column configurations, which were specifically chosen to cover a wide range of area ratios.

The modes of deformation for small groups of stone columns are examined with the aid of new parameters called compression and punching ratios. In previous studies the modes of deformation have usually been determined at ultimate conditions; however, this study examines the modes of deformation at typical working loads. This allows a direct link to be made between the deformational behaviour and settlement performance of stone columns.

The stress concentration ratio is an important parameter which compares the vertical stress in columns to the vertical stress in the surrounding soil. For this research the vertical stress used to determine this parameter is measured beneath the base of footings (i.e. at the top of stone columns). Stress concentration ratios are used in analytical design methods to determine the settlement performance and the potential of stone columns to stabilise slopes; the variation of this ratio with the modes of deformation and the key design parameters is investigated.

5.2 Details of FEA

The various configurations of columns analysed are outlined in the following section. The Bothkennar soil profile, which was validated in the previous chapter, was adopted for all of the subsequent FEA. The footings are 0.6 m thick and founded 0.6 m below ground level. The column diameter is normally not a variable in design as the poker is of fixed diameter (430 mm is the most commonly used size) and the constructed column diameter depends on the properties of the surrounding soil. A diameter of 0.6 m is typical of stone columns constructed in soft soils using the bottom feed system. The column length was increased in 1 m increments (from 0 m, i.e. no columns, to 13.9 m, i.e. the base of the Carse clay profile adopted) to examine the effect of floating and end-bearing columns (Figure 5.1).

Area ratio and column confinement

The degree of confinement provided to individual stone columns depends on A/A_C and the number of columns within a group. The influence of column confinement was determined by analysing various configurations of columns such as single columns, 2×2, 3×3, 4×4 groups

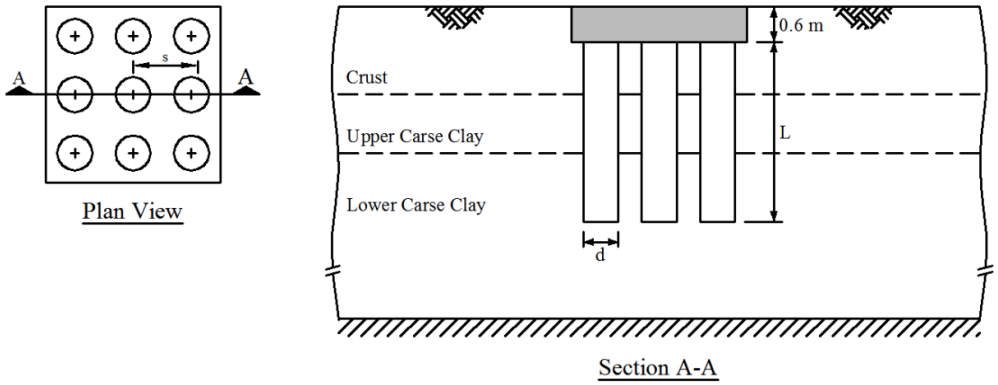

Figure 5.1 - Layout of columns in Bothkennar soil profile

and infinite grids of columns (see Figure 5.2). Single columns and infinite grids provide a useful frame of reference for the other configurations of columns as these two cases correspond to zero and full column confinement, respectively. Columns are positioned on a square grid and spaced at 1.0, 1.5 and 2.0 m, which corresponds to A/A_C of 3.5, 8.0 and 14.1, respectively. This is a typical range of A/A_C for small loaded areas, as can be seen in the settlement database developed by McCabe *et al.* (2009); columns at $A/A_C < 3.5$ would not be practicable or economic to construct and columns at $A/A_C > 14.1$ would typically be used to support wide area loadings such as embankments, which can tolerate larger settlements. The edge of the footing is located at a distance of half the column spacing (0.5×s) from the centreline of the outer row of columns; the influence of the footing overhang is examined in a subsequent parametric study.

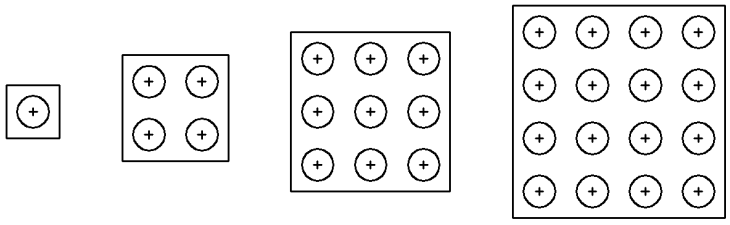

Figure 5.2 - Column configurations to examine influence of column confinement

Column arrangement

The column arrangements adopted to support a 3 m square pad footing are shown in Figure 5.3. The arrangements of 4, 5 and 9 columns are carefully chosen to allow the benefit of individual columns (i.e. centre, edge and corner) to be assessed. A comparison of the 4 and 5 column groups allows the benefit of an extra central column to be assessed, while a comparison of the 5 and 9 column groups allows the benefit of four edge columns to be

assessed. A group of 7 columns may also be adopted to support small pad footings in practice and this configuration was compared with a group of 9 columns.

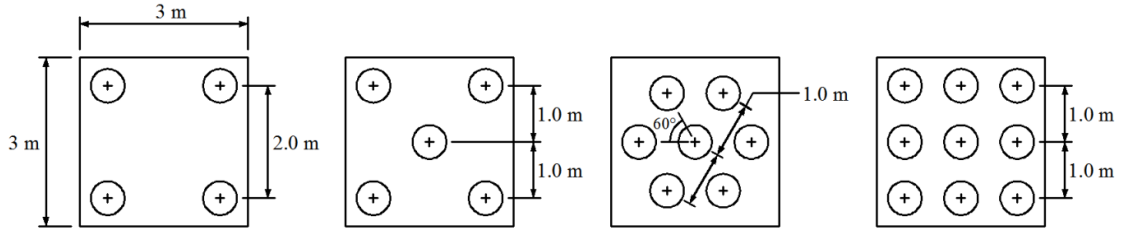

Figure 5.3 - Column configurations to examine influence of column arrangement

Column position

The effect of footing overhang and column position was examined for a 3 m square pad footing by positioning a 2×2 group of columns progressively closer to the footing edge (Figure 5.4). It is well known from elastic theory that the distribution of vertical stress beneath rigid footings is non-uniform and high vertical stress develops beneath the edge of footings. The column spacings investigated were 1.0, 1.5 and 2.0 m.

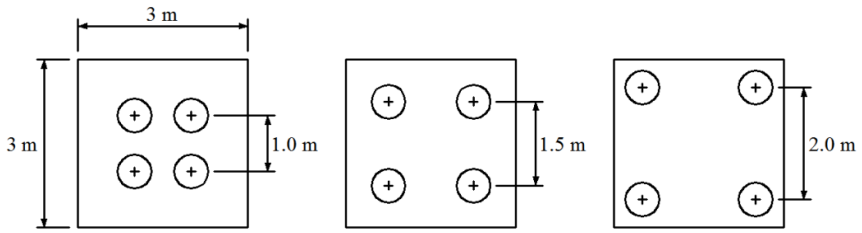

Figure 5.4 - Column configurations to examine influence of column position relative to the footing edge

Column compressibility and strength

The influence of column stiffness and strength upon the settlement performance and deformational behaviour of groups of 4, 5 and 9 columns beneath a 3 m square footing (see Figure 5.5) is investigated. The benchmark parameters adopted for the column stiffness (E_{50} = 70 MPa; E_{ur} = 210 MPa) and strength ($\varphi = 45°$; $\psi = 15°$) are developed in Section 4.6.1.

- The stiffness parameters are varied from E_{50} = 30–70 MPa on the basis of a range proposed by Barksdale & Bachus (1983). The unload-reload Young's modulus is defined by the relationship $E_{ur} = 3E_{50}$ (Brinkgreve & Broere, 2006).
- The angle of friction for the stone backfill was varied from φ = 40–50° and the angle of dilatancy was defined as $\psi = \varphi - 15°$ (Bolton, 1986).

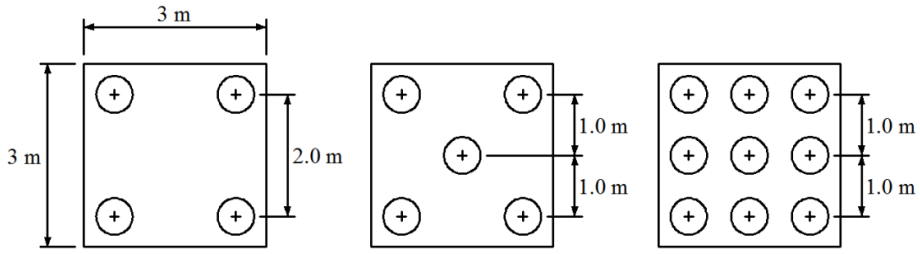

Figure 5.5 - Column configurations for parametric study of column compressibility and strength

Column installation effects

It was shown in Section 3.4.3 that the most appropriate method to simulate column installation effects in PLAXIS 3D Foundation is to increase the coefficient of lateral pressure (K_0) in the surrounding soil. A review of numerical analyses which adopted this methodology (see Section 2.4.3) suggests that K_0 is increased in the range 0.75–1.50, with an average of 1.00. As the *in situ* stress state in the upper layers at the Bothkennar test site is quite high (K_0 > 1.0), only the stress state of the lower Carse clay layer is modified to investigate the effects of column installation. A range of K_0 values (0.75, 1.00 and 1.25) were examined for the lower Carse clay.

Stiff crust layer

The soil profile adopted for the Bothkennar test site is modified to investigate the effect of the lower Carse clay and the stiff crust (Figure 5.6). The settlement performance, deformational behaviour and stress concentration ratio for various column arrangements outlined in Figure 5.5 are investigated for the various profiles shown in Figure 5.6.

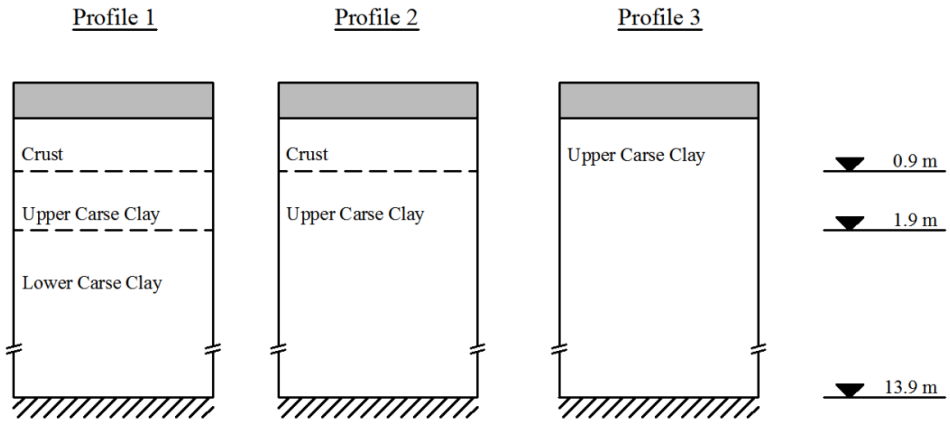

Figure 5.6 - Various profiles adopted to investigate the effect of the lower Carse clay (Profile 2) and the stiff crust (Profile 3)

5.3 Settlement analysis

As described earlier, the ultimate bearing capacity (q_{ult}) recorded by Jardine *et al.* (1995) for an unreinforced rigid footing at the Bothkennar test site was 138 kPa (see Section 4.5.3). Applying typical factors of safety (2.5–3.0) yields allowable bearing pressures in the range of 46–55 kPa. As a result, the settlement performance of stone columns was measured at 50 kPa, which was deemed a typical working load. The extent of settlement improvement is quantified by means of a settlement improvement factor (n), defined as the ratio of the settlement of an untreated footing to the settlement of a treated footing:

$$n = \frac{settlement\ of\ untreated\ footing}{settlement\ of\ treated\ footing}$$

5.3.1 Settlement performance of infinite grids of stone columns

The influence of column length upon the settlement performance of an infinite grid of stone columns is shown in Figure 5.7. A negligible reduction in footing settlement is observed in Figure 5.7(i) for columns shorter than L = 2 m. This may be attributable to the stiff upper layers at the Bothkennar test site which extend to 1.9 m beneath the footing base, as installing stone columns in an already competent layer will not reduce footing settlement. However, a significant reduction in footing settlement is observed with increasing column length thereafter which yields high settlement improvement factors (Figure 5.7(ii)). It can also be seen that the increase in settlement improvement factors with column length becomes more pronounced at low area ratios. This suggests that columns are at their most effective when closely-spaced.

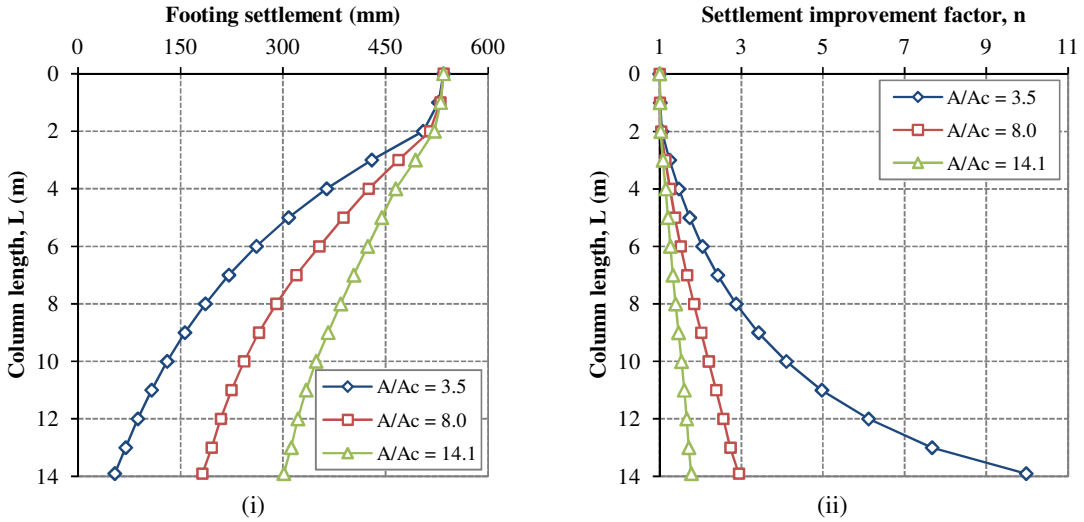

Figure 5.7 - Variation of (i) footing settlement and (ii) settlement improvement factor with column length for an infinite grid of columns

5.3.2 Settlement performance of small groups of stone columns

The influence of column length and column confinement upon the settlement performance of small groups of stone columns is shown in Figure 5.8(a). As with an infinite grid of columns, a negligible increase in settlement improvement factors is observed for all columns shorter than L = 2 m.

It can be seen in Figure 5.8(a-i) that settlement improvement factors for columns at low area ratios (i.e. A/A_C = 3.5) increase continuously with column length. A *jump* in settlement improvement factors is observed when moving from floating to end-bearing columns (i.e. L = 13→13.9 m) at low area ratios. The improved settlement performance may be explained as the proportion of applied load transferred to the base of columns is supported by a rigid stratum in the case of end-bearing columns, rather than a compressible stratum in the case of floating columns. The *jump* in settlement improvement factors suggests that closely-spaced columns transfer a significant proportion of the applied load to their base. The magnitude of the *jump* increases for larger groups of columns, which indicates that the proportion of applied load transferred to the base of columns increases for larger groups of columns. This reflects the enhanced lateral confinement associated with larger groups of columns.

The variation of settlement improvement factors with column length for various groups of columns at A/A_C of 8.0 and 14.1 is shown in Figures 5.8(a-ii) and 5.8(a-iii), respectively. Similar to columns at low area ratios, a continuous increase in settlement improvement factors is observed with increasing column length for all columns. However, the rate of increase in settlement improvement factors reduces for column lengths longer than L = 5 m. This suggests that long widely-spaced columns transfer a smaller proportion of the load to the base of columns and may be deforming closer to the ground surface.

It is clearly shown in Figure 5.8(a) that the enhanced levels of lateral confinement associated with larger groups of columns yields higher settlement improvement factors. However, it appears that the variation of settlement improvement factors with column length is dictated by area ratio rather than the number of columns, as a continuous increase in settlement improvement factors is observed with column length at low area ratios (i.e. A/A_C = 3.5), while the increase in settlement improvement factors with column length tends to reduce beyond L = 5 m at higher area ratios (i.e. A/A_C = 8.0 and 14.1).

The influence of the footing width (B) upon the settlement performance of small groups of columns is shown in Figure 5.8(b). For the column configurations analysed, it appears that A/A_C governs the variation of settlement improvement factors with column length. The classical Boussinesq (1885) solution for vertical stress distribution beneath an unreinforced square footing suggests that the stress increment applied to the footing is no longer perceived at L/B = 2 and so improving the settlement characteristics of the soil below this level, by installing stone columns, should not enhance the settlement performance. However, it appears that this significant depth (L/B = 2) does not influence settlement improvement factors of columns at low area ratios, as a continuous increase in settlement improvement factors is observed with increasing column length beyond this level.

5.3.3 Comparison of infinite grids with small groups of stone columns

The influence of A/A_C and column confinement upon the settlement performance of infinite grids and small groups of end-bearing columns is shown in Figure 5.9. It is clear that A/A_C has a significant influence on the settlement performance of stone columns, as a decrease in area ratio yields very high settlement improvement factors. The effect of column confinement is also evident as a larger group of stone columns yields higher settlement improvement factors, especially at low area ratios.

Settlement improvement factors for small groups of end-bearing stone columns (n) are normalised by settlement improvement factors for an infinite grid of end-bearing stone columns (n_{uc}) and presented in Figure 5.10. The n/n_{uc} ratio allows the influence of column confinement upon small groups of columns to be assessed, as an infinite grid of columns has full confinement and is an ideal benchmark. An increase in n/n_{uc} is observed with both an increasing number of columns and an increasing area ratio. It can be seen in Figure 5.10 that n/n_{uc} increases with area ratio, from 0.19 to 0.72 for single columns and from 0.45 to 0.82 for a 4×4 group of columns. The increase in n/n_{uc} for larger groups of columns reflects the increased level of lateral confinement. However, the increase in n/n_{uc} with increasing area ratio may be explained as the influence of lateral confinement upon settlement improvement factors reduces at high area ratios. Consequently, the difference between settlement improvement factors for small groups (n) and infinite grids (n_{uc}) of stone columns reduces at high area ratios, which yields an increase in n/n_{uc}.

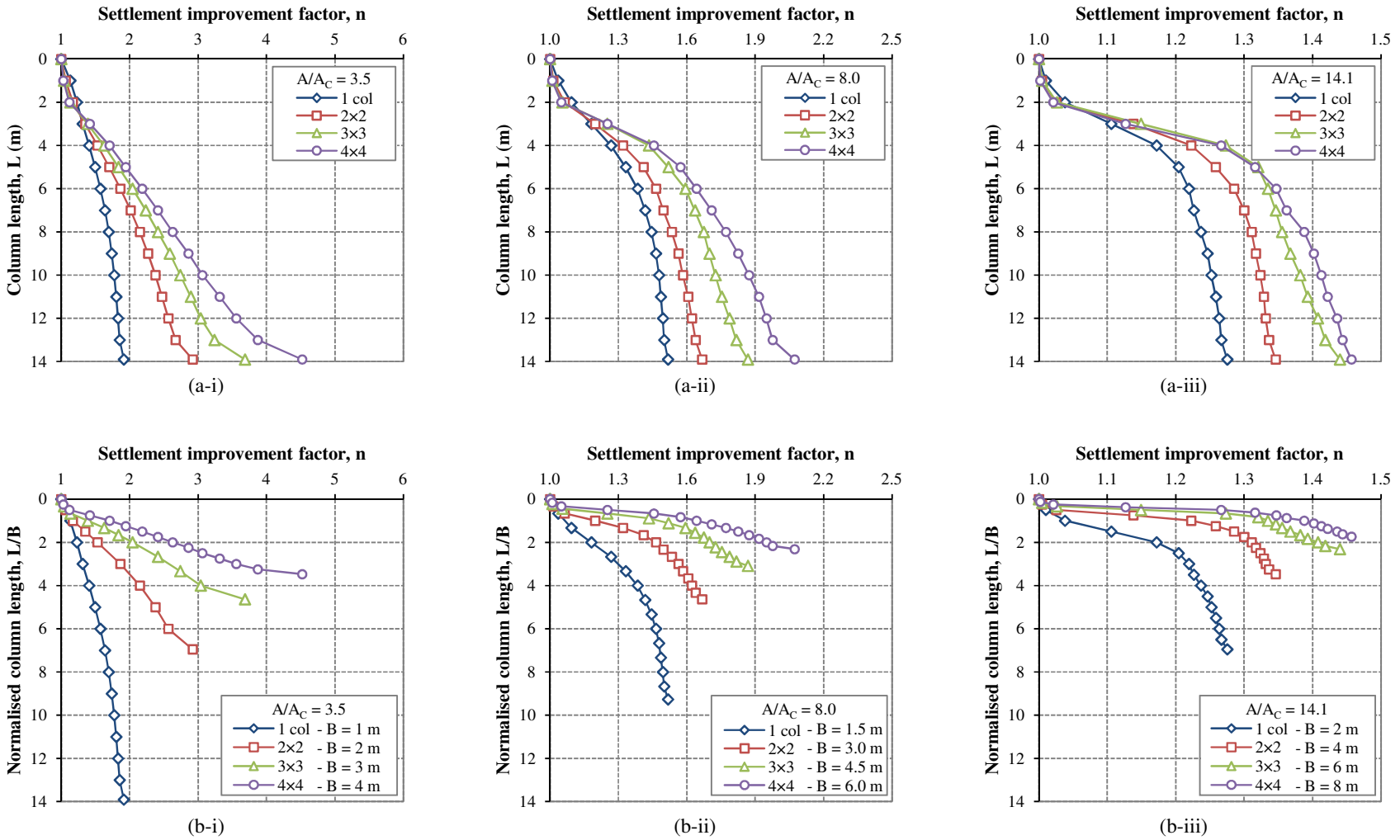

Figure 5.8 - Variation of settlement improvement factor with (a) column length (L) and (b) normalised column length (L/B) for small groups of columns, spaced at area ratios of (i) 3.5, (ii) 8.0 and (iii) 14.1

The relationship between the settlement of small groups of columns and infinite grids (s/s_{uc}) is shown in Figure 5.11. Priebe (1995) also developed a design chart (Figure 2.24) which relates the settlement of small groups of columns to infinite grids. However, Priebe (1995) does not directly account for the influence of footing area and relies on A/A_C to compensate for a decrease in s/s_{uc} with an increasing footing area. It can be seen in Figure 5.11 that both the area ratio and the number of columns have a significant influence on the settlement performance of small groups of columns. For similar area ratios, it can be seen that s/s_{uc} increases for a larger group of columns. This may be attributed to an increase in footing size for larger groups of columns. It can also be seen that the increase in s/s_{uc} for larger groups of columns is more pronounced at high area ratios (A/A_C = 14.1). This highlights the positive confining effects of closely-spaced columns.

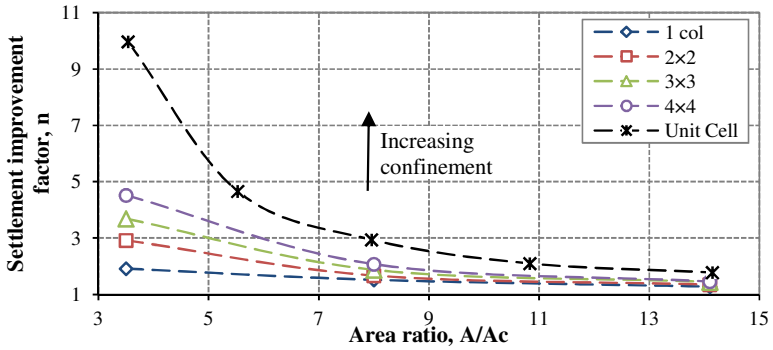

Figure 5.9 - Settlement improvement factors for small groups of end-bearing columns

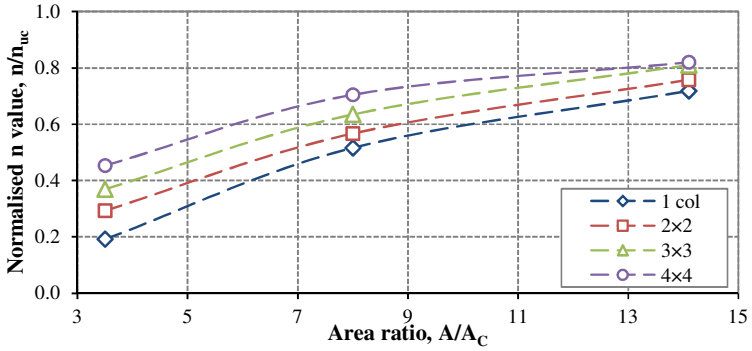

Figure 5.10 - Normalised settlement improvement factors for small groups of end-bearing columns

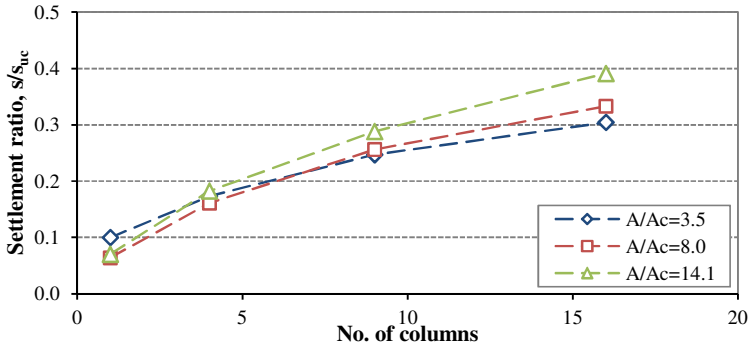

Figure 5.11 - Normalised settlement for small groups of end-bearing columns

5.3.4 Influence of column arrangement

The settlement performance of the various configurations of columns supporting a 3 m square footing (see Figure 5.3) is shown in Figure 5.12(i). As expected, it can be seen that settlement improvement factors increase with both column length and the number of columns. It appears that columns at low area ratios continue to yield higher increases in settlement improvement factors with increasing column length, which is consistent with earlier findings. A continuous increase in settlement improvement factors is observed for the 7 and 9 column groups and a *jump* in settlement improvement factors is again observed when moving from floating to end-bearing columns (i.e. L = 13→13.9 m). This suggests that the 7 and 9 column groups transfer a significant proportion of the applied load to the base of columns.

The arrangement of columns can be tailored to achieve a specific settlement performance, i.e. long columns at high area ratios or short columns at low area ratios. The volume of stone required for each configuration of columns is shown in Figure 5.12(ii). It appears that installing an extra centre column in a 2×2 group is only beneficial for long columns. It also appears that short columns at low area ratios are the most efficient configuration to achieve high settlement improvement factors. However, it must be noted that the volume of stone does not entirely reflect the overall cost of construction. Other factors such as the time taken to form stone columns must also be taken in account, i.e. a large number of short columns will take longer to construct than a small number of long columns due to the time taken to remove the poker. The longer length of time taken to construct a larger number of columns translates itself as an additional cost and must also be taken into consideration.

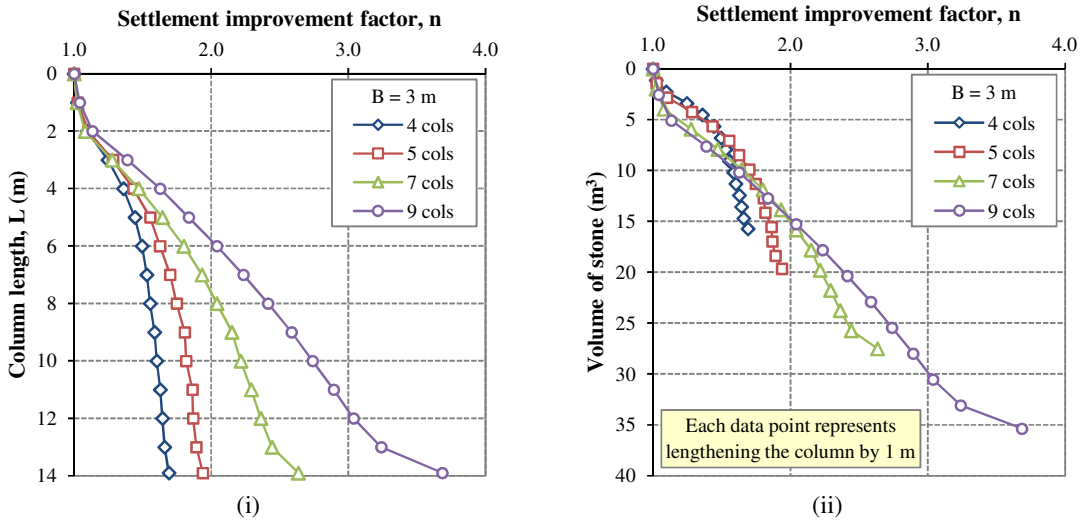

Figure 5.12 - Variation of settlement improvement factors with (i) column length and (ii) volume of stone for various arrangements of stone columns

5.3.5 Influence of column position

The influence of column position relative to the edge of footings (see Figure 5.4) upon settlement improvement factors is shown in Figure 5.13. It appears that small benefits can be gained by keeping columns closer to the footing edge. This may be attributed to high stress concentrations which occur beneath the edge of rigid footings. Therefore, columns placed in this zone have the potential to absorb more load and develop higher settlement improvement factors. A FEA by Wehr (2004) to examine the group behaviour of stone columns demonstrates that shear zones develop at the edges of a pad footing and extend to a depth beneath the centre of the footing. Positioning columns closer to the edge of footings, and thus closer to these shear zones, may also explain the enhanced settlement performance.

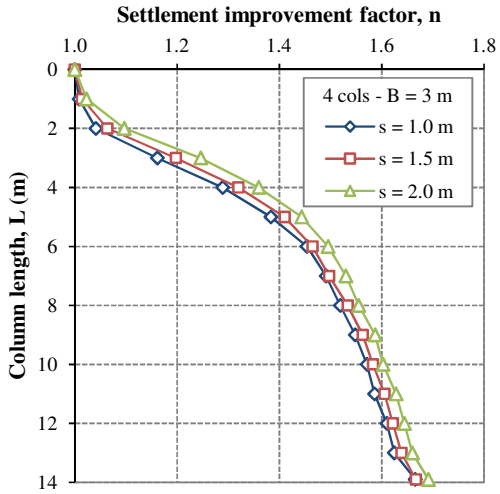

Figure 5.13 - Influence of column position upon settlement improvement factors

5.3.6 Influence of column compressibility

The influence of column compressibility upon the settlement performance of various column arrangements supporting a 3 m square footing (see Figure 5.5) is shown in Figure 5.14. As expected, settlement improvement factors increase with column stiffness ($E_{50,\ col}$). This is consistent with Domingues *et al.* (2007a) who conducted a FEA on large groups of stone columns (A/A_C = 5.3) supporting an embankment. The increase in settlement improvement factors with increasing column stiffness for end-bearing columns is shown in Table 5.1 and it can be seen that the effect of column stiffness is more significant for the group of 9 columns. The distribution of plastic points along a cross-section of 4, 5 and 9 columns is shown in Figure 5.15. The Mohr-Coulomb plastic points represent soil elements in a plastic stress state, i.e. which lie on the Mohr-Coulomb failure line. It can be seen that the extent of plasticity

reduces for larger groups of columns. This may be explained as the average applied load carried per column reduces for larger groups. This suggests that larger groups of columns are in more of an elastic state and hence are more sensitive to changes in elastic stiffness moduli.

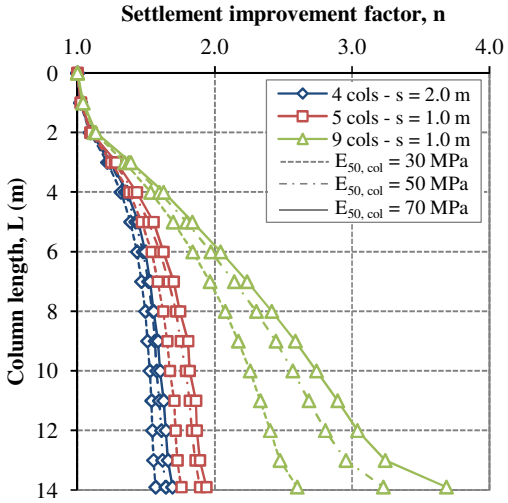

Figure 5.14 - Influence of column compressibility upon settlement improvement factors

Table 5.1 - Influence of column compressibility upon settlement improvement factors for end-bearing columns

No. of cols	Settlement improvement factors			% reduction		
	Column compressibility, E_{50} (MPa)			Column compressibility, E_{50} (MPa)		
	30	50	70	30	50	70
4	1.57	1.64	1.69	-7	-3	-
5	1.76	1.89	1.94	-9	-2	-
9	2.60	3.23	3.68	-29	-12	-

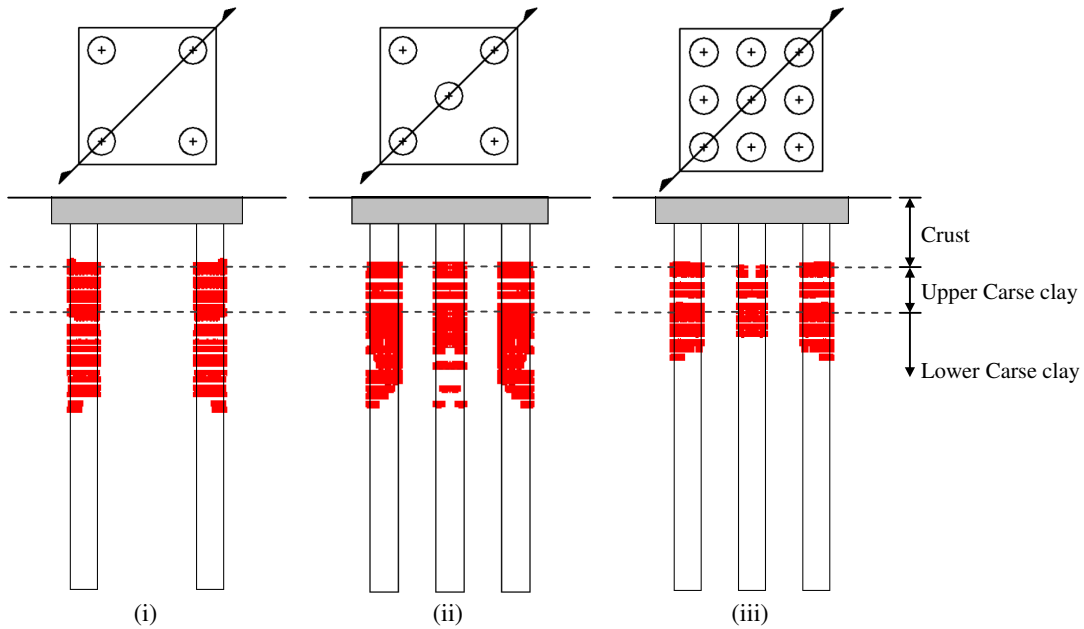

Figure 5.15 - Distribution of plastic points (Mohr-Coulomb) within a cross-section of (i) 4, (ii) 5 and (iii) 9 columns beneath a 3 m square footing (L = 6 m)

5.3.7 Influence of column strength

The influence of column strength upon the settlement performance of various column configurations supporting a 3 m square footing (see Figure 5.5) is shown in Figure 5.16 for friction angles in the range φ = 40–50°. It can be seen that settlement improvement factors increase with column strength. The increase in settlement improvement factors with increasing column strength from the benchmark strength of φ = 45° to 50° for end-bearing columns is shown in Table 5.2. It can be seen that an increase in column strength has the smallest effect on the group of 9 columns. This may be explained as the angle of internal friction only becomes mobilised once columns are in a plastic state. Therefore, increasing the angle of internal friction (i.e. increasing column strength) will have a larger influence on column configurations which exhibit the largest degree of plasticity. Similarly reducing the angle of internal friction from the benchmark strength of φ = 45° to 40° increases the extent of plasticity within columns and, consequently, has the smallest effect upon columns which exhibit the largest degree of plasticity.

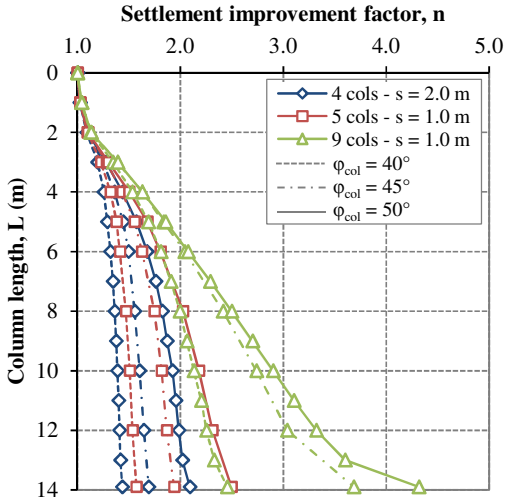

Figure 5.16 - Influence of column strength upon settlement improvement factors

Table 5.2 - Influence of column strength upon end-bearing settlement improvement factors

No. of cols	Settlement improvement factors			% reduction / increase		
	Angle of internal friction, φ (°)			Angle of internal friction, φ (°)		
	40	45	50	40	45	50
4	1.43	1.69	2.09	-15	-	24
5	1.57	1.94	2.49	-19	-	29
9	2.46	3.68	4.32	-33	-	17

5.3.8 Influence of column installation effects

The effects of column installation are investigated by increasing the coefficient of lateral earth pressure (K_0) in the lower Carse clay layer. The influence of K_0 upon the settlement performance of various configurations of columns (see Figure 5.5) is shown in Figure 5.17. It can be seen that increasing K_0 enhances the settlement performance of all column configurations, especially for groups of 4 and 5 columns. The smallest increase in settlement improvement factors is observed for the group of 9 columns (Table 5.3). This suggests that the mode of deformation for the group of 9 columns is less dependent on the lateral support provided by the surrounding soil than the groups of 4 and 5 columns. In fact, a slight decrease in settlement improvement factors is observed when increasing K_0 from 1.0 to 1.25 for a group of 9 columns. This may be explained as the untreated footing benefits more from an increase in K_0 than the settlement of a group of columns and, therefore, settlement improvement factors decrease slightly. It will be shown later on in Section 5.4.3 that columns at low area ratios tend to punch, while columns at high area ratios tend to bulge and are therefore more dependent on the lateral support provided by the surrounding soil.

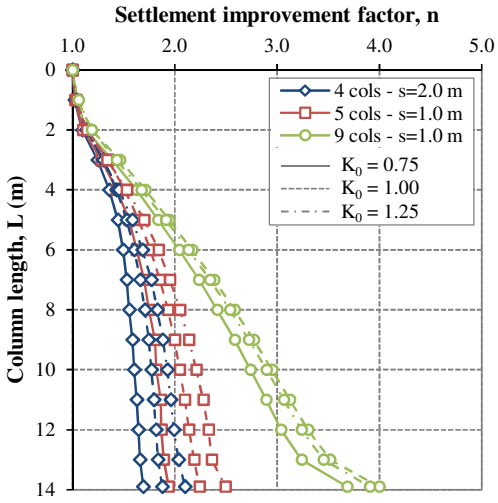

Figure 5.17 - Influence of coefficient of lateral earth pressure upon settlement improvement factors

Table 5.3 - Influence of coefficient of lateral earth pressure upon end-bearing settlement improvement factors

No. of cols	Settlement improvement factors			% reduction / increase		
	Coefficient of lateral earth pressure, K_0			Coefficient of lateral earth pressure, K_0		
	0.75	1.00	1.25	0.75	1.00	1.25
4	1.69	1.88	2.10	-	11	24
5	1.94	2.24	2.49	-	16	29
9	3.68	4.00	3.91	-	9	6

5.3.9 Influence of crust

The influence of the lower Carse clay and the stiff crust at the Bothkennar test site upon the settlement performance of various arrangements of columns (see Figure 5.5) supporting a 3 m square footing is shown in Figure 5.18. Profile 1 is the standard Bothkennar soil profile and settlement improvement factors for this profile in Figure 5.18 were presented earlier in Figure 5.12. The differences between Profiles 1, 2 and 3 are shown in Figure 5.6.

Settlement performance

Profile 2 consists of a stiff crust which is underlain by upper Carse clay. This soil profile is stiffer at depth than Profile 1, as it does not contain the lower Carse clay layer. This is reflected in Figure 5.18(i) as the untreated (L = 0 m) and treated settlements are lower than Profile 1. Profile 3 does not contain the stiff crust and consists entirely of upper Carse clay. While it is softer than Profile 1 near the surface, it is stiffer at depth and this is again reflected in Figure 5.18(i) as the treated settlements are lower than Profile 1. It is interesting to note that the untreated settlements (L = 0 m) for Profiles 1 and 3 are similar, which suggests that the increase in settlement due to the absence of the stiff crust is offset by the increased stiffness at depth, as the lower Carse clay is replaced by upper Carse clay.

Settlement improvement factors

The importance of the soil stiffness at depth is evident in the variation of settlement improvement factors with column length (Figure 5.18(ii)). It can be seen that settlement improvement factors are lowest for Profile 1. This may be related to the weak lower Carse clay which is not present in Profiles 2 and 3.

It can also be seen in Figure 5.18(ii) that settlement improvement factors increase significantly with column length up to L = 3 m in Profile 3. However, the rate of increase in settlement improvement factors with column length slows down thereafter. This is most pronounced for smaller groups of columns (i.e. higher A/A_C) and suggests that a critical length may exist for columns formed in Profile 3. This profile is similar to that used in laboratory studies described in the literature review (see Sections 2.2 and 2.3) and may explain why authors have postulated critical lengths in the past. However, it can be seen that critical lengths are less well defined for more realistic soil profiles. Therefore, this highlights the benefits of the FEM which accurately captures the influence of the stiff crust.

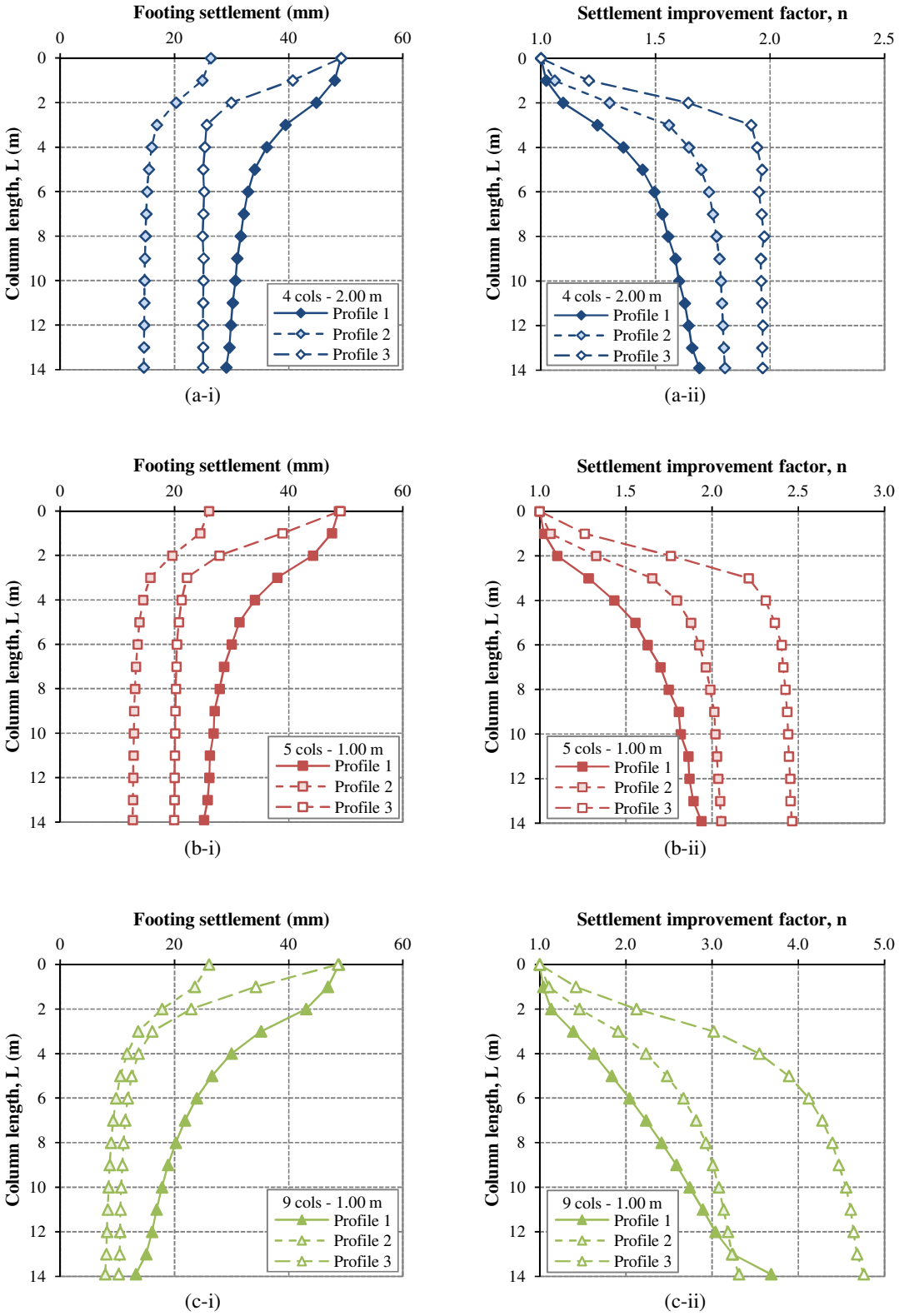

Figure 5.18 - Influence of the lower Carse clay and the stiff crust upon (i) settlement and (ii) settlement improvement factors for (a) 4, (b) 5 and (c) 9 columns beneath a 3 m square footing

5.4 Deformational behaviour of stone columns

5.4.1 Definitions of punching and compression ratios

It was shown by Muir Wood *et al.* (2000) that groups of stone columns can exhibit many modes of deformation such as punching, bulging, shearing and bending. New parameters, referred to as punching and compression ratios, were defined in this thesis to help identify the different modes of deformation.

Punching ratio

Depending on the adopted configuration of columns, a proportion of the applied load may be transferred to the base of the columns which results in columns punching vertically into the underlying soil. In order to compare the punching of columns beneath different footing sizes, the displacement at the base of columns is normalised by the displacement of the footing:

$$Punching\ ratio = \frac{u_{col} - u_{soil}}{u_{footing}} \quad \textbf{(5.1)}$$

where u_{col} = displacement at base of columns

u_{soil} = displacement of soil surrounding the base of columns

$u_{footing}$ = displacement at surface of footings

The displacement of the soil surrounding the base of columns (u_{soil}) is determined by averaging soil displacements within a zone surrounding each column. The size of the zone adopted to determine u_{soil} will influence the magnitude of the punching ratio, as soil displacement decreases with distance from columns. Two zones, shown in Figure 5.19, were compared in order to find a consistent method of calculating the punching ratio. The first zone (i) is a 1 m square zone surrounding the column and the second zone (ii) is also a square zone, whose width is equal to the column spacing. The size of the second zone will always be greater than or equal to the first zone as column spacing ranges from 1.0–2.0 m in this study.

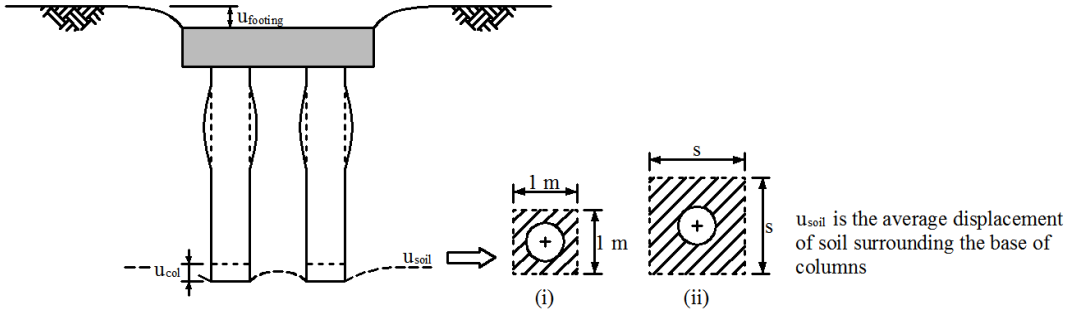

Figure 5.19 - Displacement at surface of footing, base of columns and soil surrounding base of columns

The variation of punching ratio - determined by methods (i) and (ii) - with length for an infinite grid of columns is shown in Figure 5.20. The variation of punching ratio with length for A/A_C = 3.5 is not shown as this corresponds to a column spacing of 1.0 m; the zones for methods (i) and (ii) coincide at this spacing and no difference will be observed. It can be seen in Figure 5.20 that methods (i) and (ii) predict a similar variation of punching ratio with length. It is also clear that the punching ratio is always higher for method (ii). This may be explained as the displacement of the surrounding soil is averaged over a larger area for the method (ii). This leads to a lower average displacement of the soil and, consequently, higher punching ratios, as soil displacement decreases with distance from the column. The punching ratio is determined using the method (i) for the subsequent analyses, as the zone in which the soil displacement is averaged is the same size for all column spacings and thus allows for a consistent analysis.

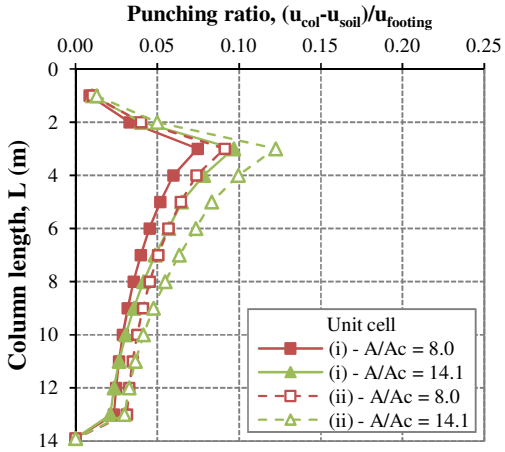

Figure 5.20 - Variation of punching ratios with length for an infinite grid of columns, with u_{soil} measured in (i) a 1 m square zone and (ii) a square zone, whose width is equal to the column spacing

Compression ratio

The compression ratio is an important indicator of the mode of deformation and is defined as the proportion of surface settlement transferred to the column base. Low compression ratios suggest that columns are transferring the load to depth, rather than deforming along their length. One limitation of the compression ratio is that is does not differentiate between axial and radial deformation. However, axial deformation due to column compressibility results in a steady increase in compression ratios, while radial deformation due to column bulging can be identified by a rapid increase in compression ratios.

$$Compression\ ratio = \frac{u_{footing} - u_{col}}{u_{footing}} \quad \textbf{(5.2)}$$

5.4.2 Deformational behaviour of an infinite grid of stone columns

The variation of punching ratio with area ratio and column length for an infinite grid of columns is shown in Figure 5.21(i). It can be seen that the punching ratio increases with column length for all columns shorter than L = 3 m. It can also be seen in Figure 5.21(ii) that the increase in punching ratio is coupled with low compression ratios. This suggests that columns do not deform along their length and punching is therefore the dominant mode of deformation for short columns.

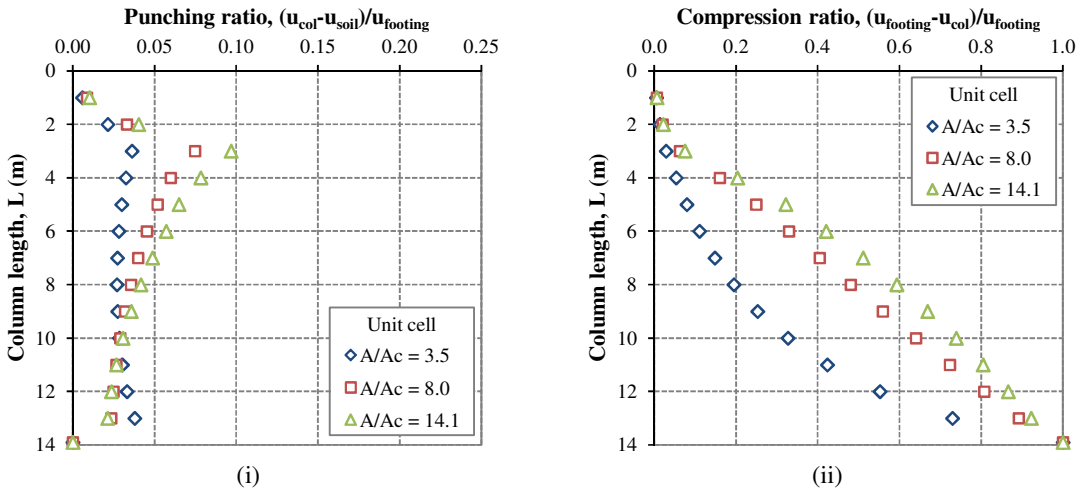

Figure 5.21 - Variation of (i) punching and (ii) compression ratios with column length for an infinite grid of columns

It can be seen in Figure 5.21(i) that the punching ratio increases with column length up to a maximum at L = 3 m. This increase may be attributed to a reduction in the stiffness of soil layers in the upper 3 m of the Bothkennar test site, i.e. the crust is the stiffest layer, followed by the upper Carse clay and then the lower Carse clay (see C_C values in Table 4.2). Therefore, as column length increases, the columns bases are founded in more compressible soil strata which results in higher punching ratios (Figure 5.22). It is interesting to note that the maximum punching ratio occurs at L = 3 m, despite the fact that the base of 2 m long columns coincides with the weakest part of the soil profile, i.e. the top of the lower Carse clay layer. It seems intuitive that the maximum punching ratio would occur when the column bases are formed in the weakest part of the soil profile. However, it can be seen in Figure 5.22(ii) that the base of 2 m long columns extends just beyond the bottom of the upper Carse clay layer, which reduces the displacement of the soil at the top of the lower Carse clay layer, thus, reducing the punching ratio.

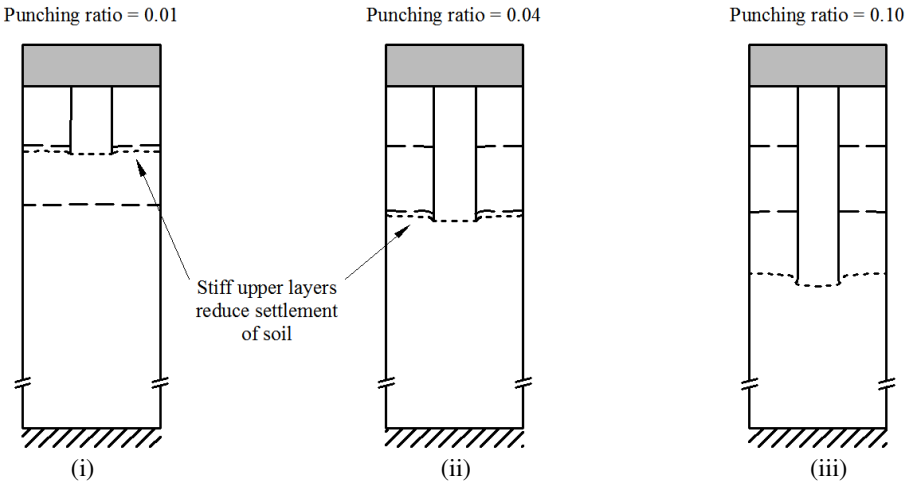

Figure 5.22 - Deformation of an infinite grid of floating stone columns at an area ratio A/A_C = 14.1 for column lengths of (i) L = 1 m, (ii) L = 2 m and (iii) L = 3 m

It is also evident in Figure 5.21(i) that the punching ratio increases with increasing area ratio and this is most pronounced at L = 3 m. The deformation of an infinite grid of 3 m long columns at various area ratios is shown in Figure 5.23. It can be seen in Figure 5.23(i) that columns at low area ratios act with the surrounding soil and punch as a single entity into the underlying soil. This mode of deformation is referred to as 'block' failure and is a form of column punching. It occurs for large groups of closely-spaced columns and is characterised by low punching and low compression ratios. High punching ratios usually denote punching failure; however, punching ratios are low for 'block' failure as columns deform with the surrounding soil. A similar mode of deformation is observed by Black (2006) for a group of three columns at low area ratios (A/A_C = 2.5 and 3.6). It can be seen in Figures 5.23(ii) and 5.23(iii) that column interaction decreases at higher area ratios, as columns tend to act more individually and punch into the underlying soil.

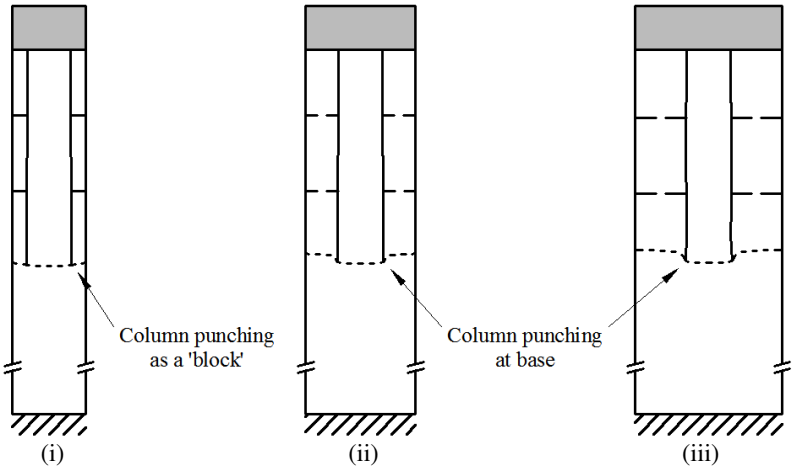

Figure 5.23 - Deformation of an infinite grid of 3 m long columns at area ratios of (i) 3.5, (ii) 8.0 and (iii) 14.1

While it can be seen in Figure 5.21 that columns at all area ratios exhibit similar variations of punching and compression ratios with column length up to L = 3 m, a marked difference is observed with area ratio thereafter:

- Columns at low area ratios continue to exhibit relatively low and constant punching ratios for column lengths L > 3 m. Compression ratios also remain relatively low, which indicates that columns do not deform significantly along their length. This suggests that 'block' failure remains the dominant mode of deformation with increasing length for an infinite grid of columns at low area ratios. A slight increase in the punching ratio is observed for column lengths L > 11 m.
- Columns at high area ratios exhibit a decrease in punching ratio and increase in compression ratio for column lengths L > 3 m. The increase in compression ratios indicates that columns are deforming along their length and may be bulging closer to the ground surface. Columns which are bulging cannot transfer the applied load to the base of columns which consequently results in low punching ratios.

5.4.3 Deformational behaviour of small groups of stone columns

Single columns and 2×2 groups

The influence of area ratio and column length upon punching ratios for single columns and 2×2 groups is shown in Figures 5.24(i) and 5.25(i), respectively. It can be seen that punching ratios increase with column length up to a maximum at L = 3 m, which is similar to an infinite grid of columns. The increase in punching ratios is again coupled with relatively low compression ratios as shown in Figures 5.24(ii) and 5.25(ii) for single columns and 2×2 groups, respectively. Therefore, it appears that punching is the dominant mode of deformation for short columns.

It can be seen in Figures 5.24(i) and 5.25(i) that an increase in area ratio leads to a decrease in punching ratio for 1 m long single columns and 2×2 groups of columns, respectively. This may be explained as the soil surrounding at the base of 1 m long columns is significantly influenced by the footing overhead. An increase in area ratio for groups of columns corresponds to an increase in footing width, and wider footings induce more displacement in the soil at z = 1 m (z = depth beneath footing). As a consequence, this reduces the differential displacement between the base of columns and the surrounding soil, which results in lower punching ratios.

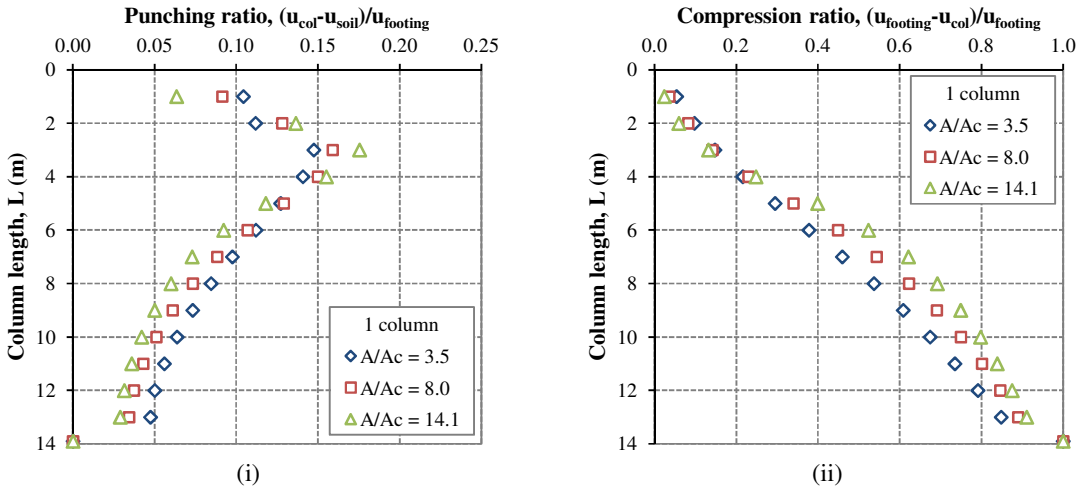

Figure 5.24 - Variation of (i) punching and (ii) compression ratios with column length for single columns

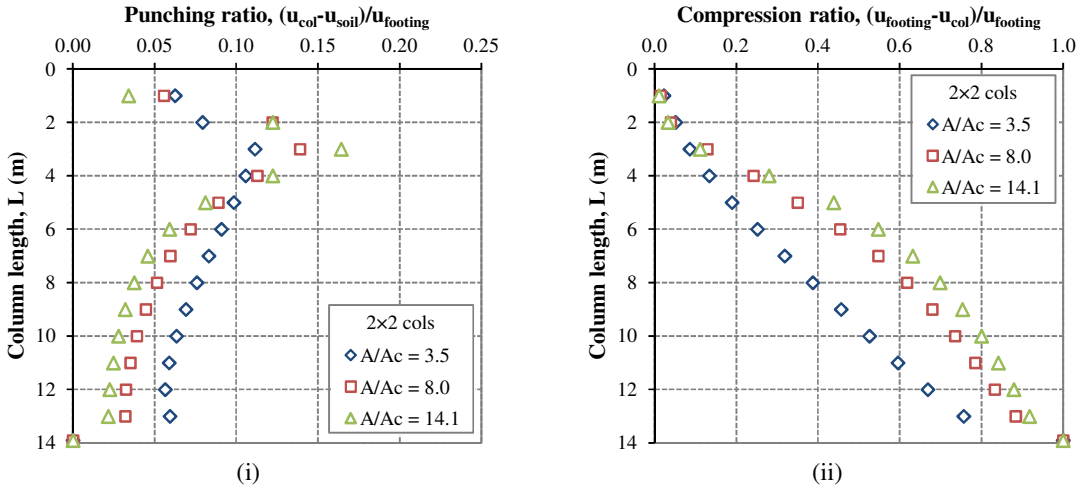

Figure 5.25 - Variation of (i) punching and (ii) compression ratios with column length for 2×2 groups of columns

However, it can also be seen that an increase in area ratio leads to an increase in punching ratios for L = 2, 3 and 4 m. It is established that punching is the dominant mode of deformation for short stone columns, which implies that columns develop shear stress and end-bearing pressure along the side and at the base of columns, respectively. An increase in area ratio corresponds to an increased footing width for groups of columns. This implies that the total load taken per column also increases with area ratio. Columns of similar length which are 'punching' have the capacity to carry similar shear force along their sides. Therefore, an increase in the total load taken per column increases the portion of the load transferred to the base of columns, which consequently increases the punching ratio.

A reduction in the punching ratio is coupled with an increase in compression ratios for single columns and 2×2 groups which are longer than L = 3 m. This suggests that columns are deforming along their length and that bulging is the dominant mode of deformation. It is interesting to note that the reduction in punching ratios and increase in compression ratios becomes more pronounced with increasing area ratio. This is consistent with the findings from an infinite grid of columns and indicates that column bulging becomes more pronounced with increasing area ratio.

3×3 and 4×4 groups

The variation of punching ratio with column length for 3×3 and 4×4 groups of columns is shown in Figures 5.26(i) and 5.27(i), respectively. Punching ratios are observed to increase with length up to a maximum at L = 3 m, which is again similar to findings from single columns, 2×2 groups and infinite grids of columns. The increase in punching ratios is coupled with low compression ratios, as shown in Figures 5.26(ii) and 5.27(ii) for 3×3 and 4×4 groups, respectively. This indicates that columns do not deform along their length and are transferring the applied load to the base of columns. Therefore, it appears that punching is again the dominant mode of deformation for short columns. It can be also seen that punching ratios increase at higher area ratios, which reflects the loss in lateral confinement and increase in the total force carried per column with increasing with area ratio.

The deformed shape of a 3×3 group of columns at L = 3 m and 6m is shown in Figure 5.28. It can be seen in Figure 5.28(i) that closely-spaced columns are acting as a 'block' with the surrounding soil. This is consistent with relatively low punching and compression ratios, evident in Figures 5.26 and 5.27 for 3×3 and 4×4 groups, respectively. It appears that 'block' failure remains the dominant mode of deformation with increasing column length for closely-spaced columns. In contrast, it can be seen that columns at higher area ratios which are longer than L = 3 m deform significantly with increasing column length. A reduction in punching ratios and increase in compression ratios suggests that columns are deforming along their length and do not transfer the applied load to the base of columns (see Figure 5.28). It can also be seen that external columns tend to bend outwards and away from central columns. This mechanism was also observed by McKelvey *et al.* (2004) in small scale laboratory tests.

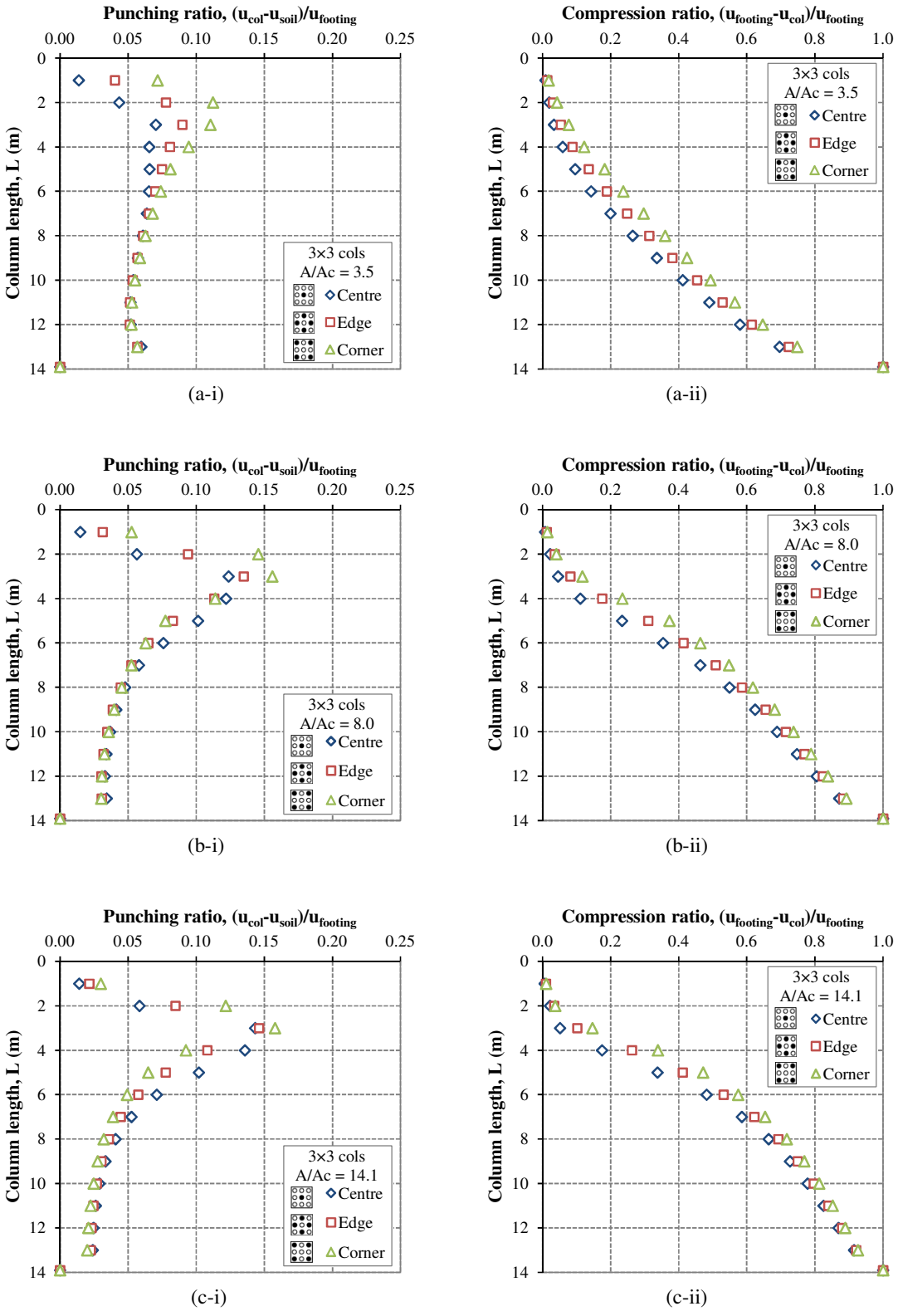

Figure 5.26 - Variation of (i) punching and (ii) compression ratios with column length for a 3×3 group of columns spaced at area ratios of (a) 3.5, (b) 8.0 and (c) 14.1

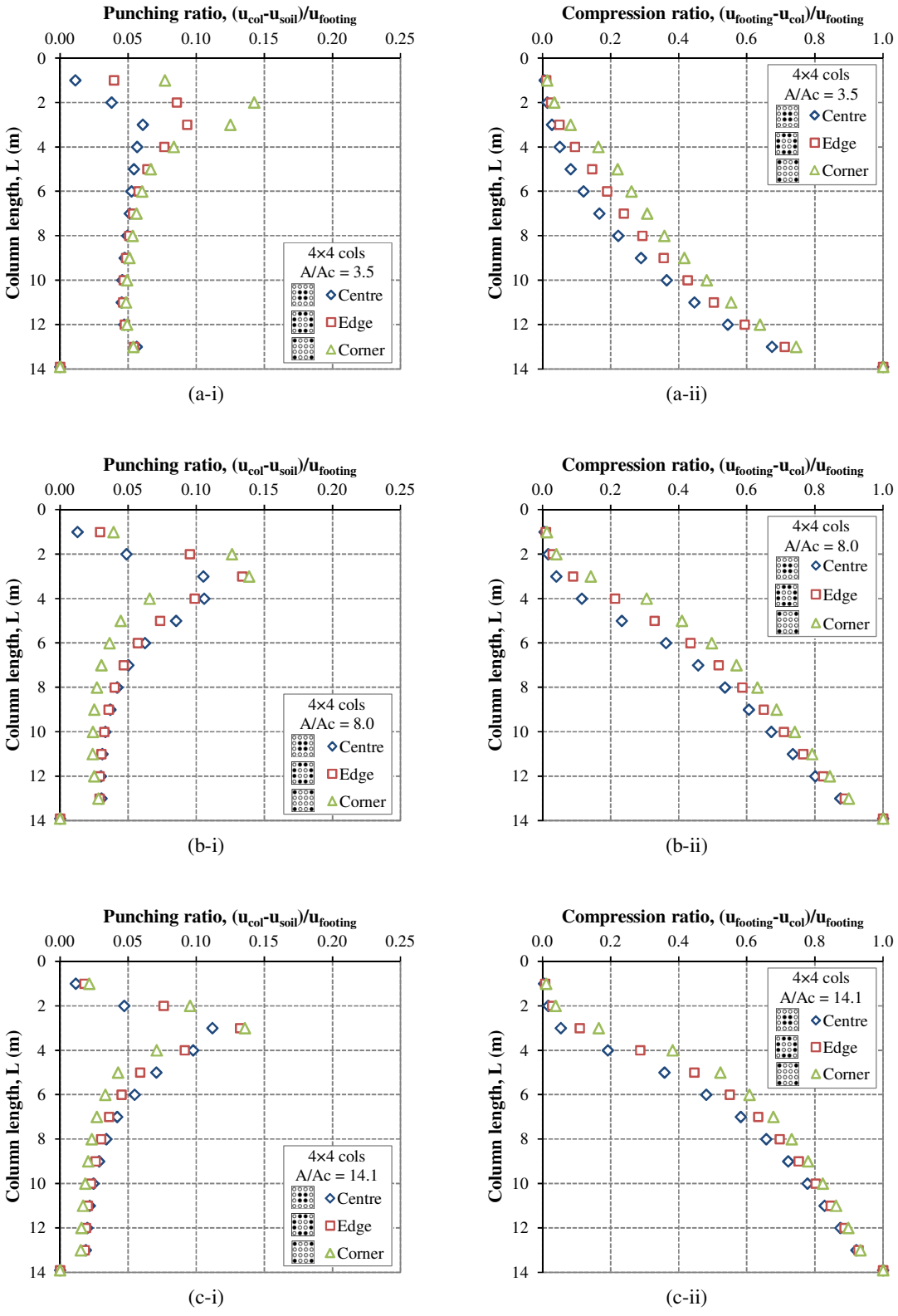

Figure 5.27 - Variation of (i) column and (ii) column ratios with column length for a 4×4 group of columns spaced at area ratios of (a) 3.5, (b) 8.0 and (c) 14.1

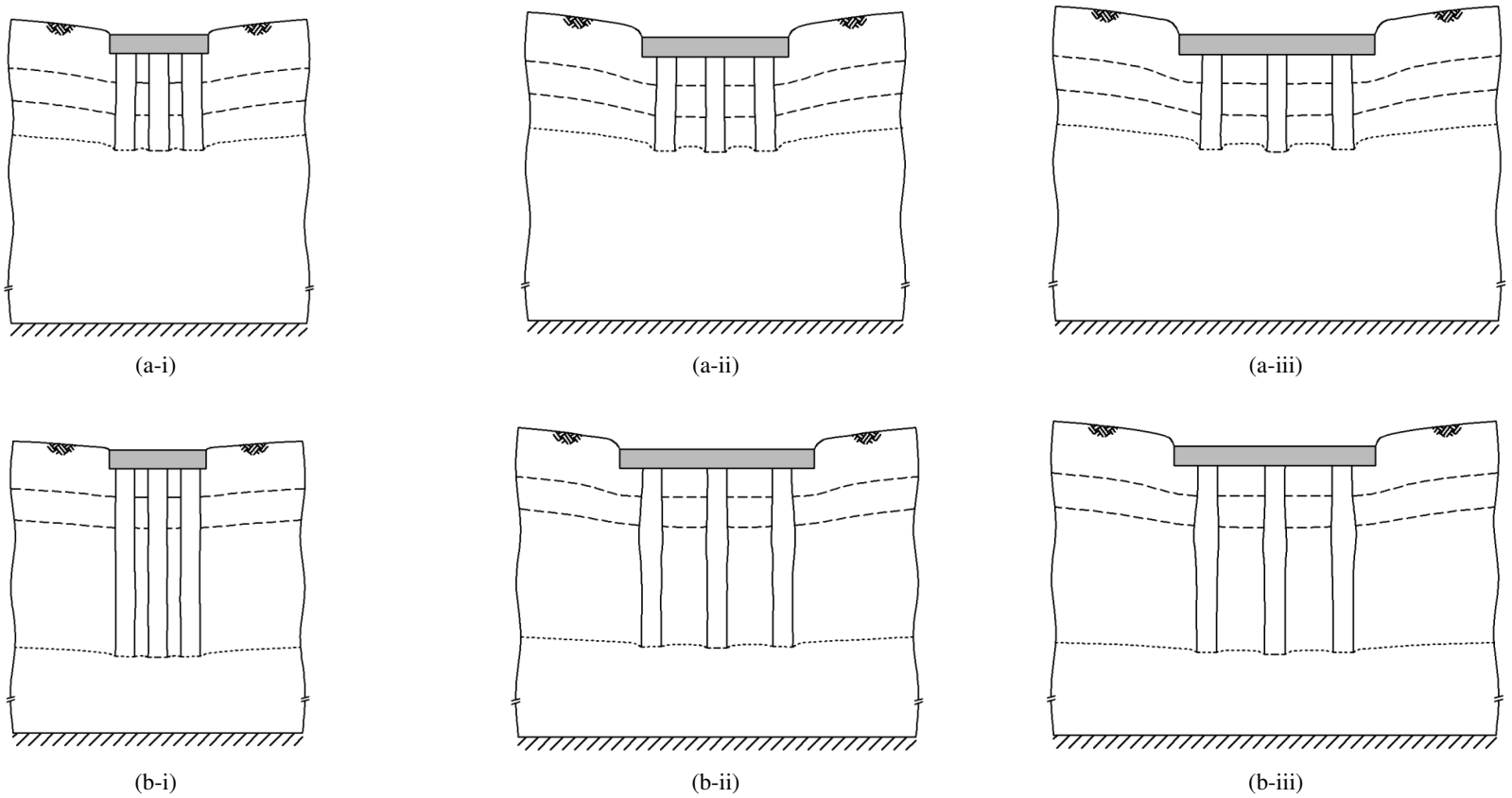

Figure 5.28 - Deformed shapes from PLAXIS 3D Foundation for 3×3 group of columns at area ratios of (i) 3.5, (ii) 8.0 and (iii) 14.1 for column lengths (a) L = 3 m and (b) L = 6 m

The variation of punching ratios for individual columns (i.e. centre, edge and corner columns) within a 3×3 and 4×4 group can also be seen in Figures 5.26 and 5.27, respectively. For columns shorter than L = 3 m, it appears that punching ratios are lowest for centre columns, followed by edge and corner columns. This trend is also evident for all lengths of closely-spaced columns (i.e. $A/A_C = 3.5$), which suggests that this variation of punching ratios with column length is associated with a punching mode of deformation. Columns which are punching impart shear stresses to the surrounding soil which tends to drag the surrounding soil downwards. Punching ratios are lowest for centre columns as the soil surrounding the base of the column is dragged downwards on all sides by edge and corner columns. However, it can be seen for widely-spaced columns (i.e. $A/A_C = 8.0$ and 14.1) which are longer than L = 3 m that punching ratios for centre columns exceeds punching ratios for corner and edge columns. It is evident in Figure 5.28 that long widely-spaced edge columns tend to bulge and bend outwards, which reduces punching at the base of columns. Centre columns are better confined and can transfer more of the applied load to the base.

5.4.4 Comparison of infinite grid with small groups of columns

The influence of column confinement upon punching and compression ratios is shown in Figures 5.29(i) and 5.29(ii), respectively. It can be seen in Figure 5.29(a-i) for columns at low area ratios that punching ratios reduce with an increasing number of columns. It was established previously that punching failure is the dominant mode of deformation for closely-spaced floating columns. Furthermore, punching ratios are lowest for interior columns within closely-spaced groups, as shear stresses from neighbouring columns drag the soil surrounding the base of columns downwards. Therefore, as the number of interior columns increases, the average punching ratio of closely-spaced groups of columns reduces.

A reduction in the punching ratio with an increasing number of columns is also observed in Figures 5.29(b-i) and 5.29(c-i) for columns at higher area ratios. It is shown in Figure 5.28(iii) that column bending occurs in the outer row of widely-spaced columns. Bending reduces the ability of columns to transfer the applied load to depth and hence results in lower punching ratios. For a constant area ratio, footing width increases with an increasing number of columns. Columns become increasingly slender as footing width increases and, consequently, are more susceptible to bending. Therefore, punching ratios reduce with an increasing number of columns at high area ratios.

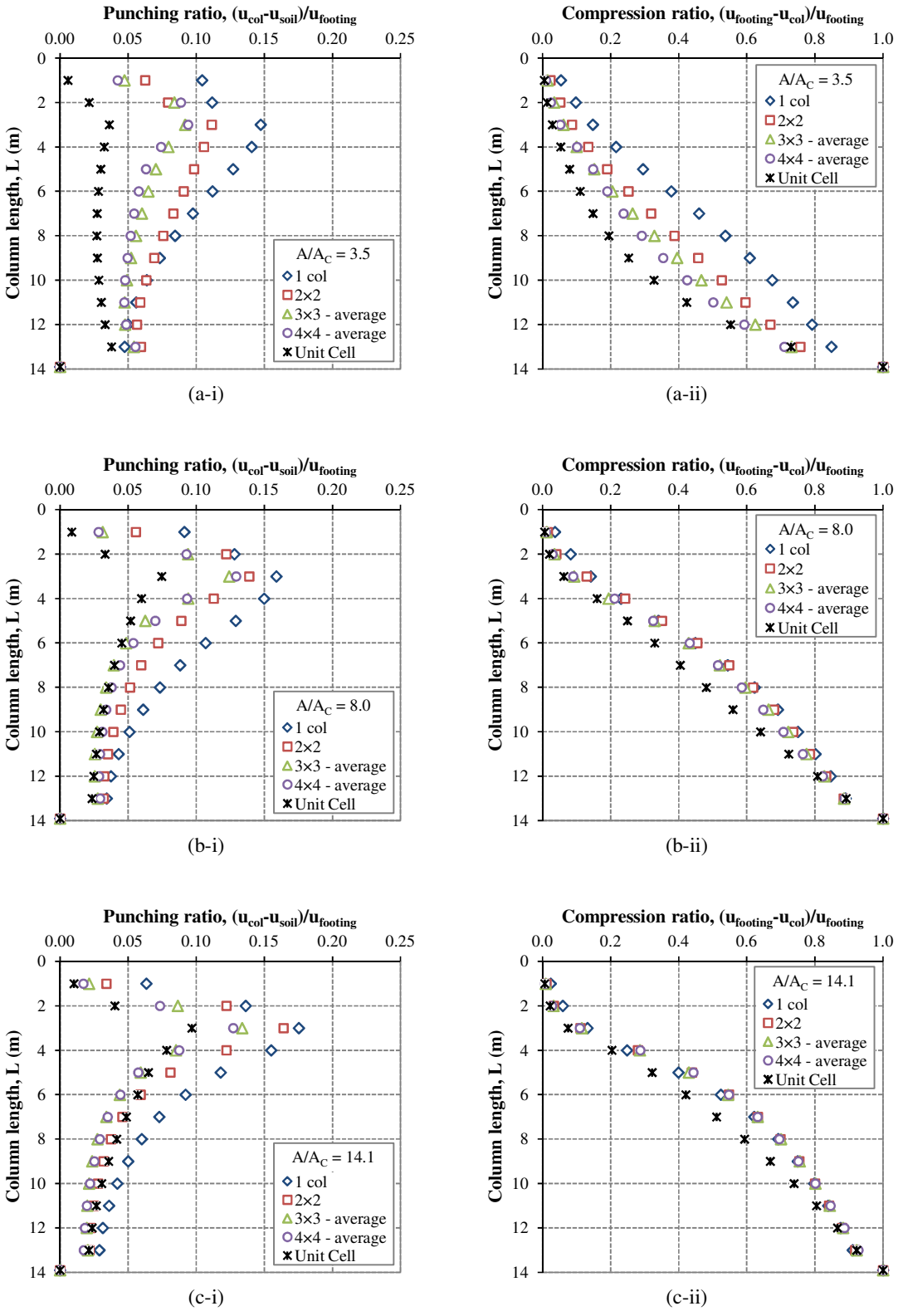

Figure 5.29 - Influence of column confinement upon (i) punching and (ii) compression ratios for various lengths and configurations of columns spaced at area ratios of (a) 3.5, (b) 8.0 and (c) 14.1

It can be seen in Figure 5.29(i) that unit cell conditions yield the lowest punching ratios for columns at low area ratios. However, this is not the case for high area ratios and it can be seen that punching ratios for the unit cell are larger than those for groups of columns longer than 7 m and 5 m in Figures 5.29(b-i) and 5.29(c-i), respectively. The external columns in groups experience a loss of lateral confinement and bend outwards, which reduces the punching ratio. An infinite grid of columns cannot bend due to symmetry and punching ratios are higher, despite the increased level of column confinement.

The relationship between column confinement and compression ratios is shown in Figure 5.29(ii). It can be seen for closely-spaced columns that the average compression ratios of a group reduces as the number of columns increases. This is consistent with findings from the settlement performance, where the *jump* in settlement improvement factors observed for end-bearing columns with an increasing number of columns. This indicates that larger groups of columns transfer higher proportions of the applied load to the base, which reduces the deformation along the length of columns.

5.4.5 Influence of column arrangement upon deformational behaviour

The variation of punching and compression ratios with length for various column arrangements (see Figure 5.3) supporting a 3 m square footing is shown in Figure 5.30. An increase in the punching ratio with length is observed for all short columns. This is coupled with relatively low compression ratios, which indicates that punching is the dominant mode of deformation. An increase in punching ratios is observed for fewer supporting stone columns. This may be related to an increase in the total load taken per column as the number of supporting columns reduces. Columns of similar length which are punching have the capacity to develop similar shear force along the sides. Therefore, any extra load taken by columns (i.e. for fewer supporting columns) is transferred to the base of columns, which results in higher punching ratios.

While all configurations of columns exhibit a similar variation of punching and compression ratios with increasing length for short columns, a marked change is observed with increasing length thereafter. The groups of 4 and 5 columns exhibit a significant reduction in punching ratio and a simultaneous increase in compression ratio. This indicates that these column groups are not transferring the applied load to the base of columns and are deforming closer

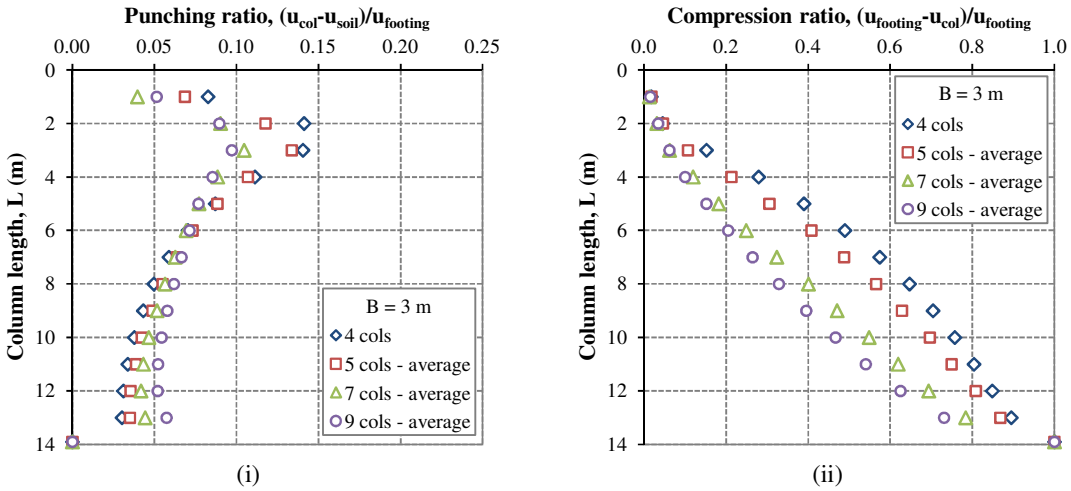

Figure 5.30 - Variation of (i) punching and (ii) compression ratios with column length for various configurations of stone columns beneath a 3 m square footing

to the ground surface. This is consistent with previous findings for long widely-spaced columns. In contrast to this behaviour, relatively low compression ratios are observed for the groups of 7 and 9 columns. This suggests that punching failure remains the dominant mode of deformation with increasing column length.

5.4.6 Influence of column position

The influence of column position relative to the edge of footings (see Figure 5.4) upon punching and compression ratios is shown in Figure 5.31. For columns shorter than L = 3 m, it can be seen that the punching ratio increases for columns positioned closer to the edge of footings. It is established that punching is the dominant mode of deformation for all short columns. Columns which are punching develop shear stress along the side of columns, which tends to drag the surrounding soil downwards. The influence of shear stress becomes more pronounced as columns are positioned closer together and the surrounding soil is displaced more uniformly, which results in lower punching ratios. However, no change in punching ratios is observed for column lengths longer than L = 3 m when bulging becomes the dominant mode of deformation for longer columns. While no change in the punching ratio occurs for columns which are bulging, the compression ratio increases for columns which are positioned closer to the edge of footings. This may be explained as closely-spaced columns are less susceptible to bending and, therefore, exhibit less compression.

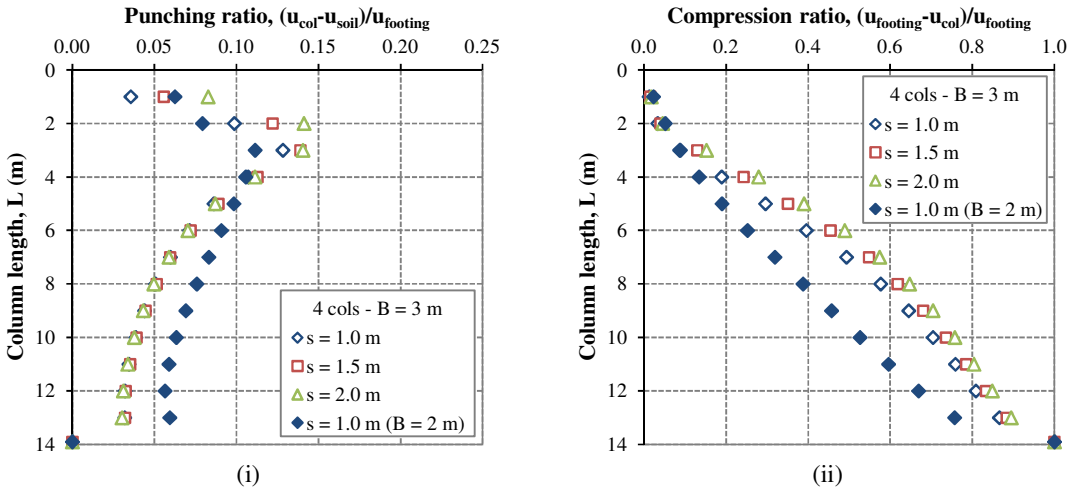

Figure 5.31 - Variation of (i) punching and (ii) compression ratios with column length for various column spacings beneath a 3 m square footing

The deformational behaviour of a 2×2 group spaced at 1.0 m and supporting a 2 m and a 3 m square pad footing is also compared in Figure 5.31. It appears that the mode of deformation is different for the group of columns beneath the 2 m square footing (i.e. $A/A_C = 3.5$). Increased punching ratios and lower compression ratios indicate that punching remains the dominant mode of deformation for all column lengths. Therefore, it is postulated that area ratio is more critical than column spacing in governing the deformational behaviour of columns.

5.4.7 Influence of column compressibility

The influence of column compressibility upon the deformational behaviour of various column arrangements supporting a 3 m square footing (see Figure 5.5) is shown in Figure 5.32. It can be seen that an increase in column stiffness results in an increase in punching ratios and decrease in compression ratios. While the increase in punching ratios is relatively uniform for all column configurations, a larger decrease in compression ratios is observed for the group of 9 columns. This is consistent with findings from the settlement performance of stone columns, as the group of 9 columns are in more of an elastic state and are therefore more influenced by changes in elastic stiffness moduli.

5.4.8 Influence of column strength

The influence of column strength upon the deformational behaviour of various column arrangements supporting a 3 m square footing (see Figure 5.5) is shown in Figures 5.33. It

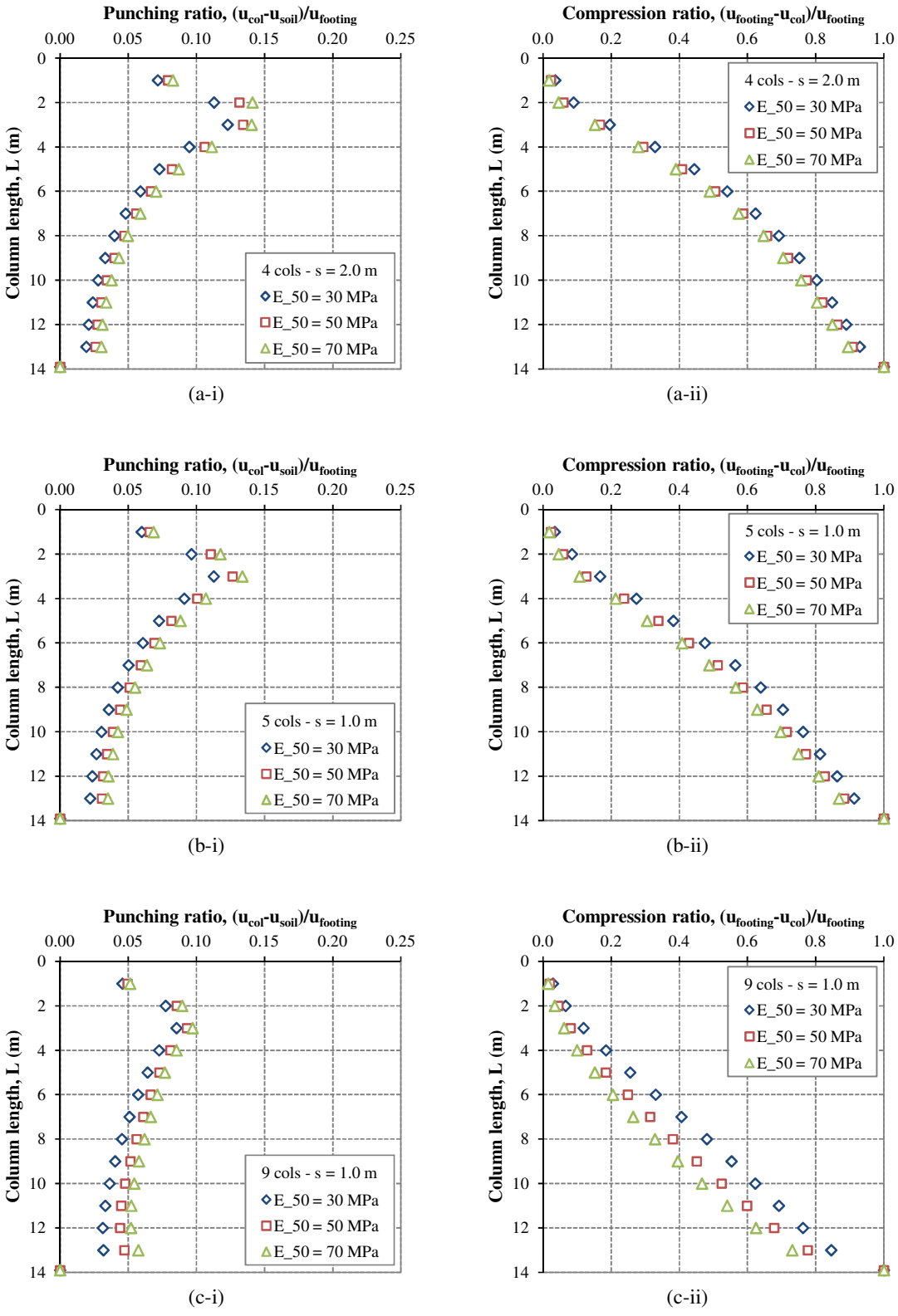

Figure 5.32 - Influence of column compressibility upon the variation of (i) punching and (ii) compression ratios with column length for a group of (a) 4, (b) 5 and (c) 9 columns beneath a 3 m square footing

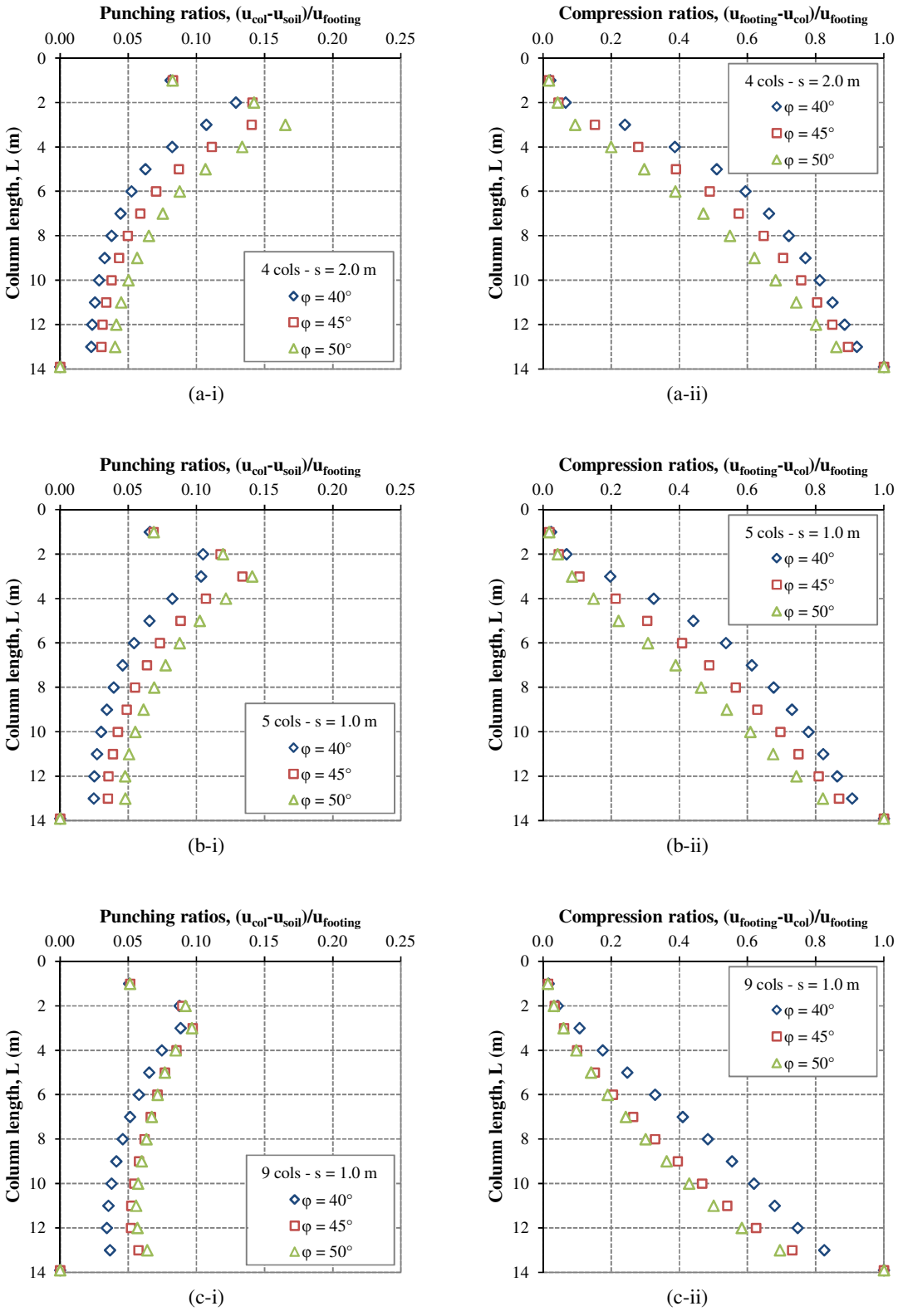

Figure 5.33 - Influence of column strength upon the variation of (i) punching and (ii) compression ratios with column length for a group of (a) 4, (b) 5 and (c) 9 columns beneath a 3 m square footing

can be seen that compression ratios decrease with an increasing angle of friction for the stone column. This results in a corresponding increase in punching ratios. The changes in punching and compression ratios are more pronounced for fewer columns and only negligible changes are observed when increasing the angle of internal friction from 45° to 50° for the group of 9 columns.

5.4.9 Influence of column installation effects

The influence of the coefficient of lateral earth pressure (K_0) for the lower Carse clay layer upon the deformational behaviour of various column arrangements supporting a 3 m square footing (see Figure 5.5) is shown in Figures 5.34. It appears that increasing K_0 has a minor influence upon punching and compression ratios. This is consistent with Kirsch (2006) who conducted a FEA on a group of stone columns and observed that column installation effects do not influence the deformational behaviour of stone columns but do enhance the settlement performance of stone columns.

5.4.10 Influence of stiff crust

The influence of the lower Carse clay and the stiff crust upon the deformational behaviour of various column arrangements (see Figure 5.5) supporting a 3 m square footing is shown in Figure 5.35. Profile 1 is the standard Bothkennar soil profile and the punching and compression ratios for this profile in Figure 5.35(i) were presented earlier in Figure 5.30.

Punching ratio

It can be seen in Figure 5.35(i) that punching ratios increase with column length up to a maximum at L = 3 m for Profile 1. A similar variation is observed for Profile 2, however punching ratios reach a maximum at L = 2 m and are lower than Profile 1 for column lengths L > 3 m. This reflects the increased stiffness at depth for Profile 2, as the lower Carse clay in the standard Bothkennar soil profile (Profile 1) is replaced with the stiffer upper Carse clay. Profile 3 consists entirely of upper Carse clay and, therefore, allows for the influence of the stiff crust to be assessed. It can be seen that punching ratios are largest near the surface for this soil profile and decrease with increasing column length thereafter. Punching ratios for Profile 3 are higher than Profiles 1 and 2 for short columns, but this trend reverses for columns longer than L = 3 m.

Compression ratio

The variation of compression ratios with column length is shown in Figure 5.35(ii). It can be seen that compression ratios are lowest for Profile 1, which indicates that columns formed in Profiles 2 and 3 are more susceptible to a bulging mode of deformation. This may be explained by a number of reasons:

(i) The lower Carse clay in Profile 1 is replaced by the stiffer upper Carse clay in Profiles 2 and 3. Therefore, the base of floating columns in Profile 2 and 3 is formed in a more competent soil layer. The enhanced support at the base of columns reduces punching and forces columns to compress more along their length.

(ii) The absence of the stiff crust (i.e. Profile 3) leads to the highest compression ratios. The stiff crust prevents bulging in the upper sections of columns, where overburden stresses are lowest.

It appears that the modes of deformation for columns formed in a homogenous soil profile, as used in the laboratory tests described in the literature review (see Sections 2.2 and 2.3), are very different to columns formed in a more realistic soil profile, as modelled in PLAXIS 3D Foundation. This is discussed in more detail in Section 7.3.3.

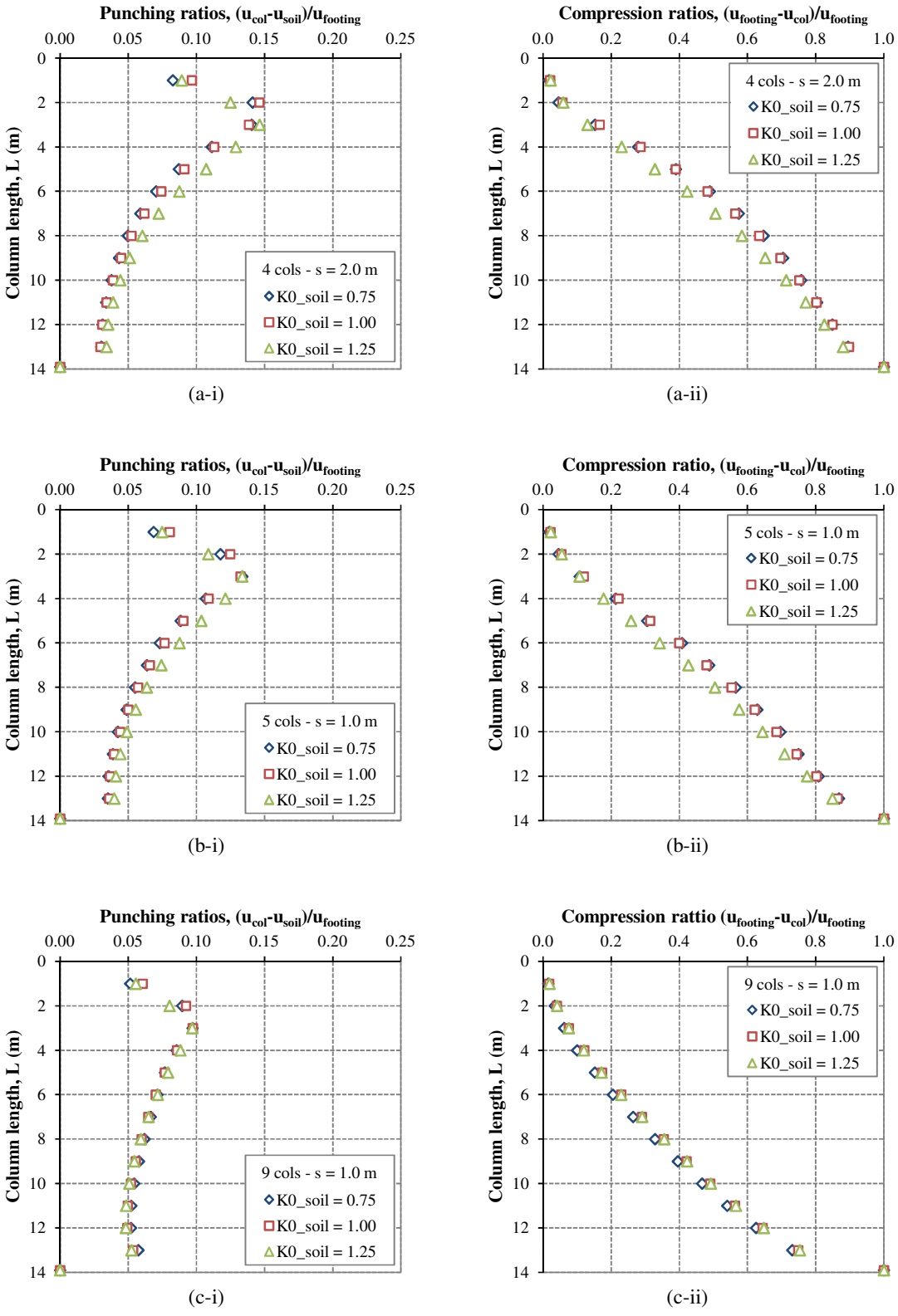

Figure 5.34 - Influence of column installation effects upon the variation of (i) punching and (ii) compression ratios with column length for a group of (a) 4, (b) 5 and (c) 9 columns beneath a 3 m square footing

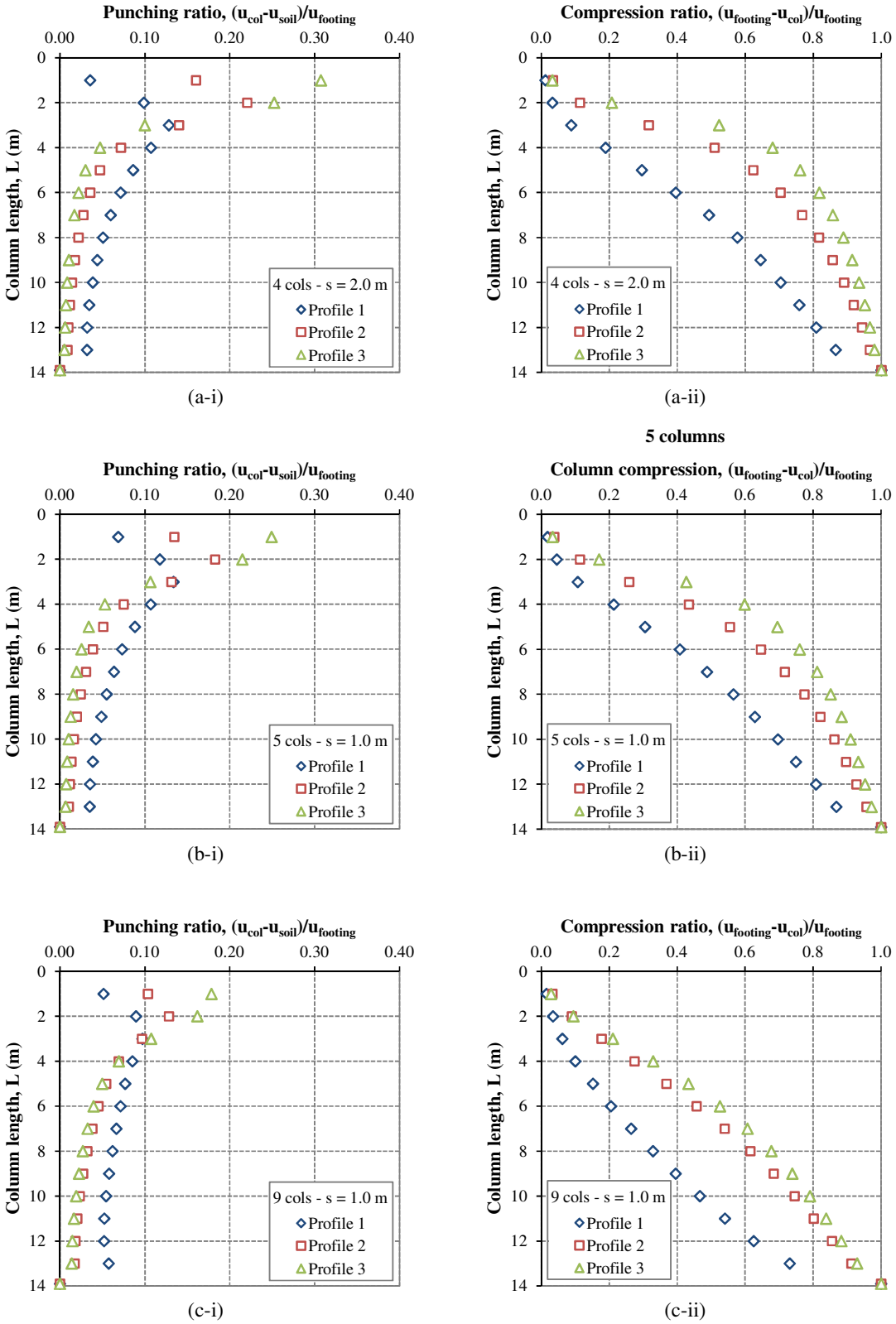

Figure 5.35 - Influence of stiff crust upon the variation of (i) punching and (ii) compression ratios with column length for a group of (a) 4, (b) 5 and (c) 9 columns beneath a 3 m square footing

5.5 Stress concentration ratio

The ratio of vertical effective stress in the column and the surrounding soil is known as the stress concentration ratio. It is an important parameter which indicates the efficiency of stone columns at enhancing the settlement performance of treated soils. The stress concentration ratio is typically measured at the top of stone columns. Stress concentration ratios from field tests (Munfakh *et al.*, 1984) and laboratory studies (Black 2006, McKelvey *et al.*, 2004 and Muir Wood *et al.*, 2000) are determined from pressure transducers which are located at discrete locations in columns and the surrounding soil, as shown in Figure 5.36(i). Stress concentration ratios are therefore relative to a specific point and hence a specific stress level. However, stress concentration ratios from numerical and analytical studies (Pulko & Majes, 2005) are measured more comprehensively, as vertical stress is averaged over the entire column and soil areas, as illustrated in Figure 5.36 (ii).

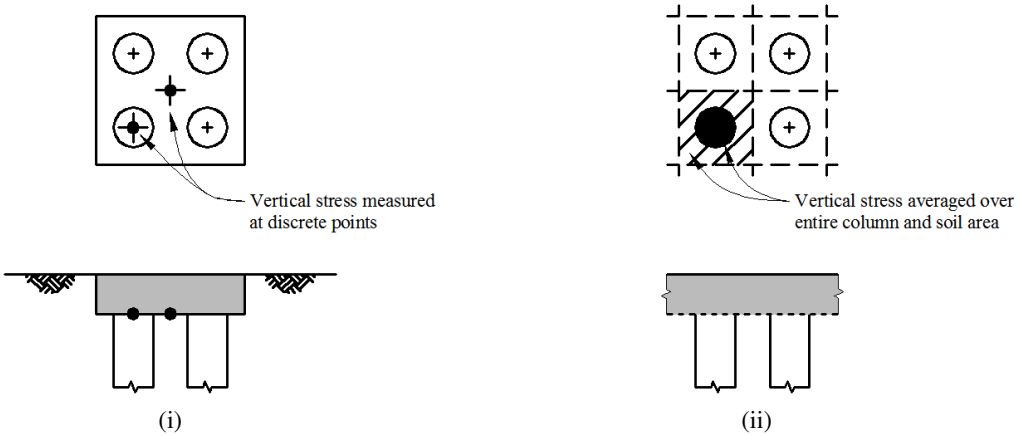

Figure 5.36 - Determination of stress concentration ratios for (i) field/laboratory studies and (ii) numerical/analytical studies

Stress concentration ratios from PLAXIS 3D Foundation are defined by two methods, which are illustrated in Figure 5.37:

(i) The first method compares the average vertical stress in each column (σ'_{col}) to the average vertical stress in the entire soil area beneath the footing ($\sigma'_{soil,\ average}$).

(ii) The second method compares the average vertical stress in each column (σ'_{col}) to the average vertical stress in the soil within a square zone of influence surrounding each column (σ'_{soil}); the width of the zone of influence is equal to the column spacing.

The first method allows the stress levels in corner, edge and centre columns to be directly compared with each other, as the average stress over the entire area of soil is used. The second method is a measure of the work each column is doing relative to the stress in the surrounding zone of influence and, therefore, indicates the efficiency of each column.

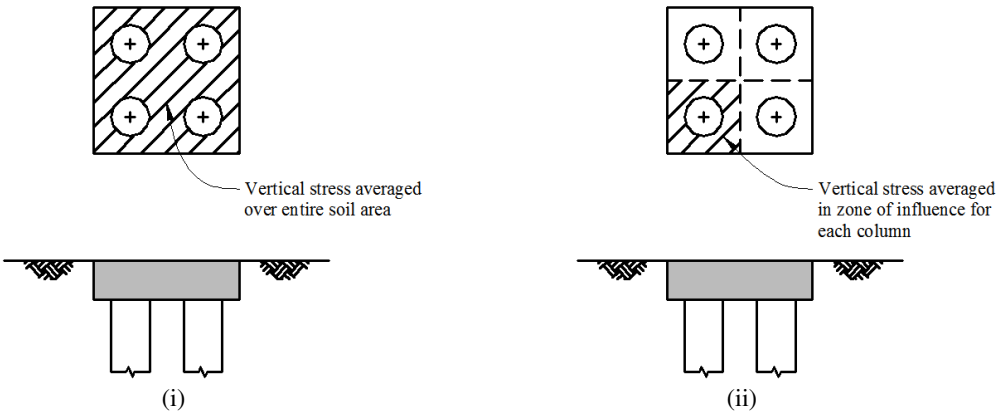

Figure 5.37 - Stress concentration ratio determined by (i) averaging stress over entire soil area and (ii) averaging stress within the zone of influence for each column

Stress concentration ratios determined from both methods will be identical for single columns, 2×2 groups and infinite grids as due to symmetry, the area of soil beneath footings corresponds to the zone of influence for each column. However, this is not the case for groups of columns larger than 2×2 configurations as the stress in the zone of influence varies for different columns. By way of example, the distribution of vertical effective stress immediately beneath a 4.5 m square concrete footing, which is (i) unreinforced (L = 0 m) and (ii) reinforced with a 3×3 group of end-bearing (L = 13.9 m) stone columns, is shown in Figure 5.38. It can be seen that high vertical stress develops beneath the edges of the rigid unreinforced footing. The high stress levels beneath the edges of the footing reduce for the reinforced case as columns absorb a larger proportion of the load and, therefore, reduce the stress on the surrounding soil.

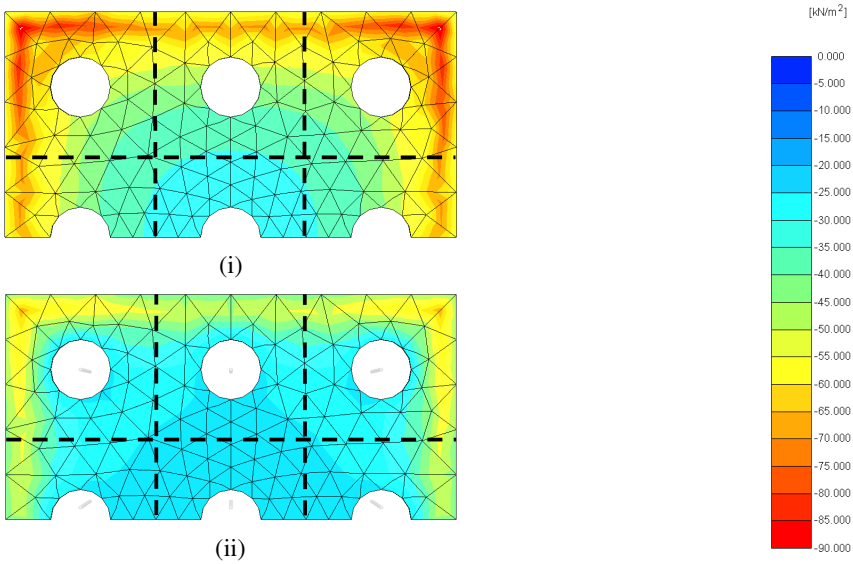

Figure 5.38 - Distribution of vertical effective stress (σ'_{vert}) immediately beneath a 4.5 m square footing, which is (i) unreinforced (L = 0 m) and (ii) reinforced with end-bearing stone columns (L = 13.9 m)

5.5.1 Stress concentration ratios for infinite grids of stone columns

The variation of stress concentration ratios with column length for an infinite grid of columns is shown in Figure 5.39. It can be seen that the stress concentration ratio remains relatively constant with increasing column length. It was shown previously (see Section 5.4.1) that an infinite grid of columns exhibit punching and bulging modes of deformation. It is also well known that all columns within an infinite grid deform equally due to symmetry. Consequently, no shear stress develops along the column-soil interface near the surface and the stress concentration ratio measured at the surface depends on the stiffness properties of the column and the surrounding soil. Therefore, the stress concentration ratio does not change with increasing column length.

A slight reduction in the stress concentration ratio is observed at high area ratios. Column confinement reduces at high area ratios, which consequently reduces the stiffness of stone columns and hence yields lower stress concentration ratios.

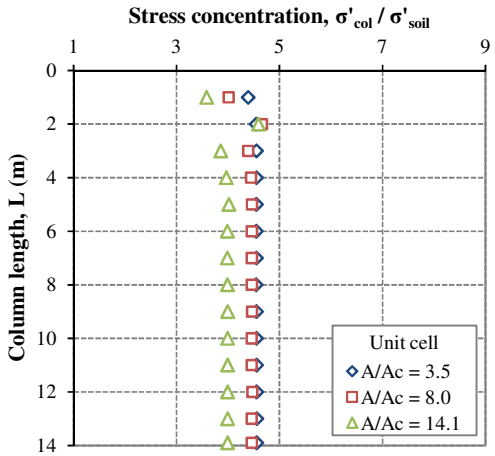

Figure 5.39 - Variation of stress concentration ratio with column length for an infinite grid of columns

5.5.2 Stress concentration ratios for small groups of stone columns

Single columns and 2×2 groups

The variation of stress concentration ratios with column length for single columns and 2×2 groups is shown in Figures 5.40(i) and 5.40(ii), respectively. An increase in stress concentration ratios with column length is observed for all columns shorter than L = 3 m. It was shown previously (see Section 5.4.2) that punching is the dominant mode of deformation for short single columns and 2×2 groups. Groups of columns which are punching develop

shear stress along the sides and end-bearing pressure at the base of columns. The load-carrying capacity of columns increases with increasing column length as shear stress can develop over a larger area. As a result, stress concentration ratios increase in concert.

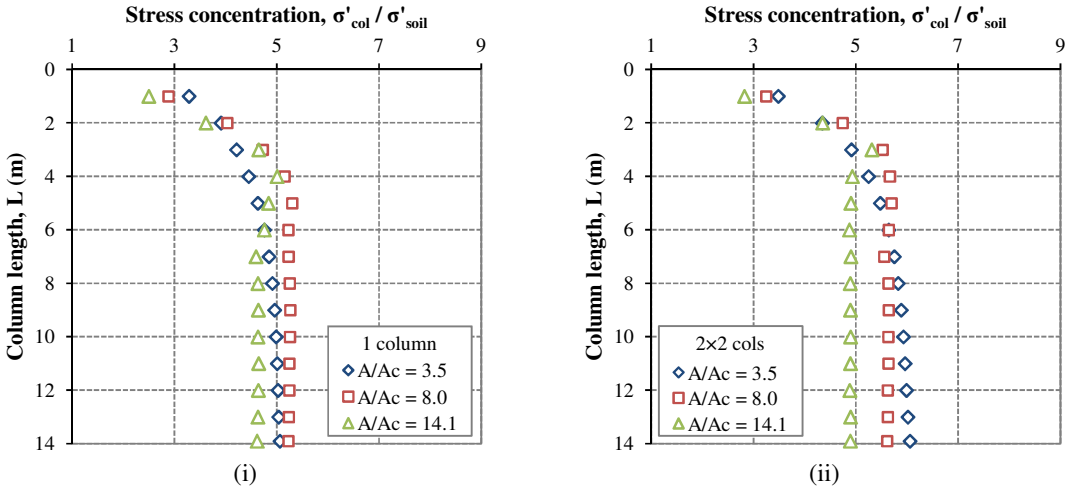

Figure 5.40 - Variation of stress concentration ratio with column length for (i) single and (ii) 2×2 groups of stone columns

Stress concentration ratios continue to increase with column length for closely-spaced columns (i.e. A/A_C = 3.5), which is consistent with previous findings that closely-spaced columns punch into the underlying soil. While large increases in stress concentration ratios are initially observed with increasing column length, the rate of increase in stress concentration ratios with column length reduces significantly for column lengths L > 3 m. This may attributed to large percentage increases in column length for short columns (100% for L = 1 → 2 m) compared to longer columns (10% for L = 10 → 11 m).

It can also be seen in Figures 5.40(i) and 5.40(ii) that stress concentration ratios for columns at A/A_C = 8.0 and 14.1 reach maximum values at L ≈ 4 m. Stress concentration ratios remain relatively constant with increasing column length thereafter for columns at A/A_C = 8.0, which indicates that the mode of deformation has changed from punching to bulging. Column bulging occurs at the point of lowest lateral support, which occurs near the top of the lower Carse clay (z ≈ 3 m). Increasing the column length for this mode of deformation does not enhance the load-carrying capacity of columns and, therefore, does not increase stress concentration ratios. A slight reduction in stress concentration ratios for columns at A/A_C = 14.1 is observed with increasing column length in the range 4–7 m and 4–5 m for single columns and 2×2 groups, respectively. A combination of punching and bulging modes of

deformation may be occurring over this range of lengths. However, bulging becomes more prevalent as column length increases and stress concentration ratios decrease slightly towards constant values.

A reduction in stress concentration ratios is observed for higher area ratios at L = 1 m. This is consistent with findings from the deformational behaviour of single columns and 2×2 groups, as shown in Figures 5.24(i) and 5.25(i), respectively, where a reduction in column punching is observed for higher area ratios at L = 1 m. The footing size increases at higher area ratios, which stresses the soil deeper and induces more displacement in the soil surrounding the base of columns at z = 1 m. Therefore, the end-bearing resistance at the base of columns, and consequently the load-carrying capacity of stone columns, reduces with increasing area ratio.

However, it is interesting to note that stress concentration ratios increase at a faster rate at higher area ratios for L = 2, 3 and 4 m. The average load carried per column increases with footing area. Therefore, a larger force is carried along the sides and at the base of columns. This results in high punching ratios, as shown in Section 5.4.3, and also forces columns to carry a larger proportion of the applied load which results in higher stress concentration ratios.

3×3 and 4×4 groups

The variation of stress concentration ratio with column length for 3×3 and 4×4 groups of columns is shown in Figures 5.41 and 5.42, respectively. The stress concentration ratio is measured using two methods, as outlined at the start of this section. The first method, which is shown in Figures 5.41(i) and 5.42(i), compares the average stress in columns with the average stress in the entire soil area beneath the footing. The second method, which is shown in Figures 5.41(ii) and 5.42(ii), compares the average stress in columns with the average stress in the soil surrounding each column.

Variation of stress concentration ratio with column position

It can be seen in Figures 5.41(i) and 5.42(i) that stress levels are highest in corner columns, followed by edge and centre columns. This is due to the position of columns relative to the edge of footings. It is well known from elastic theory that elevated stress levels develop beneath the edge of rigid footings and, therefore, positioning columns in this location gives them the potential to absorb more load. It can also be seen that the variation in stress

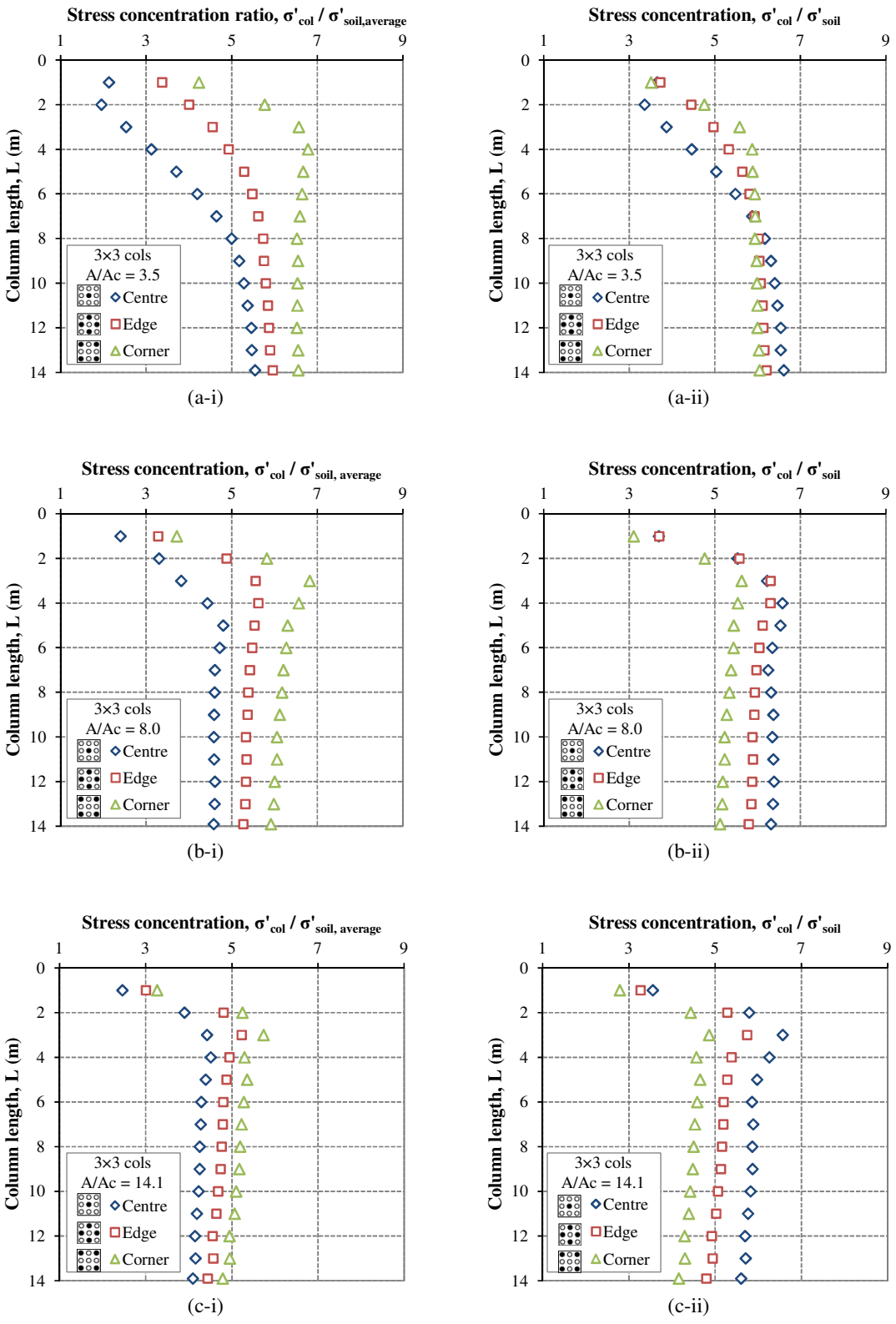

Figure 5.41 - Variation of stress concentration ratio with column length for a 3x3 group of columns, spaced at area ratios of (a) 3.5, (b) 8.0 and (c) 14.1

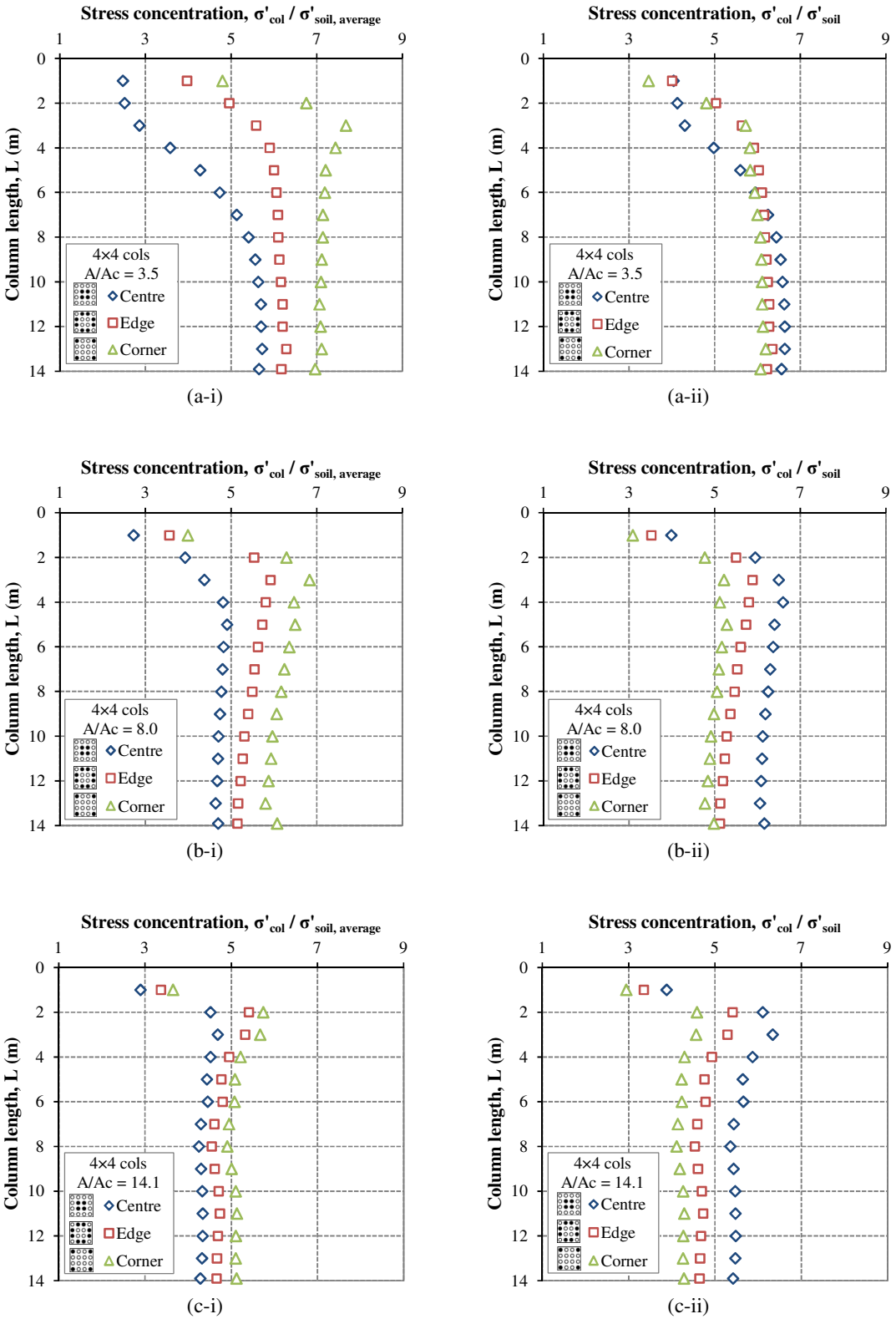

Figure 5.42 - Variation of stress concentration ratio with column length for a 4x4 group of columns, spaced at area ratios of (a) 3.5, (b) 8.0 and (c) 14.1

concentration ratios between individual columns becomes more pronounced for lower area ratios. The external row of columns are positioned a distance 0.5×s (s = column spacing) from the edge of footings. As column spacing decreases for lower area ratios, columns are positioned closer to the edge of footings and hence closer to the zone of elevated stress levels. Therefore, the variation in stress concentration ratios is most significant at low area ratios.

Variation of stress concentration ratio with column length and area ratio

The variation of stress concentration ratios with column length for 3×3 and 4×4 groups of columns at $A/A_C = 3.5$ is shown in Figures 5.41(a-i) and 5.42(a-i), respectively. An increase in stress concentration ratios with increasing column length is observed for all columns up to L = 4 m and L = 3 m for 3×3 and 4×4 groups of columns, respectively. A slight reduction in stress concentration ratios with increasing column length is subsequently observed for corner columns up to $L \approx 7$ m, while stress concentration ratios in edge and centre columns continue to increase or remain constant. As outlined previously, corner columns carry a greater proportion of the applied load due to the position of columns relative to the footing edge. However, corner columns are more susceptible to bulging and bending as column length increases. Therefore, corner columns cannot sustain the high levels of vertical stress and transfer the applied load to edge and centre columns. Consequently, stress concentration ratios continue to increase with column length for edge and centre columns.

The transfer of vertical stress from corner columns to edge and centre columns is also evident in the variation of stress concentration ratios, measured using the second method ($\sigma'_{col}/\sigma'_{soil}$). It can be seen in Figures 5.41(a-ii) and 5.42(a-ii) for 3×3 and 4×4 groups of columns, respectively, that corner and edge columns initially carry a larger proportion of the applied load relative to the surrounding soil. However, as column length increases a larger proportion of the load is carried by centre columns relative to the surrounding soil. This reflects the higher levels of lateral confinement associated with central columns.

The variation of stress concentration ratios with column length for columns spaced at high area ratios (i.e. $A/A_C = 8.0$ and 14.1) is shown in Figures 5.41(b-i) and 5.41(c-i) for 3×3 groups of columns and 5.42(b-i) and 5.42(c-i) for 4×4 groups of columns. As with closely-spaced columns, it can be seen that stress concentration ratios increase with column length up to L = 3 m. This is again consistent with a punching mode of deformation and is in keeping with previous findings for short widely-spaced columns. A slight reduction in stress

concentration ratios with increasing column length is subsequently observed for corner columns up to L ≈ 5 m, while stress concentration ratios continue to increase for centre columns at A/A_C = 8.0. This indicates that the heavily loaded corner columns transfer the applied vertical load to centre columns. No change in stress concentration ratio with increasing column length is observed thereafter, which suggests that bulging is the dominant mode of deformation. While no transfer of stress is evident for columns at an area ratio A/A_C = 14.1, it can be seen that stress concentration ratios for all columns (i.e. corner, edge and centre) reduce slightly with increasing column length up to L ≈ 6 m and are constant thereafter. The absence of stress transfer from corner to centre columns may be attributed to the relatively uniform stress levels in all columns. The slight reduction in stress concentration ratios with is also evident from single and 2×2 groups of columns and suggests that both punching and bulging modes of deformation are occurring. Bulging becomes more prevalent as column length increases and no change in stress concentration ratios is observed with increasing column length.

The positive influence of column confinement can be seen in Figures 5.41(b-ii) and 5.41(c-ii) for 3×3 groups of columns and 5.42(b-ii) and 5.42(c-ii) for 4×4 groups of columns. Stress concentration ratios - measured using the second method (i.e. the vertical stress in columns relative to the local stress level) - are highest in the centre columns. This reflects the increased levels of lateral confinement associated with centre columns. This is in contrast to edge and corner columns which bulge and bend outwards away from central columns.

5.5.3 Comparison of infinite grid with small groups of columns

The influence of the number of columns upon the variation of stress concentration ratios is shown in Figures 5.43. It can be seen in Figure 5.43(a) for closely-spaced columns (i.e. A/A_C = 3.5) that stress concentration ratios increase for larger groups of columns. In addition to the enhanced lateral confinement associated with larger groups of columns, the increase in stress concentration ratios is also due to the position of columns relative to the footing edge. The distribution of vertical stress beneath unreinforced footings for a single column, 2×2 group, 3×3 group and 4×4 group of columns is shown in Figure 5.44. As the number of columns increases, the external rows of columns are positioned progressively closer to the edge of footings. Therefore, these columns are located in the zone of elevated stress levels and have

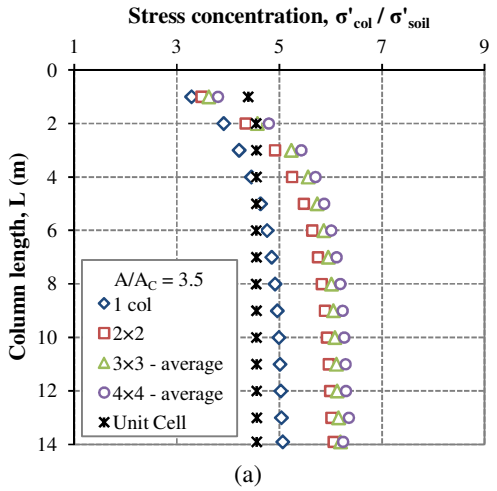

(a)

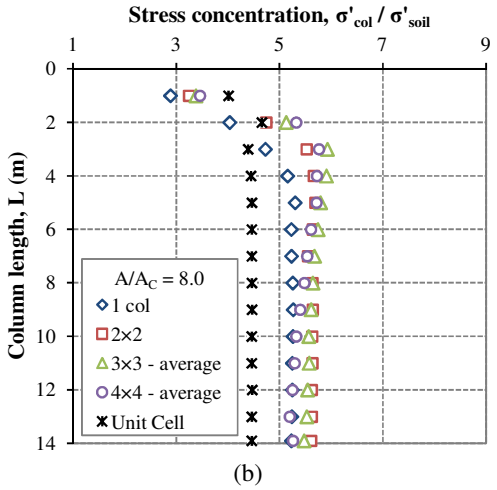

(b)

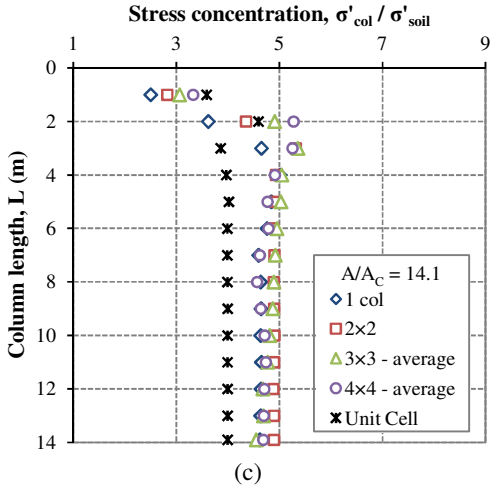

(c)

Figure 5.43 - Variation of stress concentration ratio for small groups and infinite grids of columns spaced at area ratios of (a) 3.5, (b) 8.0 and (c) 14.1

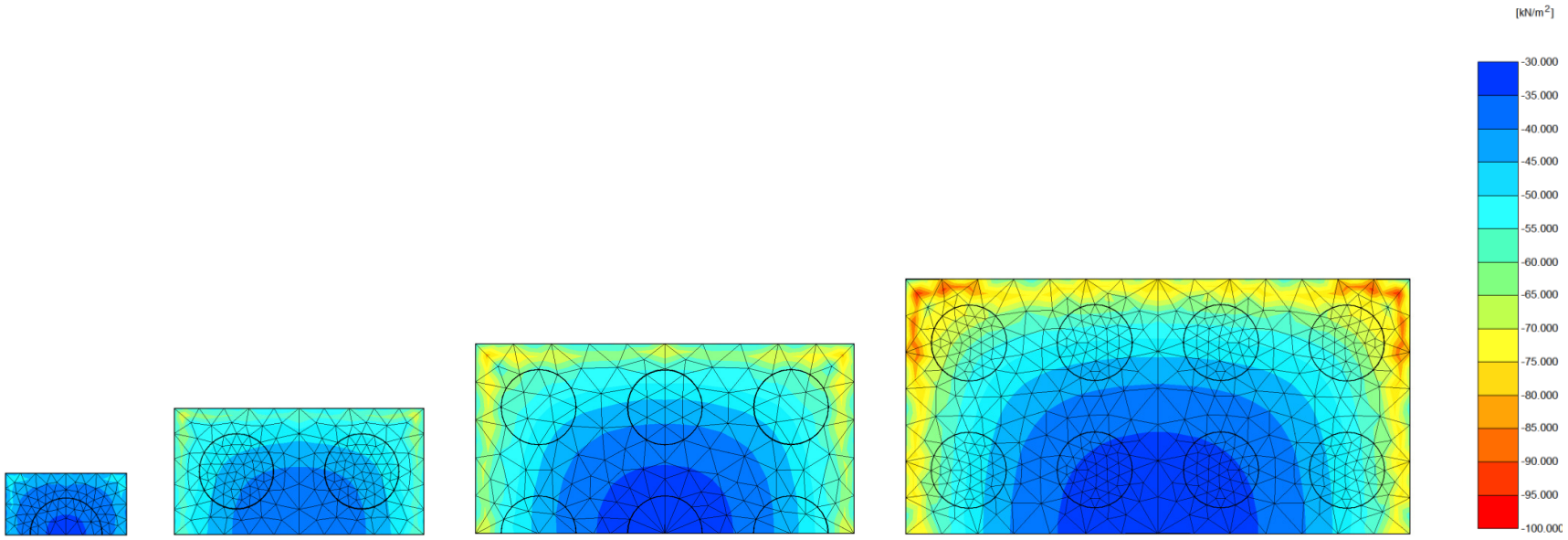

Figure 5.44 - Vertical stress beneath an unreinforced footing for (i) single column, (ii) 2×2, (iii) 3×3 and (iv) 4×4 groups of columns at an area ratio of 3.5

the potential to absorb a larger proportion of the applied load. Consequently, the average stress concentration ratios for the group of columns increases.

A similar trend is observed for short columns at higher area ratios (i.e. A/A_C = 8.0 and 14.1) in Figures 4.43(b) and 4.43(c). It was established previously that punching is the dominant mode of deformation for this configuration of columns. An increase in stress concentration ratios with an increasing number of columns is again due to the position of columns relative to the edge of the footing. However, once column length exceeds L = 3 m, the mode of deformation changes to bulging and no difference in stress concentration ratios is observed. Columns which are bulging fail at the same location (i.e. the weakest part of the soil profile). Therefore, the ultimate load is the same for all columns and is not dependent upon the position of columns relative to the edge of footings.

The stress concentration ratios for a unit cell are relatively uniform as columns are located within an infinite grid and therefore are not subject to the elevated stress levels near the edge of rigid footings.

5.5.4 Influence of column arrangement

The variation of the stress concentration ratio with column length for various arrangements of stone columns (see Figure 5.3) beneath a 3 m square footing is shown in Figure 5.45. Stress concentration ratios for groups of 4 and 5 columns (A/A_C = 8.0 and 6.4, respectively) increase with column length up to a maximum at L = 3 m. This suggests that punching is the dominant mode of deformation which corresponds with previous findings for short columns at high area ratios. A slight decrease in stress concentration ratios is observed with increasing column length up to L = 6 m, which is followed by constant stress concentration ratios thereafter. The slight reduction in stress concentration ratios with column length indicates that the mode of deformation is changing from punching to bulging. Column bulging becomes more prominent as column length increases, which results in lower stress concentration ratios. It appears that bulging is the only mode of deformation for column lengths longer than L = 6 m as stress concentration ratios are constant. Increasing the length of columns which are bulging or bending does not enhance the load-carrying capacity and, therefore, does not result in increased stress concentration ratios. It can also be seen in Figure 5.45 that stress concentration ratios are higher for the group of 4 columns than the group of 5

columns. The lower stress concentrations ratios for the group of 5 columns are observed due to the location of the central column in a region of lower stress levels (see Figure 5.44). Therefore, this column takes less of the applied load and the average stress concentration ratio for the group is reduced.

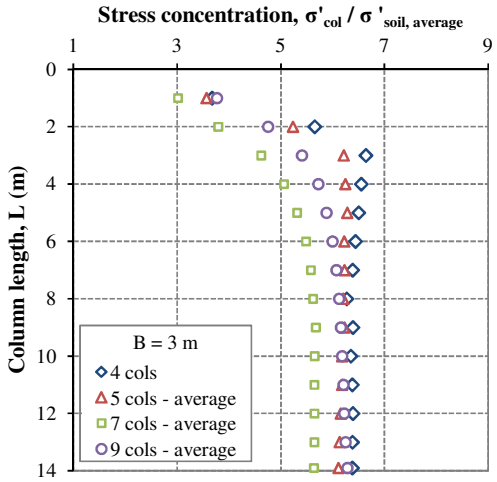

Figure 5.45 - Variation of stress concentration ratio with column length for a group of 4, 5, 7 and 9 columns beneath a 3 m square footing

The variation of stress concentration ratios with length for the groups of 7 and 9 columns is quite different to groups of 4 and 5 columns. Stress concentration ratios for groups of 7 columns and 9 columns increase at a slower rate with column length up to L = 3 m than the smaller groups of columns. Furthermore, stress concentration ratios for the groups of 7 and 9 columns continue to increase with length longer than L = 3 m, which suggests that punching remains the dominant mode of deformation with increasing column length. However, the rate of increase in stress concentration ratio reduces with increasing column length and stress concentration ratios are eventually constant for the group of 7 columns longer than L = 8 m. The magnitude of stress concentration ratios is higher for the group of 9 columns than the group of 7 columns. This is due to the position of columns relative to the footing edge. The outer ring of columns for a 9 column group are positioned closer to the footing edge and therefore closer to the elevated stress levels which develop in this region.

5.5.5 Influence of column position

The influence of column position relative to the footing edge (see Figure 5.4) upon stress concentration ratios is shown in Figure 5.46. The variation of stress concentration ratios with column length is quite similar to previous findings for columns at high area ratios. Stress

concentration ratios increase with column length up to L = 3 m, which indicates that all column configurations are punching into the underlying soil. However, no increase in the stress concentration ratio is observed with increasing column length thereafter, which indicates that the mode of deformation has changed to bulging. A slight decrease in stress concentration ratios with column length is observed in the range 3–6 m for columns spaced at 2.0 m, which indicates that a transition from punching to bulging occurs for this range of column lengths.

It can be seen in Figure 5.46 that the position of columns relative to the footing edge has a significant influence upon stress concentration ratios. Stress concentration ratios increase as columns are positioned closer to the footing edge; an increase of c.50% is observed at L = 3 m. This is due to elevated stress levels which occur beneath the edge of rigid footings, as shown in Figure 5.47. Positioning columns closer to this zone allows columns to absorb more load and hence develop higher stress concentration ratios. However, it was shown in Section 5.3.5 that the position of columns relative to the footing edge has a relatively minor influence upon the settlement performance of stone columns. Therefore, stress concentration ratios measured at the surface do not define the settlement behaviour of a group of columns. This is an interesting finding and suggests that the variation of stress concentration ratios with depth, which is not routinely measured in laboratory or field tests, may play an important role in determining the settlement performance of stone columns. The variation of stress concentration ratio with depth is investigated as part of this thesis in Section 6.3.

The influence of footing overhang upon stress concentration ratios is also investigated by comparing a 2×2 group of columns spaced at 1.0 m beneath a 2 m and a 3 m square footing. It can be seen in Figure 5.46 that stress concentration ratios for the 3 m square footing increase with column length to a maximum at L = 3 m and are constant thereafter. In contrast, a continuous increase in stress concentration ratios with increasing column length is observed for the 2 m square footing. Furthermore, it can be seen that stress concentration ratios are higher for the 2×2 group of columns beneath a 2 m footing. This is again due to the position of the columns close to the footing edge.

It appears that the position of columns and the mode of deformation both play important roles in the magnitude of stress concentration ratios.

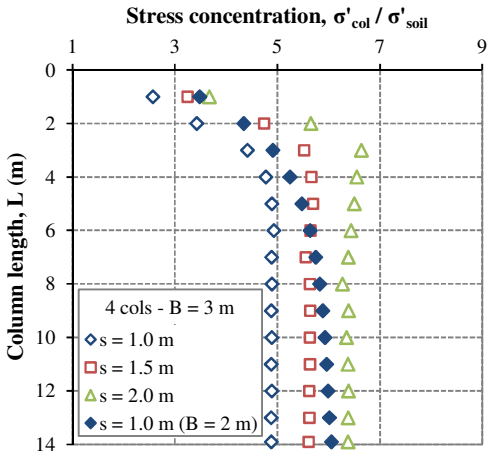

Figure 5.46 - Variation of stress concentration ratio with column length for various columns positions beneath a 3 m square footing

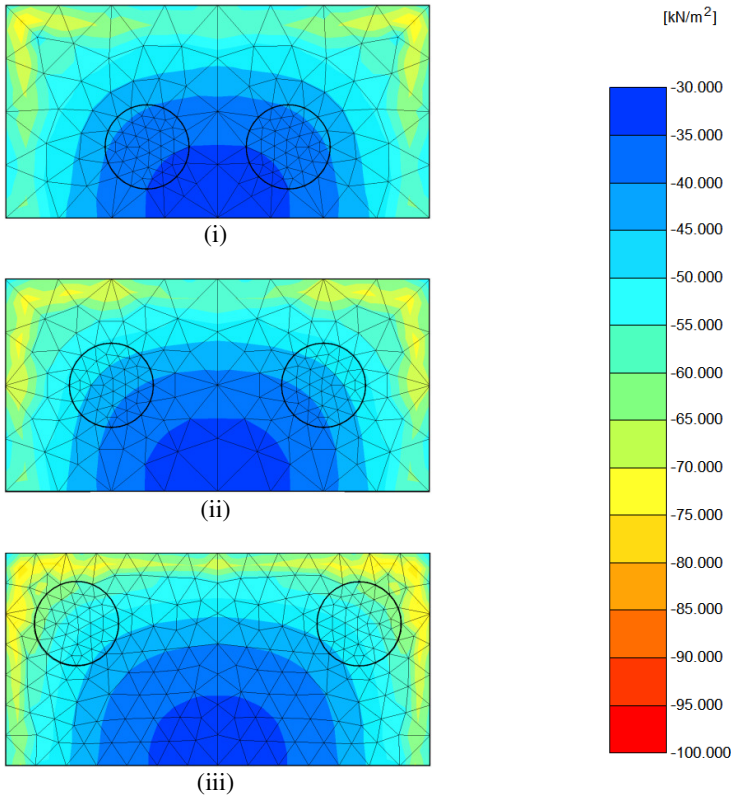

Figure 5.47 - Vertical effective stress beneath a 3 m square footing for columns spaced at (i) 1.0 m, (ii) 1.5 m and (iii) 2.0 m

5.5.6 Influence of column stiffness

The influence of column stiffness upon stress concentration ratios for various arrangements of columns (see Figure 5.5) beneath a 3 m square footing is shown in Figure 5.48. Column

stiffness is controlled by the secant Young's modulus (E_{50}) and it can be seen that an increase in E_{50} leads to higher stress concentration ratios.

It can be seen for columns shorter than L = 3 m that the influence of columns stiffness upon stress concentration ratios becomes more pronounced as column length increases up to L = 3 m. However, the variation in stress concentration ratios with E_{50} does not change with increasing column length thereafter for groups of 4 and 5 columns, as shown in Figure 5.48(a) and 5.48(b), respectively. This may be related to the bulging mode of deformation which becomes more prevalent for groups of 4 and 5 columns which are longer than L = 3 m. It was shown previously that the load-carrying capacity, and hence the stress concentration ratio, of columns which are bulging does not increase with column length.

The variation of stress concentration ratios with column length for a group of 9 columns is shown in Figure 5.48(c). As with the groups of 4 and 5 columns, the influence of column stiffness becomes more pronounced with increasing column length up to L = 3 m. Stress concentration ratios continue to increase at a slower rate with increasing column length thereafter for E_{50} = 70 MPa. However, no increase in stress concentration ratios is observed with column length for E_{50} = 30 MPa, which suggests that the mode of deformation has changed from punching to bulging.

A linear relationship appears to exist between column stiffness and stress concentration ratios as shown by stress concentration ratios for end-bearing columns in Table 5.4. Reductions in Young's moduli of 29% (E_{50} = 70 MPa→50 MPa) and 57% (E_{50} = 70 MPa→30 MPa) yield average reductions in stress concentration ratios of 12% and 31%, respectively.

Table 5.4 - Influence of column compressibility upon stress concentration ratios for end-bearing columns

	Stress concentration ratio, $\sigma'_{col} / \sigma'_{soil}$			% reduction		
No. of cols	Column compressibility, E_{50} (MPa)			Column compressibility, E_{50} (MPa)		
	30	50	70	30	50	70
4	4.6	5.7	6.4	-28	-11	-
5	4.3	5.4	6.1	-30	-11	-
9	4.1	5.3	6.3	-35	-15	-

5.5.7 Influence of column strength

The influence of column strength upon the stress concentration ratio for various arrangements of columns (see Figure 5.5) beneath a 3 m square footing is shown in Figure 5.49. The

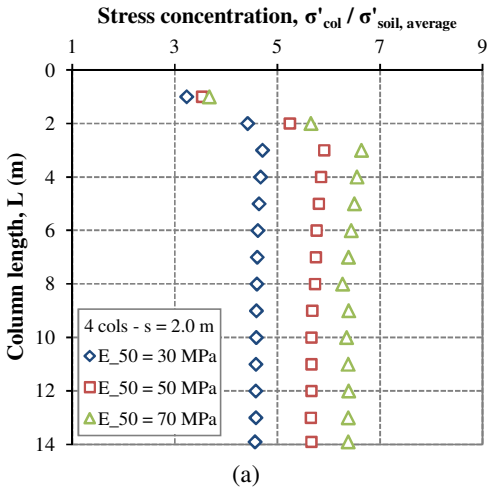

(a)

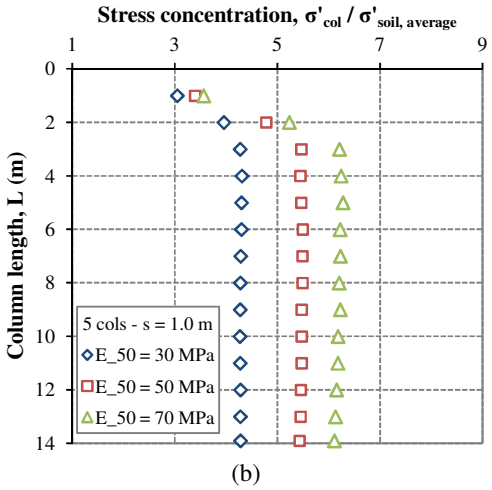

(b)

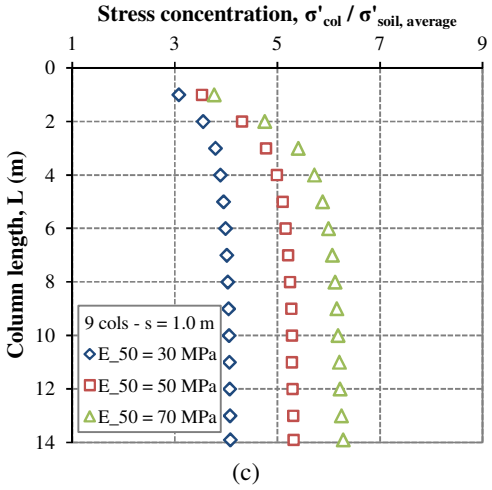

(c)

Figure 5.48 - Influence of column compressibility upon the variation of stress concentration ratios with column length for a group of (a) 4, (b) 5 and (c) 9 columns beneath a 3 m square footing

variation of stress concentration ratio with column length for groups of 4 and 5 columns is shown in Figures 5.49(a) and 5.49(b), respectively. Negligible changes in stress concentration ratios are observed with increasing column strength for short columns. However, it can be seen that increasing the strength of columns which are longer than L = 3 m leads to significant increase in stress concentrations ratios. This suggests that the influence of column strength upon stress concentration ratios is dependent on the mode of deformation. Column strength is controlled by the angle of internal friction and this parameter is only mobilised when columns are in a plastic state. Columns which are punching do not mobilise the column strength as stresses are concentrated along the column-soil interface and at the base of columns. Therefore, stress concentration ratios do not increase with column strength for columns which exhibit punching.

The variation of stress concentration ratio with column length for a group of 9 columns is shown in Figure 5.49(c). As with the groups of 4 and 5 columns, no variation of stress concentration ratios is observed with column strength for short columns. However, a decrease in column strength, from $\varphi = 45°$ to 40°, leads to a reduction in stress concentration ratios. Stress concentration ratios are relatively constant with increasing column length for columns longer than L = 3 m and defined by $\varphi = 40°$. This suggests that this configuration of columns is bulging. In contrast, a slight increase in stress concentration ratios with column length is observed for columns longer than L = 3 m and defined by $\varphi = 45°$. This is consistent with a punching mode of deformation. Furthermore, no variation of stress concentration ratios is observed when increasing column strength from $\varphi = 45°$ to 50°. Therefore, the stronger group of columns also exhibits punching and, consequently, stress concentration ratios are not influenced by a change in the column strength.

5.5.8 Influence of column installation effects

The influence of the coefficient of lateral earth pressure for the lower Carse clay layer upon stress concentration ratios for various arrangements of columns (see Figure 5.5) beneath a 3 m square footing is shown in Figure 5.49. It appears that this parameter has a negligible influence upon stress concentration ratios. However, slight increases in stress concentration ratios are observed for the groups of 4 and 5 columns at the transition from punching to bulging, i.e. for column lengths in the range of 3–5 m and 3–7 m for groups of 4 and 5 columns, respectively.

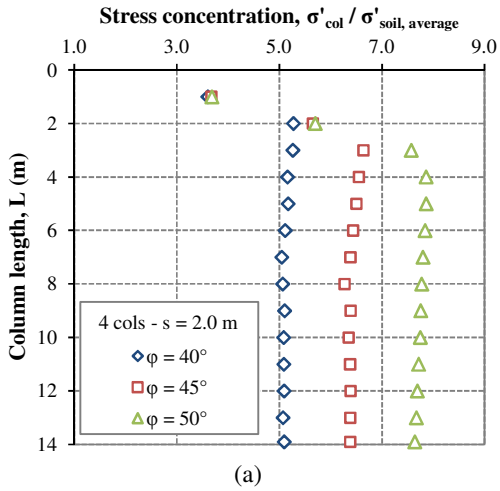

(a)

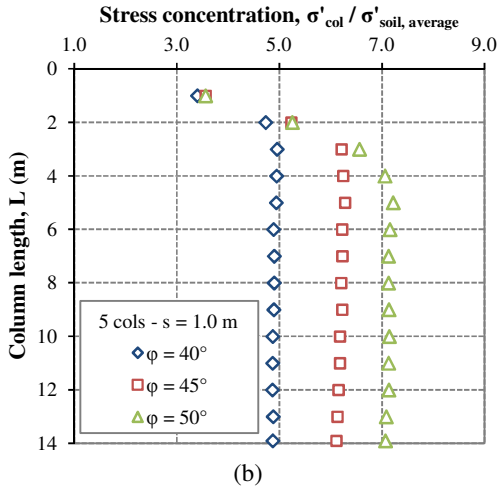

(b)

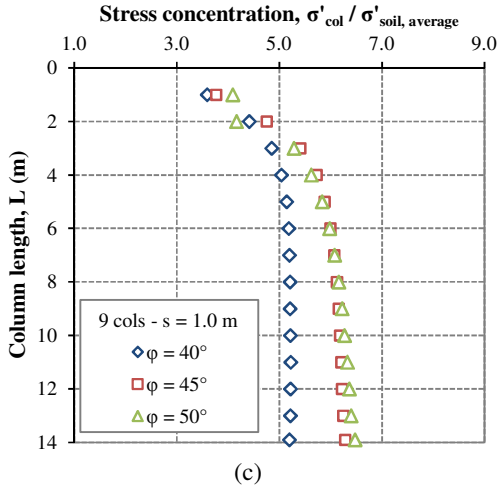

(c)

Figure 5.49 - Influence of column strength upon the variation of stress concentration ratios with column length for a group of (a) 4, (b) 5 and (c) 9 columns beneath a 3 m square footing

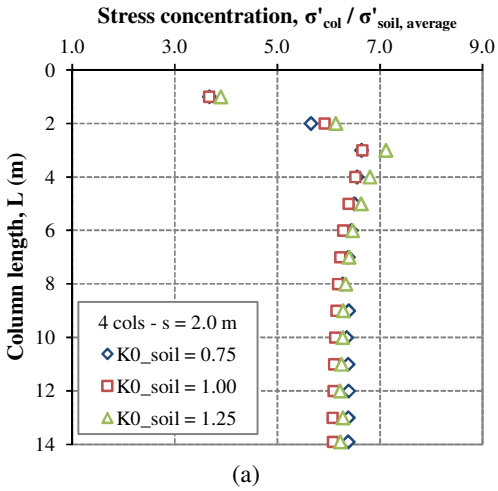

(a)

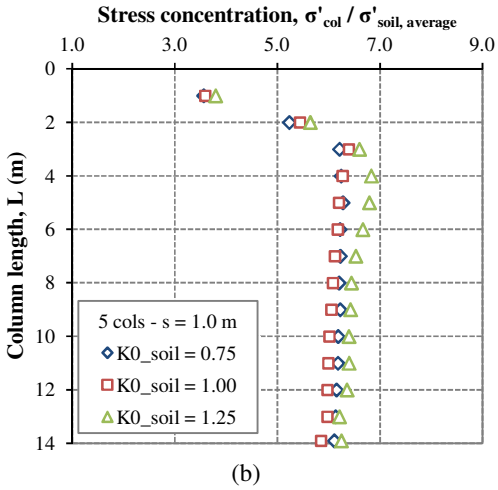

(b)

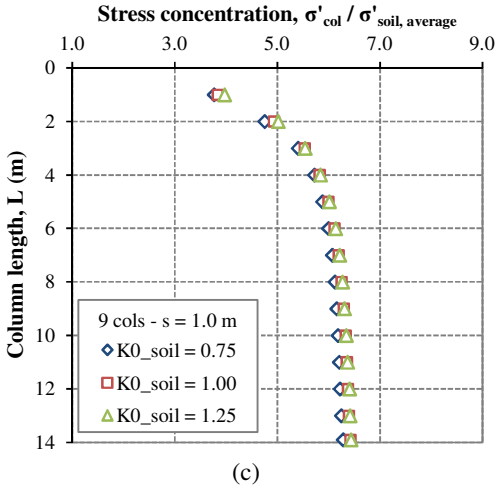

(c)

Figure 5.50 - Influence of column installation effects upon the variation of stress concentration ratios with column length for a group of (a) 4, (b) 5 and (c) 9 columns beneath a 3 m square footing

5.5.9 Influence of stiff crust

The influence of the lower Carse clay and stiff crust upon stress concentration ratios for various arrangements of columns beneath a 3 m square footing is shown in Figure 4.49. It can be seen that stress concentration ratios increase with column length up to L = 3 m for all soil profiles. This suggests that punching is the dominant mode of deformation for all short columns. It can also be seen that stress concentration ratios for columns formed in Profile 2 are higher than Profile 1. This may be related to the increased stiffness of the soil layers at depth in Profile 2 compared to Profile 1. It was shown earlier that columns formed in Profile 2 yield higher compression ratios as the base of columns are formed in stiffer soil strata. Therefore, columns formed in Profile 2 carry a larger proportion of the applied load and hence yield higher stress concentration ratios.

A further increase in stress concentration ratios is observed for columns formed in Profile 3. This is due to the absence of the stiff crust at the ground surface. The soil at the ground surface in Profile 3 consists of upper Carse clay, which yields a higher modular ratio (E_{col}/E_{soil}) than Profile 1. This results in higher levels of vertical stress in the stone columns, which consequently leads to higher stress concentration ratios.

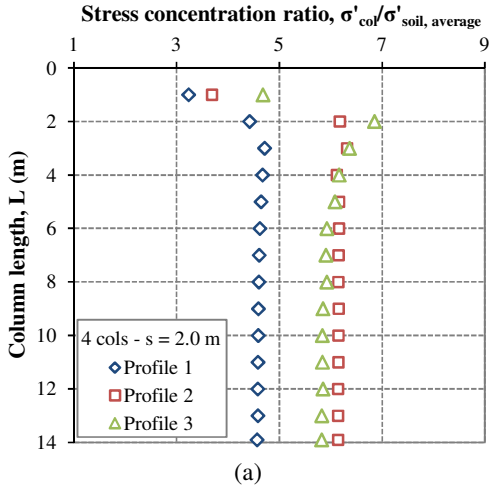

(a)

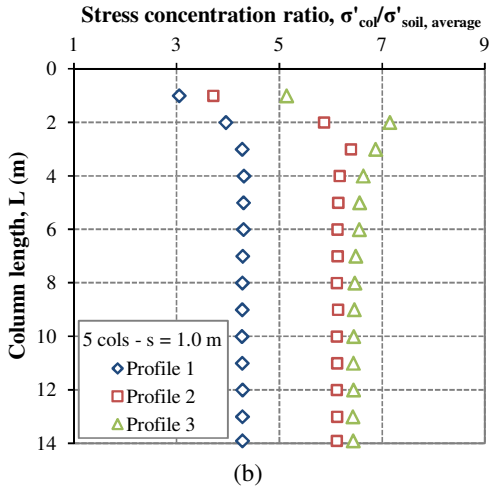

(b)

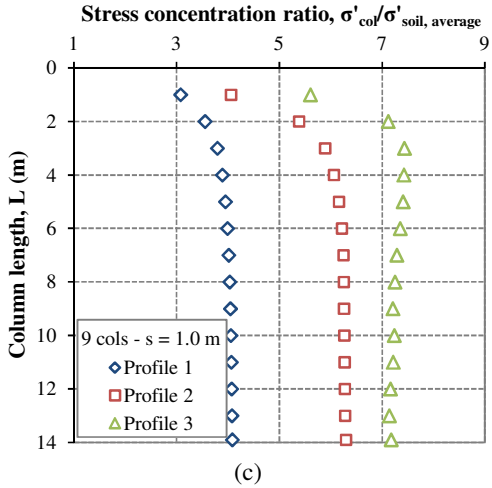

(c)

Figure 5.51 - Influence of stiff crust upon the variation of stress concentration ratios with column length for a group of (a) 4, (b) 5 and (c) 9 columns beneath a 3 m square footing

5.6 Summary of results of FEA: Settlement performance, deformational behaviour and stress concentration ratios

Various arrangements of columns were analysed over a typical range of area ratios to examine the relationship between area ratio, column length and column confinement (i.e. increasing the number of columns). The influence of key design parameters was examined for a select number of column configurations, which were specifically chosen to cover a wide range of area ratios. The settlement performance and deformational behaviour of stone columns was measured at 50 kPa, which was deemed a typical working load for the Bothkennar test site.

5.6.1 Settlement performance

The settlement performance was measured using a settlement improvement factor, n, which is defined as the ratio of the settlement for an untreated and treated footing. It was found that the area ratio, column length and column confinement all have a positive influence upon the settlement performance of stone columns. Moreover, the influence of area ratio and column length appears to be inter-related as the influence of column length becomes more pronounced at low area ratios. A continuous increase in settlement improvement factors with increasing column length was observed for columns at low area ratios, while the increase settlement improvement factors with column length tails off for long columns at higher ratios.

Influence of key design parameters:

- A trade off exists between area ratio and column length, as short closely-spaced columns and long widely-spaced columns can be adopted to achieve a specific settlement performance. This raises the possibility of optimising the design of stone columns by minimising the volume of stone; however, other factors such as construction time must also be taken into account.
- Small benefits can be gained by positioning columns closer to the edge of rigid footings. This may be attributed to the elevated stress levels in this region. However, the presence of the stiff crust may be masking the beneficial effects of column position, to a certain extent.
- The stiffness and strength of stone columns were found to a have significant influence on the settlement performance of stone columns at low and high area ratios, respectively.

The influence of these parameters is related to the degree of plasticity within columns, and hence the mode of deformation.

- The coefficient of lateral earth pressure has a positive influence on the settlement performance of stone columns and this is most pronounced at high area ratios.
- The presence of the stiff crust has a significant influence upon the settlement performance of stone columns. It was found that the improvement in settlement improvement factors tails of significantly for homogenous soils samples, i.e. without a stiff crust. This profile is similar to that adopted in laboratory studies (see Sections 2.2 and 2.3) and may explain why authors have postulated critical lengths in the past. However, critical lengths are less well defined for more realistic soil profiles.

5.6.2 Deformational behaviour

The deformational behaviour of stone columns was examined in this thesis using newly defined punching and compression ratios, which essentially are a measure of the normalised punching at the base of columns and axial strain along the length of columns, respectively. Columns which are punching transfer a significant proportion of the applied load to the base of columns and, consequently, this mode of deformation is characterised by high punching and low compression ratios. In contrast, columns which are bulging deform extensively along their length and cannot transfer the applied load to the base of columns. Therefore, the bulging mode of bulging is characterised by low punching and high compression ratios. Using these ratios, it was possible to determine which mode of deformation (i.e. punching or bulging) was most influential for each configuration of columns.

Three modes of deformation were identified from the numerical analysis: (i) punching; (ii) 'block' failure and (iii) bulging. The punching mode of deformation is observed for all short columns (i.e. $L < 3$ m), as an increase in punching ratios is coupled with relatively low compression ratios. Punching remains the primary mode of deformation for long single columns at low area ratios, as relatively high punching and low compression ratios are observed with increasing column length. 'Block' failure is characterised by low punching and compression ratios and this mode of deformation is observed for large groups of columns at low area ratios. 'Block' failure is effectively an extension of punching, as columns act as a single entity with the surrounding soil and punch uniformly, thus yielding low punching ratios. The bulging mode of deformation is observed for long columns at high area ratios, as a

significant decrease in punching ratios, coupled with an increase in compression ratios is observed with increasing column length. In culmination, it appears that the number of columns does not fundamentally change the mode of deformation, and that the deformational behaviour of columns is governed by the area ratio and column length.

Influence of key design parameters:

- The influence of column stiffness and strength is most pronounced for columns at low and high area ratios, respectively. Columns at low area ratios in more of an elastic state and, therefore, are more susceptible to changes in the elastic stiffness moduli. In contrast, the extent of plasticity within groups of columns is more pronounced at high area ratios and these configurations of columns are more influenced by changes in the strength characteristics of stone columns.
- The coefficient of lateral earth pressure does not influence the deformational behaviour of columns, which is consistent with a numerical study conducted by Kirsch (2006).
- The presence of the stiff crust has a significant influence on the deformational behaviour of stone columns. It was observed that column configurations formed in a homogenous soil sample exhibit lower punching and higher compression ratios, which suggests a bulging mode deformation is more pronounced. Column bulging occurs at the point of lowest lateral resistant, which is generally near the ground surface. Therefore, removing the stiff crust allows columns to bulge closer to the ground surface.

5.6.3 Stress concentration ratios

The stress concentration ratio is an important parameter which compares the vertical effective stress in columns (σ'_{col}) to the surrounding soil (σ'_{soil}). It is generally measured at the ground surface and is defined by two methods in this thesis:

(i) The first method compares the average vertical effective stress in columns (σ'_{col}) to the average stress in the entire soil area beneath the footing ($\sigma'_{soil, average}$).

(ii) The second method compares the average vertical stress in columns (σ'_{col}) to the average vertical stress in the soil within a square zone of influence surrounding each column (σ'_{soil}); the width of the zone of influence is equal to the column spacing.

Stress concentration ratios do not increase with column length for an infinite grid of columns. This is due to symmetry which ensures that the behaviour of an infinite grid of columns is

identical and, consequently, no shear stress develops along the side of the columns near the ground surface. Therefore, stress concentration ratios are only dependent upon the modular ratio (E_{col}/E_{soil}). In contrast, stress concentration ratios for a group of stone columns are dependent upon the mode of deformation. Columns which are punching develop low stress concentration ratios, which increase with column length. However, no increase in stress concentration ratios is observed with increasing column length for columns which exhibit a bulging mode of deformation. Bulging occurs at the point of lowest lateral resistance and increasing the column length does not enhance the load-carrying capacity of stone columns.

Influence of key design parameters:

- Stress concentration ratios measured using the method (i) indicate that corner corners carry a higher proportion of the applied load, followed by edge columns and centre columns. This may be attributed to the elevated levels of vertical stress beneath the edge of rigid footings.
- Stress concentration ratios measured using method (ii) suggests that centre columns carry the highest proportion of the applied load relative to the stress in the surrounding zone of influence. This reflects the increased levels of lateral confinement associated with centre columns.
- Increasing the stiffness and strength of columns yields higher stress concentration ratios. This is most pronounced for columns which exhibit a bulging mode of deformation, as columns which are punching transfer the applied load along the column-soil interface.
- Increasing the coefficient of lateral earth pressure has a minor influence on the stress concentration ratios of columns, which is consistent with previous findings from the mode of deformation.

Chapter 6
Results of FEA: Distribution of total shear strains and characteristic column behaviour

6.1 Background

The characteristic behaviour of individual columns is examined in the following chapter. The load-transfer mechanisms are identified for various column configurations at three specific column lengths: 3, 8 and 13.9 m. The column lengths are chosen on the basis of previous findings from the deformational behaviour of columns (see Section 5.4) to examine specific modes of deformation; 3 m long columns are chosen to investigate punching; 8 m long columns are chosen to investigate a combination of punching-bulging failure and 13.9 m end-bearing columns are chosen to investigate bulging failure, as punching is precluded.

It is established that the deformational behaviour of columns is highly dependent upon the support provided by the surrounding soil. The type of stress imparted from columns to the surrounding soil depends upon the dominant mode of deformation, i.e. columns which are bulging primarily impart radial stress, while columns which are punching impart a combination of shear and end-bearing stress. The response of the surrounding soil to each of these stresses plays a key role in determining the settlement performance of stone columns. The distribution of shear strains within columns and in the surrounding soil is therefore very important. This is investigated in the following sections and allows the modes of deformation identified in Section 5.4, which were determined by compression and punching ratios, to be verified.

The deformational behaviour of columns is also examined by investigating the distribution of vertical and horizontal strain within columns. The magnitude and location of maximum strain within columns defines the deformational behaviour of columns. The influence of column confinement, column length and area ratio upon these strains is examined in the following

chapter. The stress concentration ratio is an important parameter in determining the settlement performance of stone columns. It was shown in Section 5.5 that its magnitude at the surface does not uniquely define the settlement performance of columns. Therefore, the variation of this parameter with depth is examined.

6.2 Distribution of total shear strains

6.2.1 Total shear strains for an infinite grid of stone columns

The distribution of total shear strain (γ) for an infinite grid of columns at lengths of 3, 8 and 13.9 m is shown in Figures 6.1(a), 6.1(b) and 6.1(c), respectively. It can be seen in Figure 6.1(a) that the majority of shear strain develops beneath the base of 3 m long columns. This suggests that punching is the dominant mode of deformation. It appears that the distribution of shear strain beneath the base of columns becomes more uniform at low area ratios, which is indicative of 'block' failure (Figure 6.1(a-i)). In contrast, it can be seen in Figures 6.1(a-ii) and 6.1(a-iii) that column punching becomes more localised at higher area ratios.

The mode of deformation for 8 m long floating columns is shown in Figure 6.1(b). It can be seen in Figure 6.1(b-i) that the majority of shear strain continues to develop beneath the base of columns at low area ratios. It appears that an infinite grid of columns at low area ratios do not develop shear stress along the sides of columns and transfer the applied load to the base of columns, which is again consistent with 'block' failure. A change in the mode of deformation is observed for 8 m long columns at higher area ratios in Figures 6.1(b-ii) and 6.1(b-iii). While a fluctuation in shear strain is observed within columns, it is clear that bulging develops at the top of the lower Carse clay layer (i.e. weakest part of the soil profile). Columns at higher area ratios experience a loss of lateral confinement which results in column bulging. The loss of lateral confinement becomes more pronounced with increasing area ratio and the magnitude of shear strain increases in concert.

No punching is observed in Figure 6.1(c) as the end-bearing columns (L = 13.9 m) are resting on a rigid stratum. It can be seen that bulging always occurs at the top of the lower Carse clay layer for all area ratios. The magnitude of column bulging increases at high area ratios, which reflects the loss of lateral confinement and, also, the higher force taken per column with increasing area ratio.

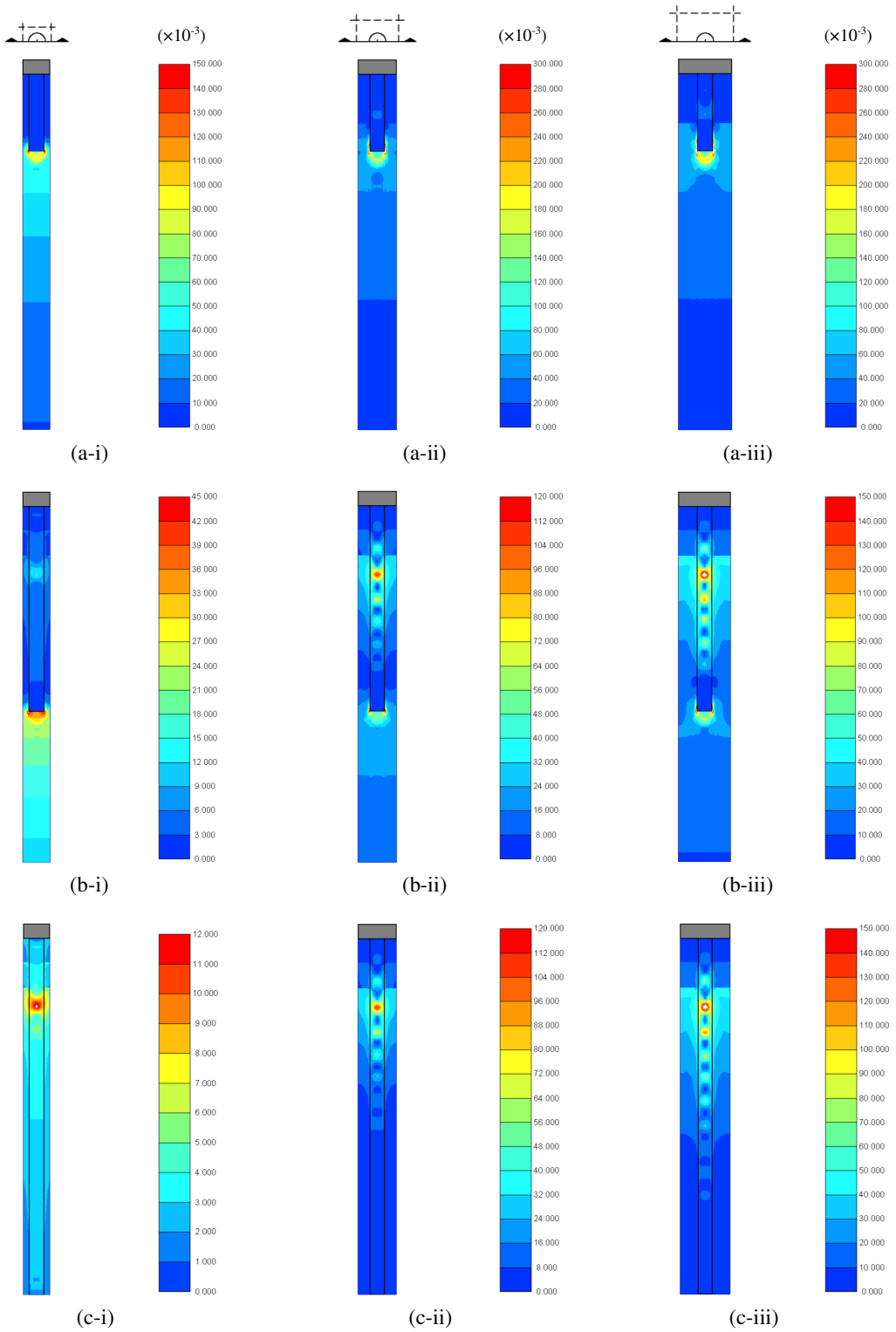

Figure 6.1 - Total shear strains for an infinite grid of columns for column lengths L of (a) 3 m, (b) 8 m and (c) 13.9 m and at area ratios A/A_C of (i) 3.5, (ii) 8.0 and (iii) 14.1

6.2.2 Total shear strains for small groups of stone columns

Single columns

The development of total shear strain for a single column at lengths of 3, 8 and 13.9 m is shown in Figures 6.2(a), 6.2(b) and 6.2(c), respectively. Similar to an infinite grid of columns, it can be seen in Figure 6.2(a) that the majority of shear strain develops beneath the base of 3 m long columns. This indicates that column punching is the dominant mode of deformation for short columns. However, it can also be seen that additional shear strain develops along the side of single columns. This is not observed for an infinite grid of columns, as columns within an infinite grid deform equally due to symmetry and consequently no shear stress develops along the side of columns.

The distribution of total shear strain for 8 m long floating columns is shown in Figure 6.2(b). It can be seen in Figure 6.2(b-i) that shear strain develops along the side and at the base of columns at low area ratios, which indicates that punching is the dominant mode of deformation. It can also be seen that the magnitude of shear strain at the base of columns is considerably reduced compared to 3 m long columns. This may be explained as longer columns can generate a larger shear force along the side of columns and also a higher base resistance is available as columns are formed in a deeper, more competent soil stratum. It can be seen in Figures 6.2(b-ii) and 6.2(b-iii) that the mode of deformation changes from punching to bulging with increasing area ratio for 8 m long columns. While some shear strain develops along the side and at the base of columns, the majority of shear strain develops within columns near the top of the lower Carse clay layer.

The distribution of shear strains for single end-bearing columns is shown in Figure 6.2(c) and indicates that no bulging occurs in columns at low area ratios. It appears that columns at low area ratios develop shear strains along the sides of columns in upper sections. In contrast, the majority of shear strain develops within columns at higher area ratios, which suggests that bulging is the primary mode of deformation.

Localised shear zones also develop beneath the edges of pad footings for columns at higher area ratios. These shear zones develop as a results of the large displacement discontinuity between the pad footing and the surrounding soil; however, they do not appear to extend beyond the stiff crust.

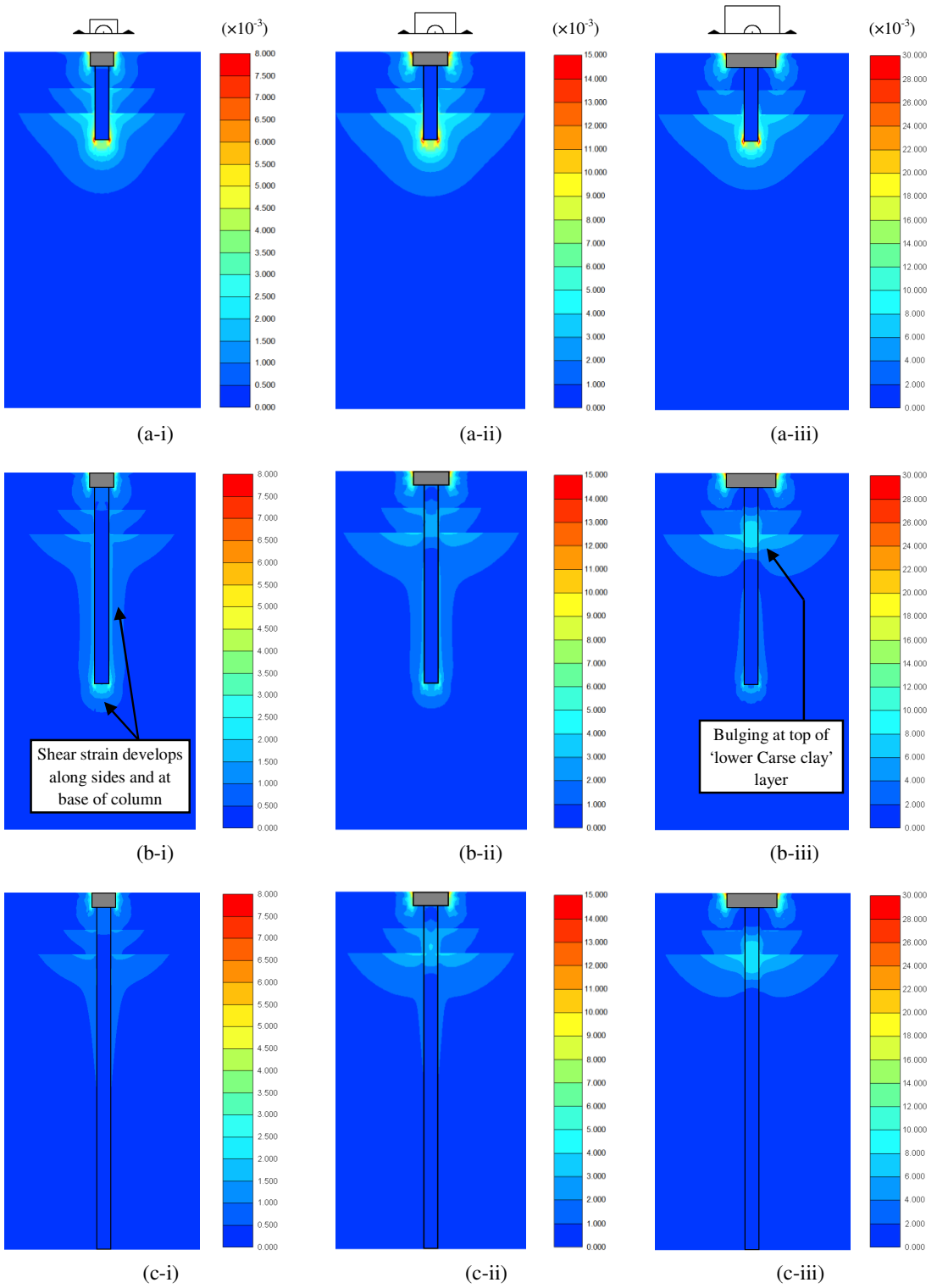

Figure 6.2 - Total shear strains for single columns for column lengths L of (a) 3 m, (b) 8 m and (c) 13.9 m and at area ratios A/A_C of (i) 3.5, (ii) 8.0 and (iii) 14.1

2×2 group of columns

The distribution of shear strain within a 2×2 group of columns for lengths of 3, 8 and 13.9 m is shown in Figures 6.3(a), 6.3(b) and 6.3(c), respectively. It can be seen in Figure 6.3(a) that the majority of shear strain develops beneath the base of 3 m long columns, which is similar to findings from single columns and infinite grids of columns. It can also be seen in Figure 6.3(a-i) that relatively uniform strain develops beneath the base of columns and no shear strain develops in the central zone of soil bounded by the columns. This suggests that columns are punching as a 'block' with the surrounding soil. The development of shear strain along the outer sides of columns is also evident in Figure 6.3(a-i). It is difficult to determine whether this strain is generated from friction along the side of columns or whether it is a shear zone extending from the corner of the pad footing. It can be seen in Figures 6.3(a-ii) and 6.3(a-iii) that column punching becomes more localised and columns tend to act more individually with increasing area ratio. The development of shear zones from the corner of pad footings to the base of columns is also observed for 2×2 groups at higher area ratios.

As column length increases, Figure 6.3(b-i) illustrates how the magnitude of shear strain beneath the base of columns reduces and a more uniform distribution of shear strain develops along the side and at the base of columns. It can be also seen that no shear strain develops in the central zone of soil bounded by the columns which again suggests that 'block' failure remains the dominant mode of deformation with increasing column length for 2×2 groups at low area ratios. In contrast, the mode of deformation appears to change from punching to bulging with increasing column length for 2×2 groups of columns at higher area ratios. Column bulging is evident in Figures 6.3(b-ii) and 6.3(b-iii) as the majority of the shear strain develops within columns, near the top of the lower Carse clay layer. Shear zones also develop from the corners of pad footings to the point of maximum bulging in columns at high area ratios. It also appears that shear zones bridge between the points of maximum bulging in columns and create a zone of undeforming soil between the base of the footing and the points of column bulging. This zone of undeforming soil was also observed by Muir Wood *et al.* (2000) and Wehr (2004) in small scale laboratory tests and numerical studies, respectively. This zone of soil moves downwards and displaces the surrounding soil, causing the columns to bulge and bend outwards.

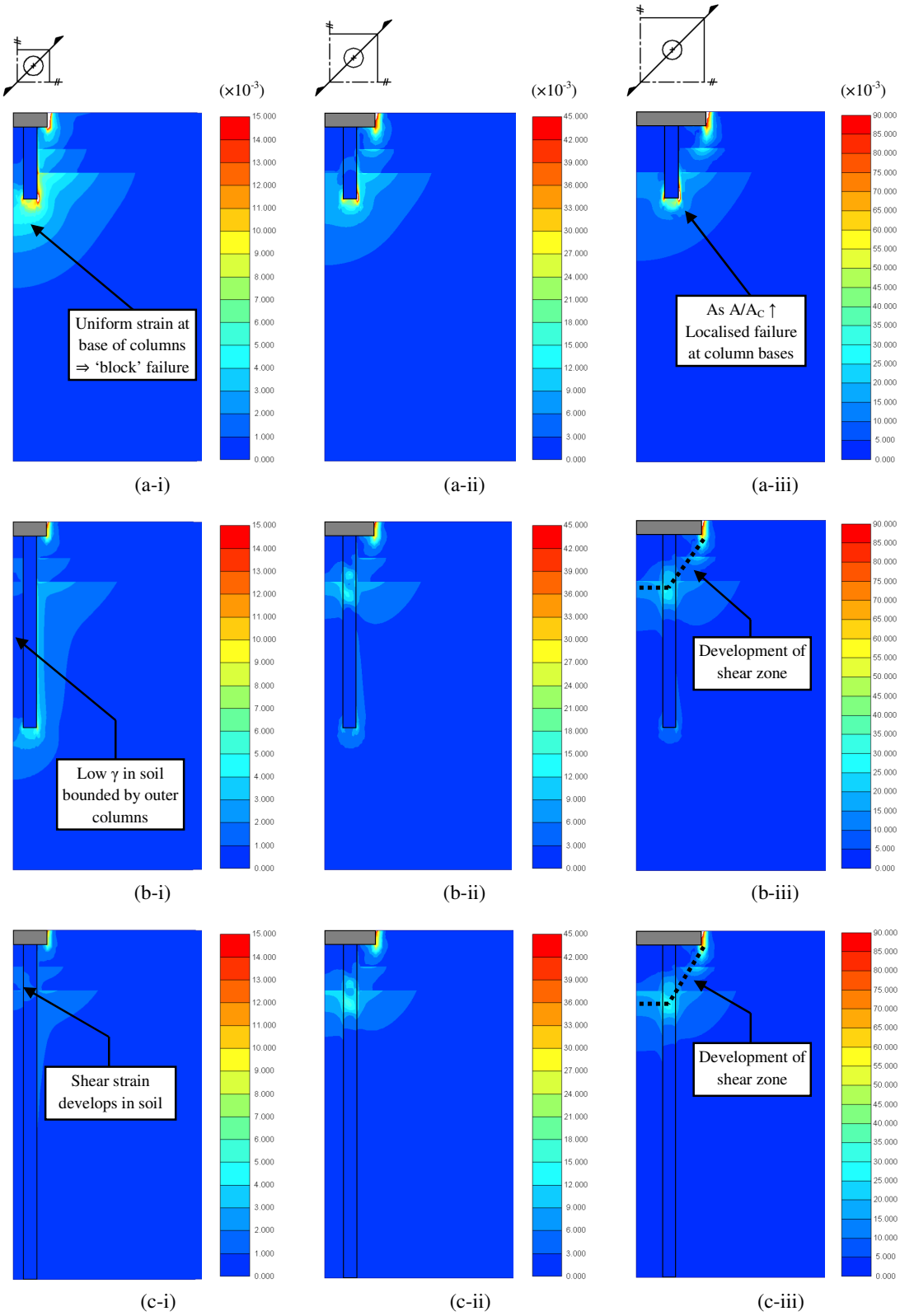

Figure 6.3 - Total shear strains for 2×2 groups of columns for column lengths L of (a) 3 m, (b) 8 m and (c) 13.9 m and at area ratios A/A_C of (i) 3.5, (ii) 8.0 and (iii) 14.1

The distribution of shear strains for end-bearing columns is shown in Figure 6.3(c). While no bulging occurs in columns at low area ratios, it appears from Figure 6.3(c-i) that shear strain develops in the soil bounded by the columns. This causes columns to bend outwards and away from the centre of the footing. Shear strains are also observed along the side of columns, which indicates that the columns may still be transferring the applied load through side friction. Figures 6.3(c-ii) and 6.3(c-iii) indicate that bulging failure continues to occur for end-bearing columns at high area ratios. The development of a shear zone, which extends from the corners of pad footings to the points of maximum bulging, and bridges the soil between columns is again evident.

3×3 group of columns

The distribution of shear strain for a 3×3 group of columns at lengths of 3, 8 and 13.9 m is shown in Figures 6.4(a), 6.4(b) and 6.4(c), respectively. It can be seen in Figure 6.4(a-i) that the majority of shear strain develops beneath the base of columns, which indicates that punching is the dominant mode of deformation for 3 m long columns at low area ratios. Similar to previous findings, Figures 6.4(a-ii) and 6.4(a-iii) illustrate that punching becomes more localised and columns tend to behave individually at higher area ratios. It appears that columns at low area ratios are behaving as a 'block' with the surrounding soil, as shear strain at the base of columns is relatively uniform and shear strains do not develop in the soil between columns. The development of a shear zone which extends from the corner of pad footings to the base of columns is also evident, especially at high area ratios.

The punching mode of failure continues to occur with increasing length for columns at low area ratios, as shown in Figure 6.4(b-i) for 8 m long columns. While some shear strain develops within the upper sections of external column, which may result in column bending, the majority of shear strain develops along the outer side of external columns and at the base of columns. Therefore, it appears that 'block' failure remains the dominant mode of deformation with increasing column length for a group of columns at low area ratios. In contrast, it can be seen in Figures 6.4(b-ii) and 6.4(b-iii) that columns at higher area ratios tend to bulge with increasing column length. Bulging occurs at the top of the lower Carse clay layer. The shear zone which extends from the corners of pad footings to the points of maximum bulging in external columns becomes more defined with increasing column length. The shear zone bridges between the points of bulging in the central and outer columns, which creates a zone of undeforming soil.

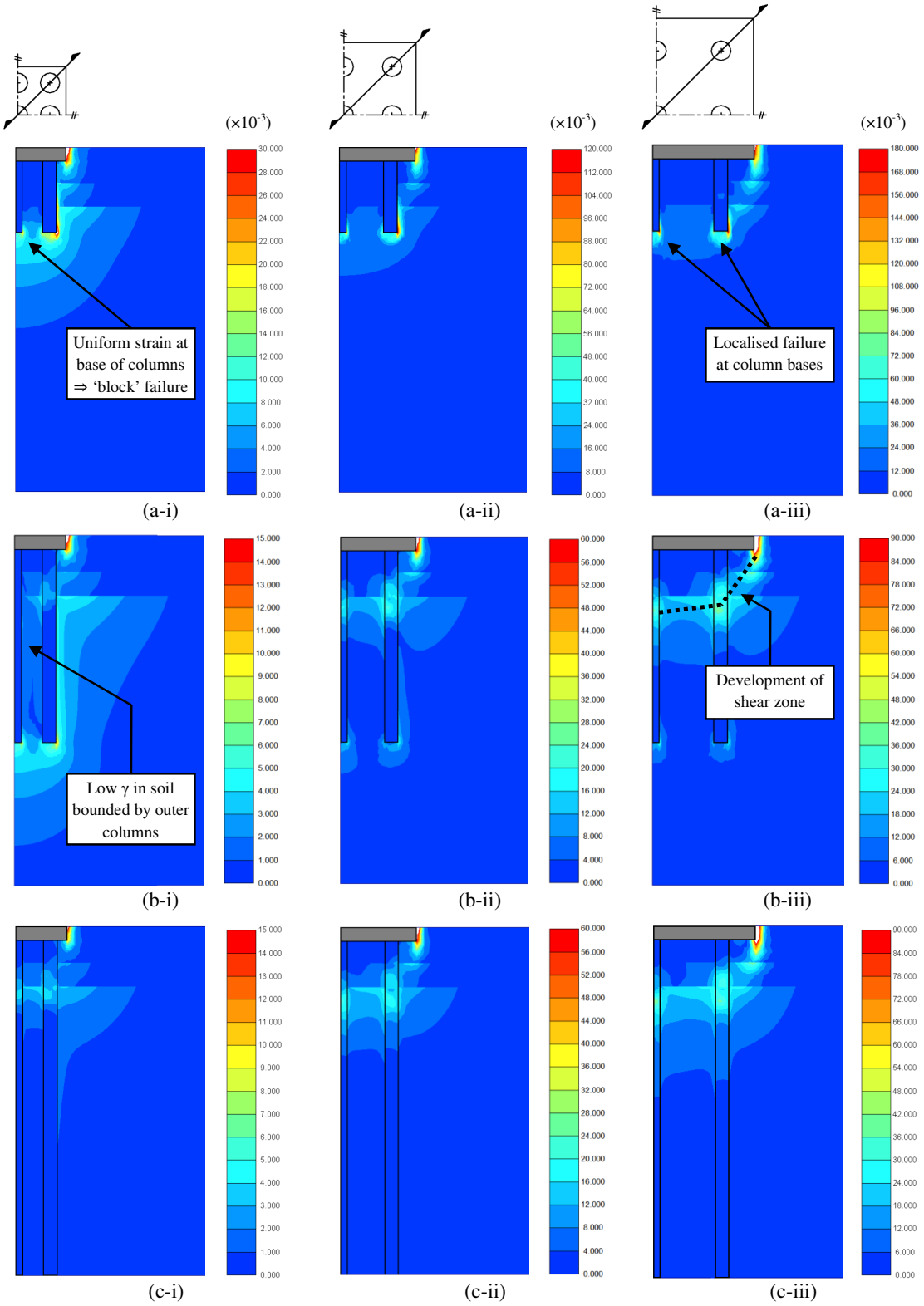

Figure 6.4 - Total shear strains for 3×3 group of columns for column lengths L of (a) 3 m, (b) 8 m and (c) 13.9 m and at area ratios A/A_C of (i) 3.5, (ii) 8.0 and (iii) 14.1

The mode of deformation changes from punching to bulging once columns are end-bearing on a rigid stratum. In contrast to single columns and groups of 2×2 columns, bulging occurs in 3×3 groups of end-bearing columns at low area ratios (Figure 6.4(c-i)). It can be seen in Figures 6.4(c-ii) and 6.4(c-iii) that the bulging mode of deformation continues to occur with increasing column length for 3×3 groups of columns at high area ratios. Furthermore, shear strain in external columns is more acute, which highlights the positive confining effect provided to the central column. It also appears that larger deformation occurs at a slightly shallower depth in external columns compared to central columns. Initially all columns tend to bulge at the same depth, i.e. at the top of the lower Carse clay. However, the bulging of external and central columns mobilises the passive resistance of the soil which is bounded by the central and exterior columns. This increases the lateral resistance at this depth, which enhances the confinement provided to the central column, and hence forces bulging deeper. The magnitude of bulging is also reduced, as bulging occurs in a deeper and stiffer soil stratum. Bulging in external columns continues to occur at the top of the lower Carse clay layer, as columns bulge and bend outwards towards the unconfined sides.

4×4 group of columns

The distribution of shear strain for a 4×4 group of columns of lengths 3, 8 and 13.9 m is shown in Figures 6.5(a), 6.5(b) and 6.5(c), respectively. It can be seen in Figure 6.5(a) that all 3 m long columns punch into the underlying soil. Figure 6.5(a-i) shows that shear strain develops along the outer sides of external columns at low area ratios. It can also be seen in Figure 6.5(a-i) that relatively uniform shear strain develops beneath the base of columns, which again suggests that columns at low area ratios are acting as a ‘block’ with the surrounding soil. It is evident in Figures 6.5(a-ii) and 6.5(a-iii) that column punching becomes more pronounced with increasing area ratio, which is consistent with findings from an infinite grid of columns, single columns, 2×2 groups and 3×3 groups of columns.

It can be seen in Figure 6.5(b-i) that punching remains the dominant mode of deformation with increasing column length for columns at low area ratios. Shear strains develop beneath the base of columns and along the outer side of external columns. It is also clear that low levels of shear strain develops in central columns and in the soil bounded by external columns, which provides further evidence to suggest that columns at low area ratios are deforming as a ‘block’. However, column bulging becomes more pronounced with increasing

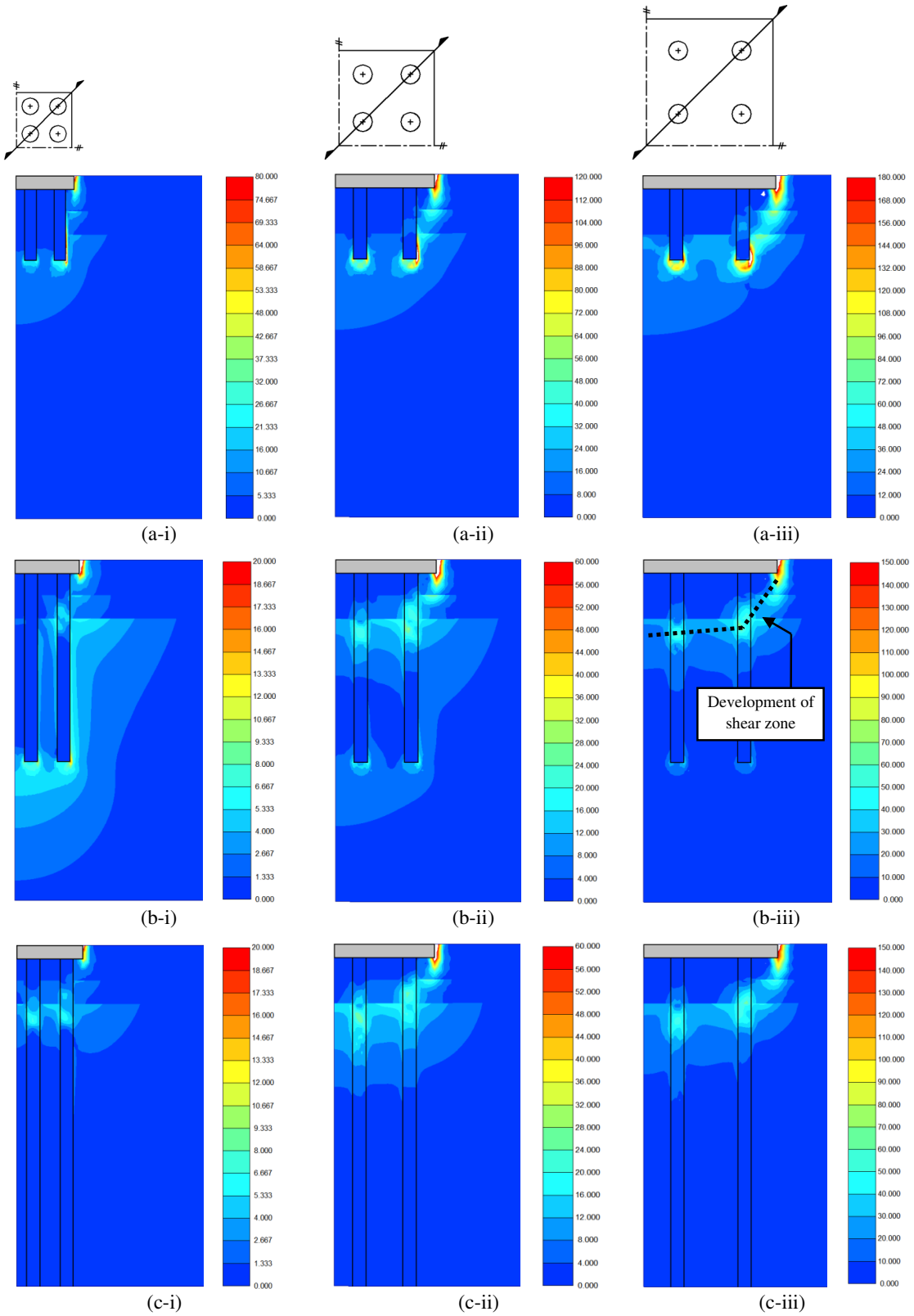

Figure 6.5 - Total shear strains for 4×4 group of columns for column lengths L of (a) 3 m, (b) 8 m and (c) 13.9 m and at area ratios A/A_C of (i) 3.5, (ii) 8.0 and (iii) 14.1

area ratio, as shown in Figures 6.5(b-ii) and 6.5(b-iii). Bulging occurs at the top of the lower Carse clay layer in external columns and occurs slightly deeper in central columns. The development of a shear zone, which extends from the corner of pad footings to the point of maximum bulging, is again observed.

The distribution of shear strain for end-bearing columns is shown in Figure 6.5(c). It can be seen that bulging occurs for all area ratios as column punching is precluded. It appears that the magnitude and location of bulging is similar for central and external columns at low area ratios. However, as the area ratio increases it can be seen that the magnitude of shear strain increases and bulging occurs at shallower depths in external columns compared to central columns. The development of shear zones from the corner of the pad footing is again evident and they join together beneath the centre of the footing to form a zone of undeforming soil.

6.3 Characteristic column behaviour

The characteristic behaviour of each column is presented in this section which shows the relationship between vertical strain (ε_y), horizontal strain (ε_h) and stress concentration ratio within the columns. The difference in behaviour for corner, edge and centre columns is also highlighted. The strains are reported in the x, y and z directions in PLAXIS 3D Foundation. However, as the columns are circular it is useful to investigate the vertical and horizontal strains. The vertical strains (ε_y) are determined directly from PLAXIS 3D Foundation and the horizontal strains (ε_h) are determined as the average of the two orthogonal strains, i.e. $\varepsilon_h = ½(\varepsilon_x + \varepsilon_z)$.

6.3.1 Infinite grid of columns

Distribution of vertical and horizontal strain

The distribution of vertical strain, horizontal strain and stress concentration ratio with depth for an infinite grid of columns is shown in Figure 6.6. It can be seen in Figure 6.6(a-i) that vertical strain is low within 3 m long columns and primarily develops beneath the base of columns. This coincides with findings from the distribution of total shear strains (see Section 6.2.1) that an infinite grid of 3 m long columns punch as a ‘block’ into the underlying soil. It can be seen in Figure 6.6(a-ii) that horizontal strain within 3 m long columns is also quite low and appears to be related to the distribution of vertical strain. The magnitude of vertical and

horizontal strain increases with area ratio, which reflects the loss of lateral confinement and increase in the total load taken per column with increasing area ratio. In addition, it is interesting to note that no horizontal strain develops in the soil below the base of columns. This indicates that the unreinforced soil is subject to one-dimensional boundary conditions, imposed by the wide area loading.

The distribution of vertical strain with depth for an infinite grid of 8 m long columns is shown in Figure 6.6(b-i). It can be seen for columns at low area ratios (i.e. $A/A_C = 3.5$) that the majority of vertical strain develops beneath the base of columns. In contrast, significant vertical strain develops within columns at higher area ratios. It is interesting to note that vertical strain within columns increases with area ratio, while the vertical strain beneath the base of columns remains unchanged. This may be explained as the wide area loading stresses the soil profile to the full depth and, therefore, induces similar vertical strain in the soil beneath the base of columns. As with 3 m long columns, it appears that the distribution of vertical strain within 8 m long columns is related to the horizontal strain (Figure 6.6(b-ii)). It appears that both vertical and horizontal strain within columns increases with area ratio and that the maximum horizontal strain occurs at the same depth ($z \approx 2.5$ m), close to the top of the lower Carse clay layer (i.e. the weakest point in the soil profile). A significant amount of horizontal strain occurs within columns at high area ratios (i.e. $A/A_C = 8.0$ and 14.1) which is consistent with column bulging.

The distribution of vertical strain for an infinite grid of end-bearing stone columns is shown in Figure 6.6(c-i). Vertical strain increases with depth to a maximum at $z \approx 2.5$ m and decreases thereafter, eventually becoming negligible at $z = 8$ m. The horizontal strain is shown in Figure 6.6(c-ii) and is similar to the distribution of vertical strain with depth. This indicates that vertical strains are primarily developed from horizontal strains.

Distribution of stress concentration ratio

The distribution of stress concentration ratios in the upper layers of the Bothkennar test site, for columns at low area ratios (i.e. $A/A_C = 3.5$) is similar for all lengths and is best illustrated in the inset in Figure 6.6(b-iii). It appears that stress concentration ratios decrease with depth within the crust. This is related to a decrease in modular ratio (E_{col}/E_{soil}) with increasing overburden pressure, as shown in Figure 6.7. The stiffness of the soil and column increases

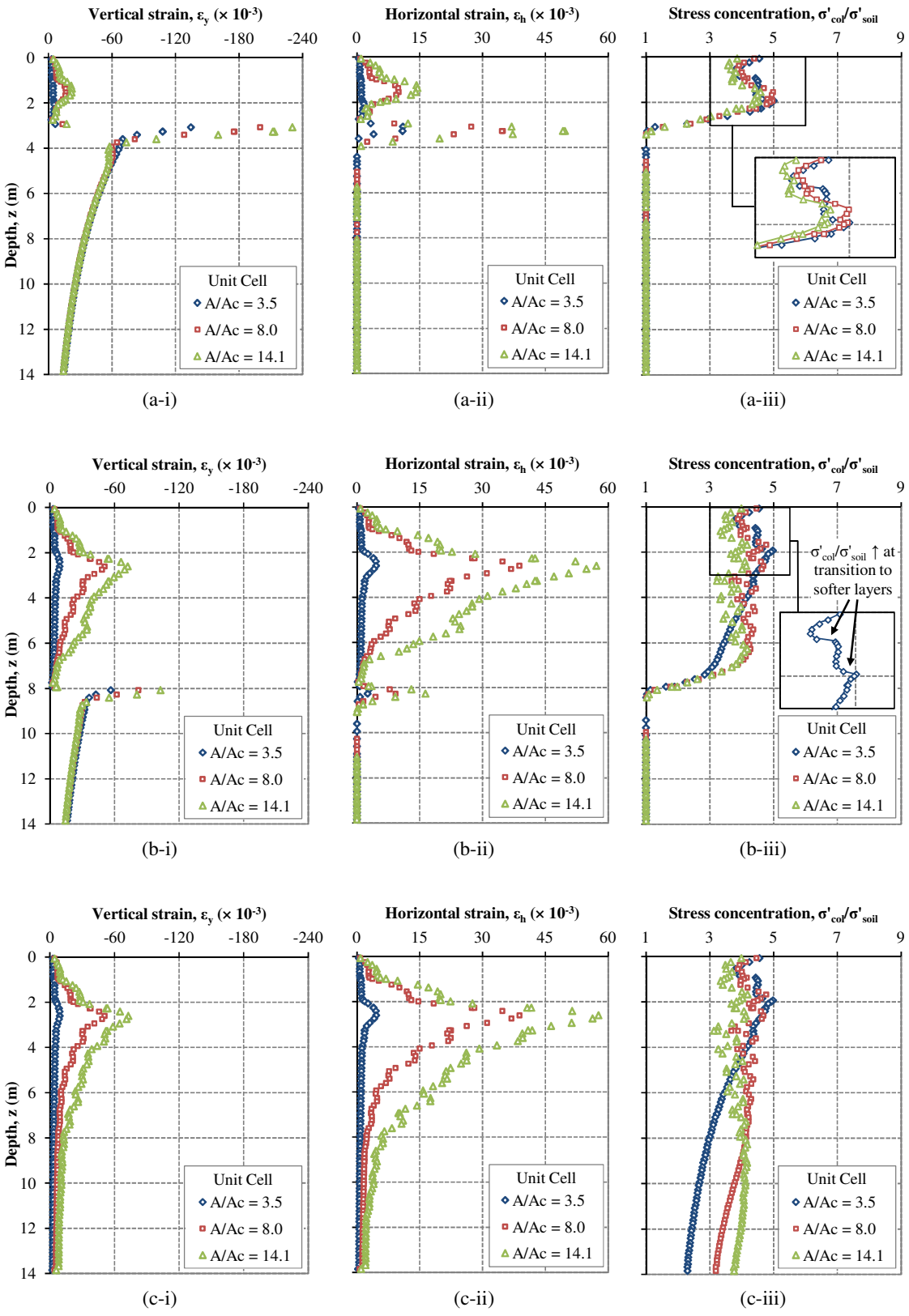

Figure 6.6 - Distribution of (i) vertical strain, (ii) horizontal strain and (iii) stress concentration ratio with depth for an infinite grid of columns at lengths L of (a) 3 m, (b) 8 m and (c) 13.9 m

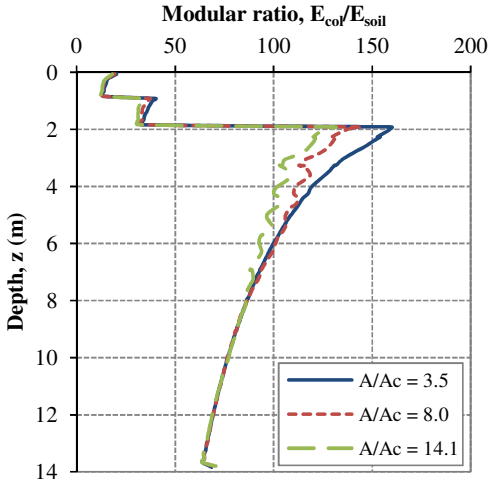

Figure 6.7 - Distribution of modular ratio E_{col}/E_{soil} with depth for an infinite grid of end-bearing stone columns at various area ratios

with depth according to the power law outlined in equation 3.3. The rate of increase in stiffness with overburden pressure is controlled by the parameter, 'm', which is defined as 0.3 and 1.0 for the column and soil, respectively. The higher 'm' value results in a faster increase in E_{soil} compared to E_{col} with depth. Therefore, E_{col}/E_{soil} reduces with depth in the crust, which leads to lower stress concentration ratios.

An increase in stress concentration ratios is observed at the transition between the crust and the softer upper Carse clay layer. This may be explained as E_{col}/E_{soil} increases sharply for this layer and columns, therefore, carry a larger proportion of the applied load. A slight reduction in stress concentration ratios with depth is again observed throughout the upper Carse clay layer, followed by a sharp increase at the transition to the softer lower Carse clay layer. Stress concentration ratios continue to reduce with depth in the lower Carse clay layer and revert to unity (i.e. $\sigma_{col}/\sigma_{soil} = 1$) at the base of floating columns, as no extra vertical load can be sustained in the columns at this level.

It can be seen in Figure 6.6(c-iii) that stress concentration ratios are related to the modular ratio for an infinite grid of columns at $A/A_C = 3.5$, as stress concentration ratios reduce by c.55% in the lower Carse clay layer ($\sigma_{col}/\sigma_{soil}$ = 5.0 to 2.3) which coincides with a similar drop in modular ratios for the same layer (E_{col}/E_{soil} = 160 to 68), as shown in Figure 6.7.

While a similar distribution of stress concentration ratio with depth is observed for all short columns (Figure 6.6(a-iii)), a marked change is observed with increasing area ratio for 8 m

and 13.9 m long columns, as shown in Figures 6.6(b-iii) and 6.6(c-iii), respectively. Despite a large degree of scatter, it appears that stress concentration ratios reduce with increasing horizontal strain. It can be seen in Figure 6.6(ii) that horizontal strain increases with increasing area ratio. This reflects the loss of lateral confinement and, also, the higher load carried per column with increasing area ratio. It can be seen that sections of columns which develop high horizontal strain cannot sustain the vertical stress and, consequently, yield low stress concentration ratios. However, it is interesting to note that in sections of columns which develop low horizontal strain, stress concentration ratios increase for higher area ratios (Figure 6.6(c-iii)).

6.3.2 Small groups of columns

Single columns

Distribution of vertical and horizontal strain

It can be seen in Figure 6.8(a-i) that vertical strain is very small in 3 m long columns at low area ratios (i.e. A/A_C = 3.5) and that the majority of vertical strain develops in the soil beneath the base of columns. It also appears that the distribution of vertical strain is closely related to horizontal strain; it can be seen in Figure 6.8(a-ii) that the majority of horizontal strain also develops beneath the base of columns. The development of horizontal strain beneath the base of single columns is in contrast to an infinite grid of columns. This may be explained as the soil beneath the base of single columns is unconfined and spreads outwards when subjected to vertical stress, thus generating horizontal strain. A slight increase in vertical and horizontal strain is also observed with increasing area ratio within 3 m long columns. This reflects the loss of lateral confinement and increase in the total force taken per column with increasing area ratio. Finally, it appears that punching is the dominant mode of deformation for all 3 m long columns as the majority of vertical strain develops beneath the base of columns.

The distribution of vertical and horizontal strain along 8 m long columns is shown in Figures 6.8(b-i) and 6.8(b-ii), respectively. A marked changed in the distribution of vertical and horizontal strain within columns is observed with increasing area ratio. It can be seen in Figure 6.8(b-i) for low area ratios that the majority of vertical strain develops beneath the base of columns, which suggests that punching remains the dominant mode of deformation.

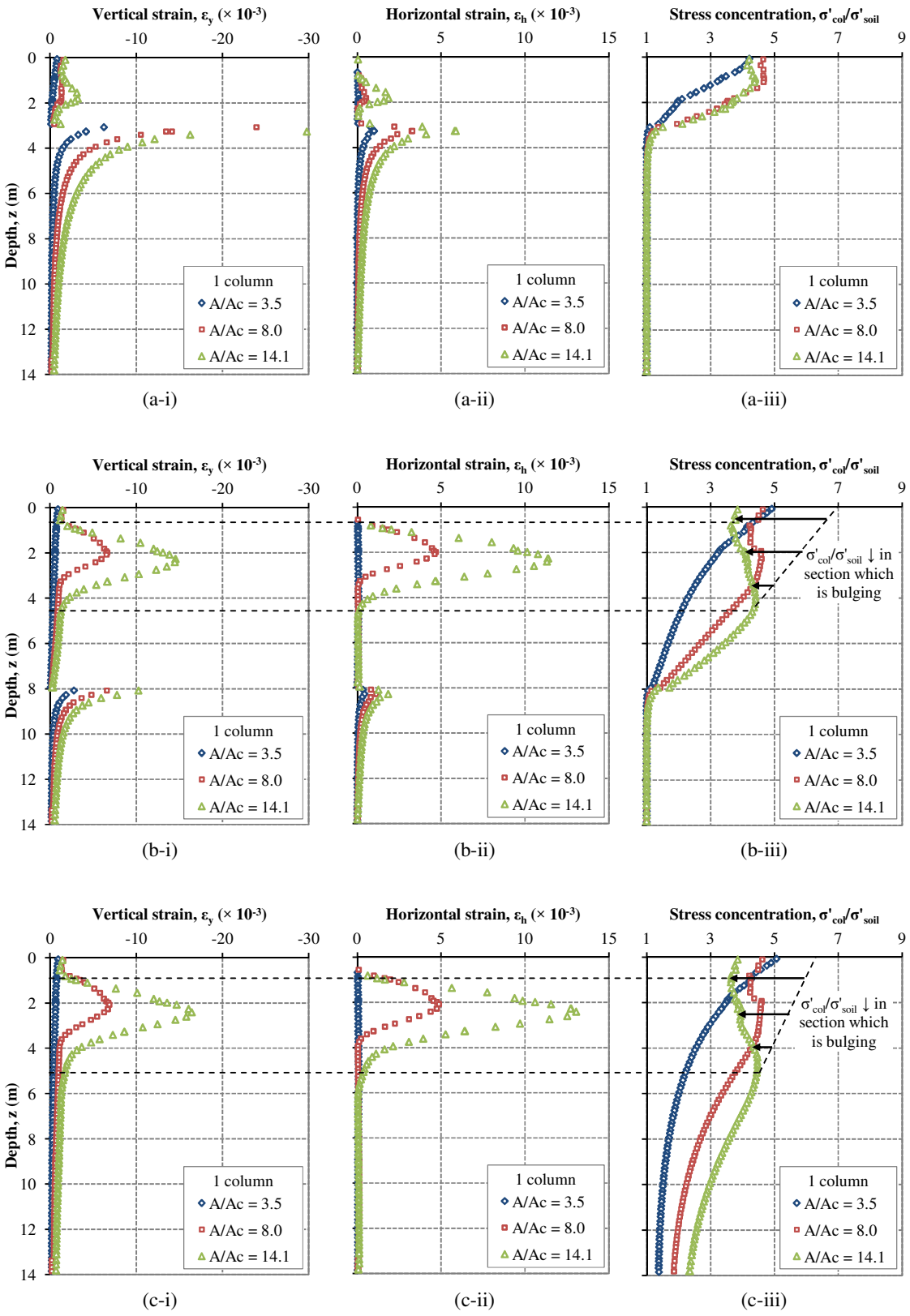

Figure 6.8 - Distribution of (i) vertical strain, (ii) horizontal strain and (iii) stress concentration ratio with depth for a single column at lengths L of (a) 3 m, (b) 8 m and (c) 13.9 m

It is interesting to note that the magnitude of vertical strain at the base of columns is reduced compared to 3 m long columns. This may be explained as the base of 8 m long columns is founded in a deeper, more competent soil stratum. It can also be seen in Figure 6.8(b-i) for columns at high area ratios that vertical strain develops within columns and beneath the base of columns. This suggests that punching and bulging modes of deformation may be occurring simultaneously. However, it can be seen that the majority of the vertical strain develops within columns rather than at the base, which suggests that bulging is the dominant mode of deformation. The development of high horizontal strains within columns is also evident in Figure 6.8(b-ii), which is consistent with a bulging mode of deformation. It can be seen in Figure 6.8(b-i) that the magnitude of vertical strain and the extent of the column which is strained both increase at high area ratios. This is due to the loss of lateral confinement and increase in the total load taken per column. Maximum bulging occurs at a depth between 2.0–2.5 m, which coincides with the top of the lower Carse clay layer and is consistent with the depth of maximum bulging for an infinite grid of columns.

The distributions of vertical and horizontal strain within end-bearing columns are shown in Figures 6.8(c-i) and 6.8(c-ii), respectively. It can be seen that no horizontal strain develops in single columns at low area ratios which indicates that columns are not bulging. However, a small amount of vertical strain is observed near the top of columns at low area ratios. This indicates that columns are transferring the applied load through shear stress along the sides of columns, which is similar to a punching mode of deformation. The bulging mode of deformation remains prevalent for columns at higher area ratios, as a significant degree of vertical and horizontal strain is observed in the upper sections of columns. Similar to 8 m long floating columns, the magnitude of strain and the extent of the column which is strained both increase with increasing area ratio.

Distribution of stress concentration ratio

The distribution of stress concentration ratios along the length of single columns is shown in Figure 6.8(iii). It can be seen in Figure 6.8(a-iii) that stress concentration ratios for 3 m long columns are high at the top and reduce with depth to unity (i.e. $\sigma'_{col}/\sigma'_{soil} = 1$) at the base of columns. It is well established that punching is the dominant mode of deformation for short columns, which implies that columns carry the applied load through a combination of shear stress and end-bearing resistance. Consequently, the applied vertical stress, and hence the

stress concentration ratio, reduces with depth. Stress concentration ratios approach unity at the base of columns as no extra vertical stress in columns can be sustained at this point.

A slightly different distribution of stress concentration ratios is observed for 3 m long columns at high area ratios in Figure 6.8(a-iii). It can be seen in Figure 6.8(a-ii) that horizontal strain increases with area ratio, which is consistent with the fact that columns at higher area ratios carry a larger proportion of the applied load. This explains the high stress concentration ratios at high area ratios in the lower sections of columns. However, the increase in stress concentration ratio with increasing area ratio is offset by the effects horizontal strain in the upper sections of columns.

The distribution of stress concentration ratios with depth for 8 m and 13.9 m long columns is shown Figures 6.8(b-iii) and 6.8(c-iii), respectively. It can be seen that stress concentration ratios increase with area ratio for sections of columns which are subject to low horizontal strains. This may be attributable to an increased load that is taken per column with increasing area ratio and is consistent with the findings from infinite grids of columns. However, it appears that the magnitude of stress concentration ratios is significantly reduced in the upper sections of columns, where column bulging occurs. Columns in a state of plasticity cannot sustain high vertical stress and, consequently, a significant reduction in vertical stress, and hence stress concentration ratios, occurs. The reduction of stress concentration ratios appears to be most pronounced at the top of the bulged section of columns.

2×2 group of columns

Distribution of vertical and horizontal strain

The distributions of vertical and horizontal strain with depth for 2×2 groups of 3 m long columns are shown in Figures 6.9(i) and 6.9(ii), respectively. It can be seen in Figure 6.9(a-i) that the majority of vertical strain develops beneath the base of 3 m long columns, which suggests that punching is the dominant mode of deformation. It also appears that the vertical and horizontal strains are closely related; the majority of horizontal strain also develops beneath the base of columns (Figure 6.9(a-ii)). The magnitude of vertical and horizontal strains is also observed to increase with increasing area ratio.

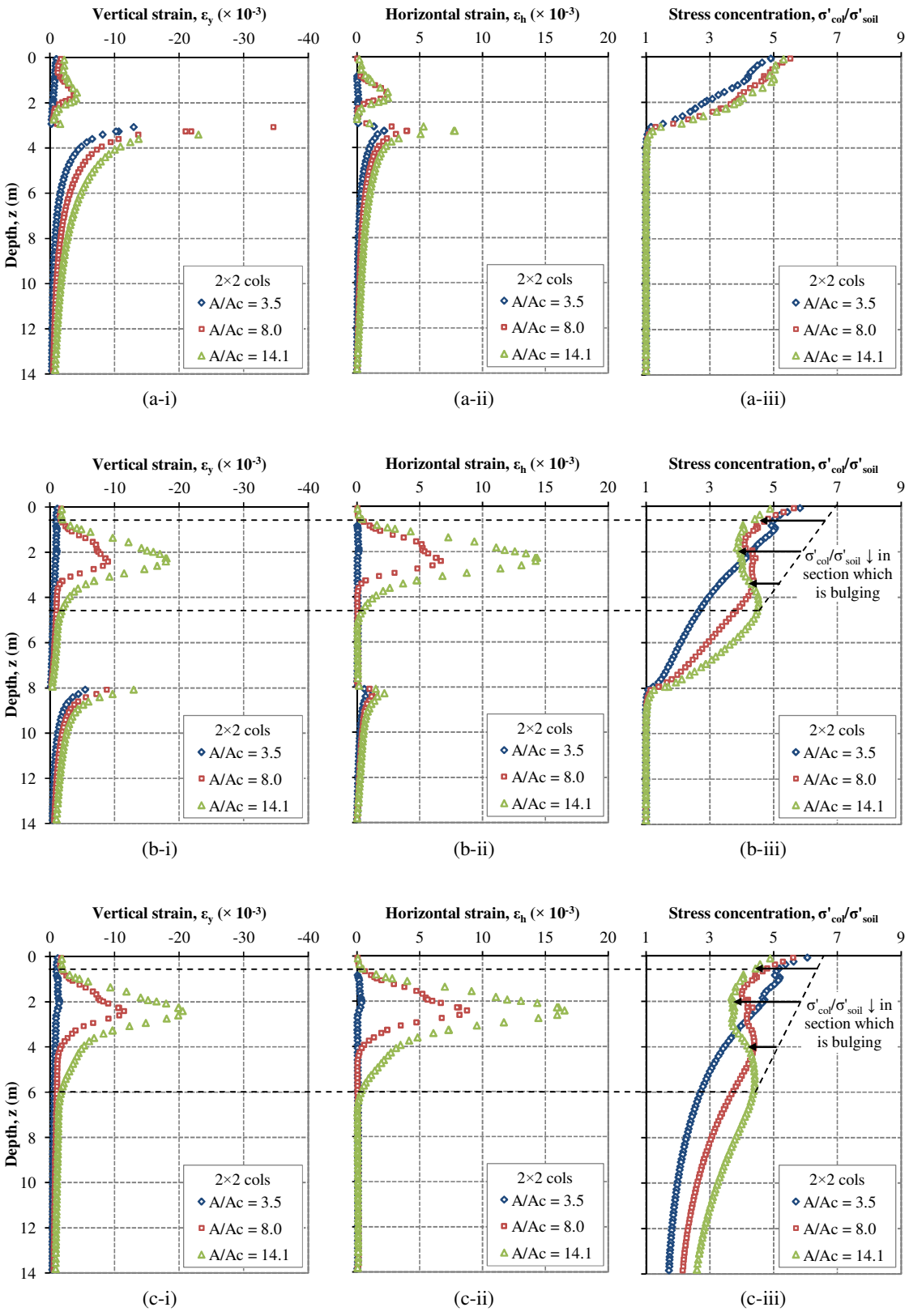

Figure 6.9 - Distribution of (i) vertical strain, (ii) horizontal strain and (iii) stress concentration ratio with depth for a 2×2 group of columns at lengths L of (a) 3 m, (b) 8 m and (c) 13.9 m

The distribution of vertical and horizontal strain with depth for 2×2 groups of 8 m long columns is shown in Figures 6.9(b-i) and 6.9(b-ii), respectively. It can be seen in Figure 6.9(b-i) for low area ratios that the majority of vertical strain develops beneath the base of columns. This is again consistent with a punching mode of deformation. In contrast, it can be seen that the majority of vertical strain develops within columns at high area ratios, which suggests that bulging is the dominant mode of deformation. It can be seen in Figure 6.9(b-ii) that columns at high area ratios develop large horizontal strains, which is consistent with a bulging mode of deformation.

The distribution of vertical and horizontal strain with depth for 2×2 groups of end-bearing columns is shown in Figures 6.9(c-i) and 6.9(c-ii), respectively. It can be seen that the vertical and horizontal strain in columns at low area ratios is quite low, which suggests that columns do not fail by bulging. This is quite interesting as punching failure is precluded for end-bearing columns. It appears that closely-spaced columns develop shear stress along the side of the columns to resist the applied load. A significant increase in horizontal strain is observed with an increasing area ratio, which indicates that columns at high area ratios are bulging.

Distribution of stress concentration ratio

The distribution of stress concentration ratio with depth is shown in Figure 6.9(iii). It can be seen for all short columns in Figure 6.9(a-iii) that stress concentration ratios are high at the surface and decrease steadily towards unity at the base of columns. This may be attributed to the punching mode of deformation as shear stress develops along the side of columns which results in a reduction of vertical stress with depth. A similar distribution of stress concentration ratio is also evident for 8 m and 13.9 m long closely-spaced columns (i.e. $A/A_C = 3.5$) in Figures 6.9(b-iii) and 6.9(c-iii), respectively.

A change in the distribution of stress concentration ratio at higher area ratios ($A/A_C = 8.0$ and 14.1) is observed as column length increases. It can be seen in Figures 6.9(b-iii) and 6.9(c-iii) that stress concentration ratios reduce with depth in the stiff crust (i.e. $z < 0.9$). This again may be explained as columns carry the applied load through shear stress along the sides of the columns in this section. However, the magnitude of stress concentration ratios at this depth is lower than stress concentration ratios for closely-spaced columns (i.e. $A/A_C = 3.5$), which is a direct result of the bulged column in the Carse clay. Columns which are bulging

are in a contained state of plasticity which reduces their load-carrying capacity and, therefore, the vertical stress in bulged sections of columns. The vertical stress increases with depth in bulged sections of columns due to overburden stress, which increases column confinement and hence allows columns to carry a larger proportion of the load. Stress concentration ratios decrease thereafter as vertical stress is carried through shear stress and also as the modular ratio reduces with increasing overburden stress.

3×3 group of columns

Distribution of vertical and horizontal strain

The distribution of vertical and horizontal strain with depth for 3×3 groups of 3 m long columns is shown in Figures 6.10(i) and 6.10(ii), respectively. It can be seen in Figure 6.10(i) that the majority of vertical strain develops beneath the base of columns, which suggests that punching is the dominant mode of deformation. The distribution of vertical and horizontal strain for individual columns (i.e. centre, edge and corner columns) with depth is also shown in Figure 6.10(i) and 6.10(ii). The variation in vertical and horizontal strain between individual columns is negligible for columns at low area ratios, but becomes more pronounced as area ratio increases. It can be seen in Figure 6.10(c-i) and 6.10(c-ii) that vertical and horizontal strains are lowest in centre columns, followed by edge and corner columns. This highlights the increased levels of confinement associated with central columns.

The distribution of vertical and horizontal strain with depth for 3×3 groups of 8 m long columns is shown in Figures 6.11(i) and 6.11(ii), respectively. It can be seen in Figure 6.11(a-i) for 8 m long columns at low area ratios that the majority of vertical strain develops beneath the base of columns, which suggests that punching remains the dominant mode of deformation. A change in the mode of deformation is observed with increasing area ratio for 8 m long columns. A significant proportion of horizontal strain is observed within columns at area ratios of 8.0 and 14.1 in Figures 6.11(b-ii) and 6.11(b-iii), respectively. While a certain amount of vertical strain develops at the base of columns, it is clear that column bulging is the dominant mode of deformation. The variation in strain levels with column position is only observed for columns at low area ratios, where the positive effects of column confinement are again evident as vertical and horizontal strains are lowest in central columns.

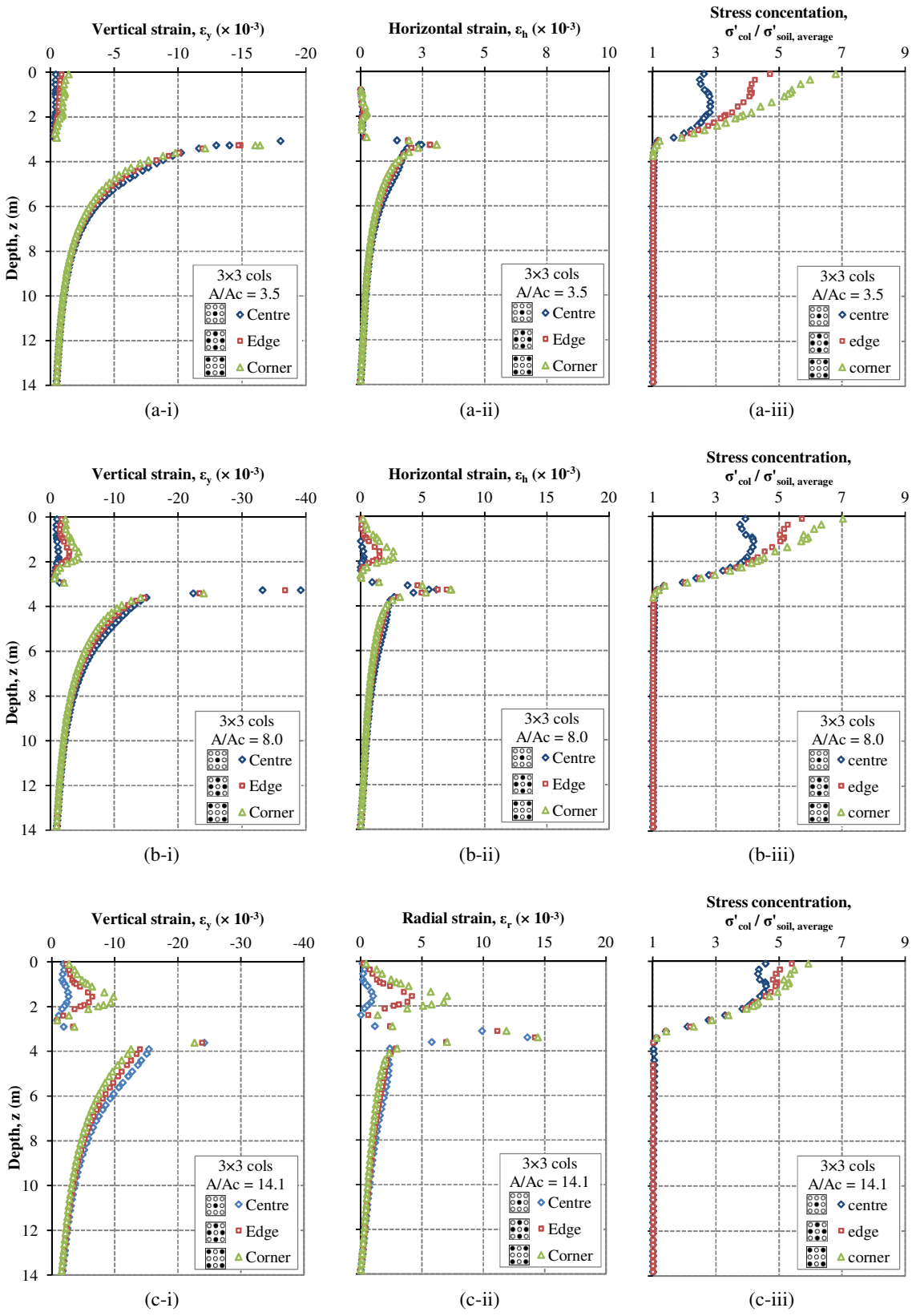

Figure 6.10 - Distribution of (i) vertical strain, (ii) horizontal strain and (iii) stress concentration ratio with depth for a 3 m long column, within a 3×3 group for A/Ac of (a) 3.5, (b) 8.0 and (c) 14.1

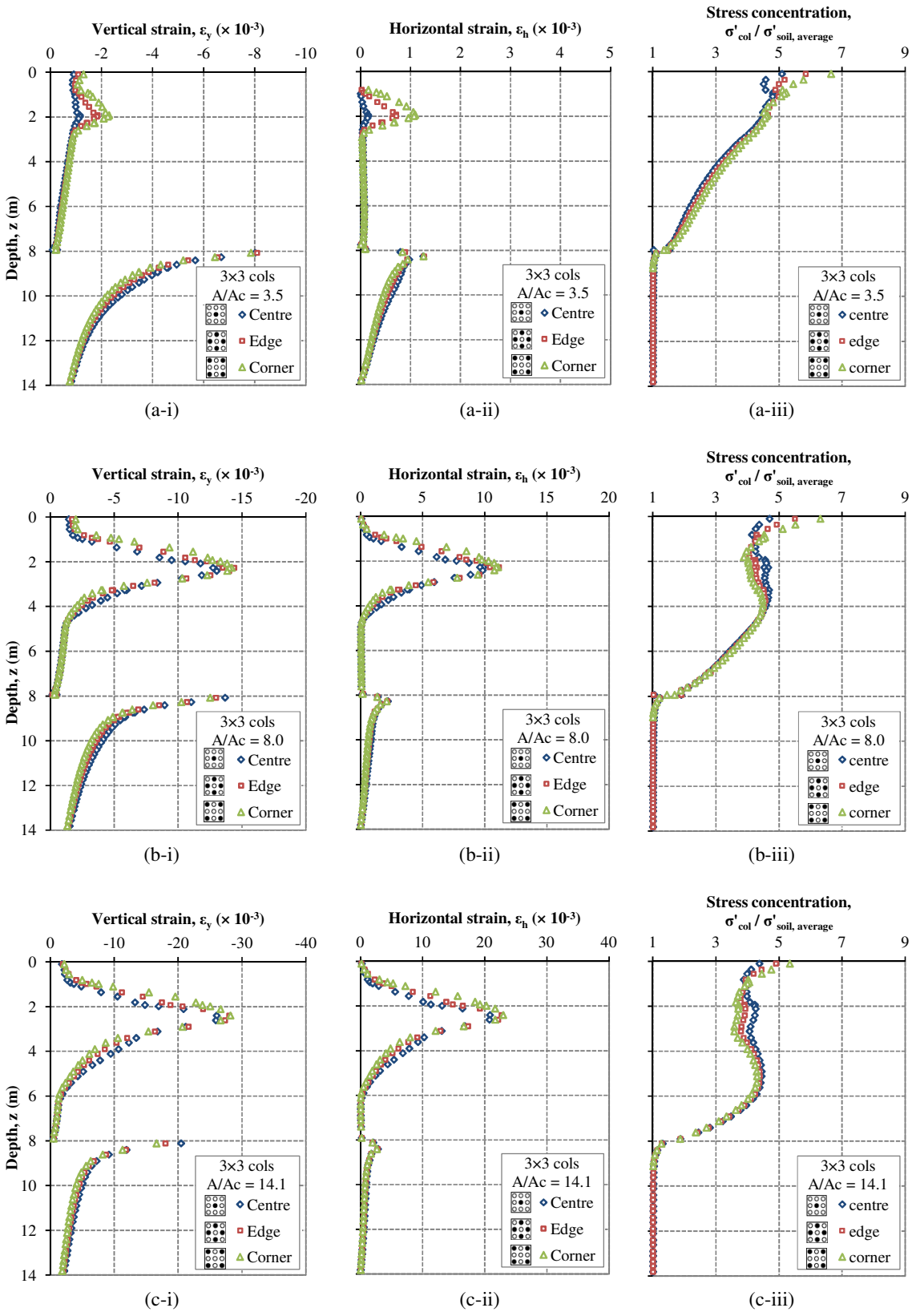

Figure 6.11 - Distribution of (i) vertical strain, (ii) horizontal strain and (iii) stress concentration ratio with depth for a 8 m long column, within a 3×3 group for A/A_C of (a) 3.5, (b) 8.0 and (c) 14.1

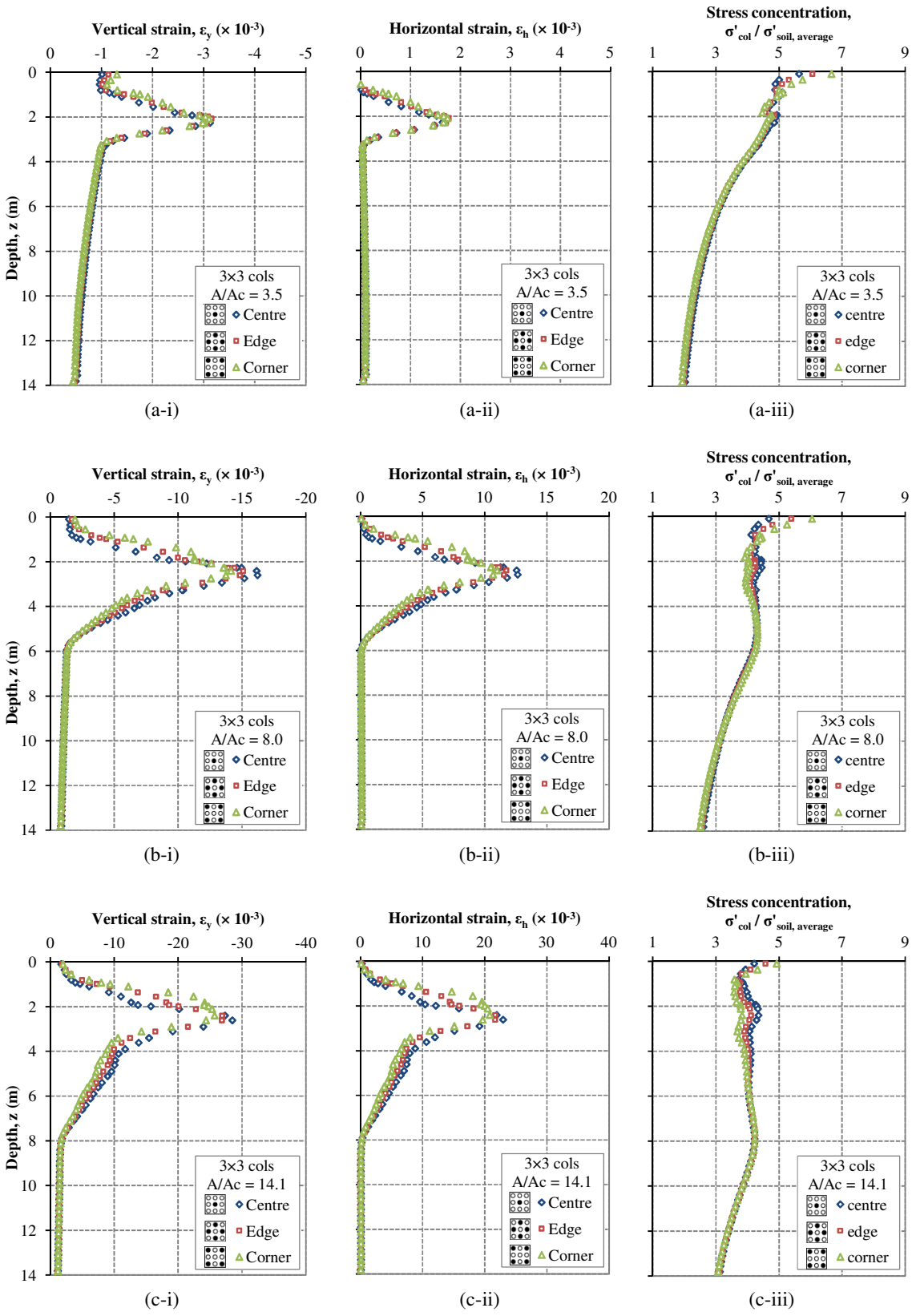

Figure 6.12 - Distribution of (i) vertical strain, (ii) horizontal strain and (iii) stress concentration ratio with depth for a 13.9 m long column, within a 3×3 group for A/A_C of (a) 3.5, (b) 8.0 and (c) 14.1

The distribution of vertical and horizontal strain for 13.9 m long columns is shown in Figures 6.12(i) and 6.12(ii), respectively. Punching failure is precluded for end-bearing columns and bulging appears to be the dominant mode of deformation for all columns. A significant increase in the magnitude of vertical and horizontal strain is observed with increasing area ratio, which may be attributed to the loss of lateral confinement and increase in the total load taken by columns with increasing area ratio. No variation in the levels of vertical and horizontal strain is observed with column position for end-bearing columns.

Distribution of stress concentration ratio

The distribution of stress concentration ratios for 3 m long columns is shown in Figure 6.10(iii). It can be seen that stress concentration ratios reduce steadily from high values, at the surface, to unity, at the base of floating columns. This is related to the punching mode of deformation and is consistent with previous findings for short single columns and 2×2 groups. A significant variation in stress concentration ratios with column position is observed in Figure 6.10(iii). It can be seen that stress concentration ratios at the surface are highest for corner columns, followed by edge and centre columns. This is due to the position of columns relative to the footing edge and is analysed in more detail in Section 5.5.2. The variation of stress concentration ratios is more pronounced at lower area ratios.

The distribution of stress concentration ratios for 8 m long columns is shown in Figure 6.11(iii). It can be seen for closely-spaced columns in Figure 6.11(a-iii) that stress concentration ratios reduce steadily with depth, which is consistent with a punching mode of deformation. However, a change in the variation of stress concentration ratios with depth is observed for higher area ratios (Figures 6.11(b-iii) and 6.11(c-iii)). It appears that stress concentration ratios for columns at high area ratios are related to horizontal strain. A significant proportion of horizontal strain occurs in long columns at high area ratios which reduces the load-carrying capacity of columns and hence results in lower stress concentration ratios. This is similar to findings for single columns and 2×2 groups. The largest drop in stress concentration ratios is evident at the top of the bulged section of columns. It can be seen that stress concentration ratios increase with depth to the bottom of the bulged section, due to overburden stress, and then decrease to unity at the base of floating columns.

The variation of stress concentration ratios with column position is also evident in Figure 6.11(iii). Vertical stress at the surface is highest for corner columns, followed by edge and

centre columns. This is again attributable to the position of columns relative to the footing edge. No change in stress concentration ratio with column position is observed with depth thereafter for closely-spaced columns. However, it can be seen for columns at higher area ratios that stress concentration ratios are highest for centre columns, followed by edge and corner columns over the bulged section of columns. This highlights the positive effects of column confinement provided to centre columns.

A similar variation of stress concentration ratios for 8 m long columns is observed for end-bearing columns in Figure 6.12(iii). It can be seen for closely-spaced columns in Figure 6.12(a-iii) that stress concentration ratios reduce steadily with depth, which is consistent with a punching mode of deformation. The distribution of stress concentration ratios for columns at higher area ratios is shown in Figures 6.12(b-iii) and 6.12(c-iii). Similar to single columns and 2×2 groups, it can be seen that the magnitude of stress concentration ratios reduces with increasing levels of horizontal strain.

4×4 group of columns

Distribution of vertical and horizontal strain

The distribution of vertical and horizontal strain with depth for 4×4 groups of 3 m long columns is shown in Figures 6.13(i) and 6.13(ii), respectively. It appears that the distributions of vertical and horizontal strain are very similar to 3×3 groups of columns. The majority of vertical strain develops beneath the base of columns which indicates that punching is the dominant mode of deformation. A variation in strain levels with column position is also observed and becomes more pronounced with increasing area ratio. It can be seen that vertical and horizontal strains are lowest in centre columns, followed by edge and corner columns. This may be attributed to the loss of lateral confinement associated with outer columns.

The distribution of vertical and horizontal strain for 8 m long columns is shown in Figures 6.14(i) and 6.14(ii), respectively. It can be seen in Figure 6.14(a-i) that punching remains the dominant mode of deformation for closely-spaced columns, as the majority of vertical strain occurs beneath the base of columns. However, a change in the mode of deformation is observed with increasing area ratio. It can be seen in Figure 6.14(ii) that considerable horizontal strain occurs in columns, which indicates that column bulging is occurring.

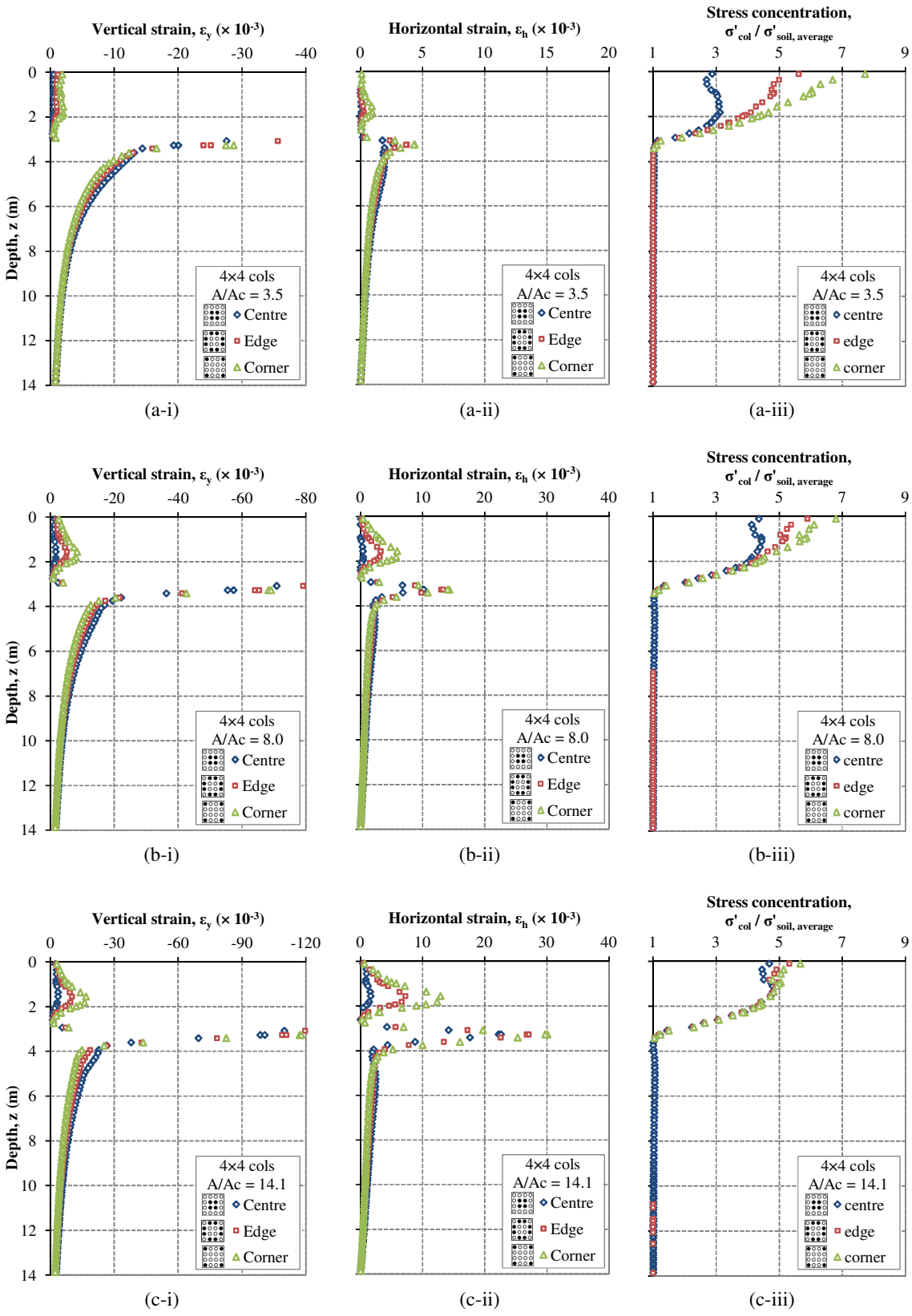

Figure 6.13 - Distribution of (i) vertical strain, (ii) horizontal strain and (iii) stress concentration ratio with depth for a 3 m long column, within a 4×4 group for A/A_C of (a) 3.5, (b) 8.0 and (c) 14.1

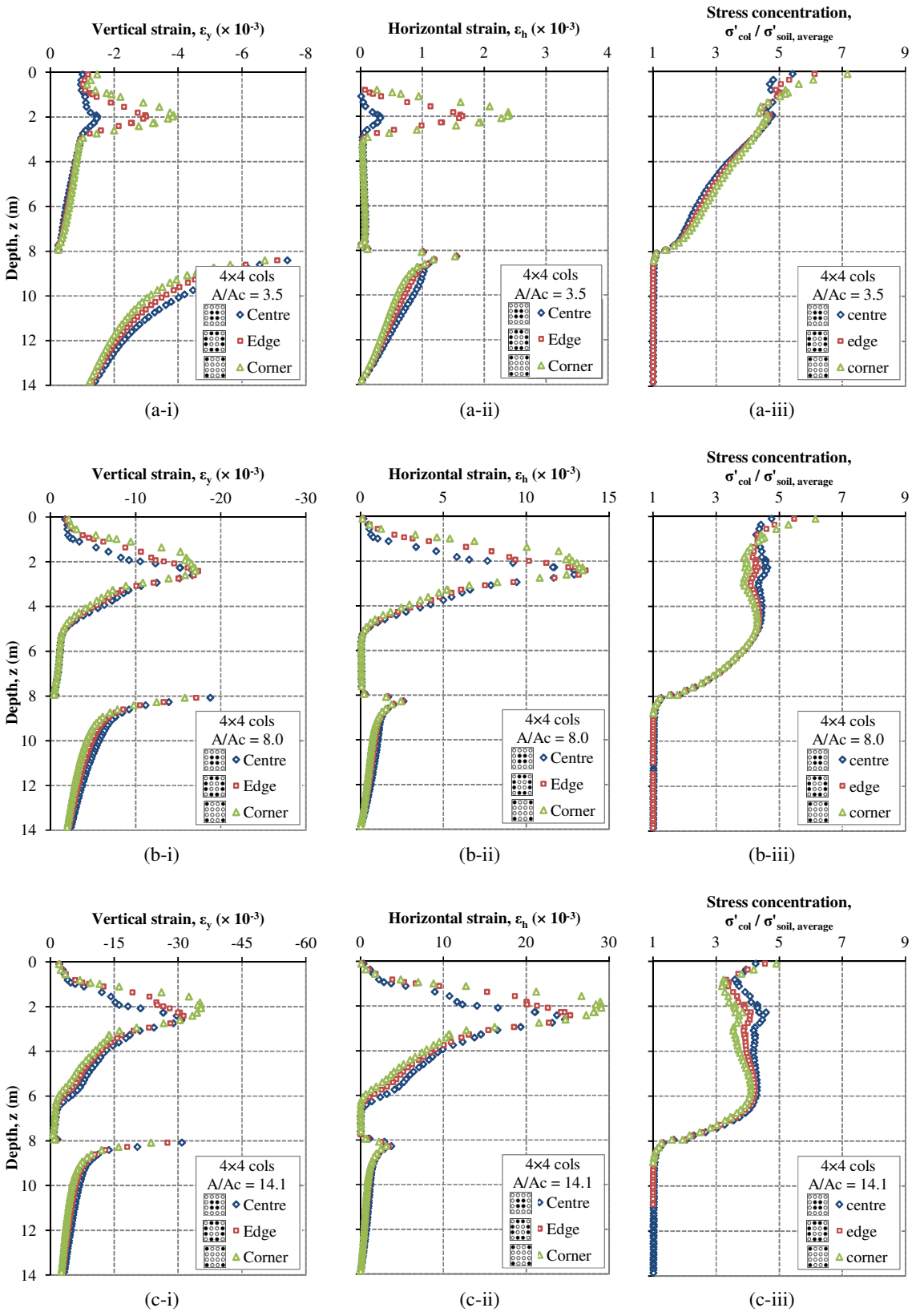

Figure 6.14 - Distribution of (i) vertical strain, (ii) horizontal strain and (iii) stress concentration ratio with depth for a 8 m long column, within a 4×4 group for A/A_C of (a) 3.5, (b) 8.0 and (c) 14.1

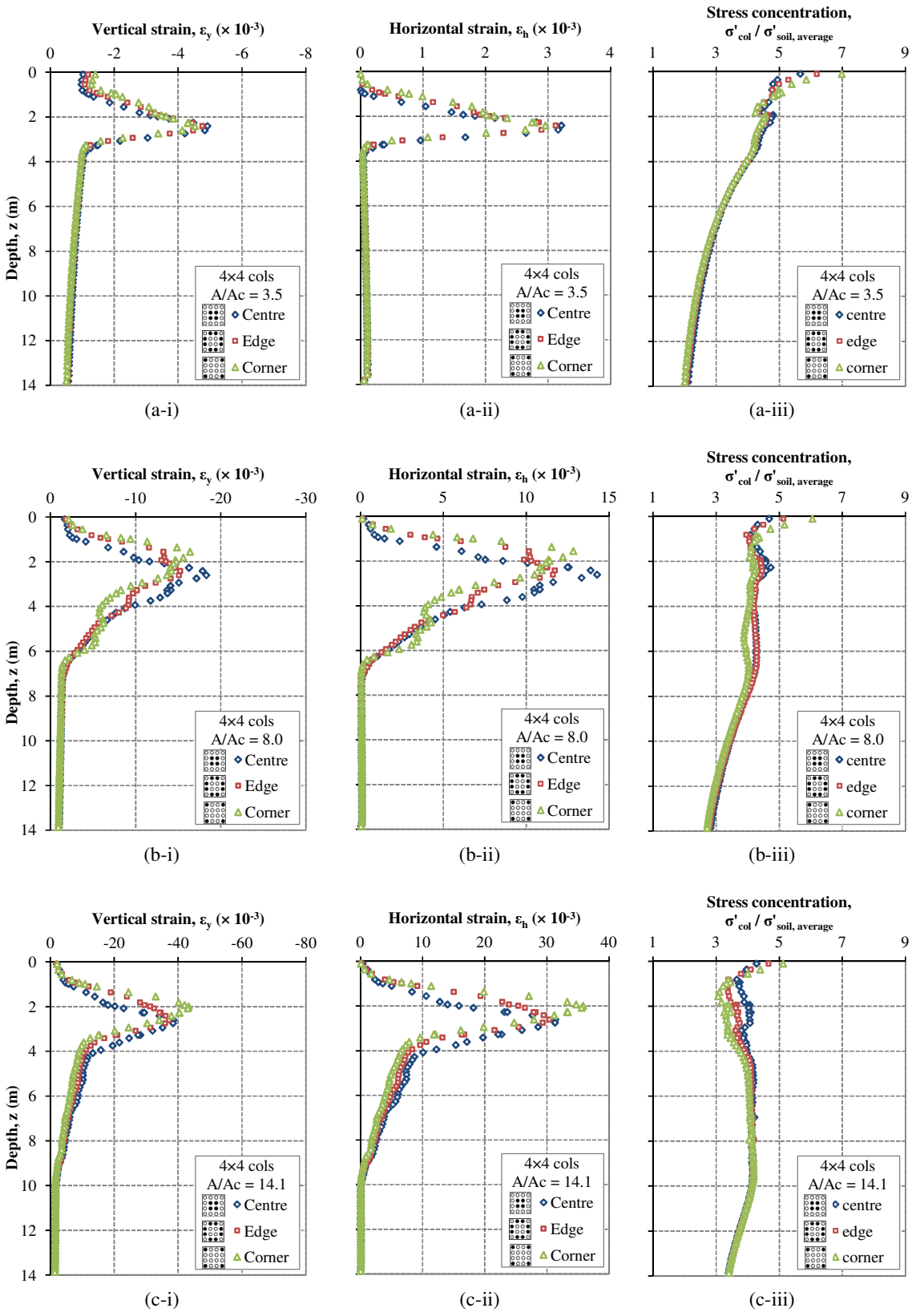

Figure 6.15 - Distribution of (i) vertical strain, (ii) horizontal strain and (iii) stress concentration ratio with depth for a 13.9 m long column, within a 4×4 group for A/A_C of (a) 3.5, (b) 8.0 and (c) 14.1

While it appears that column bulging is the dominant mode of deformation, it can still be seen that some of the applied load is transferred to the base of columns as vertical strains are developed in this region. The variation of strain level with column position is clearly visible for closely-spaced columns. The positive influence of column confinement is evident as vertical and horizontal strains are lowest for centre columns. The variation of strain level with column position is less well defined as area ratio increases. It appears that centre columns exhibit slightly lower vertical and horizontal strain.

The distribution of vertical and horizontal strain for end-bearing columns is shown in Figures 6.15(i) and 6.15(ii), respectively. It can be seen that bulging is the dominant mode of deformation for all area ratios. A significant increase in vertical and horizontal strain is also evident with increasing area ratio. The variation of strain levels with column position can also be seen for columns at higher area ratios. It can be seen in Figure 6.15(b-i) that the magnitude of vertical strain is highest and maximum strain occurs at the deepest level for centre columns spaced at A/A_C = 8.0. The maximum vertical strain also occurs deeper for centre columns which are spaced at A/A_C = 14.1. However, the maximum vertical and horizontal strain is highest for corner columns.

Distribution of stress concentration ratios

The distribution of stress concentration for 3 m long columns is shown in Figure 6.13(iii). The distribution of stress concentration ratios appears to be similar to a 3×3 group. Stress concentration ratios reduce steadily with depth from high values at the surface, which is consistent with a punching mode of deformation. The variation of stress concentration ratios with column position is also evident and this becomes more pronounced with decreasing area ratio.

The distribution of stress concentration ratios for 8 m long columns is shown in Figure 6.14(iii). The distribution of stress concentration ratio with depth for closely-spaced columns again reduces steadily with depth. This indicates that columns are punching into the underlying soil and is consistent with previous findings from single columns, 2×2 groups and 3×3 groups. However, a marked change in the distribution of stress concentration ratios is observed with increasing area ratio. It appears that stress concentration ratios are related to the horizontal strains. The development of horizontal strain in columns reduces the load-carrying capacity of columns, which results in lower stress concentration ratios. It is also

interesting to note that while stress concentration ratios are lowest for centre columns at the surface, a reverse in this trend is observed in lower sections of columns which are bulging.

The distribution of stress concentration ratios for end-bearing columns is shown in Figure 6.15(iii). It can be seen that stress concentration ratios follow a similar trend to 3×3 groups of columns and reduce steadily with depth for closely-spaced columns. However, it can be seen that the magnitude of stress concentration ratios reduces for higher area ratios, as vertical and horizontal strain increase. It can be seen that stress concentration ratios increase for centre columns in sections of columns which are bulging.

6.4 Summary of results of FEA: Distribution of total shear strains and characteristic column behaviour

Three modes of deformation were identified in Chapter 5 using newly defined punching and compression ratios. However, these ratios only indicate the general mode of deformation, and it is necessary verify these modes of deformation by conducting a more in-depth analysis of the load-transfer mechanisms. The distribution of shear strain within columns and in the surrounding soil is examined for three column lengths, namely 3, 8 and 13.9 m. These column lengths were specifically chosen to allow the load-transfer mechanism for each mode of deformation to be examined; 3 m long columns were chosen to investigate punching failure, 8 m long columns were chosen to investigate a combination of punching and bulging and 13.9 m long columns were chosen to investigate bulging failure, as punching is precluded. The distribution of vertical strain, horizontal strain and stress concentration ratio along the length of columns was also examined.

6.4.1 Distribution of total shear strain

The punching mode of deformation was evident for short columns, and also long single columns at low area ratios. This is consistent with the distribution of total shear strains, as significant shear strains develop along the side and beneath the base of columns. ‘Block’ failure becomes more prominent as the number of columns increases for columns at low area ratios. Shear strain develops along the outer side of exterior columns and beneath the base of columns, while negligible shear strain develops in the soil bounded by central and exterior columns. This indicates that the columns and surrounding soil deform as a single entity, which is consistent ‘block’ failure. Bulging failure is evident as large shear strains develop

within columns. This mode of deformation occurs for long columns at high area ratios. In addition to the three modes of deformation, the development of shear planes was also observed. The shear planes extend from the corner of pad footings to the point of maximum bulging and create a zone of undeforming soil. This is consistent with previous findings by Muir Wood *et al.* (2000); however, it is important to note that the shear planes are a secondary mode of deformation, but may become more pronounced at higher load levels.

6.4.2 Distribution of vertical strain, horizontal strain and stress concentration ratios

The distribution of vertical and horizontal strain is consistent with the shear strains. It was also observed that punching or bulging modes of deformation are not clearly defined and some combination of both modes of deformation occurs for all configurations of columns. The distribution of stress concentration ratios is significantly influenced by the vertical and horizontal strain within columns. Sections of columns which exhibit large vertical strains are in a contained state of plasticity and cannot sustain high vertical loads. Consequently, stress concentration ratios reduce in these regions.

Chapter 7
Development of simplified design method and comparison of findings with previous research

7.1 Introduction

The results from the numerical analysis regarding the settlement performance, deformational behaviour and stress concentration ratios for small groups of stone columns are placed in context to previous research in this chapter.

The loss of lateral confinement for small groups of end-bearing stone columns has been studied previously, and the findings of these studies are compared with those obtained using PLAXIS 3D Foundation. The previous research is extended through investigation of the influence of column confinement upon the settlement performance of small groups of floating stone columns. A simplified design method is proposed which allows the settlement of small groups and infinite grids of columns to be related with knowledge of the footing-width to column-length ratio and column-length to soil-thickness ratio.

Three modes of deformation referred to as "punching", "block failure" and "bulging", were identified in the previous chapters for small groups of stone columns. The development of these modes of deformation is compared with small scale laboratory studies, conducted by Muir Wood *et al.* (2000) and Black (2006). The importance of capturing the influence of the stiff crust, a salient feature of soft soil profiles, is highlighted and the existence of a critical length, proposed by previous laboratory research, is investigated.

The influence of the mode of deformation upon the settlement performance of stone columns is also investigated in the following chapter. The modes of deformations were identified using compression and punching ratios and the variation of these parameters with settlement improvement factors for different configurations of columns is presented and analysed.

Stress concentration ratios at the surface of an infinite grid of columns are compared with a database, which consists of field and laboratory measurements, and also analytical design methods. The distribution of stress concentration ratios with depth in not well understood and this is examined and compared with analytical design methods.

7.2 Settlement analysis

The behaviour of small groups of stone columns beneath pad footings is quite complex as the external columns are subject to a loss of lateral confinement and also the vertical stress decays sharply with depth. Therefore, it is helpful to conduct a three-dimensional numerical analysis to accurately capture the settlement performance of small groups of stone columns. The influence of column confinement upon the settlement performance of small groups of stone columns was examined in Chapter 5. It was found that the degree of column confinement depends on many parameters such as the number of columns, area ratio and column length. The influence of the number of columns upon the settlement performance of stone columns is expressed as a settlement ratio (s/s_{uc}), which is defined as the ratio of the settlement of small groups of columns to that of infinite grids of columns.

7.2.1 Justification of the use of s/s_{uc}

It was established in Chapters 5 and 6 that the area ratio and column length play key roles in determining the mode of deformation of stone columns. While the number of columns has a positive influence upon the settlement performance of stone columns, it does not fundamentally change the load transfer mechanisms. Therefore, it is deemed acceptable to compare the settlement of small groups with infinite grids of columns (s/s_{uc}) at similar area ratios and lengths.

7.2.2 Review of Priebe (1995)

Priebe (1995) is the only analytical method which uses the s/s_{uc} term to estimate group settlements. Design curves are presented in Figure 2.24 which relate s/s_{uc} to the number of columns and the normalised column length (L/d). The main points regarding these design curves are summarised below:

- The design curves are based on numerous calculations which account for the reduction in vertical stress with depth beneath small loaded areas and also consider a lower bearing capacity for the outer ring of columns in the column group.
- No direct reference is made to the footing area (A) in Figure 2.24 and it appears that s/s_{uc} is independent of the area ratio (A/A_C).
- However, for a given number of columns, an increase in footing area leads to larger settlements (s) due to the greater depth of stress. The corresponding increase in A/A_C leads to an increase in s_{uc}. Priebe (1995) claims that the increase in s and s_{uc} "compensate" such that s/s_{uc} ratios are acceptable for $A/A_C < 10$.

7.2.3 Review of Elshazly *et al.* (2008a)

Elshazly *et al.* (2008a) examined the influence of column confinement upon the settlement performance of stone columns and present graphs of s/s_{uc} as a function of the normalised footing width (B/L). A series of axisymmetric FEA are conducted on two soil profiles:

(i) Layered estuarine deposit, as described by Mitchell & Huber (1985)
- L = 10.8 m; end-bearing on an older marine deposit
- E_{col}/E_{soil} = 1.3–2.6

(ii) Soft clay deposit
- L = 10.8 m and 30 m; end-bearing on dense silty sand
- E_{col}/E_{soil} = 8.5

The loading is applied through a gravel distribution layer to various load levels, ranging from working loads to ultimate loads. A more detailed description of the FEA by Elshazly *et al.* (2008a) is provided in Section 2.3.3.

The variation of s/s_{uc} with B/L for the two soil profiles is shown in Figure 7.1:

- It can be seen that s/s_{uc} values increase somewhat asymptotically with B/L for profile (i). For profile (ii) a rapid increase in s/s_{uc} values is observed at low B/L followed by a gradual decrease with increasing B/L.
- It can also be seen that s/s_{uc} are much higher for profile (ii). Elshazly *et al.* (2008a) attribute this to the high modular ratio (E_{col}/E_{soil}). The Young's modulus of the stone column (E_{col}) is similar for both profiles and a higher E_{col}/E_{soil} indicates that the soil stiffness is lower for profile (ii). This suggests that the lateral support provided by the surrounding soil has a significant influence on s/s_{uc}.

The design curve developed by Priebe (1995) is adapted to match the numerical analysis by Elshazly *et al.* (2008a) (L/d = 10.8/1.06 = 10.2) and is shown in Figure 7.2. As mentioned previously, Priebe (1995) does not directly relate s/s_{uc} to the footing area. However, the footing width (B) can be determined by assuming the columns are positioned on a square grid and the distance from the centre-line of the outer row of columns to the edge of the footing is half the column spacing.

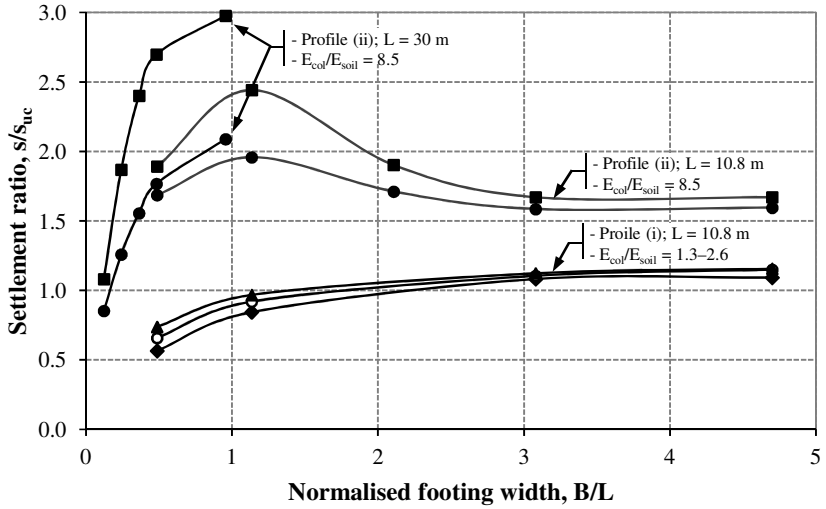

Figure 7.1- Variation of settlement ratio with normalised footing width for a layered soil and a soft clay, as determined by Elshazly *et al.* (2008a)

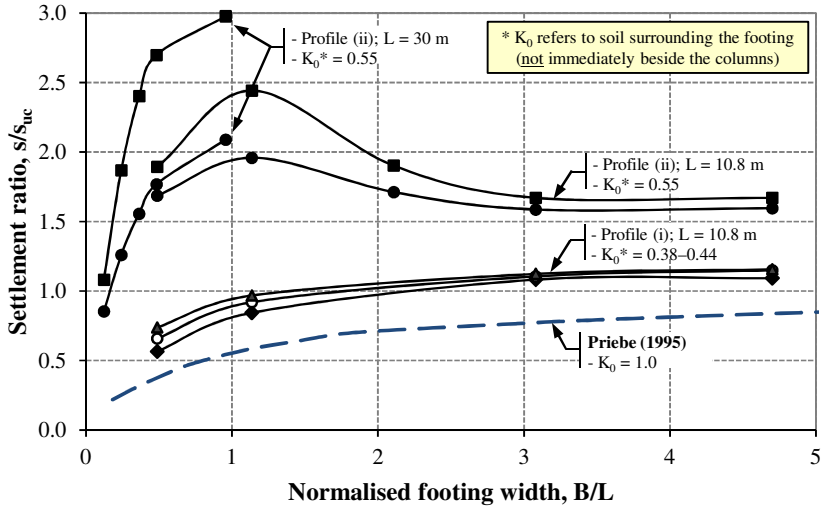

Figure 7.2 -Comparison of settlement ratios determined by Elshazly *et al.* (2008a) with Priebe (1995)

While the variation of s/s_{uc} with B/L for profile (i) is quite similar to Priebe (1995), it can be seen in Figure 7.2 that Priebe (1995) predicts lower s/s_{uc}. This may be related to the lateral support provided by the surrounding soil:

- Elshazly *et al.* (2008a) account for column installation effects by increasing K_0 in the soil immediately surrounding stone columns. However, the soil surrounding the footing (i.e. outside the outer row of columns) is modelled as a normally consolidated soil and the lateral stress is defined by $K_0 = 1 - \sin(\varphi')$ (Jaky, 1944). This results in $K_0 = 0.38–0.44$ and 0.55 for profiles (i) and (ii), respectively.
- Priebe (1995) accounts for column installation effects by adopting $K_0 = 1.0$ for the surrounding soil. A higher lateral stress state in the surrounding soil provides enhanced support to the columns and, therefore, results in lower s/s_{uc}.

Another possible explanation of the high s/s_{uc} values determined by Elshazly *et al.* (2008a) relative to Priebe (1995) is the flexible loading conditions. Elshazly *et al.* (2008a) determine s/s_{uc} from the maximum settlement, which occurs near the edge of footings (Figure 7.3). This is higher than the settlement of rigid footings, assumed by Priebe (1995), and is another contributing factor to the higher s/s_{uc} values.

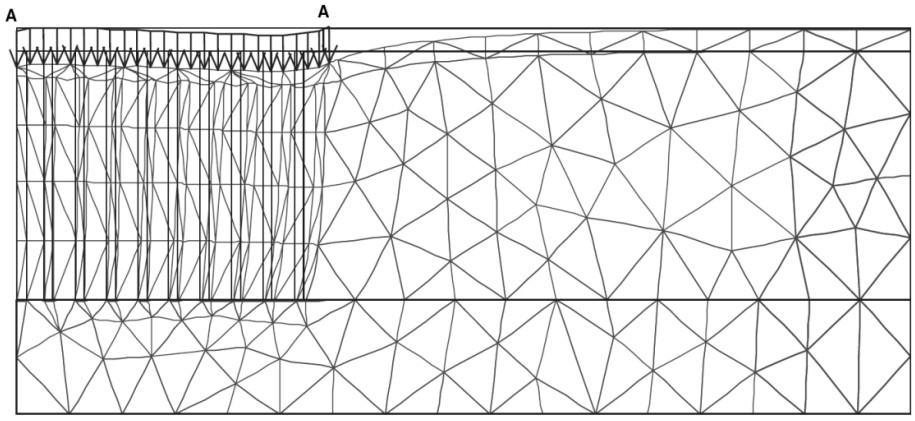

Figure 7.3 - Deformed mesh of a foundation with B/L = 3 (case of 10.8 m-thick soft clay layer with a 19×19 column arrangement) (Elshazly *et al.*, 2008a)

7.2.4 Comparison of s/s_{uc} for end-bearing columns from PLAXIS 3D Foundation & Priebe (1995)

The design curve developed by Priebe (1995) in Figure 2.24 is adapted to match the numerical analyses conducted using PLAXIS 3D Foundation (i.e. L/d = 13.9/0.6 = 23.2) and the variation of s/s_{uc} with the number of columns is shown in Figure 7.4. In order to remain consistent with the assumptions of Priebe (1995), only s/s_{uc} values for end-bearing columns from PLAXIS 3D Foundation are shown in Figure 7.4.

As expected, it can be seen in Figure 7.4 that an increase in the number of columns leads to higher s/s_{uc} values. An increase in the number of columns results in higher levels of column confinement and also higher levels of vertical stress with depth (due to larger footing areas). Therefore, the boundary conditions for groups of columns approach unit cell conditions with an increasing number of columns and s/s_{uc} values tend towards unity.

It can also be seen in Figure 7.4 that s/s_{uc} values generally increase with A/A_C and this becomes more significant for larger groups of columns. The design curve developed by Priebe (1995) agrees favourably with PLAXIS 3D Foundation for $A/A_C = 3.5$, but diverges at higher area ratios. This confirms that Priebe's (1995) method is only acceptable for column groups having low area ratios and is un-conservative for more widely-spaced columns.

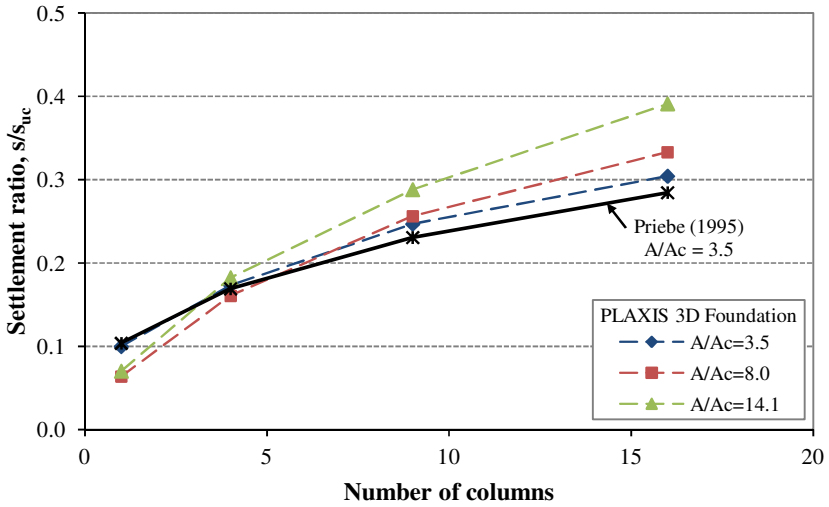

Figure 7.4 - Comparison of settlement ratios for groups of end-bearing stone columns from PLAXIS 3D Foundation with Priebe (1995)

7.2.5 Settlement ratios for floating stone columns

Currently, no study has investigated the variation of s/s_{uc} for floating stone columns. The effect of floating columns is introduced into Figure 7.5 using the L/H term, where H is the thickness of the soil deposit (= 13.9 m for the Bothkennar deposit in this research). The influence of A/A_C upon s/s_{uc} values for floating columns is also shown in Figure 7.5. For clarity, only data specific to three column lengths are presented, namely: L/H = 0.22, 0.58 and 1.00, which correspond to L = 3, 8 and 13.9 m, respectively.

Influence of L/H

For a given B/L, Figure 7.5 shows that s/s_{uc} reduces with decreasing L/H. A decrease in L/H corresponds to a thicker layer of soil beneath the base of columns. The settlement of this layer is much higher for the infinite grid of columns relative to small groups, due to the constant stress with depth. Therefore, a decrease in L/H leads to much higher s_{uc} and consequently lower s/s_{uc}.

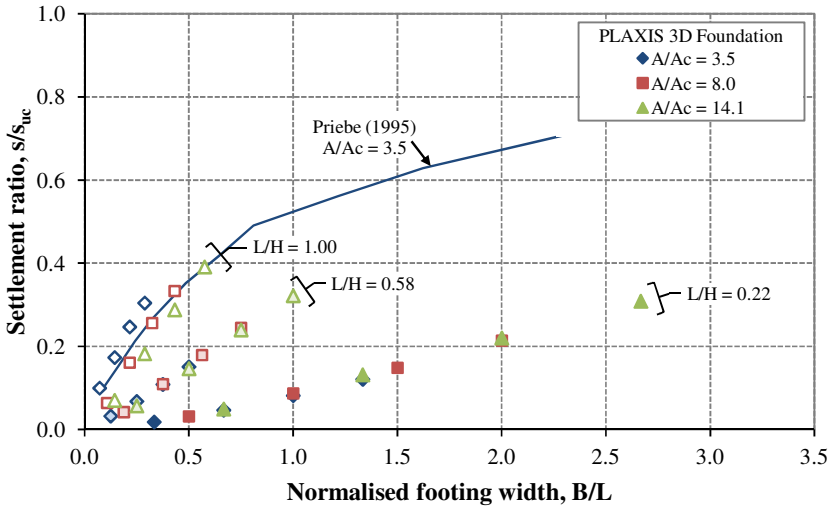

Figure 7.5 - Variation of settlement ratios with normalised footing width (B/L) and column length (L/H)

Influence of A/A$_C$

It appears that A/A_C only influences s/s_{uc} for end-bearing stone columns (L/H = 1.0). It was shown in Section 5.3.1 that the settlement performance of an infinite grid of stone columns improves significantly at low A/A_C. This is attributed to the increased levels of lateral confinement and it can be seen in Figure 5.7(ii) that the influence of lateral confinement becomes most pronounced for long columns (L > 10 m). Therefore, a significant reduction in s_{uc} occurs for long, end-bearing columns at low A/A_C, which leads to higher s/s_{uc}.

In contrast to end-bearing columns, it appears that s/s_{uc} does not vary with A/A_C for floating stone columns (L/H = 0.22 and 0.58). For a given L/H and B/L, it can be seen in Figure 7.5 that s/s_{uc} values are similar for different A/A_C. The influence of A/A_C upon the settlement performance of stone columns may be hidden in s/s_{uc}. The settlement of floating stone columns is comprised of settlement from two sections: (i) over the length and (ii) beneath the base of columns. The settlement of the soil beneath the base of columns is quite high for an infinite grid of columns, due to the constant stress with depth. This results in high s_{uc} which yields low s/s_{uc} and hence hides the influence of A/A_C upon s/s_{uc}.

Influence of B/L

A somewhat linear relationship appears to exist between s/s_{uc} and B/L for floating stone columns. However, care must be exercised in assuming a linear relationship for all B/L values as it can be seen from the distribution of s/s_{uc} with B/L for Priebe (1995) that s/s_{uc} approaches unity somewhat asymptotically at high B/L ratios.

The variation of s/s_{uc} with B/L for a wide range of column lengths is shown in Figure 7.6. It can be seen that the influence of A/A_C upon s/s_{uc} becomes more pronounced as L/H increases. This may be explained as the settlement of soil beneath the base of columns reduces at high L/H values. However, it must be noted that for the majority of column lengths, A/A_C does not influence s/s_{uc} and a near-linear relationship exists between s/s_{uc} and B/L for a given L/H.

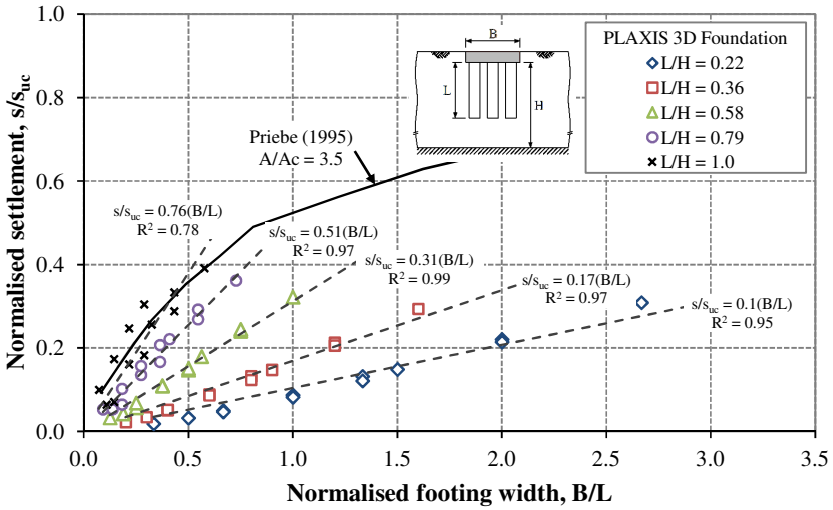

Figure 7.6 - Influence of footing width (B/L) and column length (L/H) upon settlement ratios for groups of columns

Development of a simple design equation

A simple design equation relating s/s_{uc}, B/L and L/H is developed as follows:

(i) Establish a relationship between s/s_{uc} and B/L

If s/s_{uc} and B/L are assumed to be directly proportional, then their relationship can be defined by:

$$s/s_{uc} = \alpha(B/L) \qquad \textbf{(7.1)}$$

The lines of best fit between s/s_{uc} and B/L are shown in Figure 7.6, along with their corresponding R^2 values. R^2 is the coefficient of determination and is sometimes referred

to as the proportion of explained variance. It is a measure of the relative predictive power of a model and varies between 0 and 1; the closer R^2 is to 1, the better the predictive power of the model. It can be seen that all R^2 values are close to unity, especially for floating columns, which justifies the assumption that s/s_{uc} is directly proportional to B/L.

(ii) Establish a relationship linking L/H to s/s_{uc} and B/L

The slopes of s/s_{uc} versus B/L for each L/H (defined as α) are plotted against L/H in Figure 7.7. A line of best-fit, which assumes a quadratic relationship between α and L/H, is defined by:

$$\alpha = 0.61(L/H)^2 + 0.1(L/H) + 0.06 \quad \textbf{(7.2)}$$

It can be seen that $R^2 = 1$ for this line which indicates that the quadratic equation predicts the relationship between α and L/H perfectly.

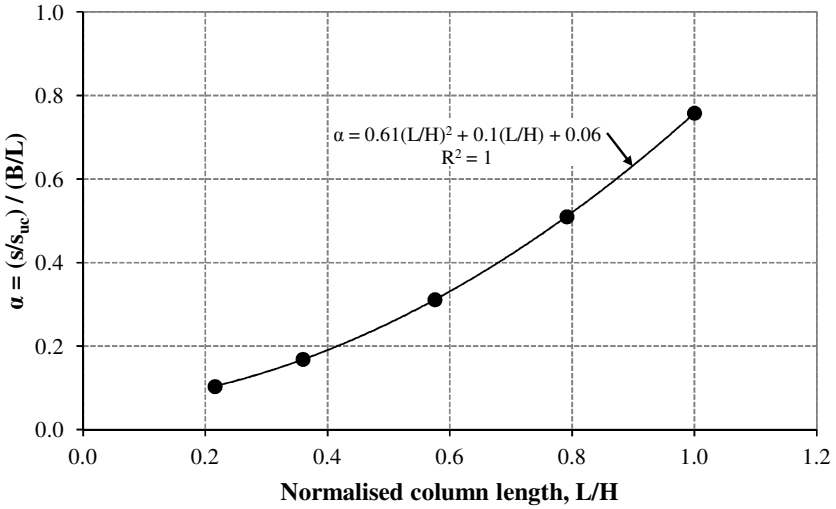

Figure 7.7 - Relationship between α (which relates the s/s_{uc} and B/L) with L/H

(iii) Combine equations 7.1 and 7.2

Equation 7.1 and 7.2 are combined to yield a simple design equation relating s/s_{uc} to B/L and L/H:

$$s/s_{uc} = \alpha.(B/L)$$

$$s/s_{uc} = (0.61(L/H)^2 + 0.1(L/H) + 0.06).(B/L) \quad \textbf{(7.3)}$$

The above equation (7.3) is an interesting and useful finding which allows designers to relate the settlement of small groups and infinite grids of columns by knowing B/L and L/H.

Therefore, instead of conducting rigorous and time consuming three-dimensional numerical analyses, the settlement of small groups of columns (s) can be easily determined from equation 7.3. The settlement of an infinite group of columns (s_{uc}) can be quickly determined from the analytical design methods described in Section 2.5.4. It was shown in Figure 4.16 that Priebe's (1995) n_2 design curve and Pulko & Majes (2005) predict the settlement performance of stone columns closest to PLAXIS 3D Foundation. However, McCabe *et al.* (2009) shows that Priebe's basic design curve (n_0) predicts the field measurements of settlement improvement factors quite well. It may be the case that Priebe's basic design curve is limited to typical field conditions and cannot capture the settlement performance of stone columns at high modular ratios (e.g. the Bothkennar soil profile).

It should be noted that equation 7.3 is specific to the benchmark parameters, developed in Sections 4.4 and 4.6.1. It was shown previously that design parameters such as modular ratios (E_{col}/E_{soil}) and the column strength (φ) have a significant influence upon the settlement performance of stone columns. However, it is difficult to predict their influence upon s/s_{uc} values, as the relative influence of E_{col}/E_{soil} and φ upon s and s_{uc} may cancel each other.

7.3 Deformational behaviour of stone columns

The deformational behaviour of stone columns was investigated in Chapters 5 and 6. The following section summarises the main findings from PLAXIS 3D Foundation and identifies the main parameters governing the deformational behaviour of stone columns. The findings from other studies regarding the deformational behaviour of stone columns are examined and placed in context of the new numerical analysis.

7.3.1 Summary of findings from PLAXIS 3D Foundation

The influence of key design parameters upon the deformational behaviour of stone columns was investigated in Section 5.3. Punching and compression ratios were defined in order to help identify three distinct modes of deformation: (i) punching, (ii) 'block' failure and (iii) bulging. The load transfer mechanisms for each of these modes of deformation were verified in Chapter 6 by analysing the distribution of total shear strain in the column and surrounding soil and, also, the distribution of stress and strain along the length of columns. It was found that A/A_C and L had a significant influence on the mode of deformation.

A short summary of the main characteristics of each mode of deformation is given below:

(i) Punching

- Typically occurs for short columns and small groups of long columns at low A/A_C.
- Characterised by low compression ratios and high punching ratios.
- Shear stress and end-bearing pressure develop along the sides and at the base of columns.

(ii) 'Block' failure

- Typically occurs for large groups of columns at low A/A_C.
- Characterised by low compression ratios and low punching ratios.
- Columns act as a single entity and displace as a 'block' into the underlying soil, which ensures low differential settlement at the base of columns and consequently low punching ratios.
- Shear stress develops along the outer sides of external columns and end-bearing pressure at the base of columns.

(iii) Bulging

- Typically occurs for long columns at high A/A_C.
- Characterised by high compression ratios and low punching ratios.
- Columns bulge at the point of lowest lateral resistance, which generally occurs near the ground surface where overburden stresses are lowest.
- Bulging precludes the transfer of the applied load to depth which yields low punching ratios.

7.3.2 Review of Black (2006)

Black (2006) conducted a series of small scale laboratory tests to investigate the settlement performance and deformational behaviour of single columns and small groups of columns. A detailed description of the study is provided in Section 2.3.2 and the main findings are summarised below:

- The deformed shape of columns was determined upon completion of loading by removing the aggregate from columns and backfilling the subsequent voids with either a hot wax or a cement-water mixture. The loading tests were terminated at high strain levels (footing settlement/diameter = 0.18–0.27), in comparison to PLAXIS 3D Foundation (footing settlement/diameter = 0.02), which implies that the deformed shape of columns was specific to ultimate conditions.

- Black (2006) observed that the displacement at the base of single columns becomes negligible for L/d > 8 and postulates that the mode of deformation changes from punching to bulging at this point.
- 'Block' failure was observed for small groups of columns whereby the columns acted as a single entity. The mode of deformation also changes from punching to bulging at L/d = 8, however d is defined as the outer diameter of the group in this instance.
- The findings by Black (2006) are consistent with McKelvey *et al.* (2004) who conducted a small scale laboratory study on small groups of stone columns and suggested that a critical column length exists and lies in the range L/d = 6–10.

7.3.3 Comparison of PLAXIS 3D Foundation with Black (2006)

The penetration at the base of single columns and footing settlement is presented by Black (2006) and these have been combined to determine compression ratios (defined in equation 5.2). The variation of compression ratios with normalised column length (L/d) from Black (2006) is compared with PLAXIS 3D Foundation in Figure 7.8.

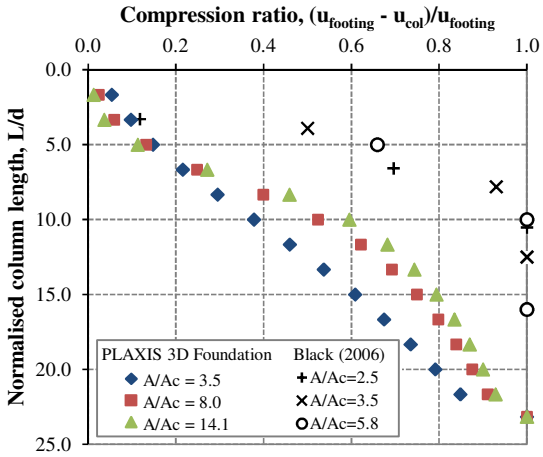

Figure 7.8 - Comparison of compression ratios from Black (2006) and PLAXIS 3D Foundation for single columns

Influence of the stiff crust

It can be seen in Figure 7.8 that compression ratios from PLAXIS 3D Foundation are much lower than Black (2006). This is due in part to the stiff crust at the Bothkennar test site, which is modelled by PLAXIS 3D Foundation, but not present in the homogeneous soil samples tested by Black (2006). The influence of the stiff crust upon the deformational behaviour of stone columns, and more specifically upon compression ratios, is shown in Section 5.4.9.

While the influence of the stiff crust upon the deformational behaviour of single columns was not investigated exclusively, it can be seen in Figure 7.9 that compression ratios increase dramatically with the absence of the stiff crust for a group of 4 columns beneath a 3 m square footing (i.e. $A/A_C = 8.0$) and agree more closely with Black (2006).

The stiff crust tends to confine columns near the surface, where columns are subject to the lowest overburden stress and hence are most susceptible to bulging. Therefore, the presence of the stiff crust enhances the load-carrying capacity of columns and allows a greater proportion of the load to be transferred to the base of columns. This highlights the advantages of the FEM, which is capable of capturing the presence of the stiff crust and, therefore, capable of modelling more realistic soil profiles.

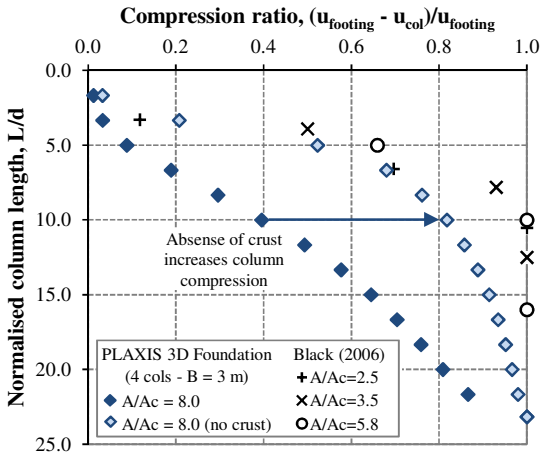

Figure 7.9 - Comparison of compression ratios from Black (2006) with PLAXIS 3D Foundation for soil profiles with and without a stiff crust

Influence of applied load level

It can be seen in Figure 7.9 that that an increase in the normalised column length (L/d) leads to an increase in compression ratios. This indicates that a larger proportion of the applied load is absorbed within columns rather than transferred to the base. Black (2006) defines column bulging when negligible displacement occurs at the base of columns and observes that the transition between punching and bulging modes of deformation is clearly defined at L/d = 8 for ultimate conditions.

However, it appears that the transition between punching and bulging is more gradual at typical working load levels, as determined by PLAXIS 3D Foundation. It can be seen in Figures 7.8 and 7.9 that compression ratios are less than 1.0 for all floating columns. This

indicates that displacement occurs at the base of all floating columns - even in the case of long columns at high area ratios (A/A_C = 8.0 and 14.1), where bulging is established as the dominant mode of deformation. This finding is quite interesting and suggests that the mode of deformation at working load levels is a combination of punching and bulging, with one particular mode more influential for a given A/A_C and L.

It was shown previously in Figure 5.15 that the extent of plasticity within columns increases for fewer supporting columns beneath a 3 m square footing, i.e. as the average load taken per column increases. Column plasticity reduces the ability of columns to transfer the applied load to the base of columns and, consequently, results in higher compression ratios. This may explain the high compression ratios observed by Black (2006) as the deformed shape of columns is determined at ultimate conditions, which ensured that columns were in an advanced state of plasticity. In contrast, columns at low working load levels are in more of an elastic state and can transfer a larger proportion of the load to the base of columns.

Influence of column length

The main aim of this thesis is to examine the key design parameters influencing the settlement performance of small groups of stone columns. Therefore, it is necessary to examine the deformational behaviour at working load levels rather than at ultimate conditions. The findings from PLAXIS 3D Foundation indicate that some degree of punching occurs at the base of all floating columns and this is most significant for columns at low A/A_C. It was shown in Section 5.3.2 that increasing the length of columns exhibiting punching enhances the settlement performance of these stone columns. Therefore, as all columns exhibit some degree of punching, the settlement performance of columns always increases with column length and in the general case no critical length exists for the settlement performance of columns.

Influence of the material parameters

Black (2006) suggests that a modular ratio E_{col}/E_{soil} = 10 is appropriate for the laboratory study. The modular ratio for an infinite grid of columns at the Bothkennar test site, modelled in PLAXIS 3D Foundation, is shown in Figure 6.7 and is much higher than Black (2006). However, it was shown in Section 5.4.6 that the effect of E_{col}/E_{soil} on compression ratios is of minor significance in the range E_{col} = 30–70 MPa.

Black (2006) used a basalt aggregate to form the stone columns. This was subject to direct shear and triaxial compression tests which indicated angles of internal friction (φ') of 46° and 43°, respectively. These values are very similar to those adopted in PLAXIS 3D Foundation (φ' = 45°) and therefore would not contribute towards the discrepancy in the results.

7.3.4 Review of Muir Wood *et al.* (2000)

Muir Wood *et al.* (2000) conducted a series of small scale laboratory tests to investigate the influence of column arrangement and length upon the deformational behaviour of groups of floating stone columns. A detailed description of the study is provided in Section 2.2.2 and the main points are summarised below:

- The deformed shape of columns was determined at the end of loading by removing the sand in the columns and backfilling the voids with plaster of Paris. Similar to Black (2006), the loading tests were terminated at high strain levels (footing settlement/diameter = 0.3) which again implies that the deformed shape of columns is specific to ultimate conditions.
- It was observed that the deformational behaviour of columns varies with the position of columns beneath the circular footings; bulging in central columns was pushed deeper due to the enhanced lateral support provided by the surrounding columns.
- It was also observed that punching was most pronounced for short, closely-spaced columns (i.e. low A/A_C) and did not occur for columns longer than L/D = 1.0. On this basis Muir Wood *et al.* (2000) suggest that a critical length may exist, but the dominant strain in columns is dependent on the footing diameter rather than on the column diameter.

7.3.5 Comparison of PLAXIS 3D Foundation with Muir Wood *et al.* (2000)

Muir Wood *et al.* (2000) present the penetration at the base of columns as a proportion of footing settlement ($u_{col}/u_{footing}$) for various configurations of columns. These values are converted into compression ratios (i.e. $1 - u_{col}/u_{footing}$) as defined in this thesis and plotted against column position in Figure 7.10; column position is defined as the normalised radial distance from the centre of the footing to the column (r/r_0), where r_0 is the radius of the footing. For clarity, only data for column lengths L/D = 1.0 is presented in Figure 7.9, as punching was not observed by Muir Wood *et al.* (2000) for longer columns.

Compression ratios from PLAXIS 3D Foundation are also presented in Figure 7.10. As with Black (2006), the laboratory tests described by Muir Wood *et al.* (2000) are conducted in a homogeneous soil sample and for consistency, the data from PLAXIS 3D Foundation is specific to soil profiles with and without a stiff crust. The column configurations from PLAXIS 3D Foundation correspond to groups of 4, 5 and 9 columns beneath a 3 m square footing, which correspond to A/A_C = 8.0, 6.4 and 3.5, respectively. In the interest of consistency, only compression ratios for 3 m long columns (i.e. L/B = 1.0) from PLAXIS 3D Foundation are presented in Figure 7.10. The position of columns for PLAXIS 3D Foundation is defined as the normalised radial distance of columns from the footing centre (r/r_0), where r_0 is the equivalent footing radius ($r_0 = B/\sqrt{\pi}$).

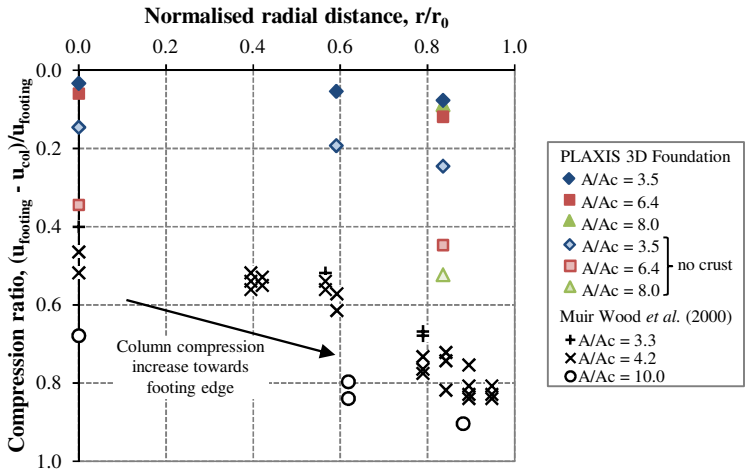

Figure 7.10 - Influence of column location upon compression ratios measured by Muir Wood *et al.* (2000) and determined PLAXIS 3D Foundation

It can be seen in Figure 7.10 that the findings from PLAXIS 3D Foundation are consistent with Muir Wood *et al.* (2000), as higher compression ratios are observed with increasing A/A_C and for columns positioned towards the footing edge.

While the absence of a stiff crust leads to an increase in compression ratios from PLAXIS 3D Foundation, it can be seen that Muir Wood *et al.* (2000) observed higher compression ratios for all A/A_C. This may be explained as follows:

- The angle of shearing resistance ($\varphi' \approx 30°$) for the sand columns in the laboratory tests is much lower than PLAXIS 3D Foundation ($\varphi' = 45°$). It was shown in Section 5.4.7 that decreasing φ from 50° to 40° had a significant influence on compression ratios, with an increase of compression ratios in the order of 0.05–0.15 observed for 3 m long columns.

- The deformed shape of columns was determined at ultimate conditions. As with Black (2006), loading was terminated at high strain levels which ensured the columns were in an advanced state of plasticity and hence yield high compression ratios.

Influence of footing width

Muir Wood *et al.* (2000) suggest that a critical length may exist for small groups of stone columns, but that the dominant strain in columns is dependent on the footing diameter (D), rather than the column diameter. The laboratory tests conducted by Muir Wood *et al.* (2000) were simulated with a plane strain FEA by Wehr (2004), who also found that the critical length is dependent on the footing diameter. Wehr (2004) observed a marked change in the deformational behaviour of columns at L/D = 1.5.

However, these findings are in contrast to McKelvey *et al.* (2004) and Black (2006) who suggest that a critical length may exist in the range L/d = 6–10, and is not dependent on the footing width. In light of these more recent findings, the data presented by Muir Wood *et al.* (2000) was re-examined in this thesis plotted in Figure 7.11.

Muir Wood *et al.* (2000) observed punching and bulging for different configurations of columns and these are plotted against L/D in Figure 7.11(i). The mode of deformation changes from punching to bulging in the range L/D = 1.0–1.5, which prompted the authors to postulate that the mode of deformation is controlled by the footing diameter. However, the observed modes of deformation are plotted against L/d in Figure 7.11(ii) and it is clear that, with the exception of two tests out of total of 14, that the mode of deformation changes from punching to bulging in the range L/d = 9.1–13.6. This is consistent with more recent findings.

The results from this thesis indicate the area ratio and column length, rather than the footing width, dictate the mode of deformation. It was established in Chapter 5 that different configurations of area ratio and column length yield either a punching-type (i.e. punching of 'block' failure) or a bulging mode of deformation. For example, it was shown in Figure 6.3(b-i) that a 2×2 group of 8 m long columns at $A/A_C = 3.5$ (i.e. B = 2 m; L/B = 4) exhibit a punching mode of deformation, while a 4×4 group of 8 m long columns at $A/A_C = 14.1$ (i.e. B = 8 m; L/B = 1) exhibit a bulging mode of deformation (Figure 6.5(b-iii)).

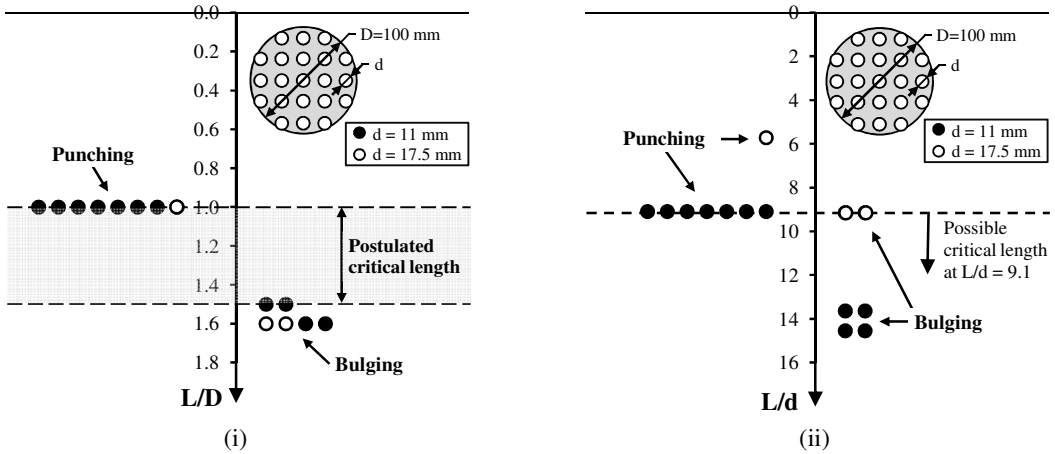

Figure 7.11 - Observations of punching and bulging for groups of columns, reported by Muir Wood *et al.* (2000), plotted against (i) L/D and (ii) L/d

7.4 Influence of deformational behaviour upon settlement performance

The settlement performance and deformational behaviour of small groups of stone columns were analysed separately in Sections 5.3 and 5.4, respectively. Compression and punching ratios were defined to help identify different modes of deformation for various configurations of columns, as summarised in Section 7.2.1. It was shown previously that an increase in column length leads to higher compression ratios, lower punching ratios (for L > 3 m) and higher settlement improvement factors (n). However, the variation of these parameters with column length depends on the mode of deformation. Essentially, the aim of this section is to form a link between the modes of deformation and the settlement performance of columns at typical working load levels.

Column punching (L ≤ 3 m and small groups of columns at A/A_C = 3.5)

Column punching typically occurs for short columns (L ≤ 3 m) and for small groups of closely-spaced columns. The occurrence of column punching is most evident for single columns at A/A_C = 3.5, as shown in Figure 7.12(a). It can be seen in Figure 7.12(a-i) that the influence of compression ratios upon n values is more significant for columns which are punching compared to columns at higher area ratios. Furthermore, it appears that the influence of compression ratios upon n values is most pronounced for short columns (i.e. L < 3 m), as the largest increase in n values with compression ratios is observed for this range of column lengths (compression ratios and n values are 0 and 1, respectively, for unreinforced footings, i.e. L = 0 m). Similarly, it can be seen in Figure 7.12(a-ii) that the influence of punching ratios upon n values is most pronounced for columns which are punching.

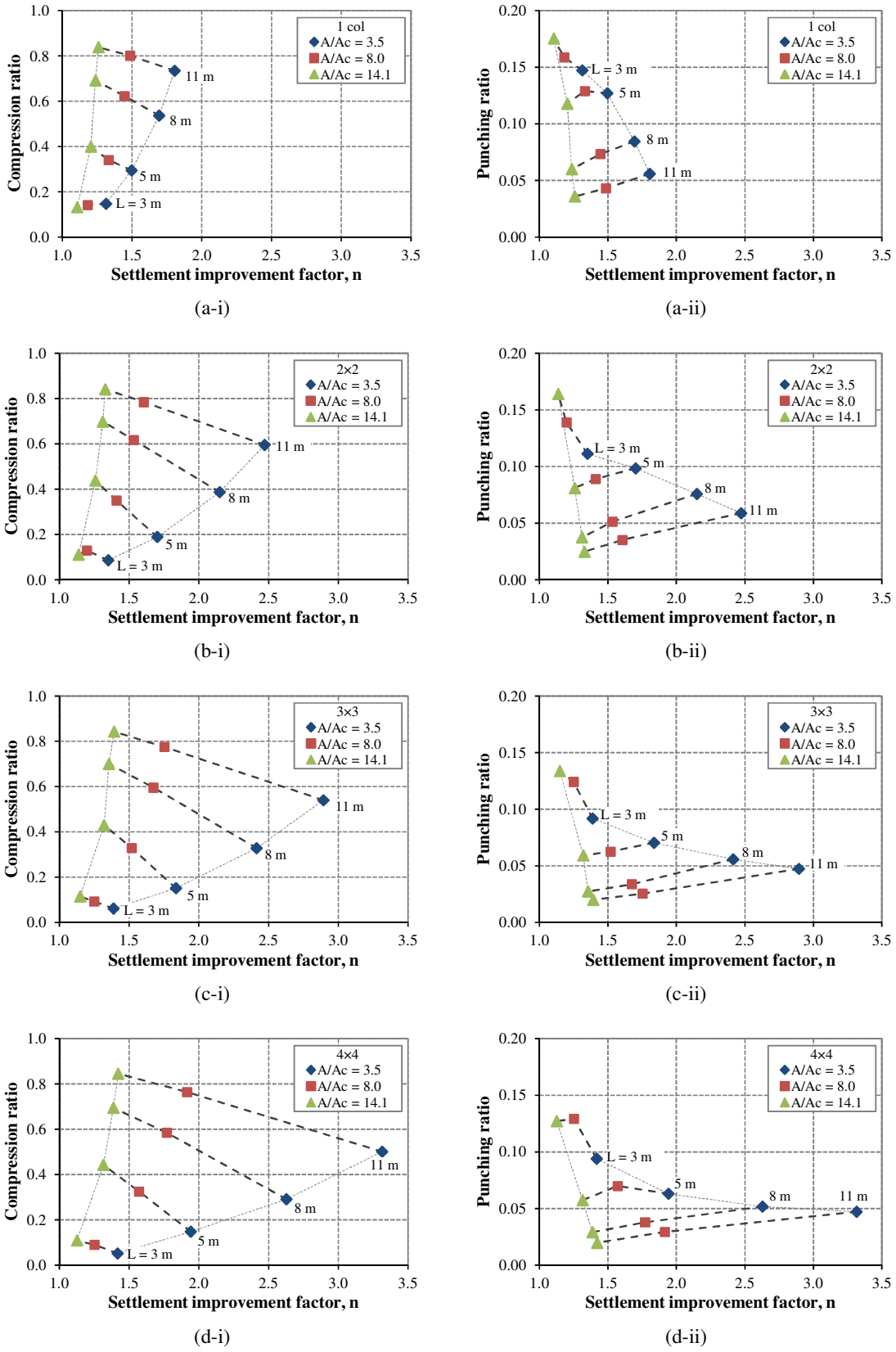

Figure 7.12 - Variation of (i) compression ratio and (ii) punching ratio with settlement improvement factor for (a) 1 column, (b) 2×2, (c) 3×3 and (d) 4×4 groups

'Block' failure (Large groups of columns at $A/A_C = 3.5$)

'Block' failure is similar to column punching and typically occurs for large groups of closely-spaced columns. The punching mode of deformation, evident in Figure 7.12(a) for single columns, transforms into 'block' failure as the number of columns increases. 'Block' failure is most clearly defined for a 4×4 group of columns at $A/A_C = 3.5$, as shown in Figure 7.12(d). It can be seen in Figures 7.12(a-i to d-i) that the line corresponding to $A/A_C = 3.5$ moves outwards and downwards, which indicates that an increase in n values and decrease in compression ratios occurs for larger groups of columns. This suggests that n values for columns exhibiting 'block' failure are more sensitive to changes in compression ratios. The influence of 'block' failure upon the variation of punching ratio with n values is shown in Figure 7.12(d-ii). It can be seen in Figures 7.12(a-ii to d-ii) that as the number of columns increase, punching ratios reduce significantly for short columns. However, punching ratios remain relatively unchanged with an increasing number of long columns. Therefore, it appears that n values for columns exhibiting 'block' failure are also very sensitive to punching ratios.

Column bulging ($L > 3$ m, $A/A_C = 8.0$ and 14.1)

Column bulging typically occurs for long widely-spaced columns and its influence upon the variation of compression ratios with n values can be seen in Figures (a-i to d-i). It appears that the increase in n values with column length for $A/A_C = 14.1$ is much lower than for punching or 'block' failure ($A/A_C = 3.5$). While the increase in n values with compression ratios becomes slightly more pronounced at closer spacings ($A/A_C = 8.0$) and for larger groups, it appears that n values are not strongly dependent upon compression ratios for the bulging mode of deformation. The variation of punching ratios with n values is shown in Figure 7.12(a-ii to d-ii). It can be seen that the variation of n values with punching ratios is similar for all configurations of columns at $A/A_C = 14.1$. Moreover, the near-vertical curve between punching ratios and n values suggests that n values are not strongly dependent upon punching ratios for the bulging mode of deformation.

Implications for design of stone columns

It was shown that the settlement performance of stone columns depends upon many factors such as the configuration of columns, material parameters and the soil profile. In order to achieve an optimum column arrangement, a trade-off exists between area ratio and column length, i.e. short closely-spaced columns or long widely-spaced columns. The relationship

between area ratio and column length is an inter-dependent one, as different configurations of columns result in different modes of deformation. Each mode of deformation has its own characteristics which makes its advantageous in different soil profiles.

It was shown in Figure 7.12 that the settlement performance of columns which exhibit punching, and especially 'block' failure, are most sensitive to changes in compression ratios. This is consistent with previous findings that the influence of column stiffness upon the settlement performance of small groups of columns is most pronounced for these modes of deformation. It was also observed that columns which exhibit punching and 'block' failure are most sensitive to changes in punching ratios. This reflects the load-transfer mechanism, as a large proportion of the applied load is transferred to the base of columns. Therefore these modes of deformation are not highly dependent upon the properties of the surrounding soil and are most efficient is soil profiles with weak upper layers.

In contrast, it can be seen that influence of compression and punching ratios upon n values diminishes for the bulging mode of deformation. Column bulging is highly dependent upon the lateral support provided by the surrounding soil and generally occurs near the ground surface, where overburden stresses are lowest. The bulging mode of deformation makes efficient use of the high stiffness properties of the stiff crust. Columns are confined in the upper layers which tends to push bulging deeper and hence increase the load-carrying capacity of columns.

7.5 Stress concentration ratio

7.5.1 Stress concentration ratios for infinite grids of stone columns

Comparison of stress concentration ratios with laboratory and field data

Stress concentration ratios (at the surface) from PLAXIS 3D Foundation are compared with laboratory and field measurements in Figure 7.13. The data presented by Aboshi *et al.* (1979) and Greenwood (1991) is from field measurements which pertain to large diameter sand columns and stone columns in soft clay, respectively. A large range of stress concentration ratios was observed by Aboshi *et al.* (1979), however, Barksdale & Bachus (1983) suggest that stress concentration ratios typically lie in the range of 2.5–5.0. In addition to the field data presented in Figure 7.13, stress concentration ratios from laboratory tests conducted by

Charles & Watts (1983) are also shown. It can be seen in Figure 7.13 that stress concentration ratios predicted by PLAXIS 3D Foundation agree quite well with field and laboratory data.

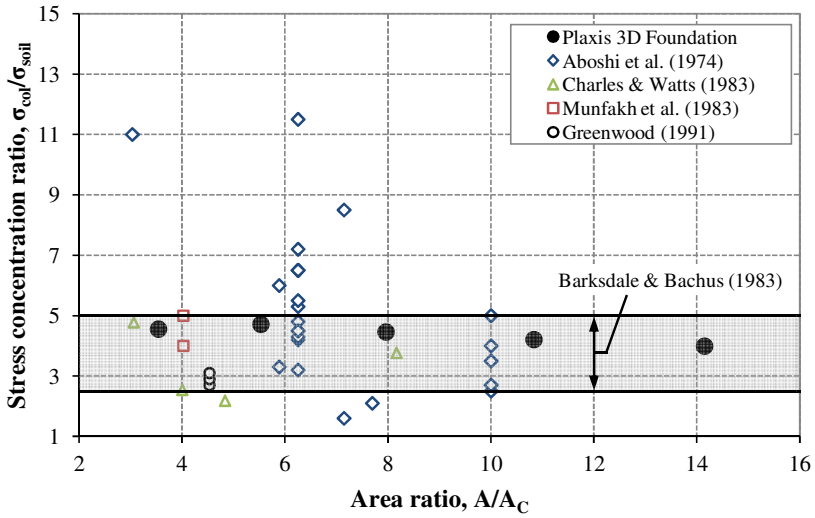

Figure 7.13 - Comparison of stress concentration ratios for an infinite grid of end-bearing columns with field data

Comparison of stress concentration ratios with analytical design methods

Stress concentration ratios determined from PLAXIS 3D Foundation at the surface are compared with analytical design methods in Figure 7.14. The data from the numerical analyses are specific to infinite grids of end-bearing columns and are therefore consistent with the assumptions of the analytical design methods.

It can be seen in Figure 7.14 that the Balaam & Booker (1981) method greatly over-estimates stress concentration ratios. This is most significant at high area ratios and is due to the assumption of elastic behaviour for the columns (Castro & Sagaseta, 2009). In contrast, PLAXIS 3D Foundation and the other analytical design methods account for plastic deformations which develop in columns and therefore predict lower, more realistic stress concentration ratios.

It can also be seen in Figure 7.14 that Priebe (1995) generally predicts lower stress concentration ratios than Pulko & Majes (2005), especially at low area ratios. This is due to the different assumptions inherent in each design method. Priebe (1995) assumes columns are in an active state throughout loading, while Pulko & Majes (2005) account for the elastic behaviour of columns at low load levels. Stress concentration ratios are much higher for columns in an elastic state and consequently Pulko & Majes (2005) predict higher stress

concentration ratios than Priebe (1995). This is most pronounced at low area ratios as columns are better confined and hence carry a larger proportion of the applied load when in an elastic state.

Perhaps the most important finding from Figure 7.14 is that both Priebe (1995) and Pulko & Majes (2005) predict higher surface stress concentrations ratios than PLAXIS 3D Foundation. This is quite interesting given that both of these design methods predict similar settlement improvement factors to PLAXIS 3D Foundation (see Section 4.6.4). Considering the equation of equilibrium developed by Aboshi *et al.* (1979) in equation (2.27), it seems intuitive that higher stress concentration ratios at the surface would yield higher settlement improvement factors. However, this is not the case and it appears that the distribution of stress concentration ratios with depth, rather than at the surface, may have more of an influence upon the settlement performance of stone columns and thus merits further investigation.

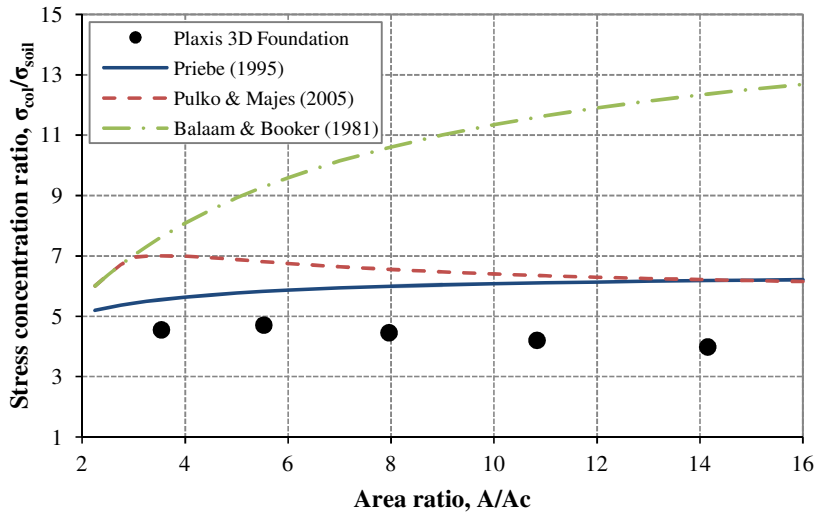

Figure 7.14 - Comparison of stress concentration ratios at the surface for an infinite grid of end-bearing columns with analytical design methods

Variation of stress concentration ratio with depth

The variation of stress concentration ratios with depth from PLAXIS 3D Foundation is compared with Priebe (1995) and Pulko & Majes (2005) in Figures 7.15(i) and 7.15(ii), respectively. The distribution of stress concentration ratios with depth from PLAXIS 3D Foundation for an infinite grid of end-bearing columns was presented and discussed previously in Section 6.3.1. The extent of plasticity within closely-spaced columns is quite low and as a result, stress concentration ratios follow a similar variation with depth to modular ratios. The maximum stress concentration ratio occurs at z = 1.9 m, which

corresponds to the top of the lower Carse clay layer (i.e. the weakest part of the soil profile). Stress concentration ratios are lower in the overlying soil, even though these soil layers are in an elastic state. This may be explained as an infinite grid of columns do not develop shear stress along their sides and hence the maximum vertical load which columns can carry at the surface is limited by the vertical stress where bulging occurs. The extent of plasticity within columns at higher area ratios (i.e. A/A_C = 8.0 and 14.1) is more significant and despite the large scatter, a constant distribution of stress concentration ratios with depth is observed in Figure 7.15 for yielded sections of columns. It can also be seen that stress concentration ratios reduce with depth in the lower sections of columns which are in an elastic state.

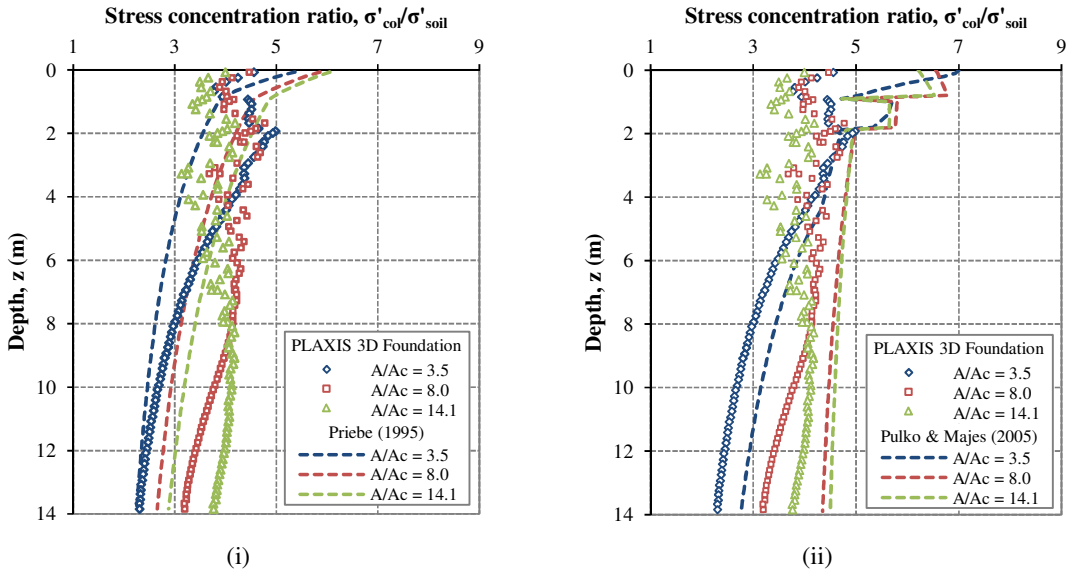

(i) (ii)

Figure 7.15 - Comparison of stress concentration ratios with depth from PLAXIS 3D Foundation with (i) Priebe (1995) and (ii) Pulko & Majes (2005) for an infinite grid of end-bearing columns

Comparison with Priebe (1995)

It can be seen in Figure 7.15(i) that Priebe (1995) predicts higher stress concentration ratios than PLAXIS 3D Foundation at the surface. This may be explained as Priebe (1995) assumes that columns are in an active state throughout loading, in comparison to PLAXIS 3D Foundation where sections of columns within the crust are in an elastic state. As mentioned earlier, stress concentration ratios at the surface of an infinite grid of columns are limited by the vertical stress at the location of column bulging and are therefore lower than Priebe (1995). This highlights the advantage of the FEM which is capable of capturing all the factors influencing the behaviour of columns, rather than treating each layer individually.

It can be seen in Figure 7.15(i) that Priebe (1995) predicts lower stress concentration ratios than PLAXIS 3D Foundation within yielded sections of columns. This is most pronounced for closely-spaced columns ($A/A_C = 3.5$) at z = 1.9 m and may be explained as Priebe (1995) fails to account for stress concentration ratios developed when columns are in an elastic state (i.e. at low load levels). However, stress concentration ratios for closely-spaced columns reduce at a faster rate with depth for PLAXIS 3D Foundation, as the lower sections of columns are in an elastic state. It can also be seen in Figure 7.15(i) that stress concentration ratios at higher area ratios (i.e. $A/_C = 8.0$ and 14.1) are relatively constant with depth in yielded sections of columns compared to Priebe (1995). This is again attributed to the assumption by Priebe (1995) that columns are in an active state throughout loading.

It is interesting to note that Priebe (1995) generally under-predicts stress concentration ratios but still yields similar settlement improvement factors to PLAXIS 3D Foundation. This may explained as stress concentration ratios determined from Priebe (1995) do not contain the modification factor for overburden stress, which is taken into account when determining settlement improvement factors (n_2).

Comparison with Pulko & Majes (2005)

As with Priebe (1995), it can be seen in Figure 7.15(ii) that Pulko & Majes (2005) predict higher stress concentration ratios in sections of columns located within the crust compared to PLAXIS 3D Foundation. This is again explained as the vertical stress at the surface of an infinite grid of columns in PLAXIS 3D Foundation is dependent upon the vertical stress at the location of column bulging. In contrast, Pulko & Majes (2005) treat each layer individually and columns are in an plastic state in the crust.

It can be seen in Figure 7.15(ii) that Pulko & Majes (2005) predict higher stress concentration ratios than Priebe (1995) and capture the variation of stress concentration ratios with depth much closer to PLAXIS 3D Foundation. This highlights the importance of considering the loading history and accounting for stress concentration ratios developed when columns are in an elastic state.

It also appears that Pulko & Majes (2005) slightly over-estimate stress concentration ratios compared to PLAXIS 3D Foundation and this may be due to the high modular ratios adopted for the analytical design methods. The soil profile adopted for the analytical design methods consists of three layers, each defined by a single Young's modulus. In contrast, PLAXIS 3D

Foundation accounts for the stress dependency of soil stiffness and captures the increase of soil stiffness with depth. The modular ratios adopted for each layer in Pulko & Majes (2005) are higher than PLAXIS 3D Foundation which increases the magnitude of stress concentration ratios and also extent of plasticity within columns.

The influence of higher stress concentration ratios upon the settlement performance of stone columns is evident in Figure 4.16, as Pulko & Majes (2005) predict higher settlement improvement factors than PLAXIS 3D Foundation at low area ratios ($A/A_C = 3.5$). This may be explained as the majority of columns are in an elastic state at low area ratios and are therefore more susceptible to differences in modular ratios. However, influence of the higher stress concentration ratios is negligible at higher area ratios, as Pulko & Majes (2005) predict similar settlement improvement factors to PLAXIS 3D Foundation (Figure 4.16). The extent of plasticity within columns is more pronounced at higher area ratio and hence the influence of modular ratios upon the settlement performance of columns reduces.

The distribution of stress concentration ratios with depth clearly indicates when columns are in an elastic and plastic stress state. This is quite useful for stability analyses where a rotational failure surface may intersect columns at different depths. However, it difficult to form a direct relationship between stress concentration ratio and settlement improvement factors for the following reasons:

(i) Settlement improvement factors are based on the increment of vertical stress ($\Delta\sigma_{col}$ and $\Delta\sigma_{soil}$) with depth rather than the total vertical stress($\sigma_{col}/\sigma_{soil}$), which is used to define stress concentration ratios, i.e. $\sigma_{col}/\sigma_{soil} == (\Delta\sigma_{col} + \gamma'_{col}.z)/(\Delta\sigma_{soil} + \gamma'_{soil}.z)$. Furthermore, the increment of vertical stress reduces with depth beneath small loaded area.

(ii) The distribution of stress concentration ratios only shows the stress state at the end of loading and does not capture the proportion of the load applied to columns in an elastic and plastic state. The majority of footing settlement is comprised from plastic strain and it is necessary to predict the yield load.

Therefore it is difficult to apply a simple equation, such as that developed by Aboshi *et al.* (1979) in equation (2.27), to estimate the settlement performance a small groups of stone columns from the distribution of stress concentration ratios with depth.

Chapter 8
Conclusions

8.1 Introduction

A series of three-dimensional FEA were undertaken to examine the influence of key design parameters upon the settlement performance and deformational behaviour of small groups of stone columns. PLAXIS 3D Foundation is adopted for this research in conjunction with the advanced elastic-plastic Hardening Soil model. A set of material parameters and soil profile were developed for the well characterised Bothkennar test site, which formed the basis of this research. The key design parameters investigated were area ratio, column length, confinement, stiffness, strength, installation effects and the presence of a stiff crust. The main conclusions are summarised in this chapter.

8.1.1 Numerical modelling preliminaries

In advance of performing the primary analyses of this thesis, it was necessary to arrive at a reliable methodology to capture the behaviour of small groups of stone columns in soft clay. The main findings from the preliminary analysis are as follows:

- The long term settlement performance of small groups of stone columns at typical working loads can be accurately modelled using drained analyses in PLAXIS 3D Foundation, as these were shown to give a similar output to more time-consuming coupled analyses (i.e. undrained loading followed by a consolidation analysis).
- Simulating column installation effects by applying large strain cavity expansions cannot be accurately implemented in a FE program which is implicitly based on small strain theory. However, an alternative approach to simulate column installation effects is to increase the coefficient of lateral earth pressure (K_0) in the surrounding soil.
- The analytical design method developed by Balaam & Booker (1981) grossly over-estimates settlement improvement factors, due to the assumption of linear elasticity for stone. It was shown that Priebe's (1995) (n_2) modified design curve (when accounting for an increased K_0 in the surrounding soil, which is not a standard adjustment) agrees quite well with PLAXIS 3D Foundation. Pulko & Majes (2005) is a more rigorous theoretical

solution than Priebe (1995), and was shown to predict a similar settlement response to PLAXIS 3D Foundation.

8.1.2 Settlement performance

The settlement performance of small groups of stone columns in the Bothkennar soil profile was determined at 50 kPa, a typical working stress for columns in soft soil. It was found that an increase in the area ratio, column length and the number of columns all have a positive influence on the settlement performance of small groups of stone columns. Moreover, the influence of column length and area ratio are somewhat coupled, as the effect of column length becomes more pronounced at low area ratios. A continuous increase in settlement improvement factors is observed with increasing column length at low area ratios, while the increase in settlement improvement factors tails off with increasing column length at high area ratios.

Influence of key design parameters and practical considerations

- For a given number of columns, their proximity to the footing edge has a relatively minor influence on the settlement performance of stone columns.
- Increasing the column stiffness and strength enhances the settlement performance of stone columns. The influence of these parameters is linked to the mode of deformation, as increasing the column stiffness and strength is most significant at low and high area ratios, respectively. This is discussed in more detail in the following section.
- Accounting for column installation effects by increasing the coefficient of lateral earth pressure (K_0) in the surrounding soil improves the settlement performance of stone columns. The influence of K_0 is most noticeable at high area ratios.
- The presence of the stiff crust also had a significant influence on the settlement performance of stone columns and this is discussed in the following section.

8.1.3 Mode of deformation

The modes of deformation for various configurations of columns were identified with the aid of new parameters, referred to as punching and compression ratios. Three distinct modes of deformation were observed: (i) punching, (ii) 'block' failure and (iii) bulging. The occurrence of each mode of deformation was verified by analysing the distribution of shear strains within

columns and the surrounding soil. The main characteristics of each mode of deformation are outlined below:

(i) Punching:

- Characterised by high punching and low compression ratios.
- Typically occurs for short columns at all area ratios and small groups of columns at low area ratios.
- High shear strains develop along the sides and beneath the base of columns which exhibit punching.

(ii) 'Block' failure:

- Characterised by low punching and high compression ratios.
- Most prominent in large groups of columns at low area ratios.
- Columns act as a single entity and punch uniformly into the underlying soil, thus resulting in low punching ratios. 'Block' failure is an extension of the punching mode of deformation, as both modes of deformation develop similar load transfer mechanisms.
- High shear strains develop along the external sides of outer columns and beneath the base of columns. No shear strains develop in the central zone of soil bounded by columns, which confirms that columns punch as a 'block' with the surrounding soil.

(iii) Bulging:

- Characterised by low punching and high compression ratios.
- Prevalent in long columns at high area ratios.
- This mode of deformation is highly dependent upon the lateral support provided by the surrounding soil and as such, bulging generally occurs near the ground surface where overburden stresses are lowest.
- High shear strains develop within columns near the top of the lower Carse clay layer, i.e. the weakest part of the soil profile.

In addition to the three modes of deformation, the development of shear planes which extend from the corners of pad footings to the point of column bulging beneath the centre of footings were also observed. It should be noted that the shear planes are a secondary mode of deformation; however they may become more prominent at higher load levels, as observed by Muir Wood *et al.* (2000).

The deformational behaviour of small groups of stone columns is governed by the area ratio and column length. While the number of columns enhances the settlement performance of

stone columns for a given area ratio, it does not fundamentally change the mode of deformation. This is an important findings which was used in the development of a simplified design method.

Influence of column length

The three modes of deformation postulated from compression and punching ratios are a simplified description of the general deformational behaviour. A more in-depth analysis of the variation of punching and compression ratios with column length reveals that some combination of punching and bulging occurs simultaneously, with one particular mode of deformation more influential for a given area ratio and column length. For example, long columns at high area ratios exhibit some degree of punching, even though bulging is established as the general mode of deformation.

The increase in settlement improvement factors with column length is most pronounced for columns at low area ratios, for which punching is the dominant mode of deformation. Shear stress develops along the sides of columns and increasing the column length directly improves the settlement performance of stone columns. A certain degree of punching is evident for all the configurations of columns analysed, which is consistent with the finding that settlement improvement factors increase with column length for all configurations of columns. Therefore, the existence of a unique critical column length, proposed from previous laboratory studies, is not supported by this numerical modelling.

Influence of stiff crust

The presence of a stiff crust, a real feature of the stratigraphy in soft soil sites that has not been recreated in previous laboratory studies, has a significant influence on the deformational behaviour of small groups of columns. The stiff crust tends to confine columns in the upper layers and forces bulging to occur in deeper layers, which enhances the columns' load-carrying capacity.

The presence of the stiff crust also contributes towards a combination of punching and bulging modes of deformation. Previous research from laboratory tests observed well-defined crossovers between punching and bulging modes of deformation at column lengths in the range L/d = 6–10. However, this has been shown to be in part due to the absence of the stiff crust in the laboratory tests (i.e. homogeneous soil samples). Columns in a homogeneous soil

sample are more susceptible to bulging near the ground surface, which reduces the ability of columns to transfer the applied load to the base of columns and hence reduces punching potential.

Influence of key design parameters and practical considerations

- The position of column relative to the footing edge has a relatively minor influence upon the deformational behaviour of small groups of columns.
- The influence of column stiffness and strength upon the settlement performance of small groups of stone columns is linked to the mode of deformation. Increasing the column stiffness is most significant at low area ratios, as columns are in more of an elastic state and thus are more susceptible to changes in elastic stiffness moduli. Conversely, increasing the column strength is most significant at high area ratios, as the extent of plasticity within columns is most pronounced.
- Increasing K_0 in the surrounding soil enhances the settlement performance of stone columns. This is most noticeable at high area ratios as columns which exhibit a bulging mode of deformation are highly dependent upon the lateral support provided by the surrounding soil. While increasing K_0 in the surrounding soil enhances the settlement performance of stone columns, it does not change their deformational behaviour.

8.1.4 Stress concentration ratios

The ratio of the vertical effective stress in columns to that in the soil is referred to as the stress concentration ratio. This parameter is generally measured at the ground surface and is quantified using two methods in this thesis:

(i) the first method compares the average vertical effective stress in columns (σ'_{col}) to the average vertical stress in the entire soil area beneath the footing ($\sigma'_{soil,\ average}$).

(ii) the second method compares the average vertical effective stress in columns (σ'_{col}) to the average vertical stress in the soil within a square zone of influence surrounding each column (σ'_{soil}); the width of the zone of influence is equal to the column spacing.

Stress concentration ratios at the ground surface

Stress concentration ratios do not vary with the mode of deformation for an infinite grid of columns. This is due to the symmetry which ensures that all columns deform identically.

Stress concentration ratios from PLAXIS 3D Foundation are in the typical range (2.5–5.0) proposed by Barksdale & Bachus (1983).

In contrast to an infinite grid of columns, stress concentration ratios for small groups of stone columns are dependent on the mode of deformation. An increase in stress concentration ratios is observed with increasing column length for columns which are punching. However, no increase in stress concentration ratios is observed with increasing column length for bulging.

Influence of key design parameters and practical considerations:

- Stress concentration ratios at the surface vary with the position of columns relative to the footing edge. Stress concentration ratios measured using method (i) are highest in corner columns, followed by edge and centre columns. This is attributed to the elevated stress levels which develop beneath the edge of rigid footings. However, stress concentration ratios measured using method (ii) are highest in centre columns, followed by edge and corner columns. This highlights the positive confining effects provided to centre columns.
- Increasing the column stiffness and strength leads to higher stress concentration ratios. This is most significant for columns exhibiting a bulging mode of deformation, as columns which are punching transfer the applied load along the column-soil interface.
- Increasing K_0 in the surrounding soil has a minor influence on stress concentration ratios. This is consistent with the previous findings that K_0 does not affect the deformational behaviour of columns.

Stress concentration ratios with depth

It is interesting to note that the position of columns relative to edge of the footing has a significant influence on stress concentration ratios, but only a minor influence on the settlement performance of stone columns. The variation of stress concentration ratios with depth was also examined and it was found that stress concentration ratios are dependent upon the deformational behaviour of columns. Stress concentration ratios are relatively constant with depth in yielded sections of columns and decrease with depth in concert with modular ratios in elastic sections of columns.

8.1.5 Simplified design method

The behaviour of small groups of stone columns is quite complex as columns are subject to a loss of lateral confinement along the outer edge and also a reduction in vertical stress with depth beneath small loaded areas. The influence of the number of columns upon the settlement performance of small groups of stone columns was quantified using a settlement ratio (s/s_{uc}), which is defined as the ratio of the settlement of a small group to that of an infinite grid of columns.

Settlement ratios for end-bearing columns increase with area ratio and were found to agree favourably with Priebe's (1995) s/s_{uc} values at low area ratios. Previous research is only focussed on end-bearing columns at low area ratios. However, this thesis examines the influence of both area ratio and floating columns (i.e. partial-depth treatment) upon s/s_{uc} for the first time.

It was observed that area ratio only influences s/s_{uc} values for end-bearing stone columns. Moreover, for a given normalised column length (L/H), a near-linear relationship exists between s/s_{uc} and the normalised footing width (B/L). Therefore, it appears that the footing width, and hence the stress distribution in the underlying soil, governs s/s_{uc} values. A simplified design method was developed which allows the settlement of a small groups of columns to be quickly estimated from B/L, L/H and s_{uc}. It is recommended that Pulko & Majes (2005) be used as an estimate of s_{uc}.

8.2 Recommendations for future research

This research has focussed on the influence of key design parameters upon the settlement performance and deformational behaviour of small groups of stone columns in soft soils. A series of three-dimensional FEA were undertaken in conjunction with the advanced elasto-plastic Hardening Soil model. A set of material parameters were developed for the well characterised Bothkennar test site, which consists of a soft uniform clay overlain by a stiff crust. The findings from the deformational behaviour of small groups of stone columns allowed a simplified method to be developed which relates the settlement of small groups and infinite grids of columns. However, this simplified method needs to be validated against field load tests on various configurations of columns. This would require measurements of

settlement at various depths, using extensometers, for unreinforced and reinforced footings. There is also further potential to extend the design method to other soil profiles:

- It was shown that the modular ratio and stress state in the surrounding soil both play an important role in the settlement performance of stone columns. It would be valuable to examine their influence upon settlement ratios for floating stone columns.
- Although the range of B/L and L/H investigated in this thesis covers a practicable range, investigating the settlement performance of small groups of stone columns in a soil profile of varying thickness would allow an even greater range of B/L and L/H to be examined.

This thesis has focussed on the long term settlement performance of small groups of columns. In addition to improving the settlement performance, stone columns also act as vertical drains and enhance the drainage capacity of soils. It is well established that the soil carries a large proportion of the vertical stress at the start of loading due to the high undrained stiffness. However, vertical stress is transferred from the soil to the stone columns as consolidation proceeds. The dissipation of excess pore pressure for small groups of stone columns has not been investigated to date and it would also be useful to examine how the position of columns relative to the footing edge affects the stress transfer during consolidation.

The installation effects associated with vibro stone columns have been touched on in this thesis. Installing stone columns imposes a complex stress regime on the surrounding soil; the displacing effects of the poker increase the soil stiffness, while the horizontal vibrations from the poker can lead to remoulding and consequently a loss of soil strength. More field measurements are essential to examine the influence of different soil types and column configurations upon column installation effects.

References

Aboshi, H., Ichimoto, I., Enoki, M. and Harada, K. (1979). The compozer - a method to improve characteristics of soft clays by inclusion of large diameter sand columns. *Proc. Int. Conf. on Soil Reinforcement: Reinforced Earth and Other Techniques*, Paris, Vol. 1, 211–216

Allman, M. A. and Atkinson, J. H. (1992). Mechanical properties of reconstituted Bothkennar soil. *Géotechnique*, Vol. 42, No. 2, 289–301

Ambily, A. P. and Gandhi, S. R. (2007). Behaviour of stone columns based on experimental and FEM analysis. *Journal of Geotechnical and Geoenvironmental Engineering*, Vol. 133, No. 4, 405–415

Andreou, P. and Papadopoulos, V. (2006). Modelling stone columns in soft clay. *Proc. 6th European Conf. on Numerical Methods in Geotechnical Engineering*, Graz, 777–780

Atkinson, J. H. and Sallfors, G. (1991). Experimental determination of soil properties. *Proc. 10th European Conf. on Soil Mechanics and Foundation Engineering*, Florence, Vol. 3, 915–956

Barksdale, R. D. and Bachus, R. C. (1983) Design and construction of stone columns, Report no. FHWA/RD-83/026, *National Information Service*, Springfield, Virginia, USA

Balaam, N. P. and Booker, J. R. (1981). Analysis of rigid rafts supported by granular piles. *Int. Journal for Numerical and Analytical Methods in Geomechanics*, Vol. 5, 379–403

Balaam, N. P. and Booker, J. R. (1985). Effect of stone column yield on settlement of rigid foundations in stabilised clay. *Int. Journal for Numerical and Analytical Methods in Geomechanics*, Vol. 9, 331–351

Balaam, N. P., Poulos, H. G. and Brown, P. T. (1977). Settlement analysis of soft clays reinforced with granular piles. *Proc. 5th Southeast Asian Conf. on Soil Engineering*, Bangkok, Vol. 1, 81–91

Baligh, M. M. (1985). Strain path method. *Journal of the Geotechnical Engineering Division*, ASCE, Vol. 111, No. 9, 1108–1136

Biarez, J., Gambin, M., Gomes-Corriea, A., Falvigny, E. and Branque, D. (1998). Using pressuremeter to obtain parameters of elastoplastic models for sands. *Proc. 1st Int. Conf. on Site Characterization*, Atlanta, Georgia, USA, 747–752

Biot, M. A. (1941). General theory of three-dimensional consolidation. *Journal of Applied Sciences*, Vol. 12, 155–164

Black, J. A. (2006). The settlement performance of a footing supported on soft clay reinforced with vibrated stone columns. *PhD thesis, Queen's University of Belfast*

Bolton, M. D. (1986). The strength and dilatancy of sands. Géotechnique, Vol. 36, No. 1, 65–78.

Boussinesq, J. (1885). *Applications des Potentiels à L'étude de L'équilibre et du Mouvement des Solides Élastiques*, Gauthier-Villars, Paris

Brauns, J. (1978). Die anfangstraglast von schottersäulen im bindigen untergrund. *Die Bautechnik*, 263–270

Brinkgreve, R. B. J and Broere, W. (2006). PLAXIS 3D Foundation Manual Version 2. *PLAXIS BV*

Castro, J. and Sagaseta, C. (2009). Consolidation around stone columns. Influence of column deformation. *Int. Journal for Numerical and Analytical Methods in Geomechanics*, Vol. 33, Issue 7, 851–877

Castro, J. (2007). Pore pressures during stone column installation. *Proc. 18th European Young Geotechnical Engineers' Conference*, Ancona

Charles, J. A. and Watts, K. S. (1983). Compressibility of soft clay reinforced with granular columns. *Proc. 8th European Conf. on Soil Mechanics and Foundation Engineering*, Helsinki, Vol. 1, 347–352

Cunze, G. (1985). Ein beitrag zur abschätzung des porenwasserüberdruckes beim rammen von verdrängungspfählen in bindigen böden. *Dissertation University of Hannover*

Debats, J. M., Guetif, Z. and Bouassida, M. (2003). Soft soil improvement due to vibro-compacted columns installation. *Proc. Int. Workshop on Geotechnics of Soft Soils - Theory and Practice*, Noordwijkerhout, Netherlands, 551–556

Domingues, T. S., Borges, J. L. and Cardoso, A. S. (2007a). Parametric study of stone columns in embankments on soft soils by finite element method. *Applications of Computational Mechanics in Geotechnical Engineering V: Proc. 5th Int. Workshop*, Guimaraes, 281–291

Domingues, T. S., Borges, J. L. and Cardoso, A. S. (2007b). Stone columns in embankments on soft soils. Analysis of the effect of the gravel deformability. *14th European Conf. on Soil Mechanics and Geotechnical Engineering*, Madrid, Vol. 3, 1445–1450

Duncan, J. M. and Chang, C. Y. (1970). Nonlinear analysis of stress and strain in soil. *ASCE Journal of the Soil Mechanics and Foundation Division*, Vol. 96, No. 5, 1629–1653

Egan, D., Scott, W. and McCabe, B. A. (2008). Installation effects of vibro replacement stone columns in soft clay. *Proc. 2nd Int. Workshop on the Geotechnics of Soft Soils*, Glasgow, 23–30

Elshazly, H. A., Hafez, D. and Mosaad, M. (2006). Back calculating vibro-installation stresses in stone columns reinforced ground. *Proc. of the ICE - Ground Improvement*, Vol. 26, Issue 2, 47–53

Elshazly, H. A., Hafez, D. H. and Mossaad, M. E. (2008a). Reliability of conventional settlement evaluation for circular foundations on stone columns. *Journal of Geotechnical and Geological Engineering*, Vol. 26, No. 3, 323–334

Elshazly, H., Elkasabgy, M. and Elleboudy, A. (2008b). Effect of inter-column spacing on soil stresses due to vibro-installed stone columns: Interesting findings. *Journal of Geotechnical and Geological Engineering*, Vol. 26, No. 2, 225–236

Gäb, M., Schweiger, H. F., Thurner, R. and Adam, D. (2007). Field trial to investigate the performance of floating stone columns. *Proc. 14th European Conf. on Soil Mechanics and Geotechnical Engineering*, Madrid, 1311–1316

Gäb, M., Schweiger, H. F., Kamrat-Pietraszewska, D. and Karstunen, M. (2008). Numerical analysis of a floating stone column foundation using different constitutive models. *Proc. 2nd Int. Workshop on Geotechnics of Soft Soils*, Glasgow, 137–142

Institution of Civil Engineers. (1992). Bothkennar soft clay test site: characterization and lessons learned. *Géotechnique*, Vol. 42, No. 2, 161–378.

Gibson, R. E. and Anderson, W. F. (1961). In-situ measurements of soil properties with the pressuremeter. *Civil Engineering and Public Works Review*, Vol. 56, No. 658, 615–618

Gill, D.R. and Lehane, B.M. (2001). An optical technique for investigating soil displacement patterns. *Geotechnical Testing Journal*, Vol. 24, 324–329

Goughnour, R. R. and Bayuk, A. A. (1979). Analysis of stone column-soil matrix interaction under vertical load. *Proc. Int. Conf. on Soil Mechanics Reinforcement*, Paris, 271–277

Greenwood, D. A. (1970). Mechanical improvement of soils below ground surface. *Geotechnical Engineering*, Proc. of Institution of Civil Engineers, London, 9–20

Greenwood, D. A. (1991). Load tests on stone columns. In *Deep Foundation Improvements: Design, Construction and Testing*, Esrig M. I. and Bachus R. C. (eds.), American Society for Testing and Materials, Philadelphia, ASTM STP 1089, 141–171

Guetif, Z., Bouassida, M. and Debats, J.M. (2007). Improved soft clay characteristics due to stone column installation. *Computers and Geotechnics*, Vol. 34, Issue 2, 104–111

Han, J. and Ye, S. L. (2001). Simplified method for consolidation rate of stone column reinforced foundations. *Journal of Geotechnical and Geoenvironmental Engineering*, ASCE, Vol. 127, No. 7, 597–603

Hight, D. W., Bond, A. J., and Legge, J. D. (1992). Characterization of the Bothkennar clay: an overview. *Géotechnique*, Vol. 42, No. 2, 303–347

Hu, W. (1995). Physical modelling of group behaviour of stone column foundations. *PhD thesis, University of Glasgow*

Hughes, J. M. and Withers, N. J. (1974). Reinforcing of soft cohesive soils with stone columns. *Ground Engineering*, Vol. 7, No. 3, 42–49

Jaky, J. (1944). The coefficient of earth pressure at rest. *Journal of the Union of Hungarian Engineers and Architects*, 355–358 (in Hungarian).

Janbu, J. (1963). Soil compressibility as determined by oedometer and triaxial tests. *Proc. European Conf. on Soil Mechanics and Foundation Engineering*, Wiesbaden, Vol. 1, 19–25

Jardine, R. J., Lehane, B. M., Smith, P. R. and Gildea, P. A. (1995). Vertical loading experiments on rigid pad foundations at Bothkennar. *Géotechnique*, Vol. 45, No. 4, 573–597

Kirsch, F. and Sondermann, W. (2003) Field measurements and numerical analysis of the stress distribution below stone column supported embankments and their stability. *Int. Workshop on Geotechnics of Soft Soils - Theory and Practice*, Noordwijkerhout, Netherlands, 595–600

Kirsch, F. (2006). Vibro stone column installation and its effect on the ground improvement. *Int. Conf. on Numerical Simulation of Construction Processes in Geotechnical Engineering for Urban Environment*, Bochum, 115–124

Kirsch, F. (2008). Evaluation of ground improvement by groups of vibro stone columns using field measurements and numerical analysis. *Proc. of the 2nd Int. Workshop on the Geotechnics of Soft Soils*, Glasgow, 241–248

Lambe, T. W. and Whitman, R. V. (1979). Soil mechanics (SI Version). *John Wiley and Sons, Inc.*

Leroueil, S., Lerat, P., Hight, D. W. and Powell, J. J. M. (1992). Hydraulic conductivity of a recent estuarine silty clay at Bothkennar. *Géotechnique*, Vol. 42, No. 2, 275–288

Mar, A. (2002). How to undertake finite element based geotechnical analysis. *NAFEMS Publication*

McCabe, B. A. (2002). Experimental investigations of driven pile group behaviour in Belfast Soft Clay. *PhD Thesis, Department of Civil Engineering, University of Dublin, Trinity College*

McCabe, B. A., McNeill, J. A. and Black, J. A. (2007). Ground improvement using the vibro-stone column technique. *Transactions of the Institution of Engineers of Ireland*, Galway

McCabe, B. A., Killeen, M. M. and Egan, D. (2008). Challenges faced in 3-d finite element modeling of stone column construction. *Proc. Joint Symposium on Concrete Research and Bridge and Infrastructure Research in Ireland*, NUI Galway, 393–400

McCabe, B. A., Nimmons, G. J. and Egan, D. (2009). A review of field performance of stone columns in soft soils. *Proc. Institution of Civil Engineers - Geotechnical Engineering*, Vol. 162, No. 6, 323–334

McKelvey, D., V. Sivakumar, Bell, A.L. and Graham, J. (2004). Modelling vibrated stone columns in soft clay. *Proc. Institution of Civil Engineers - Geotechnical Engineering*, Vol. 157, No. 3, 137–149

Mitchell, J.K. and Huber, T. R. (1985). Performance of a stone column foundation. *Journal Geotechnical Engineering*, ASCE, Vol. 11, No. 2, 205–223

Muir Wood, D., Hu, W. and Nash, D. F. T. (2000). Group effects in stone column foundations: model tests. *Geotechnique* 50(6): 689–698.

Munfakh, G. A., Sarkar, S. K. and Castelli, R. J. (1984). Performance of a test embankment founded on stone columns. *Proc. Int. Conf. on Advances in Piling and Ground Testing*, London, 259–265

Narasimha Rao, S., Madhiyan, M. and Prasad, Y. V. S. N. (1992). Influence of bearing area on the behaviour of stone columns. *Indian Geotechnical Conf.*, Calcutta, 235–237

Nash, D. F. T., Powell, J. J. M. and Lloyd, I. M. (1992a). Initial investigations of the soft clay test site at Bothkennar. *Géotechnique*, Vol. 42, No. 2, 163–181

Nash, D. F. T., Sills, G. C. and Davison, L. R. (1992b). One-dimensional consolidation testing of the soft clay from Bothkennar. *Géotechnique*, Vol. 42, No. 2, 241–256

Paul, M. A., Peacock, J. D. and Wood, B. F. (1992). The engineering geology of the Carse clay of the national soft clay research site, Bothkennar. *Géotechnique*, Vol. 42, No. 2, 183–198

Potts, D.M. and Zdravkovic, L. (1999). Finite element analysis in geotechnical engineering: theory. *Thomas Telford*

Potts, D.M. and Zdravkovic, L. (2001). Finite element analysis in geotechnical engineering: application. *Thomas Telford*

Powrie, W. (2004). Soil mechanics: concepts and applications. *Spon Press*

Priebe, H.J. (1976). Evaluation of the settlement reduction of a foundation improved by vibro-replacement. *Bautechnik*, No. 5, 160–162 (in German)

Priebe, H. J. (1995). The design of vibro replacement. *Ground Engineering*, Vol. 28, No. 10, 31–37

Pulko, B. and Majes, B. (2005). Simple and accurate prediction of settlements of stone column reinforced soil. *16th International Conference on Soil Mechanics and Geotechnical Engineering*, Osaka, Vol. 3, 1401–1404

Randolph, M. F., Carter, J. P. and Wroth, C. P. (1979a). Driven piles in clay - the effects of installation and subsequent consolidation. *Géotechnique*, Vol. 29, No. 4, 361–393

Randolph, M. F., Steenfelt, J. S. and Wroth C. P. (1979b). The effect of pile type on design parameters for driven piles. *Proc. 7th European Conf. on Soil Mechanics and Foundation Engineering,* London, 2, 107–114

Rowe, P. W. (1962). The stress-dilatancy relation for static equilibrium of an assembly of particles in contact. *Proc. Royal Society A*, Vol. 269, No. 1339, 500–527

Schanz, T., (1998). Zur modellierung des mechanischen verhaltens von reibungsmaterialen. *Habilitation, Stuttgart Universität*

Schanz, T., Vermeer, P.A., Bonnier, P.G., (1999). The hardening-soil model: Formulation and verification. *Beyond 2000 in Computational Geotechnics - 10 Years of PLAXIS International*, R. B. J. Brinkgreve (ed.), A. A. Balkema, Rotterdam, Netherlands, 281–290

Soderberg, L. O. (1962). Consolidation theory applied to foundation pile time effects. *Géotechnique*, Vol. 12, No. 3, 217–225

Sondermann, W. and Wehr, W. (2004). Deep vibro techniques, *Ground Improvement*, 2nd Edition, edited by M.P. Moseley and K. Kirsch, 57–92, Spon Press

Terzaghi, K. (1925). Erdbaumechanik auf bodenphysikalischer grundlage, F. Deuticke, Vienna

Thornburn, S. and MacVicar, R. S. L. (1968). Soil stabilization employing surface and depth vibrators. The Structural Engineer, Vol. 46, No. 10, 309–316

Wehr, J. and Herle, I. (2006). Exercise on calculation of stone columns - Priebe method and FEM. *Proc. 6th European Conf. on Numerical Methods in Geotechnical Engineering*, Graz, 773–776.

Wehr, W. (2004). Stone columns - single columns and group behavior. *Proc. 5th Int. Conf. on Ground Improvement Techniques*, Malaysia, 329–340

Wehr, J. (2006a). The undrained cohesion of the soil as a criterion for the column installation with a depth vibrator. *TRANSVIB 2006*, Gonin, Holeyman and Rocher-Lacoste (ed.), Editions du LCPC. Paris

Wehr, W. C. S. (2006b). Stone columns - group behaviour and influence of footing flexibility. *Proc. 6th European Conf. on Numerical Methods in Geotechnical Engineering,* Graz, 767–772

Witt, K. J. (1978). Versagensmechanismus einzeln belasteter schottersäulen im bindigin untergrund bei plötzlicher belastung. *B. Sc. thesis, University of Karlsruhe*

Woo-Seok Bae, Bang-Woong Shin, Byung-Chul An and Joo-Sub Kim (2002). Behaviours of foundation system improved with stone columns. *Proc. 12th Int. Offshore and Polar Engineering Conf.*, Kitakyushu, Japan, 675–678

Yu, H. (2000). Cavity expansion methods in geomechanics. *Kluwer Academic Publishers BV*, Dordrecht, NL